# ADEQUACY ASSESSMENT OF COMPOSITE GENERATION AND TRANSMISSION SYSTEMS INCORPORATING WIND ENERGY CONVERSION SYSTEMS

A Thesis

Submitted to the College of Graduate Studies and Research

in Partial Fulfillment of the Requirements

for the Degree of

**Doctor of Philosophy**

in the

Department of Electrical Engineering

University of Saskatchewan

by

**Yi Gao**

# PERMISSION TO USE

I agree that the Library, University of Saskatchewan, may make this thesis freely available for inspection. I further agree that permission for copying of this thesis for scholarly purpose may be granted to the professor or professors who supervised the thesis work recorded herein or, in their absence, by the Head of the Department or the Dean of the College in which the thesis work was done. It is understood that due recognition will be given to me and to the University of Saskatchewan in any use of the material in this thesis. Copying or publication or any other use of this thesis for financial gain without approval by the University of Saskatchewan and my written permission is prohibited.

Request for permission to copy or to make any other use of the material in this thesis in whole or part should be addressed to:

Head of the Department of Electrical Engineering

57 Campus Drive

University of Saskatchewan

Saskatoon, Saskatchewan

Canada S7N 5A9

# ABSTRACT

The development and utilization of wind energy for satisfying electrical demand has received considerable attention in recent years due to its tremendous environmental, social and economic benefits, together with public support and government incentives. Electric power generation from wind energy behaves quite differently from that of conventional sources. The fundamentally different operating characteristics of wind energy facilities therefore affect power system reliability in a different manner than those of conventional systems. The reliability impact of such a highly variable energy source is an important aspect that must be assessed when the wind power penetration is significant. The focus of the research described in this thesis is on the utilization of state sampling Monte Carlo simulation in wind integrated bulk electric system reliability analysis and the application of these concepts in system planning and decision making. Load forecast uncertainty is an important factor in long range planning and system development. This thesis describes two approximate approaches developed to reduce the number of steps in a load duration curve which includes load forecast uncertainty, and to provide reasonably accurate generating and bulk system reliability index predictions. The developed approaches are illustrated by application to two composite test systems.

A method of generating correlated random numbers with uniform distributions and a specified correlation coefficient in the state sampling method is proposed and used to conduct adequacy assessment in generating systems and in bulk electric systems containing correlated wind farms in this thesis. The studies described show that it is possible to use the state sampling Monte Carlo simulation technique to quantitatively assess the reliability implications associated with adding wind power to a composite generation and transmission system including the effects of multiple correlated wind sites. This is an important development as it permits correlated wind farms to be incorporated in large practical system studies without requiring excessive increases in computer solution time. The procedures described in this thesis for creating monthly and seasonal wind farm models should prove useful in situations where time period models are required to incorporate scheduled maintenance of generation and transmission facilities.

There is growing interest in combining deterministic considerations with probabilistic assessment in order to evaluate the quantitative system risk and conduct bulk power system planning. A relatively new approach that incorporates deterministic and probabilistic considerations in a single risk assessment framework has been designated as the joint deterministic-probabilistic approach. The research work described in this thesis illustrates that the joint deterministic-probabilistic approach can be effectively used to integrate wind power in bulk electric system planning. The studies described in this thesis show that the application of the joint deterministic-probabilistic method provides more stringent results for a system with wind power than the traditional deterministic N-1 method because the joint deterministic-probabilistic technique is driven by the deterministic N-1 criterion with an added probabilistic perspective which recognizes the power output characteristics of a wind turbine generator.

# ACKNOWLEDGEMENTS

I would like to express my deepest gratitude and appreciation to my primary supervisor Dr. Roy Billinton for his invaluable guidance, support and encouragement, for his patience, motivation, enthusiasm, and immense knowledge. Dr. Billinton's guidance helped me in all the time of research and writing of this thesis. I could not have imagined having a better advisor and mentor for my graduate study.

I also would like to give my sincere appreciation to my co-supervisor Dr. Rajesh Karki for his consistent support, and guidance me all the time during research.

I would like to express my appreciation to the members of my Advisory Committee and my graduate study teachers for strengthening my knowledge on electrical engineering.

Financial assistances from the Department of Electrical and Computer Engineering at the University of Saskatchewan in the form of a Graduate Scholarship, and from the Natural Science and Engineering Research Council of Canada in the form of research support are gratefully acknowledged.

I would like to give my special thanks to my husband, Yapeng Zhang, and my beloved daughter, Xinbei for their support, patience and love throughout the research. Thanks to my parents, Lingzhi Gao and Guilan Yang, for loving me and encouraging me throughout my life.

# TABLE OF CONTENTS

# LIST OF TABLES

# LIST OF FIGURES

# LIST OF ABBREVIATIONS

| | |
|---|---|
| A | Annual Equivalent Capital |
| ARMA | Auto-Regressive and Moving Average |
| CF | Capacity Factor |
| COPT | Capacity Outage Probability Table |
| CRF | Capital Return Factor |
| D | Deterministic N-1 criterion |
| DAFOR | Derating Adjusted Forced Outage Rate |
| DAFORW | Derating Adjusted Forced Outage Rate of a Wind Farm |
| DC | Direct Current |
| DPLVC | Daily Peak Load Variation Curve |
| DPUI | Delivery Point Unreliability Index |
| EDC | Expected Damage Cost |
| EDLC | Expected Duration of Load Curtailment |
| EENS | Expected Energy Not Supplied |
| ELCC | Effective Load Carrying Capacity |
| FOR | Forced Outage Rate |
| GA | Genetic Algorithm |
| hrs | Hours |
| HL | Hierarchical Levels |
| HL-I | Hierarchical Level-I |
| HL-II | Hierarchical Level-II |
| HL-III | Hierarchical Level-III |
| IEEE-RTS | IEEE Reliability Test System |
| IEAR | Interrupted Energy Assessment Rate |
| kWh | Kilowatt-hours |
| LDC | Load Duration Curve |

| | |
|---|---|
| LFU | Load Forecast Uncertainty |
| LOEE | Loss of Energy Expectation |
| LOLE | Loss of Load Expectation |
| LOLP | Loss of Load Probability |
| MCS | Monte Carlo Simulation |
| MECORE | Monte Carlo Simulation and Enumeration Composite System Reliability Evaluation Program |
| MLDC | Modified Load Duration Curve |
| MRBTS | Modified RBTS |
| MRRBTS | Modified Reinforced RBTS |
| MRTS | Modified IEEE-RTS |
| M1MRTS | Modified MRTS (1) |
| M2MRTS | Modified MRTS (2) |
| MTTF | Mean Time to Failure |
| MTTR | Mean Time to Repair |
| MW | Megawatt |
| MWh | Megawatt-hours |
| NID | Normally Independent Distributed |
| occ. | Occur |
| OPF | Optimal Power Flow |
| P | Probabilistic Criterion |
| PLCC | Peak Load Carrying Capacity |
| p.u. | Per unit |
| PV | Present Value |
| R | Cross-correlation Coefficient |
| RBTS | Roy Billinton Test System |
| Rc | Probabilistic risk criterion |
| RMLDC | Reduced Modified Load Duration Curve |
| SI | Severity Index |
| SLDC | Summer Load Duration Curve |
| TI | Total Investment cost |

| | |
|---|---|
| WECS | Wind Energy Conversion System |
| WLDC | Winter Load Duration Curve |
| WTG | Wind Turbine Generator |
| yr | Year |

# 1. Introduction

## 1.1. Power System Reliability Evaluation

A power system can be very complex, involving the integration of different types of generating resources to provide electricity to a wide range of customers with varying requirements. It is not possible for the supply of electrical energy to be continuously available on demand due to random failures of equipment and the system. Electric power utilities, therefore, attempt to provide an acceptable degree of system reliability in the planning, design and operation of their systems within the existing economic constraints. The term “reliability” when associated with a power system is a measure of the ability of the system to meet the customer requirements for electrical energy. Power system reliability evaluation has been extensively developed over the last sixty years and there are many publications available on this subject [1-8].

The general area of “reliability” is usually divided into the two aspects of system adequacy and system security [9, 10], as shown in Figure 1.1.

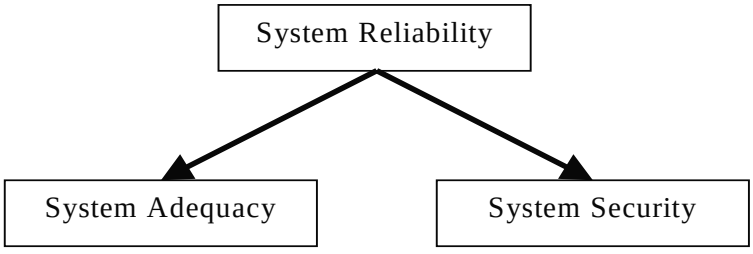


Figure 1.1: Subdivision of system reliability

The North American Electric Reliability Corporation (NERC) defines adequacy and security to be [11]:

Adequacy - The ability of the electric system to supply the aggregate electrical demand and energy requirements of the end-use customers at all times, taking into account scheduled and reasonably expected unscheduled outages of system components.

Security - The ability of the electric system to withstand sudden disturbances such as electric short circuits or unanticipated loss of system elements.

This thesis is restricted to adequacy assessment of power systems.

The basic techniques for adequacy assessment can be categorized in terms of their application to segments of a complete power system. These segments are shown in Figure 1.2 and can be defined as the functional zones of generation, transmission and distribution [12]. Hierarchical levels are created by combining the functional zones.

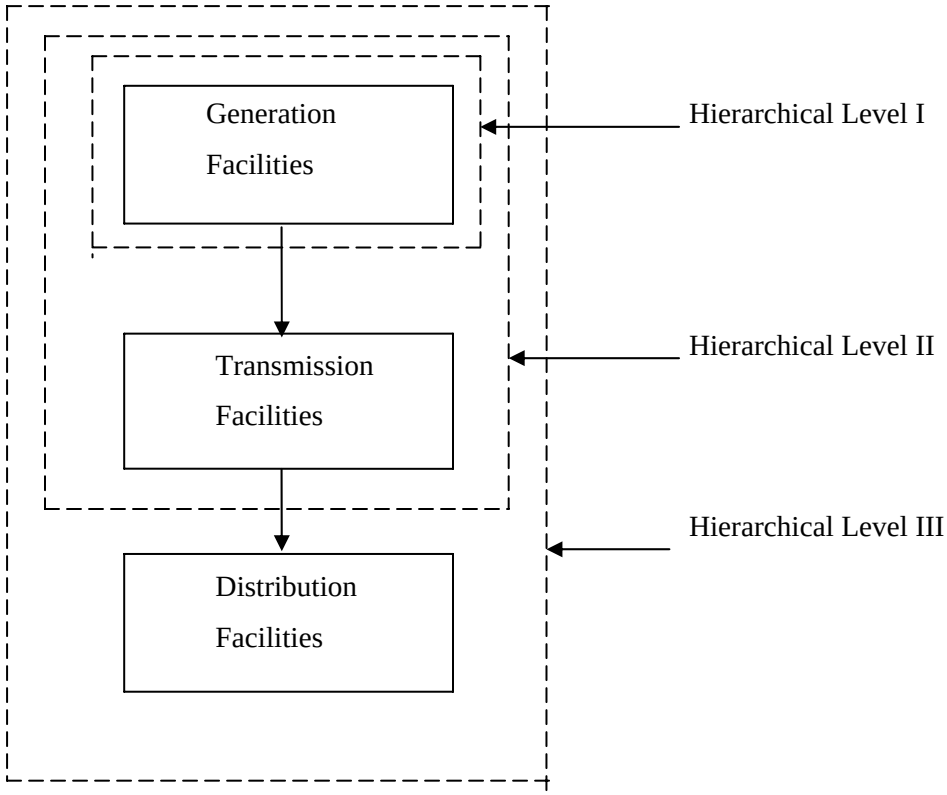


Figure 1.2: Hierarchical level structure

Reliability assessment at hierarchical level I (HL-I) is solely concerned with the generation facilities. At this level, the total system generation including interconnected assistance is examined to determine its ability to meet the total system load demand. Reliability assessment at HL-I is normally defined as generating capacity reliability evaluation. Reliability evaluation at hierarchical level II (HL-II) includes both the generation and transmission in an assessment of

the integrated ability of the composite system to deliver energy to the bulk supply points. This analysis is usually termed as composite system or bulk power system reliability evaluation. Overall assessment considering all three functional segments is known as HL-III analysis. The research described in this thesis is conducted at HL-II and is focused on adequacy analysis.

Reliability analysis of a power system can be conducted using either deterministic or probabilistic techniques. Deterministic techniques provide a reliability analyst with information on how a system failure can happen or how system success can be achieved. The most common deterministic criterion dictates that specific credible outages will not result in system failure. The traditional deterministic criterion used particularly in bulk electric systems (BES) is known as the N-1 security criterion [13] under which the loss of any bulk system component will not result in system failure. The essential weakness of deterministic criteria is that they do not respond to the stochastic nature of system behavior, customer demands or component failures. System behavior is stochastic in nature, and therefore it is logical to consider probabilistic methods that are able to respond to the actual factors that influence the reliability of the system. Probabilistic techniques provide quantitative indices, which can be used to decide if system performance is acceptable or if changes need to be made. There is, however, considerable reluctance to using probabilistic techniques in many areas due to the difficulty in interpreting the resulting numerical indices. Deterministic criteria are easier for system planners, designers and operators to understand than a numerical risk index determined using probabilistic techniques. This difficulty can be alleviated by incorporating the acceptable deterministic N-1 and probabilistic considerations to provide a resulting soft criterion. A combination of the basic deterministic and probabilistic concepts is illustrated in [14] and designated as system well-being analysis. An alternate approach to the well-being technique designated as the joint deterministic-probabilistic (D-P) approach is presented in [15] and applied in the research described in this thesis.

## 1.2. Concept of Bulk Electric System Reliability Analysis

As noted earlier, the analysis conducted at HL-II is usually termed as composite system or bulk power system reliability evaluation. Composite power system reliability evaluation provides an assessment of the ability of an electric power system to satisfy the load and energy requirements

at the major load points and for the overall system. The most significant quantitative indices in composite power system reliability evaluation are those that relate to load curtailment. Analytical methods or Monte Carlo simulation techniques are two fundamental approaches to bulk system reliability assessment [9].

Analytical methods such as contingency enumeration [16] represent the system by a mathematical model and evaluate the reliability indices from the model using direct numerical solutions. An analytical method will always give the same numerical result for the same system, same model and same set of input data. These methods, therefore, tend to provide a high degree of confidence in the reliability evaluation results as they are obtained by an exact solution from an accepted system model. Analytical techniques, however, usually require assumptions to simplify the solutions. This is particularly the case when complex systems and operating procedures have to be modeled. The resulting analysis can therefore lose some of its significance. This difficulty can be reduced or eliminated by using a simulation approach. Monte Carlo simulation methods estimate the reliability indices by simulating the actual process and random behavior of the system. The method, therefore, treats the problem as a series of experiments. There are merits and demerits in both methods. Generally, Monte Carlo simulation requires a large amount of computing time compared to analytical methods. Monte Carlo simulation techniques, however, can theoretically take into account virtually all aspects and contingencies inherent in the planning, design and operation of a power system [9, 10].

Considerable work has been done in the last two decades on the subject of composite generation and transmission system reliability evaluation using analytical or Monte Carlo simulation techniques, or a hybrid of both methods [3-8]. There has been a growing interest and an increasing trend in applying Monte Carlo simulation approaches to bulk electric system reliability analysis during the last decade due to the development and availability of high speed computation facilities. The two basic Monte Carlo methods used in power system reliability evaluation are generally known as the sequential and non-sequential techniques. Non-sequential techniques are widely used for power system reliability evaluation and can be divided into the two categories of state sampling and state transition sampling. Sequential simulation can fully take into account the chronological behavior of the system, while the non-sequential method

involves non-chronological system state considerations. Both sequential and non-sequential simulation techniques, however, have advantages and disadvantages.

### 1.3. Power Systems with Wind Energy

Renewable energy resources are receiving considerable attention in the continued growth and development of bulk electric power systems. The most promising renewable electrical energy generating source at the present time is wind power. Wind power is a clean, emissions-free power generation technology. Like all renewable sources, it is based on capturing the energy from natural forces and has none of the polluting effects associated with 'conventional' fuels. Over the past ten years, global wind power capacity has continued to grow at an average cumulative rate of over 30%, and 2008 was another record year with more than 27 GW of new installations, bringing the total up to over 120 GW. In 2008, Canada became the 12th country in the world to surpass the 2,000 MW mark in installed wind energy capacity – ending the year with 2,369 MW. Canada's wind farms now produce enough power to meet almost 1% of Canada's electricity demand [17]. Improvements in wind generation technologies will continue to encourage the use of wind energy in both grid-connected and stand-alone systems. Wind energy is now "utility scale" and can affect utility system planning and operations for both generation and transmission [18].

Since wind power production is dependent on the wind, the output of a turbine and wind farm varies over time, under the influence of meteorological fluctuations. These variations occur on all time scales: by seconds, minutes, hours, days, months, seasons and years. The fundamentally different operating characteristics of wind energy affect power system reliability in a different manner than conventional technology systems. As power generation plants using wind energy are increasingly integrated into existing power systems, it becomes particularly important to evaluate the reliability of these plants and assess the effects that they will have on the overall system reliability. Most of the reported work has been done since 1988 [5-8] on modeling wind power generation and on the use of such models for generating system adequacy evaluation. Bulk electric system reliability evaluation is a relatively complicated task that involves detailed

modeling of both the generation and transmission facilities [9]. Considerably less work has been done on the reliability evaluation of bulk electric systems incorporating wind energy.

### 1.4. Research Objectives and Overview of the Thesis

The fundamentally different operating characteristics of wind energy affect power system reliability in a different manner than conventional technology systems due to the random nature of the wind. The increasing use of wind power as an important electrical energy source clearly indicates the importance of assessing the reliability of bulk systems containing significant amounts of wind energy. Monte Carlo simulation can be effectively used in composite system reliability evaluation. The most basic non-sequential Monte Carlo simulation method is the state sampling technique. The major advantages of the state sampling method are relatively low computation times and memory requirements for large practical system studies. Multi-state components can also be incorporated in the analysis without a significant increase in computing time. This research work is focused on the utilization of state sampling Monte Carlo simulation in wind integrated bulk electric system reliability analysis and the application of these concepts in system planning and decision making. The following list of conducted tasks indicates the specific objectives of the research described in this thesis.

1. The development of appropriate load models for adequacy evaluation considering load forecast uncertainty.
2. A detailed investigation of bulk electric system adequacy assessment incorporating correlated wind energy conversion systems (WECS) using the state sampling Monte Carlo simulation method.
3. An examination of the ability to develop and utilize time period WECS and load models in composite system adequacy evaluation including wind energy.
4. An investigation of wind power considerations in bulk electric system reliability planning using the joint deterministic-probabilistic method.
5. An examination of reliability improvement economic analysis using reliability cost/reliability worth considerations for optimum system reinforcement planning associated with WECS additions.

This thesis is organized into eight chapters:

Chapter 1 introduces some of the basic concepts related to power system reliability evaluation and power systems including wind power. It also outlines the research objectives and the scope of the thesis.

Chapter 2 briefly describes relevant system reliability indices. Three techniques used in power system adequacy evaluation, i.e. the analytical technique, and the non-sequential and sequential Monte Carlo simulation techniques are illustrated. A composite generation and transmission system reliability evaluation software known as MECORE [19] is introduced in this chapter. The two study systems designated as the Roy Billinton Test System (RBTS) [20] and the IEEE Reliability Test System (RTS) [21], which are used extensively in this thesis, are introduced. The basic annual reliability indices for the two systems obtained using the MECORE software are presented.

Bulk system adequacy assessment incorporating load forecast uncertainty is presented in Chapter 3. Two basic methods that can be used to include the load forecast uncertainty in the reliability assessment of a power system are presented. Reliability indices obtained by applying the two methods in generating capacity adequacy assessment are compared. Approximate load model techniques for incorporating load forecast uncertainty in bulk system reliability evaluation are also presented and compared with the two basic methods. The impacts of load forecast uncertainty on the system and load point reliability indices for the two study systems are investigated using MECORE.

Chapter 4 presents research conducted on wind integrated bulk system adequacy assessment considering wind speed correlation. A genetic algorithm method [22-24] is used to adjust the wind speed models to simulate correlated wind speeds for multiple wind farms. A wind energy conversion system (WECS) model involving wind turbine generators (WTG) and the wind speed characteristics is described. An approach for use with the state sampling method to conduct adequacy assessment in power systems containing correlated WECS is developed and discussed. Using this approach, the MECORE software was modified to incorporate two dependent wind farms. The original RBTS and IEEE-RTS systems were modified to represent the conditions

existing in a wide range of practical systems. A detailed investigation of bulk system adequacy assessment incorporating correlated WECS is conducted using the modified systems.

Wind integrated bulk system adequacy assessment considering wind energy seasonal characteristics is presented in Chapter 5. Procedures for creating time period wind speed models and associated multi-state WECS models are presented. The effects in a wind integrated RBTS HL-I analysis of time period wind power outputs are investigated. The differences in the system risk indices between using the developed period WECS models and using an annual model are examined using the composite RBTS and IEEE-RTS. The impacts on the bulk system reliability indices of varying seasonal wind speed correlation levels between dependent wind farms are also investigated.

Chapter 6 extends the joint deterministic-probabilistic (D-P) technique [15] in a wind integrated bulk power system reliability planning context. The basic concepts behind the traditional deterministic N-1 criterion (D), the basic probabilistic (P) technique, and the D-P approach are presented in this chapter. The capacity value of wind generation using various approaches and how this capacity value can be utilized under a deterministic N-1 criterion are examined. The procedures used in the application of the D, P and D-P methods to a bulk power system incorporating a single and multiple WECS are illustrated. The benefits in terms of system peak load carrying capacity (PLCC) [9] in a WECS planning context are investigated using the three techniques.

Large-wind integrated bulk system reinforcement planning is considered in Chapter 7. The IEEE-RTS is modified and the modified system associated with WECS is considered as a basic study system. The procedures in applying the D- P technique for long-term bulk system planning are illustrated and compared with an analysis using the P method. Planning alternatives are proposed that meet the N-1 criterion over the planning time frame and candidate planning schemes are selected from the proposed alternatives using the D-P and P approaches. Economic assessment is then conducted on the candidate alternatives using the two approaches. Investment and risk costs for the candidate schemes are investigated using the present value method [25, 26].

The impacts on the system risk indices and investments in the planning period of considering long-term load forecast uncertainty are also examined.

Chapter 8 summarizes the research work described in the thesis and presents some general conclusions.

# 2. Basic Concepts in Power System Adequacy Assessment

## 2.1. Introduction

As noted in Chapter 1, power system adequacy is usually expressed in the form of indices that reflect the system capability and the service provided to the system customers. Adequacy indices can be used to predict the performance of different system designs, reinforcements and expansion plans and the related cost/worth of the alternatives. Significant effort has been applied to develop techniques for predicting and assessing the adequacy performance of actual power systems [1-8]. The fundamental approaches used to calculate adequacy indices in a probabilistic evaluation can be generally described as being either analytical evaluation or Monte Carlo simulation. Analytical techniques represent the system by analytical models and evaluate the system adequacy indices from these models using mathematical solutions. Monte Carlo simulation techniques, on the other hand, estimate the adequacy indices by simulating the actual process and the random behavior of the system. Both approaches have advantages and disadvantages, and each of them can be very powerful with proper application.

This chapter provides a brief description of some of the analytical methods for generating capacity adequacy evaluation. Non-sequential and sequential Monte Carlo simulation techniques are also presented in this chapter. The reliability indices used in this research and an evaluation software known as MECORE [19] are introduced. The concepts are illustrated by application to two composite test systems.

## 2.2. General Assessment Techniques

### 2.2.1. Analytical Techniques

Analytical techniques represent the system by analytical models and evaluate the system risk indices from these models using mathematical solutions. The analytical approach can in many

cases provide accurate probabilistic indices in a relatively short calculation time. Analytical techniques have been extensively developed for HL-I and HL II studies [1-8]. Analytical techniques, however, usually require assumptions to simplify the solutions. This is particularly the case when complex systems and operating procedures have to be modeled. The resulting analysis can therefore lose some of its significance. Analytical techniques are applied in some of the HL-I studies described in this thesis.

The basic modeling approach in an HL-I analysis is shown in Figure 2.1. The generation model and the load model are combined to produce the risk model. The risk indices obtained are overall system adequacy indices and do not include transmission constraints and transmission reliabilities.

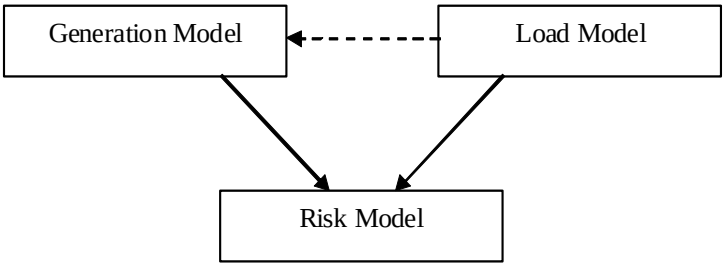


Figure 2.1: Conceptual tasks in HL- I evaluation

In most analytical techniques, the generation model is normally in the form of an array of capacity levels and their associated probabilities. This representation is known as a capacity outage probability table (COPT) [9]. Each generating unit in the system is represented by either a two-state or a multi-state model. In the two state model, the generating unit is considered to be either fully available (Up) or totally out of service (Down) as shown in Figure 2.2.

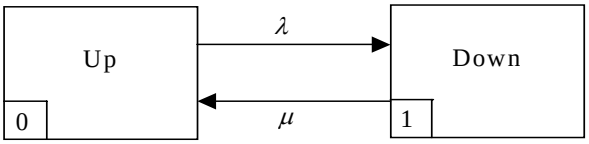


Figure 2.2: Two-state model for a generating unit

where $\lambda$ = unit failure rate
$\mu$ = unit repair rate

A multi-state generating unit is a unit that can exist in one or more derated or partial output states as well as in the fully up and fully down states [9]. The simplest model that incorporates derating is shown in Figure 2.3. This three-state model includes a single derated state in addition to the full capacity and failed states.

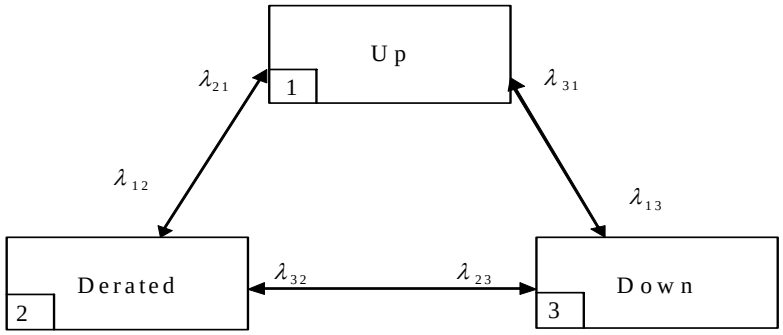


Figure 2.3: Three-state model for a generating unit

where $\lambda_{ij}$ is the transition rate between state "*i*" and state "*j*".

The COPT can be constructed using a recursive technique [9]. This technique is very powerful and can be used to add both two-state and multi-state generating units.

The load models used in the analytical methods depend on the reliability indices adopted, the availability of load data and the evaluation methods used. The load model is usually represented by either the daily peak load variation curve (DPLVC) or the load duration curve (LDC). The DPLVC is a cumulative load model formed by arranging the individual daily peak loads in descending order. The load duration curve is created by arranging the hourly load values in descending order. The DPLVC is used extensively, due to its simplicity. The LDC, however, is a more realistic representation of the system load.

The basic generating capacity reliability indices, such as the loss of load probability (LOLP), the loss of load expectation (LOLE), the loss of energy expectation (LOEE), can be calculated using the loss of load method [9]. In this method, the generation system represented by the COPT is convolved with the load characteristic represented by either the DPLVC or the LDC. The LOLE presents the expected number of days (or hours) in the specified period in which the daily peak

load (or hourly load) exceeds the available capacity. The LOLE can be expressed by Equation (2.1).

$$LOLE = \sum_{k=1}^{n} p_k \times t_k \qquad (2.1)$$

where $n$ is the number of capacity outage state in excess of the reserve. $p_k$ is the probability of the capacity outage state *k*. $t_k$ is the time for which load loss will occur.

The LOEE index is the expected energy not supplied by the generating system due to load demand exceeding the available generating capacity and is given by Equation (2.2).

$$LOEE = \sum_{k=1}^{n} p_k \times E_k \qquad (2.2)$$

where $E_k$ is the energy curtailment of capacity outage state $k$ .

The LOLE and LOEE methods are described in detail in [9], together with information on other techniques for HL-I evaluation.

### 2.2.2. Monte Carlo Simulation

As noted in Chapter 1, there are two general approaches for assessing power system reliability: the analytical method and the simulation method. Monte Carlo methods are more flexible when complex operating conditions and system considerations need to be incorporated. Considerable work has been done in the last two decades on the application of Monte Carlo simulation to power system reliability evaluation [1-10]. These simulations utilize random number generators and probabilistic techniques to model the behavior of the power system. The two basic Monte Carlo methods used in power system reliability evaluation are generally known as the sequential and non-sequential techniques. Sequential evaluation involves a chronological analysis of the system and the component states. Non-sequential techniques are widely used for power system reliability evaluation and can be divided into the two categories of state sampling and state transition sampling. The following is a brief description of the basic techniques.

**Non-Sequential Methods: State Sampling Approach**

In this approach, the system state depends on the combination of all the component states irrespective of the event chronologies and each component state can be determined by sampling

using the probability that the component appears in that state [27-29]. The basic sampling procedure is conducted by generating pseudo-random numbers and assuming that the behaviour of each component can be categorized by a uniform distribution under [0, 1]. Each consecutive sample of system states is randomly selected independently from previous and subsequent samples. The component can be represented by a two-state or multi-state model. In the case of a two-state component, each component has the two states of failure and success and component failures are independent events. The state of the system containing $n$ components including generating units, transmission lines, transformers, etc., can be expressed by the vector $S$, where $S = (S_1, \ldots, S_i, \ldots, S_n)$, $S_i$ is the state of the $i_{th}$ component. When $S$ equals zero, the system is in the normal state. When $S$ is not equal to zero, the system is in a contingency state due to component outage(s). The following steps describe the process of this method.

Step 1. Generate a uniform random number $U_i$ for the $i_{th}$ component.

Step 2. Determine the state of component $i$ using the following expression:

$$S_i = \begin{cases} 0 & (success \quad state) \quad if \quad U_i \geq FOR_i \\ 1 & (failure \quad state) \quad if \quad 0 \leq U_i < FOR_i \end{cases} \tag{2.3}$$

where $FOR_i$ is the $i_{th}$ component's forced outage rate.

Step 3. The system state $S$ is obtained by applying Step 2 to all the components.

Step 4. Determine the system state. If $S$ equals zero, the system is in the normal state. If $S$ is not equal to zero, the system is in a contingency state.

Step 5. A linear programming optimization model [10] is usually used to reschedule generation, alleviate line overloads and to avoid load curtailment if possible or to minimize the total load curtailment if unavoidable.

Step 6. Reliability indices for each load point and the system are accumulated and Steps 1 to 5 are repeated until the stopping criterion is reached.

One of the advantages of the system state sampling method is that multi-state components can be incorporated in the analysis without a significant increase in computing time. The probabilities of the $i_{th}$ component including a single derated state for Step 2 are expressed in Equation (2.4), where $PDR_i$ is the probability of the single derated state of the $i_{th}$ component.

$$S_i = \begin{cases} 0 & (up \quad state) \quad if \quad U_i \geq PDR_i + FOR_i \\ 1 & (down \quad state) \quad if \quad PDR_i \leq U_i < PDR_i + FOR_i \\ 2 & (derated \quad state) \quad if \quad 0 \leq U_i < PDR_i \end{cases} \tag{2.4}$$

Additional derated states can be simulated in a similar manner.

The basic state sampling technique is relatively simple. It only involves the generation of uniformly distributed random numbers in the range of 0 to 1 instead of sampling a distribution function, and only basic reliability data in the form of component-state probabilities are required. The state sampling approach has a relatively short computation time with small memory requirements. The major disadvantage of the state sampling technique is that it cannot be used by itself to calculate the actual frequency index, as this approach estimates the frequency of load curtailments as the sum of the occurrences of load curtailment states and it cannot recognize the impact of failure state transitions and transitions associated with a chronological load model.

**Non-Sequential Methods: State Transition Sampling Approach**

The state transition sampling technique [30, 31] focuses on system state transitions, instead of component states or component state processes. In this method, the state transition of any component leads to a system state transition and all the state residence times are assumed to be exponentially distributed. The state transition sampling method can be used to calculate an exact frequency index without sampling the distribution function and storing chronological information as in the sequential technique. The main restriction in this technique is that it only applies to exponentially distributed component state durations. This technique is usually computationally slower than the state sampling simulation approach.

**Sequential Method**

The sequential or state duration approach [32, 33] is based on sampling the probability distributions of the component state durations. In this approach, chronological component state transition processes for all components are first simulated by sampling. The chronological system state transition process is then created by combining all the chronological component state transition processes. This technique can be used to model all the contingencies and

operating characteristics inherent in the system. Chronological load models can also be easily incorporated.

The sequential method can be used to calculate the actual frequency index as well as related indices and can incorporate different state duration distributions. The statistical probability distributions of the adequacy indices can also be assessed in addition to their expected values. This method, however, requires more computation time and storage than the state sampling approach since it is necessary to generate and store information on the chronological state transition processes of all the system components in a long time span.

The state sampling technique is used to conduct the reliability studies described in this thesis.

## 2.3. Adequacy Indices for the HL-I and the HL-II Studies

There are many possible indices that can be used to measure the adequacy of a power system and different countries and utilities use different indices. Most adequacy indices are expected values of random variables. The basic indices in generating system adequacy are the LOLP, LOLE and LOEE as noted in the previous section. These indices can be calculated using either the analytical methods or Monte Carlo simulation techniques.

The adequacy index concepts used in HL-I studies can be extended to composite system assessments. Additional indices are, however, required to reflect the composite system characteristics. Both load point and system indices are necessary to provide a complete assessment of composite system adequacy. The indices can be categorized as annualized and annual values. Annualized adequacy indices are determined using a single load level in a one-year period and the system peak load is normally used. Annual adequacy indices, however, are calculated based on the actual time-varying load throughout the year. These indices include the expected customer unsupplied energy and can be used to determine the expected damage costs for the system. The basic adequacy indices used in composite system studies are presented in the following section with reference to the MECORE program.

## 2.4. The MECORE Software

The MECORE software is a Monte Carlo based composite generation and transmission system reliability evaluation tool designed to perform reliability and reliability worth assessment of bulk electric power systems. MECORE was initially developed at the University of Saskatchewan and subsequently enhanced at BC Hydro [19].

It can be used to assess composite generation and transmission reliability, generation reliability in a composite system and transmission reliability in a composite system, and provides a wide range of reliability indices for the system and for the individual load points. It also provides unreliability cost indices, which reflect reliability worth. The indices produced by the program can be used to aid in comparing different planning alternatives from a reliability point of view. MECORE is based on a combination of Monte Carlo simulation (state sampling technique) and enumeration techniques. The state sampling technique is used to simulate system component states and to calculate annualized indices at the system peak load level. A hybrid method utilizing an enumeration approach for aggregated load states is used to calculate annual indices using an annual load curve [19]. MECORE is designed to handle up to 1000 buses and 2000 branches.

In MECORE, the generating unit states are modeled using multi-state random variables. This program was initially designed to model generating units with up to two derated states. In order to examine appropriate multi-state renewable energy models, the MECORE program was modified to recognize up to ten derated states. Transmission lines are represented by two-state models. The MECORE program uses DC load flow and a linear programming Optimal Power Flow (OPF) model is utilized to reschedule generation (change generation patterns), alleviate line overloads and avoid load curtailments if possible or minimize total load curtailments if unavoidable.

A priority order policy is used in MECORE to make load shedding decisions to alleviate system constraints and maintain system stability. One common method to determine the priority order is based on economic factors which recognize the customer cost associated with failure of supply. The most convenient index for this purpose is the Interrupted Energy Assessment Rate (IEAR),

as it measures the customer monetary loss as a function of the energy not supplied [9]. The higher the IEAR, the more disruptive is the loss of supply and a higher priority order is applied. The overall system IEAR is calculated using the following equation [9].

$$Average\,system \quad IEAR = \sum_{k=1}^{NB} IEAR_k q_k \tag{2.5}$$

where $NB$ is the total number of load buses in the system, $IEAR_k$ is the IEAR at load bus $k$, and $q_k$ is the fraction of the system load utilized by the customers at load bus $k$.

A brief description of the capabilities of MECORE is presented in the following and the capabilities are further described in [19].

I. Failure modes:
   - Independent failures of generators, lines and transformers
   - Common cause outages of transmission lines
   - Generating unit derating states

II. Failure criteria:
   - Capacity deficiency
   - Line overload
   - System separation-load loss
   - Bus isolation-load loss

III. Load model:
   - Annual, seasonal, and monthly load curve
   - Multi-step models
   - Bus load proportional scaling and flat level model

IV. Probability indices:
   - System and bus indices
   - Annualized and monthly/seasonal/annual indices
   - Basic and IEEE-proposed indices [9, 10]

**Basic Indices**

(1) Probability of load curtailment (PLC)

$$\text{PLC} = \sum_{i \in S} P_i \tag{2.6}$$

where $P_i$ is the probability of system state $i$ and $S$ is the set of all system states associated with load curtailments.

(2) Expected number of load curtailment (ENLC)

$$\text{ENLC} = \sum_{i \in S} F_i \quad \text{occ./yr} \tag{2.7}$$

The ENLC is the sum of the occurrences of the load curtailment states and is therefore an upper boundary of the actual frequency index. The system state frequency $F_i$ can be calculated by the following relationship between the frequency and the system state probability $P_i$:

$$\text{F}_\text{i} = P_i \sum_{K \in N} \lambda_K \quad \text{occ./yr} \tag{2.8}$$

where $\lambda_k$ is the departure rate of component $k$ and $N$ is the set of all components of the system.

(3) Expected duration of load curtailment (EDLC)

$$\text{EDLC} = \text{PLC} \times 8760 \quad \text{hrs/yr} \tag{2.9}$$

(4) Average duration of load curtailment (ADLC)

$$\text{ADLC} = \text{EDLC/EFLC hrs/disturbance} \tag{2.10}$$

(5) Expected load curtailment (ELC)

$$\text{ELC} = \sum_{i \in S} C_i F_i \quad \text{MW/yr} \tag{2.11}$$

where $C_i$ is the load curtailment of system state $i$.

(6) Expected demand not supplied (EDNS)

$$\text{EDNS} = \sum_{i \in S} C_i P_i \quad \text{MW} \tag{2.12}$$

(7) Expected energy not supplied (EENS)

$$\text{EENS} = \sum_{i \in S} C_i F_i D_i = \sum_{i \in S} 8760 C_i P_i \quad \text{MWh/yr} \tag{2.13}$$

where $D_i$ is the duration of system state $i$.

(8) Expected damage cost (EDC)

$$\text{EDC} = \sum_{i \in S} C_i F_i D_i W \quad \text{k\$/yr} \tag{2.14}$$

where $C_i$ is the load curtailment of system state $i$; $F_i$ and $D_i$ are the frequency and the duration of system state $i$; $W$ is the unit damage cost in \$/kWh.

**IEEE Proposed Indices**

(9) Bulk power interruption index (BPII)

$$\text{BPII} = \frac{\sum_{i \in S} C_i F_i}{L} \text{ MW/MW-yr} \qquad (2.15)$$

where $L$ is the annual system peak load in MW.

(10) Bulk power/energy curtailment index (BPECI)

$$\text{BPECI} = \frac{EENS}{L} \text{ MWh/MW-yr} \qquad (2.16)$$

(11) Bulk Power-supply average MW curtailment index (BPACI)

$$\text{BPACI} = \frac{ELC}{EFLC} \text{ MW/disturbance} \qquad (2.17)$$

where EFLC is expected frequency of load curtailment:

$$\text{EFLC} = \sum_{i \in S} (F_i - f_i) \text{ occ./yr} \qquad (2.18)$$

$F_i$ is the frequency of departing system state $i$ and $f_i$ is the portion of $F_i$ which corresponds to not going through the boundary wall between the loss-of-load state set and the no-loss-of-load state set.

(12) Modified bulk energy curtailment index (MBECI)

$$\text{MBECI} = \frac{EDNS}{L} \text{ MW/MW} \qquad (2.19)$$

(13) Severity index (SI)

$$\text{SI} = BPECI \times 60 \text{ system min/yr} \qquad (2.20)$$

The basic indices can be applied to an overall system or to a single load point, while the IEEE proposed indices apply to the overall system. The advantage of the IEEE proposed indices is that they can be used to compare the adequacy of systems having different sizes. When the MECORE program is used in HL-I studies, the transmission elements in the test system are assumed to be 100% reliable. The basic indices of LOLP, LOLE and LOEE used in HL-I analyses are the same as the PLC, EDLC and EENS respectively used in MECORE.

The rate of convergence in a Monte Carlo simulation of a composite system is different for the various load bus and system indices. A larger number of samples leads to higher accuracy but involves more computing time. The coefficient of variation of a particular index can be used as the convergence criterion. The coefficient of variation for the EDNS index is most often used and is outputted with the calculated results.

## 2.5. Two Composite Test Systems

The two test systems used in this chapter are the Roy Billinton Test System (RBTS) [20] and the IEEE Reliability Test System (IEEE-RTS) [21]. The single line diagrams of the RBTS and the IEEE-RTS are shown in Figures 2.4 and 2.5 respectively.

The RBTS is a small composite system developed for educational and research purposes at the University of Saskatchewan. It is a six-bus test system with five load buses. It has 11 generators, 9 transmission lines and 7 branches. The total installed capacity is 240 MW and the system peak load is 185 MW. The system voltage level is 230 KV.

The IEEE-RTS is a relatively large system compared with the RBTS. It was developed by an IEEE Task Force to provide a practical representative bulk power system for research and comparative study purposes. The generating system contains 32 generators with capacities from 12 to 400 MW. The transmission system has 24 buses, which include 10 generator buses, 10 load buses, and 4 connection buses, connected by 33 lines and 5 autotransformers at two voltages levels: 138KV and 230 KV. The total installed capacity of the IEEE-RTS is 3405 MW and the system peak load is 2850 MW.

Both the RBTS and the RTS use the same per-unit load model, designated as the IEEE-RTS load model [9, 10]. This load model can be used to create 8760 hourly chronological loads on a per unit basis. The basic data for the two test systems are given in Appendix A.

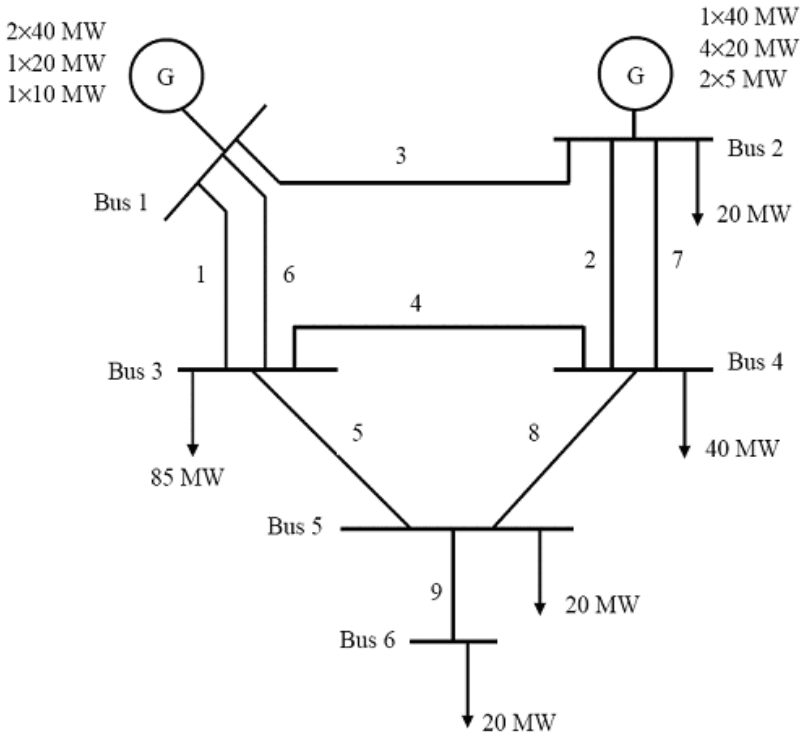


Figure 2.4: Single line diagram of the RBTS

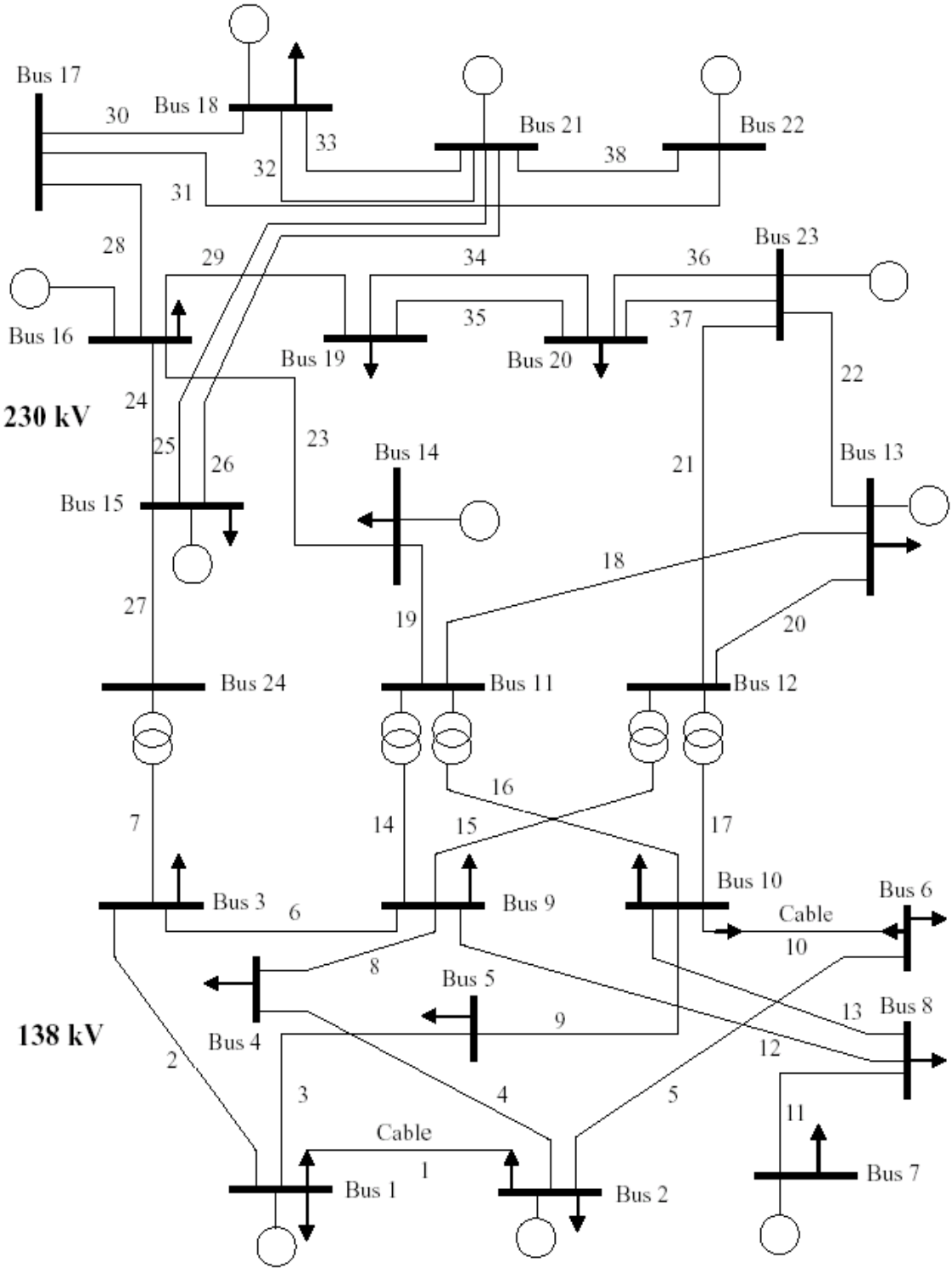


Figure 2.5: Single line diagram of the IEEE-RTS

## 2.6. Initial Studies on the RBTS and IEEE-RTS

Base case studies provide a reference framework for system modification and data sensitivity analyses. Many factors can be included in a composite system assessment, such as the derated states of generating units, common mode failures of transmission lines, station originated failures and so on. In order to clearly understand the base case results, it is important to appreciate which factors are included and which factors are not considered. The following conditions were used in the base case analyses of the RBTS and IEEE-RTS in the research described in this thesis.

- The economic priority order for load curtailment is utilized.
- The step-down transformers at transformer stations are assumed to be customer owned and the reliability indices are calculated at the high voltage bus bars.
- Station configurations are not incorporated in the evaluation process.
- Transmission line common mode failures are not considered.

The IEAR values for each load point [34] and the corresponding priority order for the RBTS load points are given in Table 2.1. The values for each load point [34] of the IEEE-RTS and the corresponding priority order are shown in Table 2.2. The number of simulation samples should be carefully selected in order to obtain meaningful reliability results. Studies conducted earlier [34] show that acceptable accuracy at HL-II can be achieved when the numbers of samples for the RBTS and the IEEE-RTS are 2,000,000 and 500,000 respectively. These sample sizes are used in the HL-II adequacy analyses described in this thesis.

Table 2.1: Bus IEAR values and priority order in the RBTS

| Bus No. | IEAR ($/kWh) | Priority Order |
|---|---|---|
| 2 | 7.41 | 1 |
| 3 | 2.69 | 5 |
| 4 | 6.78 | 2 |
| 5 | 4.82 | 3 |
| 6 | 3.63 | 4 |

Table 2.2: Bus IEAR values and priority order in the IEEE-RTS

| Bus No. | IEAR ($/kWh) | Priority Order |
|---|---|---|
| 1 | 6.20 | 1 |
| 2 | 4.89 | 9 |
| 3 | 5.30 | 8 |
| 4 | 5.62 | 3 |
| 5 | 6.11 | 2 |
| 6 | 5.50 | 4 |
| 7 | 5.41 | 5 |
| 8 | 5.40 | 6 |
| 9 | 2.30 | 16 |
| 10 | 4.14 | 10 |
| 13 | 5.39 | 7 |
| 14 | 3.41 | 14 |
| 15 | 3.01 | 15 |
| 16 | 3.54 | 13 |
| 18 | 3.75 | 11 |
| 19 | 2.29 | 17 |
| 20 | 3.64 | 12 |

The initial annual indices were calculated using a 20-step load model shown in Appendix B. The annual load point and system indices of the RBTS under these conditions are shown in Tables 2.3 and 2.4 respectively.

Table 2.3: Annual load point indices for the RBTS

| Bus No. | PLC | ENLC (1/ yr ) | ELC (MW/yr) | EDNS (MW) | EENS (MWh/yr ) |
|---|---|---|---|---|---|
| 2 | 0.00000 | 0.00000 | 0.000 | 0.00000 | 0.000 |
| 3 | 0.00014 | 0.07874 | 0.891 | 0.00143 | 12.561 |
| 4 | 0.00000 | 0.00106 | 0.006 | 0.00000 | 0.029 |
| 5 | 0.00000 | 0.00550 | 0.060 | 0.00003 | 0.293 |
| 6 | 0.00120 | 1.18219 | 15.489 | 0.01575 | 137.942 |

Table 2.4: Annual system indices for the RBTS

| Indices | Annual value |
|---|---|
| ENLC (1/yr ) | 1.257 |
| ADLC (hrs/disturbance) | 9.319 |
| EDLC (hrs/yr ) | 11.713 |
| PLC | 0.00134 |
| EDNS (MW) | 0.01722 |
| EENS (MWh/yr ) | 150.83 |
| EDC (K$/yr) | 666.65 |
| BPII (MW/MW- yr ) | 0.08890 |
| BPECI (MWh/MW- yr ) | 0.81527 |
| BPACI (MW/disturbance) | 13.09 |
| MBECI (MW/MW) | 0.00009 |
| SI (system minutes/yr ) | 48.92 |

It can be seen from Table 2.3 that the EENS values at load buses 3 and 6 are much larger than those at the other load buses. It shows that Bus 3 and 6 are the least reliable load points in the RBTS, as Bus 3 has the lowest priority and Bus 6 has the second lowest priority among all the load buses in Table 2.1. Bus 6 has the highest annual EENS because Bus 6 is connected to the rest of the system by a single radial line and is relatively far from the generating units, as shown in Figure 2.4.

The annual system and load point indices of the IEEE-RTS are shown in Tables 2.5 and 2.6 respectively.

Table 2.5: Annual system indices for the IEEE-RTS

| Indices | Annual value |
|---|---|
| ENLC (1/yr ) | 1.137 |
| ADLC (hrs/disturbance) | 11.445 |
| EDLC (hrs/year ) | 13.018 |
| PLC | 0.00149 |
| EDNS (MW) | 0.19119 |
| EENS (MWh/yr ) | 1674.80 |
| EDC (K$/yr) | 7067.65 |
| BPII (MW/MW- yr ) | 0.05347 |
| BECI (MWh/MW- yr ) | 0.58765 |
| BPACI (MW/disturbance) | 133.99 |
| MBECI (MW/MW) | 0.00007 |
| SI (system minutes/yr ) | 35.26 |

Table 2.6: Annual load point indices for the IEEE-RTS

| Bus No. | PLC | ENLC (1/yr ) | ELC (MW/yr) | EDNS (MW) | EENS (MWh/yr ) |
|---|---|---|---|---|---|
| 1 | 0.00000 | 0.00000 | 0.000 | 0.00000 | 0.000 |
| 2 | 0.00000 | 0.00080 | 0.024 | 0.00002 | 0.192 |
| 3 | 0.00000 | 0.00035 | 0.013 | 0.00001 | 0.099 |
| 4 | 0.00000 | 0.00000 | 0.000 | 0.00000 | 0.000 |
| 5 | 0.00000 | 0.00000 | 0.000 | 0.00000 | 0.000 |
| 6 | 0.00000 | 0.00075 | 0.055 | 0.00004 | 0.310 |
| 7 | 0.00000 | 0.00041 | 0.003 | 0.00000 | 0.015 |
| 8 | 0.00000 | 0.00002 | 0.000 | 0.00000 | 0.001 |
| 9 | 0.00083 | 0.65554 | 38.777 | 0.04890 | 428.392 |
| 10 | 0.00000 | 0.00321 | 0.161 | 0.00016 | 1.359 |
| 13 | 0.00000 | 0.00005 | 0.001 | 0.00000 | 0.010 |
| 14 | 0.00014 | 0.12319 | 7.366 | 0.00848 | 74.290 |
| 15 | 0.00047 | 0.37877 | 31.499 | 0.03795 | 332.480 |
| 16 | 0.00007 | 0.05775 | 2.076 | 0.00231 | 20.248 |
| 18 | 0.00002 | 0.02078 | 1.502 | 0.00156 | 13.661 |
| 19 | 0.00149 | 1.13619 | 69.293 | 0.08997 | 788.151 |
| 20 | 0.00004 | 0.03772 | 1.633 | 0.00178 | 15.590 |

Table 2.6 illustrates that the EENS at load buses 9, 14, 15 and 19 are larger than those at the other buses in the IEEE-RTS. These four buses have the four lowest priorities, as shown in Table 2.2.

It can be also seen from Tables 2.3 and 2.5 that the indices of the load points with low priority order are higher than at other load points, which indicates that the individual load point indices are highly dependent on the load curtailment priority order.

## 2.7. Summary

This chapter briefly describes some basic concepts and evaluation techniques utilized in HL-I and HL-II analyses. The basic indices used in generating system reliability evaluation are briefly introduced in this chapter, followed by the basic indices used in bulk power systems.

Adequacy at these two hierarchical levels can be assessed either by analytical techniques or by Monte Carlo simulation methods. Three basic Monte Carlo simulation techniques designated as

state sampling, state transition sampling and sequential analysis are introduced in this chapter. Each approach has its own advantages and disadvantages. The MECORE program is based on the state sampling approach and is designed to conduct reliability and reliability worth assessments of composite systems. Its capabilities are briefly presented in this chapter. The basic adequacy indices provided by the MECORE program are presented. These indices can be used to measure the reliability at an individual load bus or for the entire system. The MECORE program has been utilized in the research described in this thesis to conduct bulk system adequacy studies.

Two composite test systems known as the RBTS and the IEEE-RTS are used in this research. The RBTS is a small system designed for education and research purposes. The IEEE-RTS is relatively large compared to the RBTS. The annual indices for the original RBTS and IEEE-RTS are given in this chapter. These results provide a base case reference for the system conditions covered in subsequent chapters.

# 3. Bulk System Adequacy Assessment Incorporating Load Forecast Uncertainty

## 3.1. Introduction

Load forecast uncertainty always exists in an actual power system as power utilities have to face a wide range of financial, societal and environmental uncertainties. Load forecast uncertainty is relatively small for short lead times but can be quite significant when looking further into the future. Load forecast uncertainty, therefore, is an extremely important parameter in electric power system reliability evaluation, planning and operating.

A number of papers [35-41] discuss the risk or impact due to load forecast uncertainty. References 9, 38 and 39 show that load forecast uncertainty can have a significant effect on the calculated reliability indices in a generating capacity study. The effects of system and bus load uncertainty in composite system adequacy assessment are examined using the sequential Monte Carlo simulation technique in [40]. Reference 41 investigates the impacts of bus load uncertainty and correlation at HL-II using a state sampling technique. There has been relatively little additional work on incorporating system load forecast uncertainty in bulk system adequacy assessment using a state sampling Monte Carlo simulation technique, such as that applied in MECORE.

One of the main objectives in incorporating load forecast uncertainty is to take into account the inherent probability that the system load differs from the expected forecast value. This chapter describes two methods that can be used to include the effects of load forecast uncertainty in the reliability assessment of power systems. Development and utilization of appropriate load models incorporating overall system load forecast uncertainty in generating system and bulk system adequacy assessment are presented and examined in this chapter using the RBTS and the IEEE-RTS.

## 3.2. Methods for Considering Load Forecast Uncertainty in Power System Adequacy Assessment

### 3.2.1. Basic Methods for Incorporating Load Forecast Uncertainty

The uncertainty in load forecasting can be included in a reliability evaluation using two basic methods.

***Method 1***

Published data suggests that the load forecast uncertainty can be reasonably described by a normal distribution. The distribution mean is the forecast peak load. The distribution can be divided into a discrete number of class intervals in which the load representing the class interval mid-point is assigned the designated probability for that class interval. It has been found that there is relatively little difference in the end result between representing the distribution of load forecast uncertainty by seven steps or forty-nine steps [9]. The normal distribution divided into seven steps is, therefore, used in the studies described in this thesis. Figure 3.1 shows a seven-step approximation of the normal distribution. The class interval probabilities in this figure are 0.006 (±3), 0.061(±2), 0.242(±1) and 0.382(0) respectively.

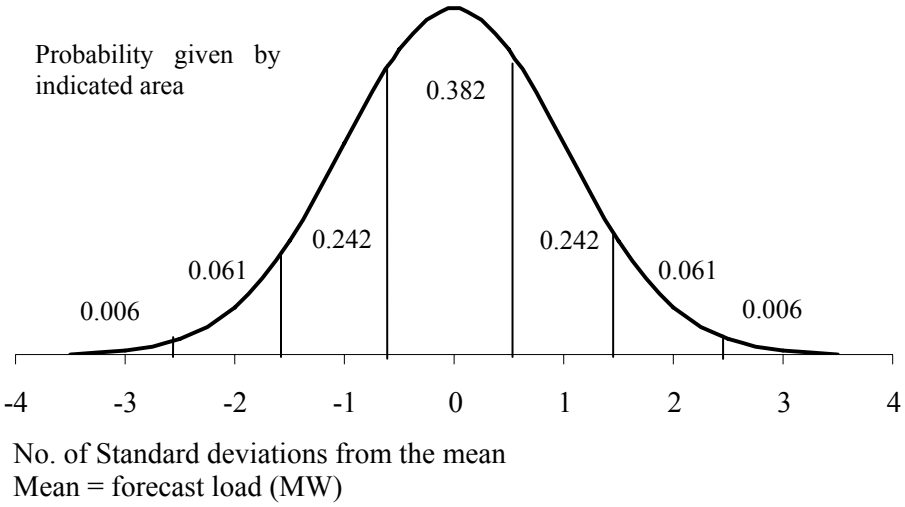


Figure 3.1: Seven-step approximation of the normal distribution

The reliability index for each peak load level represented by the class interval is calculated. The seven individual values are then weighted by the probability of existence of that peak load level. The final system reliability index is the expected value for the forecast peak load.

***Method 2***

The reliability indices including uncertainty can be found using a different approach. The system load duration curve in this case is modified to produce a load profile which includes uncertainty. If uncertainty is fixed at some specified value and the load shape remains unchanged, considerable saving in computer time can be achieved by using the modified load duration curve as input data in a range of studies [9]. The modified load duration curve is obtained using a group of conditional load shape segments. The procedure used to modify the load duration curve is briefly illustrated as follows:

Step 1. Determine the number of conditional load shapes. This is the number of discrete class intervals of a probability distribution as shown in Figure 3.1. Each forecast load is represented by the class interval mid-value.

Step 2. The conditional load shapes represent the set of conditional load duration curves (LDC), each with a probability of existence.

Step 3. Calculate the expected time segment corresponding to each load level to determine the time-duration values in the conditional load shapes.

Step 4. Create the modified load duration curve using the time-duration values and the step load levels in the condition load duration curves. The modified load duration curve is now composed of a group of conditional segments.

A detailed description of *Method 2* is illustrated in [9]. The modified load duration curve can be represented in *MW* of peak load or expressed in percentage or per-unit of the forecast peak load. It can also be utilized with any load forecast peak assuming the basic characteristic and on the condition that the uncertainty remains constant. The definition of conditional load curves to obtain a modified curve can be quite useful in conducting a wide range of studies on composite system reliability indices with considerable savings in computer time [9].

### 3.2.2. Application of the Two Basic LFU Methods

This section describes the application of the described procedures to obtain reliability indices which include uncertainty using the two basic approaches. The RBTS generating capacity is used to illustrate the methods. The system forecast peak load is 185 MW with uncertainty as shown by the seven discrete class interval model in Figure 3.1. The system LOLE is calculated assuming that the standard deviation describing the uncertainty is 2% of the forecast peak load. The analytical technique and MECORE are used to examine the effect of load forecast uncertainty on the system reliability indices.

**Application of *Method 1***

In this method, the system LOLE is calculated for each peak load level. The seven individual values are then weighted by the probability of that peak load level. The final LOLE is the expected value of the seven weighted LOLE. The LOLE for the RBTS with and without considering load uncertainty (LFU) are shown in Table 3.1 using an analytical method. The LOLE values are calculated using a Capacity Outage Probability Table [9] and using the RBTS generating system data shown in Appendix A and the 20-step load model shown in Appendix B.

Table 3.1: The LOLE (hrs/yr) for the RBTS with and without LFU obtained using the analytical technique

| Peak Load (MW) | 165 | 175 | 185 | 195 | 205 |
|---|---|---|---|---|---|
| Without load uncertainty | 0.1671 | 0.5689 | 1.1655 | 2.8974 | 6.4834 |
| With load uncertainty (*Method 1*) | 0.1839 | 0.5882 | 1.2622 | 3.0258 | 7.0240 |

Table 3.1 shows that the HL-I system LOEE values for a peak load of 185 MW using the analytical method is 1.1655 hrs/yr. The transmission elements of the system are considered to be 100% reliable when the MECORE program is used for an HL-I study. This is accomplished by inputting zero values for the transmission element unavailabilities. Reference 29 notes that acceptable accuracy at HL-II can be achieved when the number of samples for the RBTS is 2,000,000. As noted in Chapter 2, this sample size is used in the HL-II adequacy analyses described in this thesis. This sample size is also used in the RBTS generating capacity studies to retain consistency. The system LOLE obtained using MECORE with and without LFU and the sample size of 2,000,000 are given in Table 3.2.

Table 3.2: The LOLE (hrs/yr) for the RBTS with and without LFU obtained using MECORE

| Peak Load (MW) | 165 | 175 | 185 | 195 | 205 |
|---|---|---|---|---|---|
| Without load uncertainty | 0.1728 | 0.6273 | 1.1756 | 2.9077 | 7.1314 |
| With load uncertainty (*Method 1*) | 0.1866 | 0.6351 | 1.2735 | 3.0222 | 7.4277 |

Tables 3.1 and 3.2 show that the LOLE values increase when the load forecast uncertainty is considered. This is a general conclusion documented in many publications [1-8]. The number of samples utilized in MECORE is the reason that causes the difference of the system LOLE between obtained using the state sampling technique and using the analytical method.

**Application of *Method 2***

The 20-step load model shown in Figure 3.2 is modified in *Method 2*. There are seven conditional load duration curves as the seven-step distribution of load forecast uncertainty is utilized in this thesis. In the case of a system forecast peak load of 185 MW, the peak loads of the conditional LDC vary from to173.9 MW to 196.1 MW in increments of 3.7 MW. When the peak loads of the conditional LDC are expressed in per-unit of the forecast peak load, they change from 0.94 to 1.06 with a step value of 0.02.

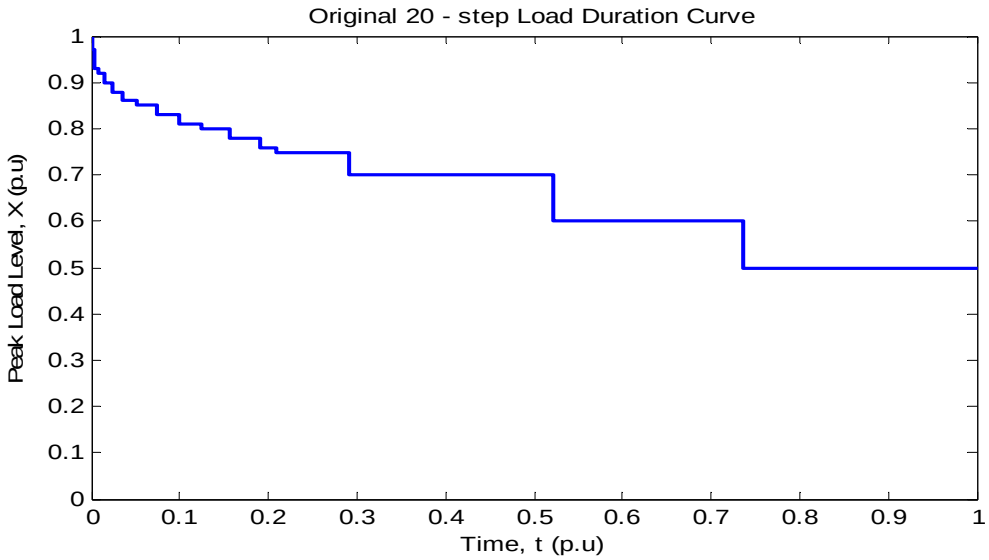


Figure 3.2: The original 20-step load duration curve

The modified load duration curve is shown in Figure 3.3. The number of stepped load levels in Figure 3.3 is 140.

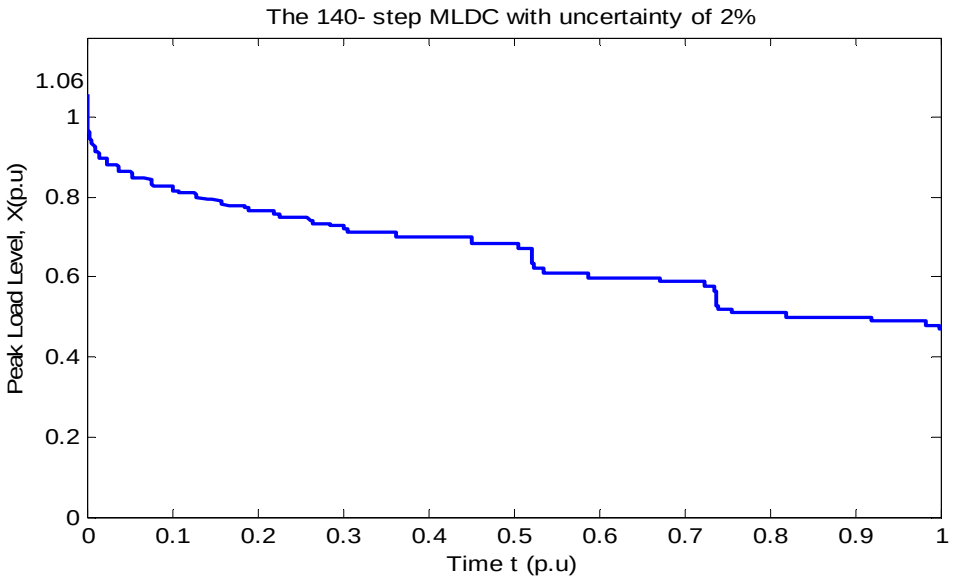

Figure 3.3: The 140-step MLDC with uncertainty of 2%

In order to demonstrate the process, the five time segments of the 140 total segments are illustrated in the following:

Segment 1 at the Peak Level of $X_1$=1.06 p.u.

The time segment $t_{S1}$= 1.3800e-006 for 1.0494≤X≤1.06

Segment 30 at the Peak Level of $X_{30}$=0.9504 p.u.

The time segment $t_{S30}$= 0.0041 for 0.949≤X≤0.9504

Segment 70 at the Peak Level of $X_{30}$=0.8601 p.u.

The time segment $t_{S70}$=0.0545 for 0.8480≤X≤0.8601

Segment 110 at the Peak Level of $X_{110}$=0.75 p.u.

The time segment $t_{S110}$=0.2261 for 0.75≤X≤0.752

Segment 140 at the Peak Level of $X_{140}$=0.47 p.u.

The time segment $t_{S140}$=1 for 0<X<0.47

The LOLE for the RBTS obtained using the modified LDC (MLDC) shown in Figure 3.3 and the analytical method are shown in Table 3.3. The RBTS LOLE without considering LFU are listed in Table 3.3 for comparison purposes.

Table 3.3: The LOLE (hrs/yr) for the RBTS with and without LFU obtained using the analytical technique

| Peak Load (MW) | 165 | 175 | 185 | 195 | 205 |
|---|---|---|---|---|---|
| Without load uncertainty | 0.1671 | 0.5689 | 1.1655 | 2.8974 | 6.4834 |
| With load uncertainty (*Method 2*) | 0.1839 | 0.5882 | 1.2622 | 3.0258 | 7.0240 |

A comparison of the LOLE shown in Tables 3.1 and 3.3 indicates that when using the analytical method, *Method 1* and *Method 2* provide the same system LOLE values.

The modified load duration curve shown in Figure 3.3 can be used as input data in a range of repetitive studies, with considerable savings in computer time. The MECORE software, however, only can handle up to 100 step-load levels in a multi-step load duration curve model. This capability limits the application of the *Method 2* in the reliability evaluation of composite systems. In order to use the modified load duration model as input data to MECORE, it is necessary to reduce the final model to one containing 100 or less step-load levels. This involves creating an approximate model which will reduce the accuracy associated with the analysis.

### 3.2.3. Approximate Modified LFU Analysis Methods

As noted above, a load duration curve with 100 or less step - load levels can be used in the MECORE program. The 140-step modified load duration curve (MLDC) shown in Figure 3.3 cannot be directly used in MECORE to analyze the impact on the system reliability indices of load forecast uncertainty. The 140-step LDC is used as the base load model in this study and two approximate approaches are applied to reduce the original 140 load levels in order to provide relatively satisfactory results. The two approaches are designated as *Method 2A* and *Method 2B*.

**Application of *Method 2A* to Reduce the 140-step MLDC**

Table 3.3 shows that the RBTS LOLE for the peak load of 185 MW is 1.2622 hrs/yr when LFU of 2% is considered. Each load level probability and LOLE value for the 140-step MLDC obtained using the analytical method are listed in Table 3.4. The load levels are in per unit of the annual peak load.

Table 3.4: Load level LOLE (hrs/yr) values for the 140-step MLDC for a peak load of 185 MW

| Load Level | Level Prob. | Level LOLE | Load Level | Level Prob. | Level LOLE | Load Level | Level Prob. | Level LOLE |
|---|---|---|---|---|---|---|---|---|
| *1.0600* | 0.00000138 | 0.00014 | *0.9900* | 0.00004202 | 0.00307 | *0.8986* | 0.00279026 | 0.05563 |
| *1.0494* | 0.00000066 | 0.00006 | *0.9879* | 0.00001986 | 0.00145 | *0.8986* | 0.00098210 | 0.01958 |
| *1.0420* | 0.00000342 | 0.00029 | *0.9870* | 0.00010431 | 0.00762 | *0.8980* | 0.00370540 | 0.07387 |
| *1.0400* | 0.00001403 | 0.00120 | *0.9853* | 0.00041382 | 0.03024 | *0.8978* | 0.00014178 | 0.00283 |
| *1.0296* | 0.00000671 | 0.00058 | *0.9830* | 0.00021774 | 0.01591 | *0.8967* | 0.00149072 | 0.02972 |
| *1.0240* | 0.00001026 | 0.00075 | *0.9800* | 0.00005566 | 0.00407 | *0.8947* | 0.00020191 | 0.00403 |
| *1.0223* | 0.00003477 | 0.00255 | *0.9702* | 0.00002662 | 0.00059 | *0.8921* | 0.00001026 | 0.00020 |
| *1.0200* | 0.00005566 | 0.00408 | *0.9699* | 0.00003696 | 0.00081 | *0.8813* | 0.00389620 | 0.07760 |
| *1.0098* | 0.00002662 | 0.00195 | *0.9693* | 0.00020191 | 0.00445 | *0.8810* | 0.00440446 | 0.08772 |
| *1.0059* | 0.00001026 | 0.00075 | *0.9680* | 0.00041382 | 0.00911 | *0.8809* | 0.00144143 | 0.02871 |
| *1.0046* | 0.00010431 | 0.00765 | *0.9660* | 0.00065322 | 0.01438 | *0.8800* | 0.00234740 | 0.04675 |
| *1.0027* | 0.00013794 | 0.01011 | *0.9633* | 0.00013794 | 0.00304 | *0.8798* | 0.00015276 | 0.00304 |
| *1.0000* | 0.00008786 | 0.00642 | *0.9600* | 0.00001403 | 0.00031 | *0.8784* | 0.00037576 | 0.00748 |
| | | | *0.9519* | 0.00005820 | 0.00128 | *0.8761* | 0.00001986 | 0.00040 |
| | | | *0.9516* | 0.00037576 | 0.00827 | *0.8640* | 0.00615020 | 0.01465 |
| | | | *0.9506* | 0.00080102 | 0.01763 | *0.8639* | 0.00571846 | 0.01362 |
| | | | *0.9504* | 0.00000671 | 0.00015 | *0.8634* | 0.00279026 | 0.00665 |
| | | | *0.9490* | 0.00065322 | 0.01438 | *0.8632* | 0.00155306 | 0.00370 |
| | | | *0.9467* | 0.00041382 | 0.00911 | *0.8621* | 0.00059170 | 0.00141 |
| | | | *0.9437* | 0.00003477 | 0.00073 | *0.8618* | 0.00014316 | 0.00034 |
| | | | *0.9400* | 0.00000138 | 0.00003 | *0.8601* | 0.00003696 | 0.00009 |
| | | | *0.9339* | 0.00059170 | 0.01242 | *0.8480* | 0.00019866 | 0.00047 |
| | | | *0.9339* | 0.00006918 | 0.00145 | *0.8470* | 0.00902666 | 0.02151 |
| | | | *0.9333* | 0.00149072 | 0.03128 | *0.8467* | 0.00389620 | 0.00928 |
| | | | *0.9320* | 0.00126442 | 0.02653 | *0.8466* | 0.00616132 | 0.01468 |
| | | | *0.9306* | 0.00000066 | 0.00001 | *0.8458* | 0.00070333 | 0.00168 |
| | | | *0.9300* | 0.00041382 | 0.00868 | *0.8455* | 0.00145546 | 0.00347 |
| | | | *0.9274* | 0.00010431 | 0.00219 | *0.8441* | 0.00005820 | 0.00014 |
| | | | *0.9240* | 0.00000342 | 0.00007 | *0.8320* | 0.00201971 | 0.00410 |
| | | | *0.9162* | 0.00070333 | 0.01402 | *0.8301* | 0.00571846 | 0.01160 |
| | | | *0.9160* | 0.00234740 | 0.04680 | *0.8300* | 0.00972572 | 0.01973 |
| | | | *0.9158* | 0.00009660 | 0.00193 | *0.8294* | 0.00098210 | 0.00199 |
| | | | *0.9150* | 0.00235312 | 0.04691 | *0.8293* | 0.00577412 | 0.01171 |
| | | | *0.9134* | 0.00080102 | 0.01597 | *0.8281* | 0.00006918 | 0.00014 |
| | | | *0.9110* | 0.00010431 | 0.00208 | *0.8268* | 0.00020754 | 0.00042 |
| | | | *0.9080* | 0.00001026 | 0.00020 | *0.8160* | 0.00801262 | 0.01625 |
| | | | | | | *0.8134* | 0.00616132 | 0.01250 |
| | | | | | | *0.8131* | 0.00144143 | 0.00292 |
| | | | | | | *0.8130* | 0.00911452 | 0.01849 |
| | | | | | | *0.8122* | 0.00009660 | 0.00020 |
| | | | | | | *0.8112* | 0.00210999 | 0.00428 |
| | | | | | | *0.8056* | 0.00009792 | 0.00016 |
| | | | | | | *0.8000* | 0.01264802 | 0.02111 |

(Continue Table 3.4)

| Load Level | Level Prob. | Level LOLE | Load Level | Level Prob. | Level LOLE | Load Level | Level Prob. | Level LOLE |
|---|---|---|---|---|---|---|---|---|
| *0.7968* | 0.00155306 | 0.00259 | *0.6860* | 0.05605204 | 0.01165 | *0.5880* | 0.05215826 | 0.00072 |
| *0.7967* | 0.00577412 | 0.00964 | *0.6720* | 0.01412882 | 0.00293 | *0.5760* | 0.01314733 | 0.00018 |
| *0.7962* | 0.00014178 | 0.00024 | *0.6580* | 0.00138972 | 0.00029 | *0.5640* | 0.00129318 | 0.00002 |
| *0.7956* | 0.00837078 | 0.01397 | *0.6360* | 0.00129318 | 0.00003 | *0.5300* | 0.00157536 | 0.00000 |
| *0.7950* | 0.00049314 | 0.00082 | *0.6240* | 0.01314733 | 0.00028 | *0.5200* | 0.01601616 | 0.00002 |
| *0.7904* | 0.00099552 | 0.00166 | *0.6120* | 0.05215826 | 0.00092 | *0.5100* | 0.06353952 | 0.00005 |
| *0.7840* | 0.00801262 | 0.01337 | *0.6000* | 0.08233246 | 0.00146 | *0.5000* | 0.10029792 | 0.00007 |
| *0.7805* | 0.00145546 | 0.00242 | | | | | | |
| *0.7802* | 0.00015276 | 0.00025 | | | | **Load Level** | **Level Prob.** | **Level LOLE** |
| *0.7800* | 0.01321338 | 0.02195 | | | | | | |
| *0.7800* | 0.00501359 | 0.00833 | | | | *0.4900* | 0.06353952 | 0.00005 |
| *0.7752* | 0.00394944 | 0.00656 | | | | *0.4800* | 0.01601616 | 0.00001 |
| *0.7680* | 0.00201971 | 0.00336 | | | | *0.4700* | 0.00157536 | 0.00000 |
| *0.7650* | 0.01988998 | 0.03305 | | | | | | |
| *0.7644* | 0.00837078 | 0.01391 | | | | | | |
| *0.7642* | 0.00014316 | 0.00024 | | | | | | |
| *0.7600* | 0.00623424 | 0.01036 | | | | | | |
| *0.7520* | 0.00019866 | 0.00005 | | | | | | |
| *0.7500* | 0.03139658 | 0.00831 | | | | | | |
| *0.7488* | 0.00210999 | 0.00056 | | | | | | |
| *0.7448* | 0.00394944 | 0.00105 | | | | | | |
| *0.7420* | 0.00138972 | 0.00037 | | | | | | |
| *0.7350* | 0.01988998 | 0.00527 | | | | | | |
| *0.7332* | 0.00020754 | 0.00005 | | | | | | |
| *0.7296* | 0.00099552 | 0.00024 | | | | | | |
| *0.7280* | 0.01412882 | 0.00334 | | | | | | |
| *0.7200* | 0.00501359 | 0.00119 | | | | | | |
| *0.7144* | 0.00009792 | 0.00002 | | | | | | |
| *0.7140* | 0.05605204 | 0.01326 | | | | | | |
| *0.7050* | 0.00049314 | 0.00012 | | | | | | |
| *0.7000* | 0.08847884 | 0.01840 | | | | | | |

It can be seen from Table 3.4 that the lower load level steps make relatively small contributions to the system LOLE although these level probabilities are relatively high. The probabilities of relatively high load level steps are less than 0.00001. The following procedure is used to reduce the 140-step MLDC in *Method 2A*.

Step 1. The 140-step MLDC is divided into several class intervals based on the load level p.u value.

Class interval 1: maximum load level $\geq$ load level $\geq 1.0$
Class interval 2: $1.0 >$ load level $\geq 0.9$
Class interval 3: $0.9 >$ load level $\geq 0.8$

Class interval 4: $0.8 > \text{load level} \geq 0.7$
Class interval 5: $0.7 > \text{load level} \geq 0.6$
Class interval 6: $0.6 > \text{load level} \geq 0.5$
Class interval 7: $0.5 > \text{load level} \geq \text{minimum load level}$

Step 2. The load level probability for each class interval except Class interval 7 is given based on the fact that lower levels have larger given load level probabilities. These given load level probabilities are shown in Table 3.5. It should be note that the selection of the class interval load level probability values can be varied for different load profiles if considered necessary.

Table 3.5: Given load level probability for each class interval

| Class interval | Given load level probability |
|---|---|
| 1 | 0.00001 |
| 2 | 0.0001 |
| 3 | 0.002 |
| 4 | 0.01 |
| 5 | 0.01 |
| 6 | 0.1 |
| 7 | n/a |

Step 3. Each individual load level probability is compared with the corresponding given class interval load level probability shown in Table 3.5. If the probability of a load level is greater than or equal to the corresponding given class interval load level probability, it is considered to be a retained load level. If the probability of a load level is less than the given load level probability, this load level is removed and the corresponding load level probability is added to an upper retained load level. It should be note that the maximum load level is always kept as the new load model first load level and the probability of the last load level is the summation of all load level probabilities in the last class interval.

An example is used to illustrate the application of the procedure in *Method 2A* and shown in Table 3.6. The selected load level is in Class interval 2 with a given load level probability of 0.0001.

Table 3.6: An example of reducing load levels in *Method 2A* (In Class interval 2)

| Load Level (p.u) | Level Probability | → | New Load Level (p.u) | New Level Probability |
|---|---|---|---|---|
| 0.9830 | 0.00021774 | | 0.9830 | 0.00033698 |
| 0.9800 | 0.00005566 | | | |
| 0.9702 | 0.00002662 | | 0.9693 | 0.00020191 |
| 0.9699 | 0.00003696 | | | |
| 0.9693 | 0.00020191 | | | |

The 140-step MLDC with uncertainty of 2% shown in Figure 3.3 is reduced to a 64-step load model using *Method 2A*. The reduced 64-step MLDC is shown in Figure 3.4 and designated as the 64-step RMLDC.

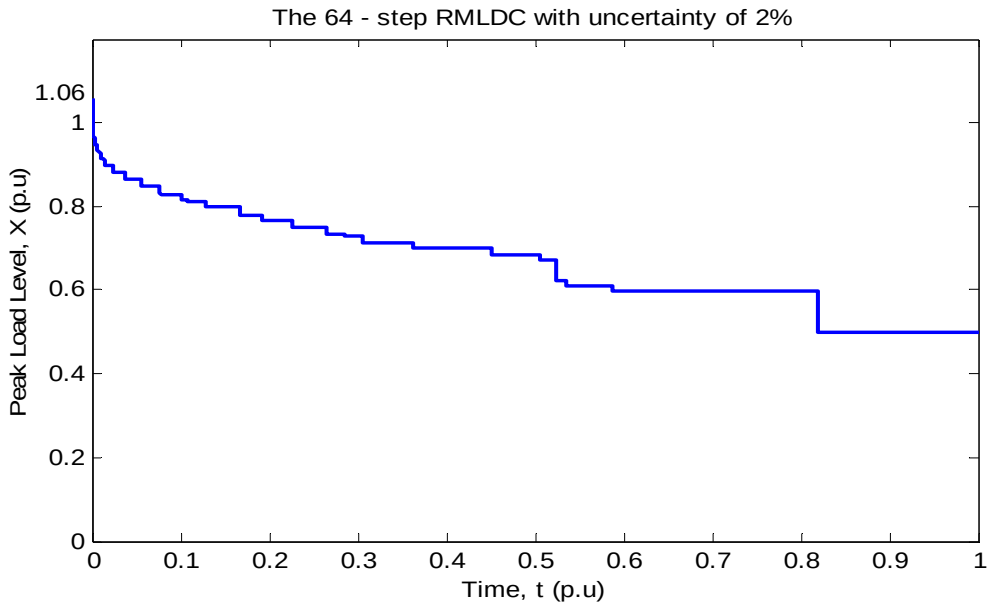


Figure 3.4: The reduced 64-step MLDC (RMLDC) with uncertainty of 2% using *Method 2A*

The RBTS LOLE results for varying peak load obtained using the 64-step RMLDC are shown in Table 3.7. The percentage values listed in this table are the differences between the results obtained using the 140-step MLDC and the 64-step RMLDC. It can be seen from Table 3.7 that there is relatively little difference in the system LOLE values for using the two load models. The key to producing an acceptable reduced LDC is to retain a large number of steps in the high risk portion of the original LDC.

Table 3.7: The system LOLE (hrs/yr) for the RBTS obtained using the multi-step load models with uncertainty of 2%

| Peak Load (MW) | The 140-step MLDC | The 64-step RMLDC | Difference |
|---|---|---|---|
| 165 | 0.1839 | 0.1855 | 0.87 % |
| 175 | 0.5882 | 0.5896 | 0.24 % |
| 185 | 1.2622 | 1.2677 | 0.44 % |
| 195 | 3.0258 | 3.0348 | 0.30 % |
| 205 | 7.0240 | 7.1112 | 1.24 % |

*Method 2A* was also studied assuming that the standard deviation describing the uncertainty is 5% of the peak load. The 140-step MLDC with uncertainty of 5% is shown in Figure 3.5. This load model was reduced to a 73-step RMLDC and shown in Figure 3.6.

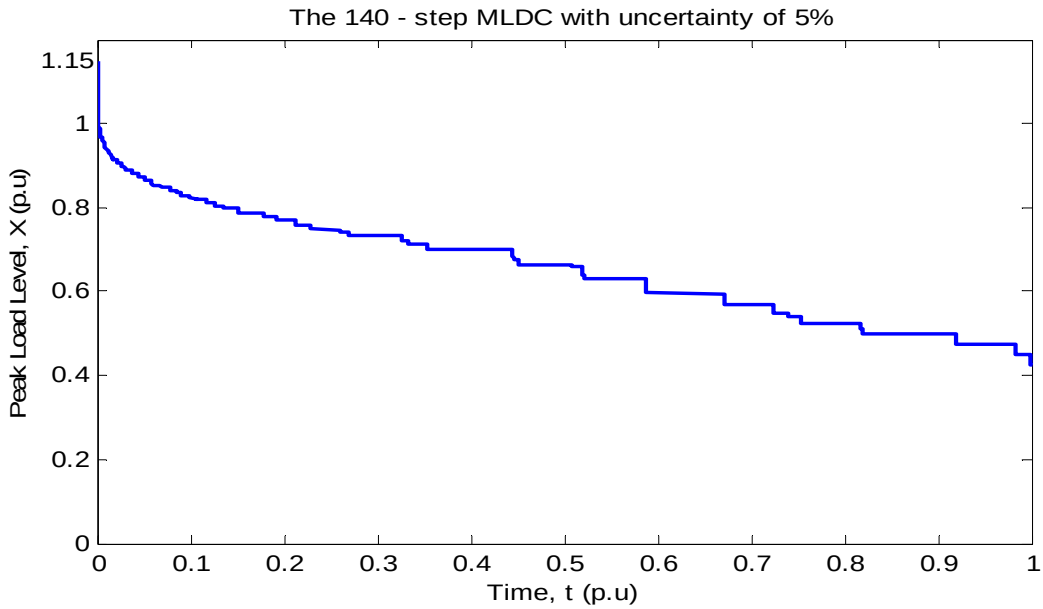


Figure 3.5: The 140-step MLDC with uncertainty of 5%

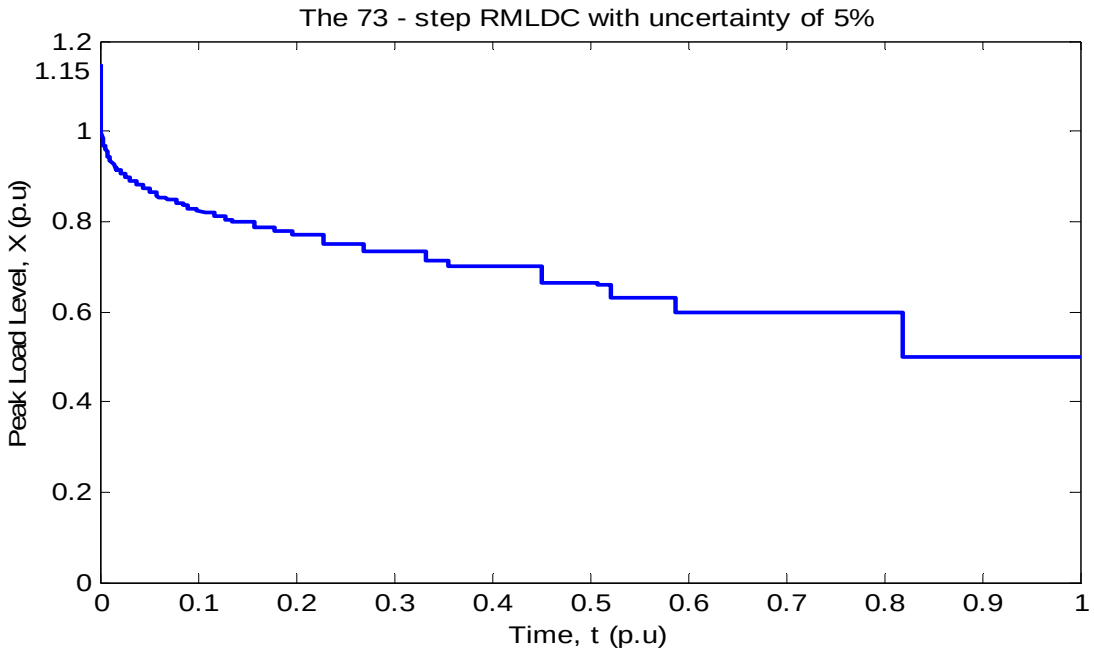


Figure 3.6: The 73-step RMLDC with uncertainty of 5% obtained using *Method 2A*

The system LOLE for the RBTS generating system calculated using the analytical method when the standard deviation is 5% are shown in Table 3.8. The percentage difference between the results obtained using the 140-step MLDC and the 73-step RMLDC are also listed in this table.

Table 3.8: The RBTS LOLE (hrs/yr) with considering load uncertainty standard deviation of 5%

| Peak Load (MW) | The 140-step MLDC | The 73-step RMLDC | Difference |
|---|---|---|---|
| 165 | 0.2631 | 0.2647 | 0.61 % |
| 175 | 0.7210 | 0.7271 | 0.85 % |
| 185 | 1.7338 | 1.7365 | 0.16 % |
| 195 | 4.0570 | 4.0680 | 0.27 % |
| 205 | 9.2549 | 9.2997 | 0.48 % |

Table 3.8 shows that there is very small impact on the system LOLE values due to reducing the number of load levels from 140 to 73. Tables 3.7 and 3.8 indicate that it is acceptable to use *Method 2A* to reduce the modified load duration curve created by incorporating load forecast uncertainty.

**Application of *Method 2B* to reduce the 140-step MLDC**

There are three steps in *Method 2B* to reduce a MLDC. The first two steps, that is, dividing the MLDC into several class intervals based on the load level p.u values and the given load level probability for each class interval, are the same as those used in *Method 2A.*

In Step 3 of *Method 2B*, if the probability of a load level is greater than or equal to the corresponding given class interval load level probability, it is considered as a retained load level. If the probability of a load level is less than the given load level probability, then further following load level probabilities are examined until a probability greater than the given value is found. The retained load level is the weighted mean of these load levels and its corresponding probability is the summation of the applied load level probabilities. Table 3.9 illustrates the weighted mean approach used in Step 3.

Table 3.9: An example of using the weight mean method in Step 3 (In Class interval 2)

| Load Level (p.u) | Level Probability | | New Load Level (p.u) | New Level Probability |
|---|---|---|---|---|
| 0.9830 | 0.00021774 | → | 0.9830 | 0.00021774 |
| 0.9800 | 0.00005566 | | 0.9747 | 0.00011924 |
| 0.9702 | 0.00002662 | | | |
| 0.9699 | 0.00003696 | | | |
| 0.9693 | 0.00020191 | | 0.9693 | 0.00020191 |

The 140-step MLDC with uncertainty of 2% shown in Figure 3.3 was reduced using *Method 2B* to a 96- step load model and shown in Figure 3.7.

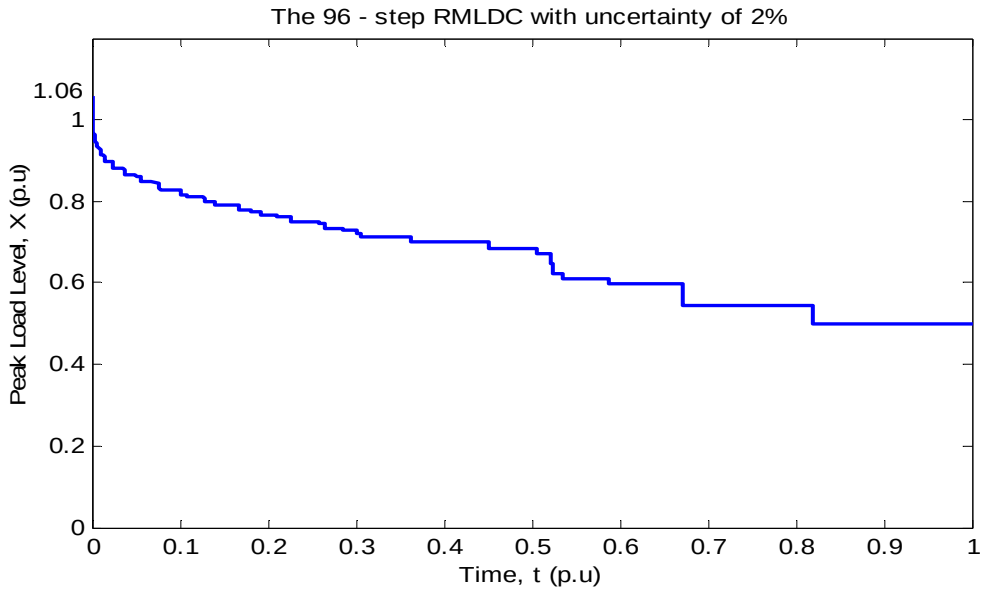


Figure 3.7: The 96-step RMLDC with uncertainty of 2% obtained using *Method 2B*

The 140-step MLDC with uncertainty of 5 % shown in Figure 3.5 was reduced using *Method 2B* to a 101- step load model and is shown in Figure 3.8.

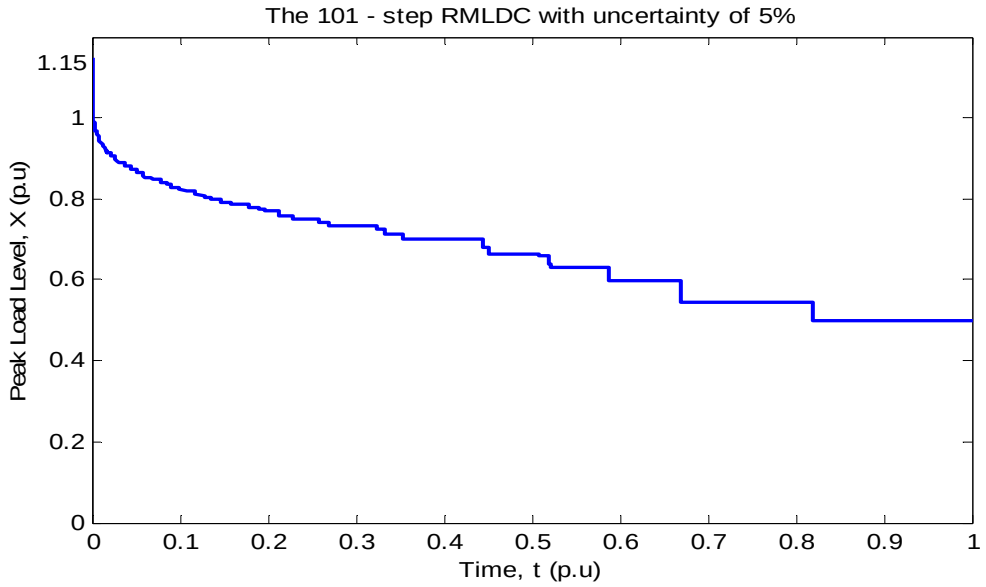


Figure 3.8: The 101-step RMLDC with uncertainty of 5% obtained using *Method 2B*

The RBTS LOLE for the peak load of 185 MW obtained using the 96-step RMLDC with uncertainty of 2% is 1.2665 hrs/yr. The system LOLE calculated using the 140-step MLDC and

the two reduced load profiles are shown in Table 3.10. The percentage values in Table 3.10 are the differences between using the reduced and the 140-step MLDC.

Table 3.10: Comparison of the system LOLE for peak load of 185 MW obtained using the different load models (uncertainty of 2%)

| Load Model | LOLE (hrs/yr) | Difference |
|---|---|---|
| The 140-step MLDC | 1.2622 | / |
| The 64-step RMLDC (*Method 2A*) | 1.2677 | 0.44 % |
| The 96-step RMLDC (*Method 2B*) | 1.2665 | 0.34 % |

The number steps in the RMLDC obtained using *Method 2A* is less than that obtained using *Method 2B*. The two methods used to reduce the number of load levels provide similar LOLE results for the RBTS. Similar studies were conducted considering uncertainty of 5% and the system LOLE results for a peak load of 185 MW are shown in Table 3.11.

Table 3.11: Comparison of the system LOLE for peak load of 185 MW obtained using the different load models (uncertainty of 5%)

| Load Model | LOLE (hrs/yr) | Difference |
|---|---|---|
| The 140-step MLDC | 1.7338 | / |
| The 73-step RMLDC (*Method 2A*) | 1.7365 | 0.16 % |
| The 101-step RMLDC (*Method 2B*) | 1.7347 | 0.05 % |

Table 3.11 indicates that using the 101-step RMLDC provides similar LOLE to that obtained using the 73-step RMLDC, and has 28 more steps than the 73-step RMLDC, which means more computing time is required in MECORE. As noted in Section 3.2.2, the MECORE software as currently formatted can only handle up to 100 step-load levels in a multi-step load duration curve model. The RMLDC obtained using *Method 2B*, therefore, cannot be used in MECORE as the step number exceeds the load level limit.

The remaining studies in this chapter were conducted using the load models developed using *Method 2A*. The results listed in Tables 3.7, 3.8, 3.10 and 3.11 indicate that *Method 2A* can be used to reduce the number of step in a multi-step load duration curve and provide acceptable system reliability indices.

### 3.3. Effect of Load Forecast Uncertainty on Bulk System Adequacy Assessment

This section illustrates the application of *Method 1* presented in Section 3.2.1 and *Method 2A* described in Section 3.2.3 to examining the effects of load forecast uncertainty in the reliability assessment of a bulk system. Two standard deviations of *2%* and *5%* of the forecast peak load are considered. The MEOCRE program was used to conduct the studies on the RBTS and IEEE-RTS composite systems. The system EENS, which is one of the most common indices in bulk system reliability assessment, is used as the basic reliability index in this study.

In applying *Method 1* in these studies, the uncertainty in each forecast peak load is assumed to be represented by the seven-step probability distribution shown in Figure 3.1. The MECORE software was therefore run seven times in each study, to produce seven sets of reliability indices. Each individual set of indices was weighted by their probabilities of existence. The final system indices are expected values of a group of expected indices. In applying *Method 2A*, the 64-step RMLDC for 2% load standard deviation shown in Figure 3.4 and the 73-step for 5% load standard deviation shown in Figure 3.6 are used directly in MECORE.

#### 3.3.1. The RBTS System Studies

The adequacy of the RBTS with load forecast uncertainty is evaluated assuming that the system forecast peak load is increased from 165 MW to 205 MW in steps of 10 MW. Tables 3.12 and 3.13 show the system EENS including load forecast uncertainty using *Method 1* and *Method 2A* respectively. It requires about 85 seconds of computing time for each peak load level to obtain the RBTS reliability indices using *Method 1*. It requires approximate 210 seconds in MECORE to calculate the RBTS reliability indices using *Method 2A*. The calculation time was assessed by running the MECORE software on an Intel Pentium D computer.

Table 3.12: The RBTS system EENS (MWh/yr) with different load forecast uncertainties obtained applying *Method 1* (calculation time: 7×85 sec)

| LFU | Peak Load | | | | |
|---|---|---|---|---|---|
| | 165 MW | 175 MW | 185 MW | 195 MW | 205 MW |
| 0% | 124.732 | 136.496 | 150.822 | 174.682 | 228.006 |
| 2% | 124.836 | 136.831 | 151.659 | 176.256 | 232.717 |
| 5% | 125.463 | 138.803 | 156.292 | 186.619 | 261.194 |

Table 3.13: The RBTS system EENS (MWh/yr) with different load forecast uncertainties obtained applying *Method 2A* (calculation time: 210 sec)

| LFU | Peak Load | | | | |
|---|---|---|---|---|---|
| | 165 MW | 175 MW | 185 MW | 195 MW | 205 MW |
| 0% | 124.732 | 136.496 | 150.822 | 174.682 | 228.006 |
| 2% | 126.676 | 138.891 | 153.945 | 179.154 | 236.919 |
| 5% | 127.729 | 141.523 | 159.998 | 191.423 | 268.408 |

The results shown in Tables 3.12 and 3.13 indicate that the risk increases as the uncertainty in the system peak load increases. The utilization of *Method 2A* in MECORE requires a shorter computing time than *Method 1.* Assuming that the system EENS obtained using *Method 1* are exact values. *Method 2A* can be considered to provide approximate values due to the required reduction in the number of steps in the load model used in MECORE. The values in Table 3.13 with LFU are higher than those in Table 3.12.

The EENS at the load buses for the peak load of 185 MW with and without consider load forecast uncertainty are shown in Table 3.14.

Table 3.14: The EENS (MWh/yr) at load buses for the peak load of 185 MW obtained using *Method 1*

| Bus Name | LFU | | |
|---|---|---|---|
| | 0% | 2% | 5% |
| Bus 2 | 0.000 | 0.000 | 0.000 |
| Bus 3 | 12.561 | 13.383 | 17.962 |
| Bus 4 | 0.029 | 0.030 | 0.036 |
| Bus 5 | 0.291 | 0.294 | 0.306 |
| Bus 6 | 137.942 | 137.952 | 137.988 |

Table 3.14 shows that the EENS at Bus 3 increases as the LFU increases. The EENS at bus 6 remains relatively constant with increase in the load forecast uncertainty. The reason is that Bus 6 is supplied by a single radial line. The conclusion can be drawn from the study results that the risk impacts on the EENS are different for different buses. A comparison of load point EENS values obtained using the two methods is shown in Figure 3.9 and indicates that the two methods provide relatively close load point EENS values.

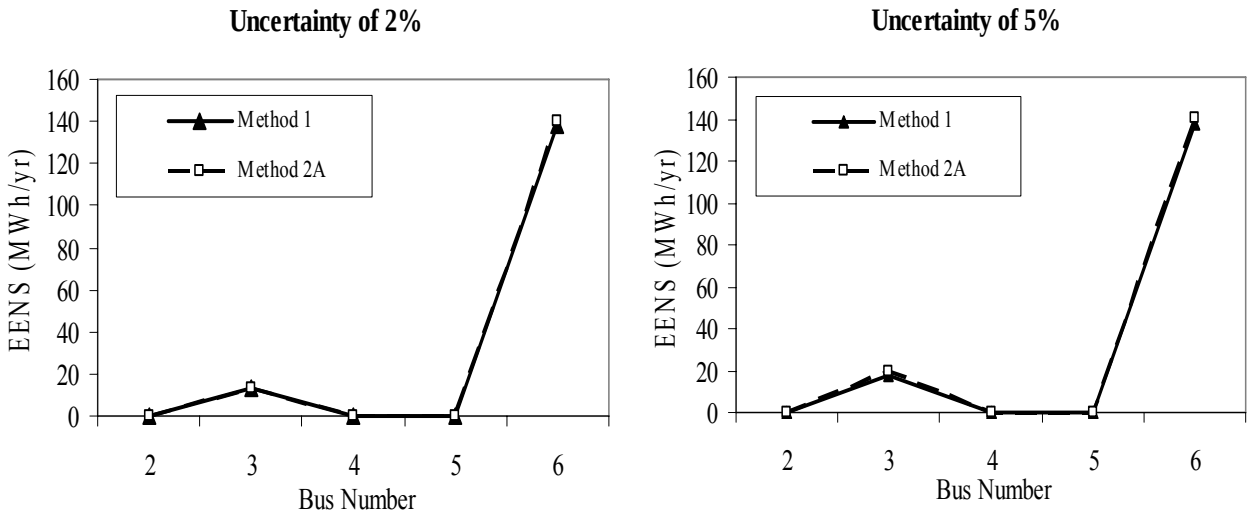


Figure 3.9: Comparison of the EENS at the load points for a peak load of 185 MW obtained using the two methods

### 3.3.2. The IEEE-RTS System Studies

The studies conducted on the IEEE-RTS are similar to those conducted on the RBTS. It is assumed that the system forecast peak load is increased from 2750 MW to 2900 MW in steps of 50 MW. The IEEE-RTS is a large system compared to the RBTS and has a relatively strong transmission network. The MECORE computing times are much more than those required for the RBTS system. Tables 3.15 and 3.16 show the system EENS with and without load forecast uncertainty as a function of peak load obtained using *Method 1* and *Method 2A* respectively.

Table 3.15: The IEEE-RTS system EENS (MWh/yr) with different load forecast uncertainties obtained applying *Method 1* (calculation time: 7×300 sec)

| LFU (%) | Peak Load | | | |
|---|---|---|---|---|
| | 2750 MW | 2800 MW | 2850 MW | 2900 MW |
| 0% | 767.800 | 1143.989 | 1674.799 | 2428.441 |
| 2% | 826.283 | 1227.434 | 1797.401 | 2598.784 |
| 5% | 1176.848 | 1728.426 | 2505.413 | 3583.205 |

Table 3.16: The IEEE-RTS system EENS (MWh/yr) with different load forecast uncertainties obtained applying *Method 2A* (calculation time: 550 sec)

| LFU (%) | Peak Load | | | |
|---|---|---|---|---|
| | 2750 MW | 2800 MW | 2850 MW | 2900 MW |
| 0% | 767.800 | 1143.989 | 1674.799 | 2428.441 |
| 2% | 843.538 | 1253.538 | 1835.540 | 2653.388 |
| 5% | 1248.451 | 1820.536 | 2625.849 | 3742.553 |

Table 3.15 and Table 3.16 show that the system EENS values for the IEEE-RTS increase as the load standard deviations increases. *Method 2A* involves considerably less computing time than that required by *Method 1*. As noted earlier in the RBTS study, the EENS values obtained using the reduced LDC in *Method 2A* are higher than those obtained using *Method 1*.

Buses 19 and 9 were selected from the 24 buses as the two buses have the lowest and second lowest load curtailment priority as shown in Table 2.2. The EENS at Bus 19 and Bus 9 as a function of the peak load with and without LFU obtained using *Method 1* are shown in Figure 3.10 and Figure 3.11 respectively.

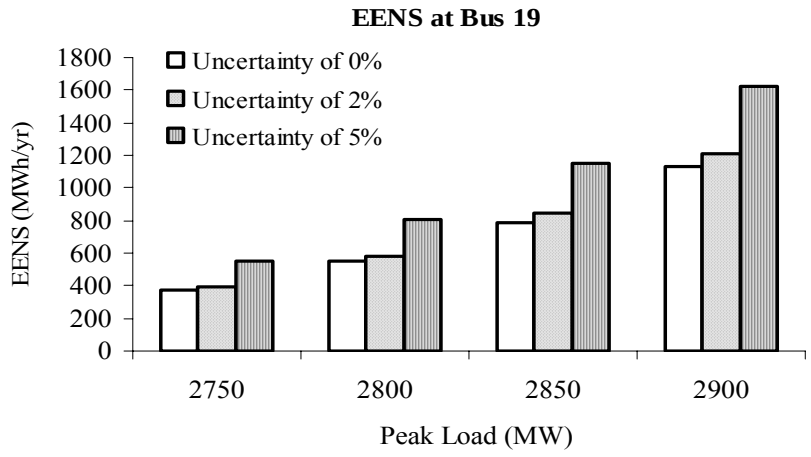


Figure 3.10: Effect of LFU on the EENS at IEEE-RTS Bus 19

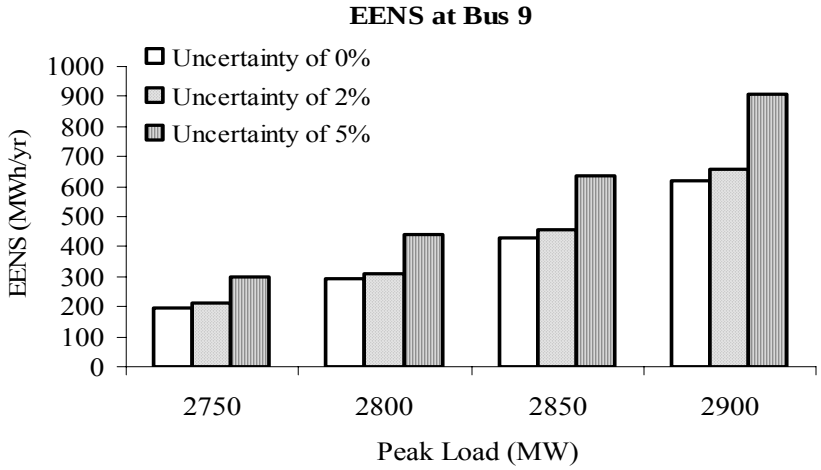


Figure 3.11: Effect of LFU on the EENS at IEEE-RTS Bus 9

Figures 3.10 and 3.11 show that the load point EENS values in the IEEE-RTS increase as the LFU increases. The impacts of LFU on the lower priority load points in the IEEE-RTS are similar due to the fact that the IEEE-RTS has a strong transmission system and these load points are not dominated by transmission deficiencies.

The relative errors in the system reliability indices considering LFU obtained by applying *Method 1* and *Method 2A* in MECORE increase as the standard deviation of the forecast peak load increases.

## 3.4. Conclusions

This chapter illustrates two basic methods for considering load forecast uncertainty that can be used in generating capacity or bulk system reliability assessment. *Method 1* is a conventional approach in which the load levels associated with the uncertainty distribution are used to calculate a set of reliability indices. These indices are then weighted using the associated probabilities to produce expected indices that include the uncertainty conditions. *Method 2* develops a modified load duration curve model that incorporates the load forecast uncertainty probability distribution. Reliability indices that include the uncertainty in the load forecast are then directly obtained using the modified load model. The studies conducted on the RBTS at HL-I show that the two methods provide virtually identical system reliability indices.

*Method 2* involves the use of a modified load duration curve with a large number of load steps. The MECORE software as currently formatted can handle up to 100 load steps in a multi-step load duration curve model. This capability limits the application of *Method 2* in the reliability evaluation of composite systems. It is necessary to reduce the final model to one containing 100 or less steps in order to use the modified load duration model as input data to MECORE. This involves creating an approximate model which reduces the accuracy associated with the analysis.

Two approximate approaches are proposed in this chapter to reduce a modified load duration curve and are designated as *Method 2A* and *Method 2B* respectively. Analytical procedures are introduced and used to create reduced modified load duration curves using the approximate approaches. Analyses on the RBTS at HL-I show that the two approximate approaches provide

reasonable reliability index results. The number of load steps in a modified load duration curve obtained using *Method 2A* is less than that obtained by applying *Method 2B*. The number of load steps in the final load duration models obtained using the two approximate approaches is dependent on the standard deviation of the load forecast uncertainty. The final load duration models obtained using *Method 2B* was not used in MECORE in this chapter as the step number exceeded the load level limit.

*Method 1* and *Method 2A* can be used in bulk system analysis incorporating load forecast uncertainty. The analyses conducted on the RBTS and the IEEE-RTS indicate that the utilization of *Method 1* and *Method 2A* in MECORE provide similar system reliability indices. The two methods as applied in MECORE have advantages and disadvantages. *Method 2A* requires much less computing time than *Method 1.* It is, however, a complicated procedure to modify the input load data file of MECORE to use the *Method 2A* load duration curve. The application of *Method 1* is much simpler to understand and implement.

The studies conducted on the RBTS and the IEEE-RTS also illustrate the effect of LFU on the system and load bus adequacy in the form of the EENS. The study results show that the system reliability indices increase with increased load forecast uncertainty. The effects of load forecast uncertainty on individual load point EENS are quite different and very dependent on the topology of the system, and the system load curtailment philosophy.

# 4. Wind Integrated Bulk System Adequacy Assessment Considering Wind Speed Correlation

## 4.1. Introduction

Wind energy is now “utility scale” and can affect utility planning and operation of both generation and transmission [42]. Utilities with significant wind potential in their service territories are actively studying the technical and economic impacts of incorporating wind plants in their systems [43]. Considerable research has been conducted to develop mathematical models and techniques for reliability evaluation of power systems containing wind energy [44-59]. References 44 to 49 focus on developing mathematical models. In actual power systems containing multiple wind sites, the wind farms are neither completely dependent nor independent but are correlated to some degree if the distances between sites are not very large. Reference 50 shows that the degree of wind correlation increases as the distance between wind sites decreases. The effect of wind site correlation is considered in [48-54]. References 48 and 49 are focused on generating system reliability evaluation incorporating multi-site wind farms using analytical methods. The sequential Monte Carlo simulation technique is used in References 51 to 53 to calculate the frequency indices in addition to other related indices and can incorporate different state duration distributions. The most comprehensive approach to incorporate wind energy in a power system reliability evaluation is to use sequential Monte Carlo simulation. This method, however, can require considerable computation time particularly when applied to large bulk systems [33, 58-60]. It is, therefore, necessary to develop suitable methods and models for wind farms that can be easily incorporated in more conventional approaches to bulk system adequacy assessment without requiring excessive increases in computer solution time, such as the Monte Carlo state sampling technique.

Relatively little published material has been done on the reliability evaluation of bulk systems incorporating multiple dependent wind energy facilities using the Monte Carlo state sampling technique. This chapter focuses on developing techniques and models to permit dependent wind

energy facilities to be incorporated in generating and bulk systems adequacy evaluation using the state sampling Monte Carlo simulation technique. This is a practical approach that can be used in a wide range of actual systems. This chapter presents the effects of incorporating large scale wind energy facilities in bulk system adequacy evaluation using the developed approaches, models and the state sampling Monte Carlo simulation technique. The RBTS and IEEE-RTS are modified to create four study bulk systems to represent general conditions that exist in actual power systems. The impacts of wind speed correlation levels, the wind farm locations and system load are examined.

## 4.2. Wind Speed Modeling

One of the first steps for a utility company to consider when developing wind as an energy source is to survey the available wind resource. Unfortunately, reliable wind speed data suitable for wind resource assessment are difficult to obtain, and many records that have been collected are not available to the general public. Many utilities and private organizations, however, are now engaged in collecting comprehensive wind speed data. These data can be used to create site specific wind speed models.

### 4.2.1. Wind Speed Model

A time series model has been developed [46] to incorporate the chronological nature of the actual wind speed. Historical wind speeds are obtained for a specific site, based on which, future hourly data are predicted using the time series model. This model has been utilized to perform reliability studies in both grid-connected and stand-alone power systems containing wind energy [47, 56-59, 61]. This time series model is also used in the research described in this thesis to generate synthetic wind speeds based on measured wind data at a specific location.

In the time series model [46], the simulated wind speed $SW_t$ can be obtained from the mean wind speed $\mu_t$ and its standard deviation $\sigma_t$ at time $t$ as follows:

$$SW_t = \mu_t + \sigma_t \times y_t \tag{4.1}$$

The original data series set $y_t$ can be used to create a wind speed time series referred to as an ARMA (n, m) series model (Auto-Regressive and Moving Average Model). This is shown in Equation (4.2).

$$y_t = \phi_1 y_{t-1} + \phi_2 y_{t-2} + \ldots + \phi_n y_{t-n} + \alpha_t - \theta_1 \alpha_{t-1} - \theta_2 \alpha_{t-2} - \ldots - \theta_m \alpha_{t-m} \quad (4.2)$$

where $\phi_i$ ( i=1,2,…,n ) and $\theta_j$ ( j=1,2,…,m ) are the auto-regressive and moving average parameters of the model respectively, $\{\alpha_t\}$ is a normal white noise process with zero mean and variance of $\sigma_a^2$, (a white noise process is a random process of random variables that are uncorrelated, have mean zero, and a finite variance denoted as $\sigma^2$), i.e., $\alpha_t \in NID(0, \sigma_a^2)$, where NID denotes Normally Independent Distributed. Equation (4.2) permits new values of $y_t$ to be calculated from current random white noise $\alpha_t$ and previous values of $y_{t-i}$. The hourly wind speeds incorporating the wind speed time series can be generated using Equation (4.1).

The ARMA time series models for different locations are different as each site experiences different wind regimes. The wind speed model and data for the Swift Current and Regina sites located in the province of Saskatchewan, Canada have been used in the studies described in this thesis. Table 4.1 shows the hourly mean wind speed and standard deviation at the Regina and Swift Current sites.

Table 4.1: Wind speed data for the two sites

| Sites | Regina | Swift Current |
|---|---|---|
| Mean wind speed (km/h) , $\mu$ | 19.52 | 19.46 |
| Standard deviation (km/h), $\sigma$ | 10.99 | 9.70 |

The ARMA models for the two sites are given in (4.3) and (4.4) respectively. The Regina wind model shown in Equation (4.3) was developed and published in [46]. The Swift Current wind model was developed and published in [52].

Regina: ARMA (4, 3):

$$y_t = 0.9336 y_{t-1} + 0.4506 y_{t-2} - 0.5545 y_{t-3} + 0.1110 y_{t-4} + \alpha_t - 0.2033 \alpha_{t-1} - 0.4684 \alpha_{t-2} + 0.2301 \alpha_{t-3} \quad (4.3)$$

$$\alpha_t \in NID(0, 0.409423^2)$$

Swift Current: ARMA (4, 3):

$$y_t = 1.1772 y_{t-1} + 0.1001 y_{t-2} - 0.3572 y_{t-3} + 0.0379 y_{t-4} + \alpha_t - 0.5030 \alpha_{t-1} - 0.2924 \alpha_{t-2} + 0.1317 \alpha_{t-3} \quad (4.4)$$

$$\alpha_t \in NID(0, 0.524760^2)$$

Figure 4.1 shows the simulated hourly wind speed for a first 100 hours using the Regina and Swift Current site data and ARMA model respectively.

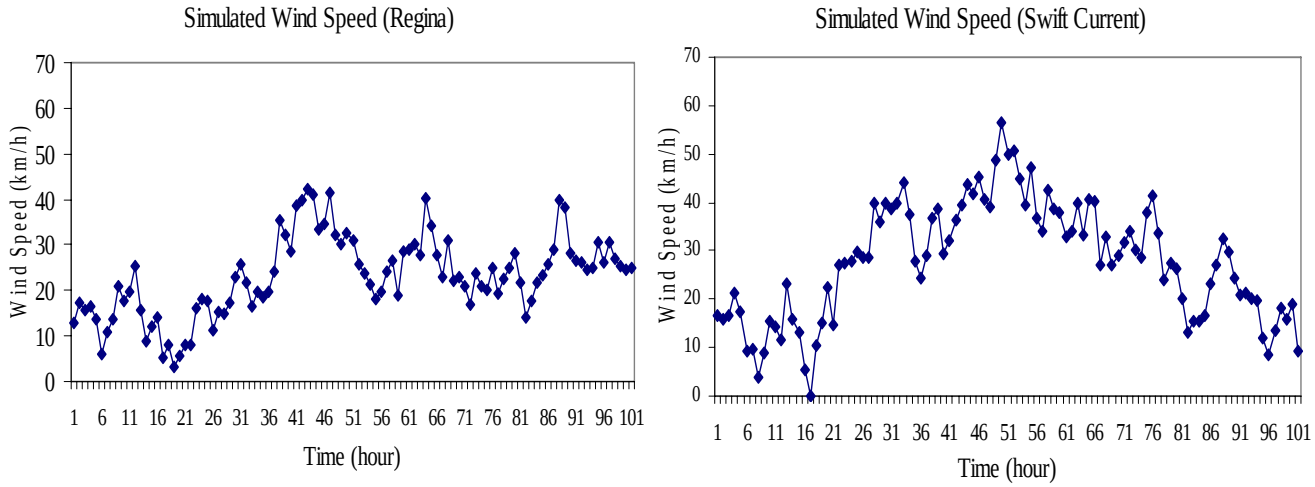


Figure 4.1: Simulated wind speeds for the Regina and Swift Current sites

Figure 4.2 shows a comparison of the observed wind speed probability distributions for the original 20 years of Swift Current wind speed data and the simulated wind speed probability distribution obtained using the ARMA (4, 3) model for a Swift Current site and a large number (8,000) of simulated years. The observed average wind speed is 19.46 km/h, and the simulated value is 19.52 km/h. The observed wind speed probability distribution is not as continuous as the simulated distribution, as it is based on only 20 years of data.

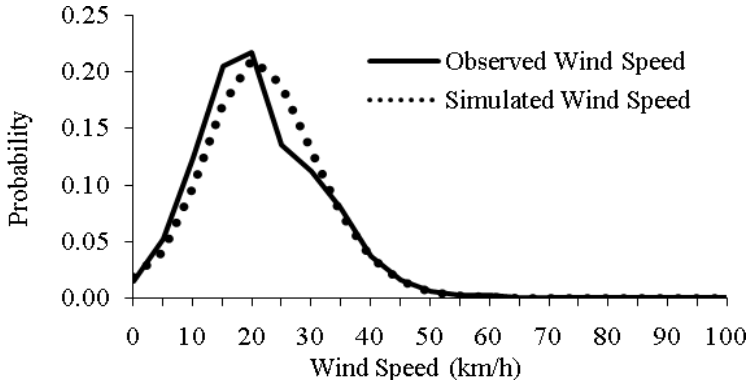


Figure 4.2: Observed and simulated wind speed distributions for the Swift Current site

Figure 4.2 shows that the ARMA (4, 3) model provides a reasonable representation of the actual wind regime. The observation is often made that wind speed can be represented by a Weibull distribution [10]. Simulation results are used to generate the wind speed probability distributions in the system adequacy studies described later in this thesis.

### 4.2.2. Genetic Algorithm Applied to Adjust the Simulated Wind Speed Correlation

In practice, wind farms are neither completely dependent nor independent but are correlated to some degree if the distances between sites are not very large. The wind speed correlation between two wind farms can be calculated using cross correlation. The cross-correlation coefficient equation is shown in (4.5).

$$R_{xy} = \frac{\frac{1}{n}\sum_{i=1}^{n}(x_i - \mu_x)(y_i - \mu_y)}{\sigma_x \sigma_y} \tag{4.5}$$

where $x_i$ and $y_i$ are elements of the first and second time series respectively, $\mu_x$ and $\mu_y$ are the mean values of the first and second time series, $\sigma_x$ and $\sigma_y$ are the standard deviations of the first and second time series, and n is the number of points in each time series.

The ARMA time series model has two parts, one part is the autoregressive (AR) model involving lagged terms in the time series itself, the other one is the moving average (MA) model involving lagged terms in the noise or residuals. It is possible to adjust the wind speed correlation level

between two or more different wind locations by selecting the random number seeds (initial numbers) for a random number generator process used in the MA model. Reference 52 uses a trial and error process to generate appropriate random number seeds by selecting a factor K between the dependent wind locations. This is a relatively straightforward method, but can require considerable time and effort and is not very flexible.

A genetic algorithm (GA) [22-24] is a search technique used in computing to find exact or approximate solutions to optimization and search problems. The simplest form of genetic algorithm involves three types of operators: selection, crossover, and mutation [22]. The major advantage of genetic algorithms is their flexibility and robustness as a global search method. A genetic algorithm is, therefore, applied in this study to select the optimum random number seeds in the ARMA model to adjust the degree of wind speed correlation for two multiple wind sites.

The basic procedure of the genetic algorithm used in this study is described as follows. Selected terms are defined in Appendix C.

Step 1. Generate a random population of *n* chromosomes which are parents. In this study, the population size is 20. The string size is 16 and each parent string size (a bit string size) is 8.

Step 2. Decode the parent gene's value. The control factors must have an upper and lower bound declared. This range is divided into the number of intervals that can be expressed by the gene's bit string. The size of interval would be $range/(2^L-1)$, where $L$ is a bit string length. The range of control factor K is from 0 to 5 in this study.

Step 3. Evaluate the fitness $f(x)$ of each chromosome $x$ in the population. A fitness function is a particular type of objective function that quantifies the optimality of a solution in a genetic algorithm. In this study, the fitness function is defined as the absolute error of the cross-correlation coefficient Rxy between the specified value and its measured value. The program stops when the fitness value is less than a prespecified value of 0.02.

Step 4. Create a new population by repeating the following steps until the new population is complete.

> Selection: Select two parent chromosomes from a population according to their fitness. The Rouleetwheel selection breeding method and the elitism method [24] are used to generate offspring.

Crossover: With a crossover probability, cross over the parents to form a new offspring. If no crossover was performed, the offspring is an exact copy of the parents. Single point crossover is used and the probability of crossover is 0.85.

Mutation: With a mutation probability, mutate new offspring at each locus (position in chromosome). The probability of mutation is 0.02.

Accepting: Place new offspring in a new population

Step 5. Use the new generated population for a further run of algorithm

Step 6. If the end condition is satisfied, the program will be stop, and return the best solution in the current population. If the end condition is not satisfied, go to Step 2.

The flow chart of the ARMA wind speed models coupled with a genetic method is shown in Figure 4.3 [62].

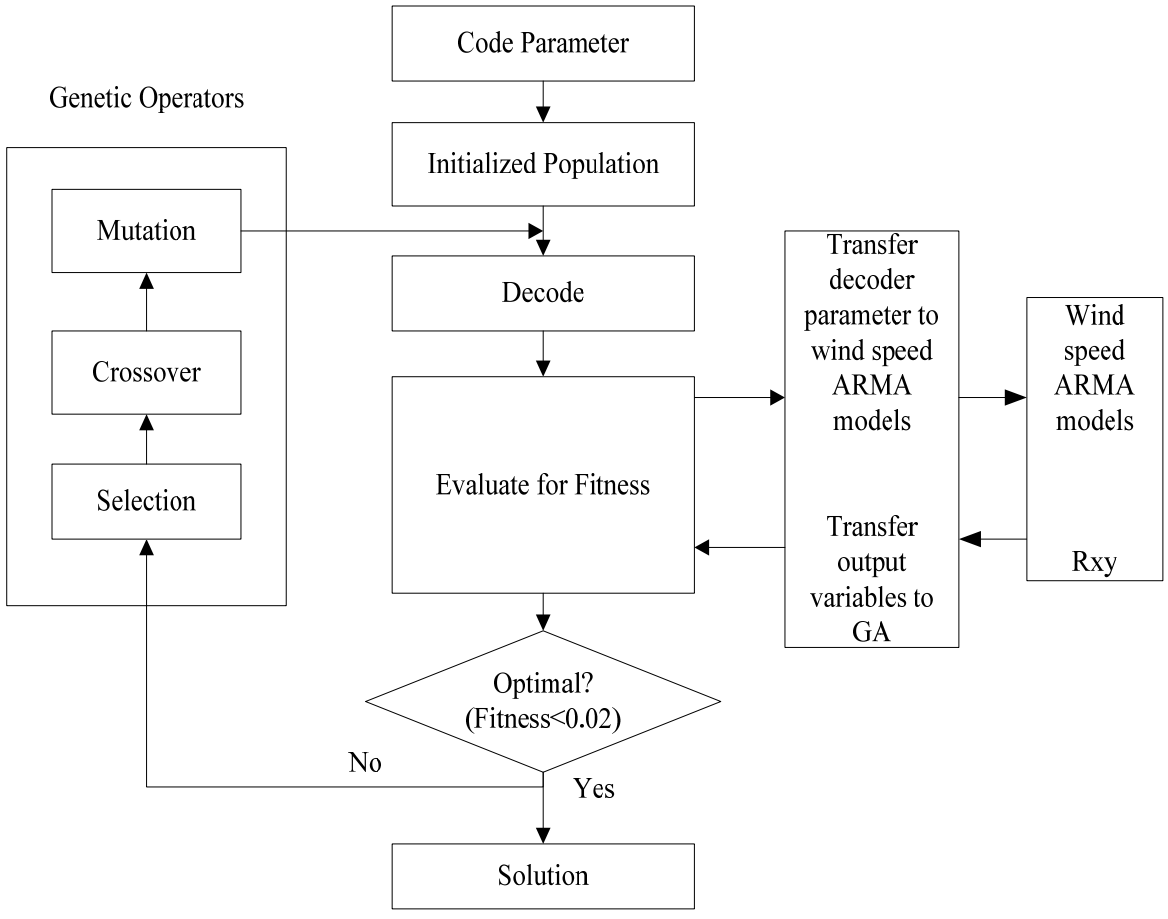


Figure 4.3: The flow chart of the ARMA wind speed models coupled with a GA

### 4.2.3. Simulation of Wind Speeds Considering Wind Speed Correlation Levels

The simulated wind speed time series during a selected period for the Regina and Swift Current sites with high correlation level (Rxy=0.8), middle correlation level (Rxy=0.5) and low correlation level (Rxy=0.2) are shown in Figure 4.4. The simulated average wind speeds for the Regina and Swift Current sites are 19.58 km/h and 19.52 km/h respectively.

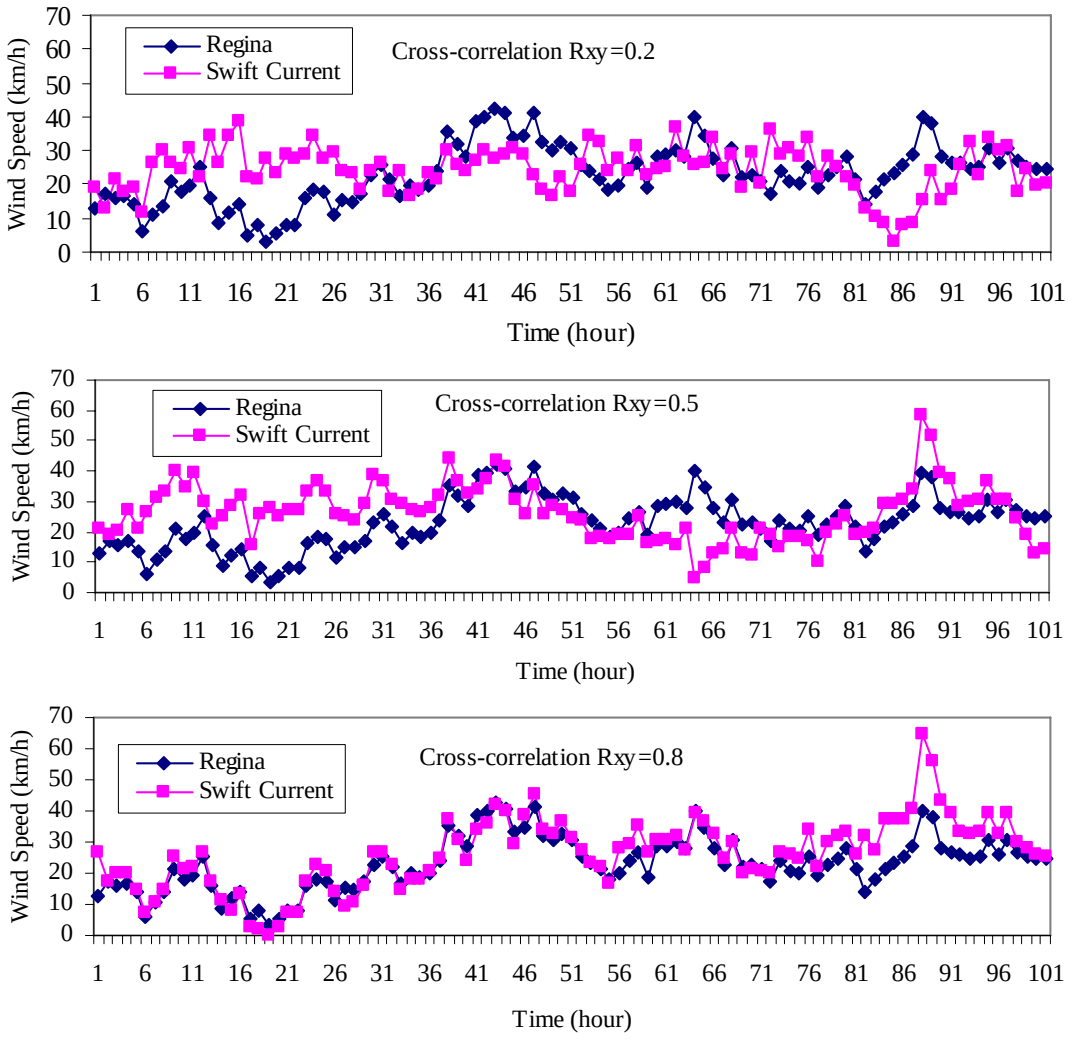


Figure 4.4: Different simulated wind speed correlation levels between the Regina and Swift Current sites

The technique of ARMA models coupled with a genetic algorithm can also be used for three or more wind site simulations in which the correlations between wind farms are taken into account. This is illustrated using Saskatoon wind site as the third wind site. The developed ARMA(3,2)

model for Saskatoon [46] is given in Equation (4.6). The average wind speed and stand deviation for Saskatoon wind site are 16.78 km/h and 9.23 km/h respectively.

Saskatoon: ARMA (3, 2):

$$y_t = 1.5047 y_{t-1} - 0.6635 y_{t-2} + 0.1150 y_{t-3} + \alpha_t - 0.8263 \alpha_{t-1} + 0.2250 \alpha_{t-2} \quad (4.6)$$

$$\alpha_t \in NID(0, 0.447423^2)$$

Figure 4.5 shows the simulated wind speed time series during a selected period for the Regina, Swift Current and Saskatoon wind sites with moderately correlated wind speeds between the three locations.

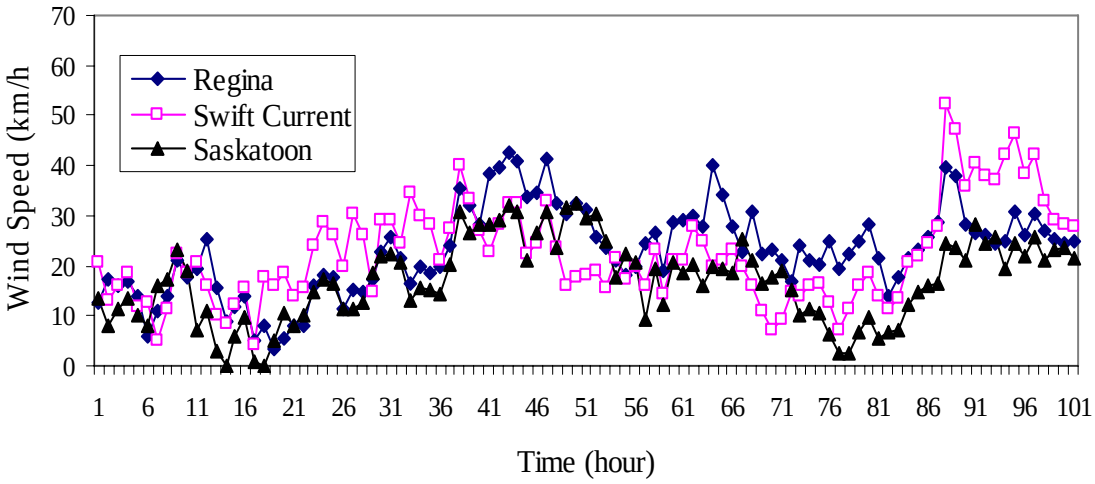


Figure 4.5: Simulated wind speed for the three partially correlated wind sites

A genetic algorithm can quickly scan a vast solution set. Bad proposals do not impact the end solution negatively as they are simply discarded. It is a very useful method coupled with ARMA models to adjust the simulated wind speed correlation levels for different wind sites.

## 4.3. Wind Turbine Generator Modeling

The power output characteristics of a WTG are quite different from those of a conventional generating unit. The output of a WTG depends strongly on the wind regime as well as on the performance characteristics and the efficiency of the generator. A 2 MW WTG with cut-in speed

of 14.4 km/h, rated speed of 36 km/h and cut-out wind speeds of 80 km/h [47, 52] is used in the studies described in this thesis.

### 4.3.1. Wind Turbine Generator Modelling

After the hourly wind speed is obtained, the next step is to determine the power output of the WTG as a function of the wind speed. This function is described by the operational parameters of the WTG. The parameters commonly used are the cut-in wind speed (at which the WTG starts to generate power), the rated wind speed (at which the WTG generates its rated power) and the cut-out wind speed (at which the WTG is shut down for safety reasons). Equation (4.7) is used to obtain the hourly power output of a WTG from the simulated hourly wind speed.

$$P(SW_t) = \begin{cases} 0 & 0 \le SW_t < V_{ci} \\ (A + B \times SW_t + C \times SW_t^{\,2}) \times P_r & V_{ci} \le SW_t < V_r \\ P_r & V_r \le SW_t < V_{co} \\ 0 & SW_t \ge V_{co} \end{cases} \tag{4.7}$$

where $P_r, V_{ci}, V_r$ and $V_{co}$ are the rated power output, the cut-in wind speed, the rated wind speed and the cut-out wind speed of the WTG respectively [63]. The constants $A$, $B$, and $C$ depend on $V_{ci}$, $V_r$ and $V_{co}$ as expressed in Equation (4.8) [63].

$$\begin{aligned} A &= \frac{1}{(V_{ci} - V_r)^2}\left\{V_{ci}(V_{ci} + V_r) - 4V_{ci}V_r\left[\frac{V_{ci} + V_r}{2V_r}\right]^3\right\}, \\ B &= \frac{1}{(V_{ci} - V_r)^2}\left\{4(V_{ci} + V_r)\left[\frac{V_{ci} + V_r}{2V_r}\right]^3 - (3V_{ci} + V_r)\right\}, \\ C &= \frac{1}{(V_{ci} - V_r)^2}\left\{2 - 4\left[\frac{V_{ci} + V_r}{2V_r}\right]^3\right\}. \end{aligned} \tag{4.8}$$

The relationship can also be illustrated graphically as shown in Figure 4.6 and is often referred to as the “Power Curve”.

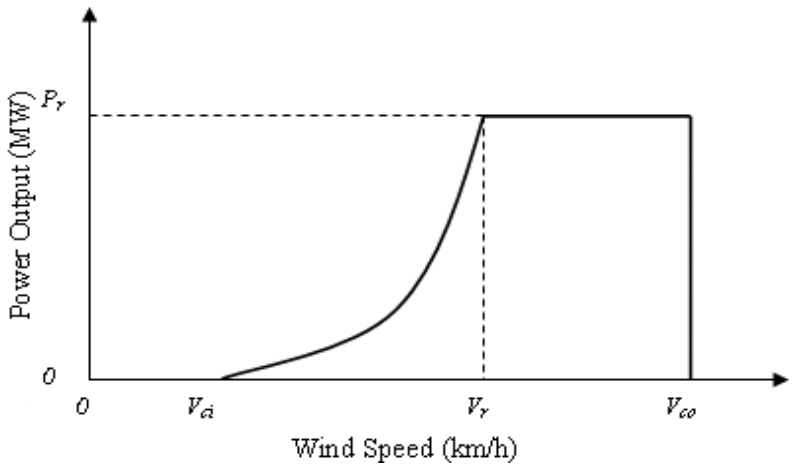


Figure 4.6: Wind turbine generator power curve

At a specific time, the hourly output power of a WTG can be obtained from the simulated hourly wind speed using Equation (4.7). Figure 4.7 presents the simulated output power of the 2 MW WTG over a one week period.

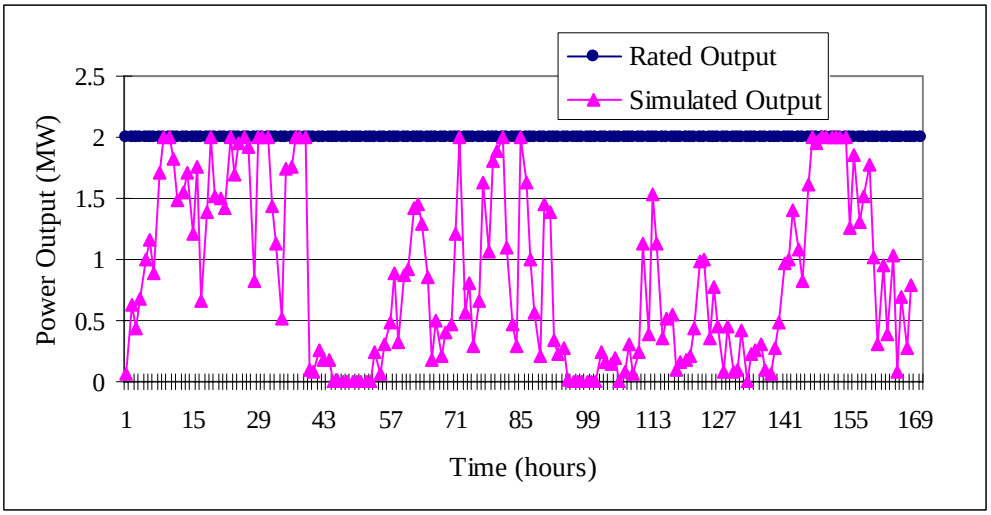


Figure 4.7: Simulated output power of a 2 MW WTG for a sample week (Swift Current data)

Figure 4.7 shows that the output power of the generator reaches its rated value for only a few hours in the week. The reason is the fact that the simulated wind speeds are seldom between the rated and cut-out wind speeds of the WTG during the sample week when the WTG unit is in the operating state. It can also be seen from Figure 4.7 that there is no power output from the WTG unit in some hours of the sample week. The reason for no power output is that the simulated

wind speed is either lower than the cut-in wind speed or higher than the cut-out wind speed of the WTG at these time points.

### 4.3.2. Wind Farm Power Output Considering Wind Speed Correlation Levels for Two Wind Sites

The simulated hourly wind power output for the two wind farms are generated using the ARMA models considering wind speed correlation and the WECS power curves. Figure 4.8 shows the simulated wind power output time series during a selected period for the Regina and Swift Current sites with different wind speed cross-correlation levels.

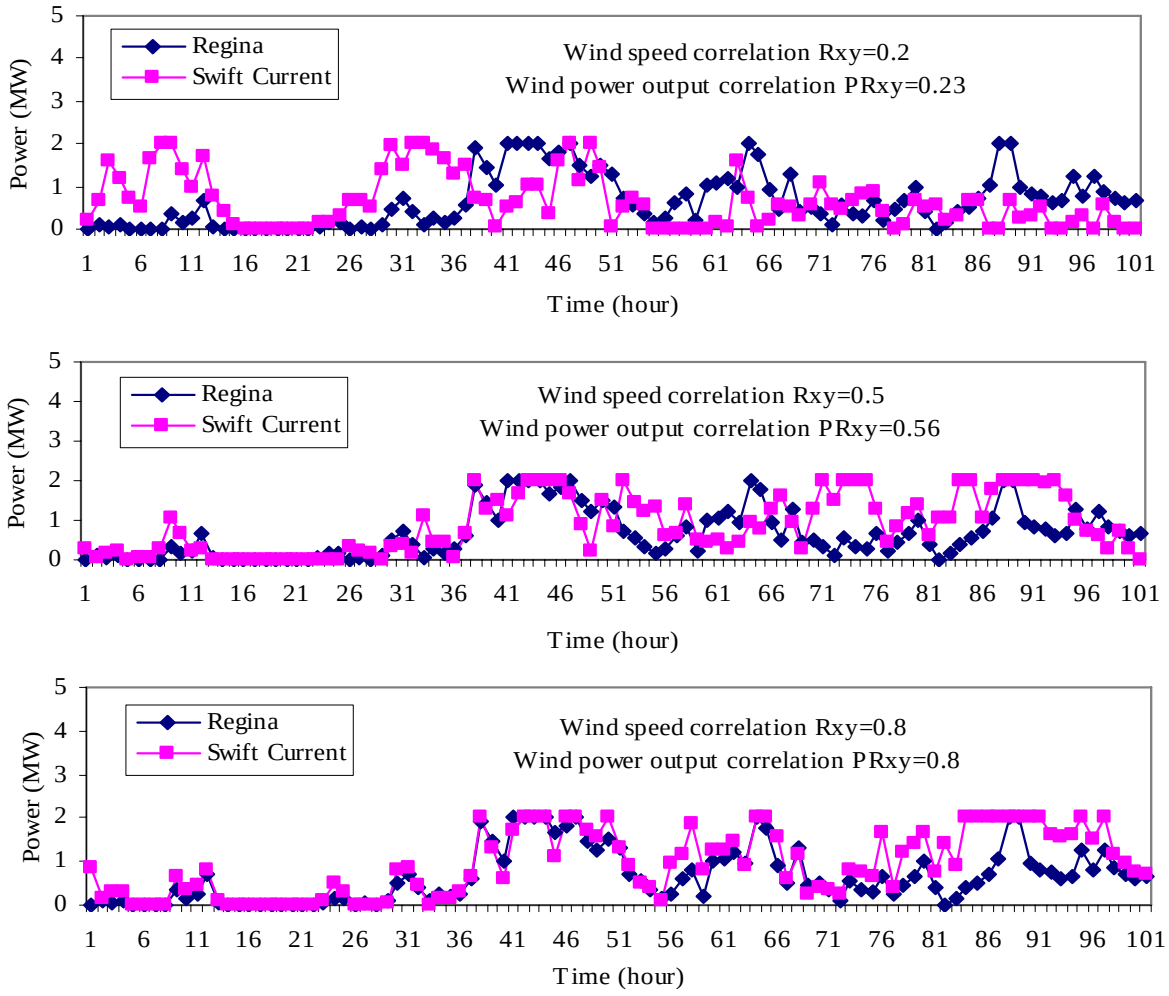


Figure 4.8: Simulated wind power outputs for different simulated wind speed correlation levels between the Regina and Swift Current wind sites

The cross-correlation coefficient of the wind power outputs for two wind sites can be calculated using (4.5) and is designed as PRxy. The calculated wind power output cross-correlations PRxy are shown in Table 4.2 for different wind speed cross-correlation coefficients.

Table 4.2: Comparison of the cross-correlation coefficients Rxy and PRxy

| Rxy | 0.1 | 0.2 | 0.3 | 0.4 | 0.5 | 0.6 | 0.7 | 0.8 | 0.95 |
|---|---|---|---|---|---|---|---|---|---|
| PRxy | 0.13 | 0.23 | 0.34 | 0.45 | 0.56 | 0.64 | 0.71 | 0.8 | 0.92 |

It can be seen from Figure 4.8 and Table 4.2 that the power output cross-correlation coefficient PRxy between the two sites are similar to the wind speed cross-correlation coefficient Rxy. The reason is that the wind power output is mainly distributed in the range of 0%- 25% of the rated power output [47]. It should be noted that this is not a general conclusion. The PRxy is extremely dependent on the wind regime and will change if the facilities are located at a site where higher wind velocities are experienced.

## 4.4. WECS Models

### 4.4.1. The Capacity Outage Probability Table of the WTG

The hourly mean wind speeds and output power for a WTG unit without considering its unavailability or forced outage rate (FOR) are generated using the ARMA time series model and the power curve respectively. The capacity outage probability table (COPT) of a WTG unit can be created by applying the hourly wind speed to the power curve. The procedure is briefly described by the following steps [47]:

1. Define the output states for a WTG unit as segments of the rated power.
2. Determine the total number of times that the wind speed results in a power output falling within one of the output states.
3. Divide the total number of occurrences for each output state by the total number of data points to estimate the probability of each state.

The WTG COPT can be formed using this approach. Two cases are illustrated in this example. The first case utilizes the actual observed 20 years of Swift Current data. The second case uses

the 8,000 simulated years of data. Figure 4.9 shows the two capacity outage probability distributions. The class interval width is 5% in this figure and the indicated capacity outage level is the midpoint of the class.

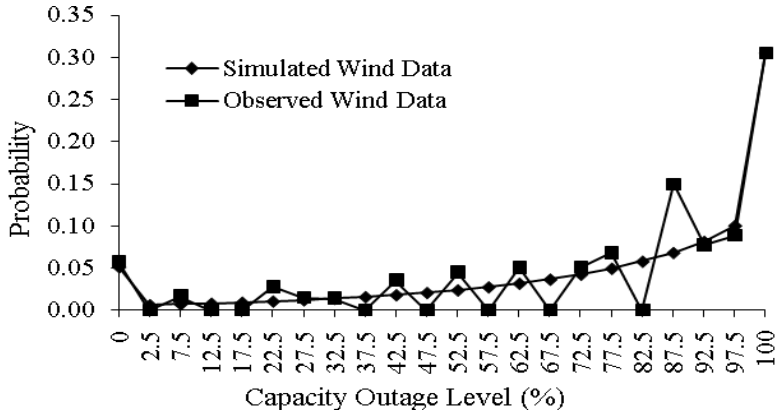


Figure 4.9: Capacity outage probability profile for the WTG unit

Figure 4.9 shows that the observed data probability profile is discontinuous due to the limited wind data collection and that the simulated wind data provides a reasonable representation for adequacy assessment. The power output characteristics of a WTG are very different from those of conventional generating units. The WTG can be considered as a generating unit with many derated states [47]. Figure 4.9 shows that the probability of having full WTG output (0% capacity outage) is relatively low for this wind regime. There are many derated states in which the output of a WTG can reside in over the course of its operating history. A basic requirement in practical adequacy assessment is to represent the WTG by an acceptable reduced number of derated states.

### 4.4.2. Multi-state WECS Models

The apportioning method [9, 64] can be used to create selected multi-state models for a WTG and the WECS. In this approach, the residence times of the actual derated states are apportioned between the completely up, selected derated and completely down states. A wind energy conversion system (WECS) can contain one or more WTG. A WECS has two basic parts: one is the wind resource and the other is the actual WTG units. If the WECS consists of identical WTG units with zero FOR, the WECS multi-state model is basically the same as that of the single

WTG unit. If the FOR of the WTG units is not zero, the WECS derated state capacity outage probability table is not the same as that of a single WTG unit. An analytical procedure used to create WECS multi-state models including the WTG FOR is described in [47]. Analysis results in [47] show that the changes in the FOR of the WTG units do not have a significant impact on the calculated system reliability indices and a five-state WECS model can be used to provide a reasonable assessment in practical studies using the analytical method or a state sampling Monte Carlo simulation method. It is, therefore, assumed in this thesis that the two installed capacity WECS consist of identical WTG units with zero forced outage rates.

The independent five-state WECS models for the Regina and Swift Current sites are developed from the 22-state model in Figure 4.9 using the Apportioning Method and shown in Table 4.3. These models will be used in later studies in this thesis.

Table 4.3: The two independent WECS models obtained using the apportioning method

| | Regina | Swift Current |
|---|---|---|
| Capacity Outage (%) | Probability | Probability |
| 0 | 0.07585 | 0.07021 |
| 25 | 0.06287 | 0.05944 |
| 50 | 0.11967 | 0.11688 |
| 75 | 0.23822 | 0.24450 |
| 100 | 0.50340 | 0.50897 |

### 4.4.3. Conditional COPT for the Two Correlated WECS

Reference 48 illustrates an approach to construct a joint capacity outage probability table for two dependent WECS. The procedure involves building a table of capacity levels for given wind speed at the first site and conditional capacity levels and corresponding probabilities at the second site. These values are then combined to create a conditional wind farm model of the two sites, at the given wind speed of the first. The conditional wind-farms are then combined to obtain an overall wind-farm model using the conditional probability theorem and the additive property of mutually exclusive events.

The approach presented in [48] is extended in this study. Site 1 located in Regina is considered to be the base site and Site 2 is located in Swift Current. There are five capacity outage levels $C_{1i}$ of

Site 1, where the subscript 1 means Site 1 and *i* is the level number, which is from 1 to 5. There are five conditional capacity outage levels $C_{2j}|\ C_{1i}$ of Site 2 at a given capacity outage level of Site 1, where the subscript 2 means Site 2 and *j* is from 1 to 5. The simulated hourly wind power output for the two wind farms are generated using the ARMA models considering wind speed correlation and the WECS power curves. The number of occurrences for each output state of Site 2 at a given capacity outage level of Site 1 are determined. The probability of each state of Site 2 at a given capacity outage level of Site 1 are estimated by dividing the total number of occurrences of each output state by the total number of data points. In order to simplify the analysis, five capacity outage levels of Site 1 are obtained directly in the program by considering a class interval width of 25% in which the indicated capacity outage level is the midpoint of the class. The independent COPT for the two sites are shown in Table 4.4. This approach provides slightly different COPT than those shown in Table 4.3 obtained using the apportioning method.

Table 4.4: The independent COPT of the WECS located at the two sites

| | Regina | Swift Current |
|---|---|---|
| Capacity Outage (%) | Probability | Probability |
| 0 | 0.07452 | 0.06892 |
| 25 | 0.06159 | 0.05807 |
| 50 | 0.11698 | 0.11383 |
| 75 | 0.23046 | 0.23579 |
| 100 | 0.51645 | 0.52337 |

A set of conditional capacity outage levels ($C_{2j}|\ C_{1i}$) of Site 2 is shown in Table 4.5. This table shows the conditional capacity outage levels and corresponding probabilities for Site 2 when the wind speed correlation coefficient between the two sites is 0.2.

Table 4.5: The conditional capacity outage levels and corresponding probabilities of Site 2 (Swift Current)

| $C_{2j}\|C_{1i}$(%) / $C_{1i}$ (%) | 0 | 25 | 50 | 75 | 100 |
|---|---|---|---|---|---|
| 0 | 0.16526 | 0.10382 | 0.16567 | 0.24943 | 0.31582 |
| 25 | 0.10431 | 0.08087 | 0.14611 | 0.25978 | 0.40894 |
| 50 | 0.08352 | 0.06940 | 0.13200 | 0.25437 | 0.46071 |
| 75 | 0.06491 | 0.05755 | 0.11561 | 0.24281 | 0.51912 |
| 100 | 0.04976 | 0.04653 | 0.09774 | 0.22361 | 0.58236 |

The overall wind energy conversion system consists of Sites 1 and 2. A series of overall wind energy conversion system models considering different wind speed correlation levels between the two wind farms is shown in Table 4.6. The values in Table 4.6, when Rxy=0.2, were obtained by combining the Regina site data shown in Table 4.4 with the appropriate values in Table 4.5.

Table 4.6: The COPT of the overall wind energy conversion system consisting of Sites 1 and 2 with variation in Rxy

| Capacity Outage (%) | Probability | | | |
|---|---|---|---|---|
| | Rxy=0.2 | Rxy=0.4 | Rxy=0.6 | Rxy=0.8 |
| 0 | 0.01232 | 0.02056 | 0.03059 | 0.04087 |
| 12.5 | 0.01416 | 0.01911 | 0.02395 | 0.02776 |
| 25 | 0.02710 | 0.03169 | 0.03455 | 0.03475 |
| 37.5 | 0.05066 | 0.05040 | 0.04767 | 0.04402 |
| 50 | 0.09394 | 0.07798 | 0.06613 | 0.06010 |
| 62.5 | 0.10562 | 0.09731 | 0.08990 | 0.08388 |
| 75 | 0.16033 | 0.14742 | 0.13389 | 0.12725 |
| 87.5 | 0.23512 | 0.22315 | 0.20165 | 0.16438 |
| 100 | 0.30076 | 0.33238 | 0.37165 | 0.41698 |

Table 4.6 shows that the probabilities associated with the capacity levels of the overall WECS are a function of the wind speed correlation coefficient between the two wind sites. The probabilities of the 0% and 100% capacity outage levels increase as the wind speed cross correlation coefficient increases. The overall WECS models shown in Table 4.6 can be combined with the capacity outage probabilities models for other units in the system to create an overall generating system COPT.

## 4.5. Adequacy Assessment of the RBTS Generating System Incorporating Two 20 MW Wind Farms

### 4.5.1. Analytical Method

Analytical methods represent the system by analytical models and evaluate the system risk indices from these models using mathematical solutions [9]. In this approach, the generating capacity is represented by the system COPT. The conventional units in the RBTS are represented

by two-state models. Models of the wind energy facilities consisting of two 20 MW wind farms are shown in Table 4.6. The overall generating system model was constructed using a recursive algorithm [9]. The system COPT was then combined with the load model to determine the system reliability indices. The system LOLE and LOEE are shown in Table 4.7.

Table 4.7: The system LOLE (hrs/yr) and LOEE (MWh/yr) using the analytical method

| | Original RBTS | Independent WECS Rxy=0 | Correlated WECS | | | | Completely Dependent WECS Rxy=1.0 |
|---|---|---|---|---|---|---|---|
| | | | Rxy=0.2 | Rxy=0.4 | Rxy=0.6 | Rxy=0.8 | |
| LOLE | 1.16 | 0.6306 | 0.6499 | 0.6681 | 0.6878 | 0.7057 | 0.7140 |
| LOEE | 12.00 | 6.0254 | 6.2450 | 6.4590 | 6.7011 | 6.9409 | 7.2533 |

It can be seen from Table 4.7 that the two 20 MW WECS have a significant impact on the RBTS reliability indices. The positive impact on system reliability when the degree of correlation between the wind farms decreases can also be observed.

### 4.5.2. State Sampling Method

The basic state sampling procedure is conducted assuming that the behaviour of each component can be categorized by a uniform distribution under [0, 1] and component outages are independent events [10]. The RBTS conventional units and independent WECS follow this assumption. This assumption, however, is not applicable to partially dependent WECS. The conventional generating unit states are represented by two-state models and the WECS are represented by five-state models in the following studies.

Random numbers distributed uniformly under [0, 1] are divided into two clusters in this study. Random numbers in the first cluster represent conventional units or independent WECS. Random numbers between 0 and 1 in the second cluster represent correlated WECS. The problem is to generate correlated random numbers which have a uniform distribution and specified correlations in the simulation process. Based on the basic concept of independent random numbers with a uniform distribution $(-\frac{1}{2}, \frac{1}{2})$ [65], the case of two uniform numbers X1

and X2, which have a specified correlation coefficient of R and uniform distributions, is used to illustrate the solution to this problem. The proof is as follows [62]:

*Given:*

*U1* and *U2* are independent uniform random variables on $(-\frac{1}{2},\frac{1}{2})$,

Let *X1=U1* with probability 1,

Let *X2=U1* with probability *P*, *X2=U2* with probability (1-*P*).

*Proof:*

Based on the given condition, *X1=U1*

$$X2 = I_A U1 + I_{\bar{A}} U2 \qquad I_A = \begin{cases} 1 & w \in A \\ 0 & w \in \bar{A} \end{cases}$$

$$P(A) = P$$

where *A* is a random variable vector with uniform distribution on $(-\frac{1}{2},\frac{1}{2})$.

The expected (E) values of $I_A$, *U1* and *U2* are:

$E(I_A) = P(A) = P$, and $E(U1)=E(U2)=0$

The determination of the covariance of *X1* and *X2* is as follows

$$\begin{aligned} Cov(X1, X2) &= E(X1X2) - E(X1)E(X2) \\ &= E(X1X2) \\ &= E[U1 \times (I_A U1 + I_{\bar{A}} U2)] \\ &= E(I_A U1^2) \\ &= E(I_A)E(U1^2) \\ &= PVar(U1) \end{aligned}$$

The variance of *X1*, $Var(X1) = Var(U1)$.

Then, the variance of *X2*,

$$\begin{aligned} Var(X2) &= E[(I_A U1 + I_{\bar{A}} U2)^2] \\ &= E[I_A{}^2 U1^2 + I_{\bar{A}}{}^2 U2^2 + 2 I_A I_{\bar{A}} U1U2] \\ &= E[I_A{}^2 Var(U1) + I_{\bar{A}}{}^2 Var(U2)] \\ &= Var(U1) \times [E(I_A{}^2) + E(I_{\bar{A}}{}^2)] \\ &= Var(U1) \times [E(I_A) + E(I_{\bar{A}})] \\ &= Var(U1) \end{aligned}$$

From the above, the cross-correlation coefficient *R* of *X1* and *X2*

$$R = Corr(X1, X2) = \frac{Cov(X1, X2)}{\sqrt{Var(X1)*Var(X2)}}$$
$$= \frac{P*Var(U1)}{Var(U1)}$$
$$= P$$

If *V1*, *V2* are independent uniform random variables on $(0,1)$,

Let *Y1*=*V1* with probability 1,

Let *Y2*=*V1* with probability *P*, *Y2*=*V2* with probability (1-*P*),

The cross-correlation coefficient *R* of *Y1* and *Y2* is same as that of *X1* and *X2*, that is,

$Corr(Y1, Y2) = Corr(X1, X2) = P$.

This conclusion is used in the state sampling simulation method to generate correlated random numbers which represent the correlated WECS. Two random numbers X1, X2 between 0 and 1 in the second cluster are used to represent the two correlated WECS. Assuming U1, U2 and U3 are three independent uniform random variable sets in the second cluster. U3 used to determine X2 is generated from U1 or U2. The first random vector containing X1 is generated from the first independent random number set U1 with probability of 1. The second random vector X2 is generated from U1 and U2 with probability P and (1-P) respectively by sampling a uniform distribution between 0 and 1 using the P and 1– P values.

The procedures are described as follows:

$U1=[U_{11}, U_{12}, U_{13}.... U_{1n}]$;

$U2=[U_{21}, U_{22}, U_{23}.... U_{2n}]$;

$U3=[U_{31}, U_{32}, U_{33}.... U_{3n}]$

where n is a sample number.

If $U_{3n} < P$, then $X2_n=U_{1n;}$

If $U_{3n} > P$, then $X2_n=U_{2n;}$

X2 is then generated from U1 with probability P and generated from U2 with probability 1-P.

For example: Given P=0.7

The first sample: $U_{11}$=0.13, $U_{21}$=0.75, $U_{31}$=0.45

$U_{31} < P$

then $X2_1$=0.13

The second sample: $U_{12}$=0.41, $U_{22}$=0.06, $U_{32}$=0.90

$U_{32} > P$

then $X2_2$=0.06

The MECORE program was modified based on this conclusion to generate correlated and uncorrelated random numbers in the simulation process in order to incorporate two dependent wind farms. The initial seed value for generating random numbers in the two clusters is 16807 in the modified MECORE program. This program will be used in the future studies described in this thesis.

The models shown in Table 4.4 were applied in the analyses conducted using the analytical method and therefore the five-state model of a WECS located at Site 2 and the WECS model for Site 1 shown in Table 4.4 are used in the state sampling method in order to compare the analysis results with those obtained using the analytical method. The system LOLE and LOEE of the RBTS with and without the two 20 MW WECS are shown in Table 4.8.

Table 4.8: The system LOLE and LOEE using the state sampling simulation method

| | Original RBTS | Independent WECS Rxy=0 | Correlated WECS | | | | Completely Dependent WECS Rxy=1.0 |
|---|---|---|---|---|---|---|---|
| | | | Rxy=0.2 | Rxy=0.4 | Rxy=0.6 | Rxy=0.8 | |
| LOLE | 1.17 | 0.6297 | 0.6477 | 0.6694 | 0.6810 | 0.6953 | 0.7136 |
| LOEE | 12.24 | 6.1136 | 6.2894 | 6.5709 | 6.7724 | 6.9485 | 7.2430 |

The results shown in Tables 4.7 and 4.8 using the analytical method and the state sampling method respectively are graphically portrayed in Figure 4.10.

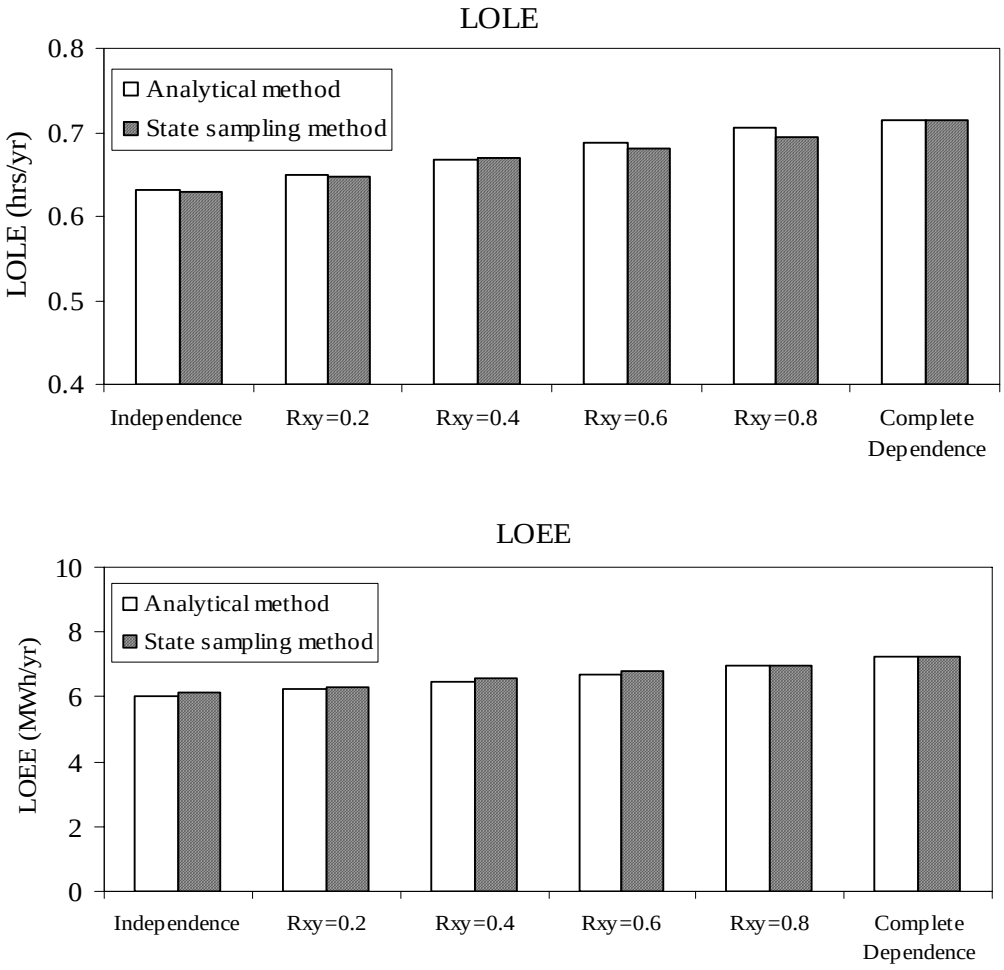


Figure 4.10: RBTS reliability indices including two 20 MW WECS with different wind speed correlation levels

The system reliability indices obtained utilizing the analytical method are considered to be the base values in this study. It can be seen from Figure 4.10 that the results calculated using the state sampling method are very close as those obtained using the analytical method. The conclusion can be drawn that the state sampling method can therefore be used in generation adequacy assessment considering wind speed correlation of WECS by generating correlated and uncorrelated random numbers in the simulation process.

### 4.5.3. Reliability Benefit Assessment of WECS

In this section, the capability of the proposed state sampling technique is presented and studies based on this method used to illustrate its application. The multi-state WECS models created for

independent wind sites can be used in the state sampling simulation method to represent WECS considering wind speed correlation between the wind farms. The five-state models for the Regina and Swift Current sites shown in Table 4.3 are used in this study.

The state sampling technique is applied to the RBTS modified by the addition of the two 20 MW WECS in order to quantitatively assess the benefit of the WECS. The system benefit in the form of the increase in peak load carrying capability (IPLCC) is used as an index to compare the adequacy effects of adding WECS to the system. The IPLCC is the increase in load carrying capability of the system attributable to the added generation (WTG) measured at the criterion reliability level [9]. The LOLE indices of the RBTS before and after adding two 20 MW WECS considering different wind speed correlation levels are shown as functions of the annual peak load in Figure 4.11. The LOLE of the RBTS with an installed capacity of 240 MW and an annual peak load of 185 MW is 1.17 hrs/yr using MECORE. The annual peak load was varied from 180 MW to 200 MW using 5 MW increments.

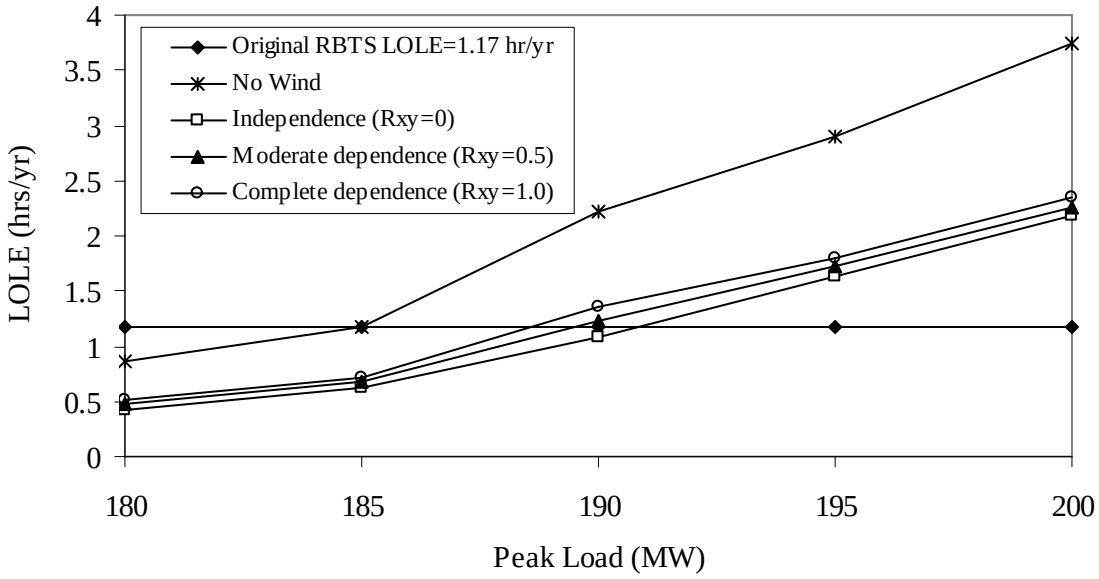


Figure 4.11: Variation in the RBTS LOLE with the degree of wind speed correlation and the annual peak load

It can be seen from Figure 4.11 that there are observable load carrying capability benefits from the WECS additions. The IPLCC increases as the wind site wind speed correlation levels

decrease. The IPLCC are approximately 5.1 MW, 4.3 MW and 3.5 MW after independent, partially dependent and totally dependent two 20 MW WECS are added to the RBTS. It should be noted that the relative reliability benefits from wind energy depend on many factors, such as the wind speed and terrain topology at the WECS sites.

### 4.5.4. Effect of the WECS Installed Capacity

The WECS installed capacity is expanded from 40 MW to 80 MW by adding 20 MW increments to the original RBTS. The wind power penetration level therefore varies from 16.7% to 33.3%. The effects on the system LOLE are illustrated in Figure 4.12 which shows the system LOLE for selected wind speed correlation levels as a function of the added wind power. The added wind power is equally divided between the two wind sites.

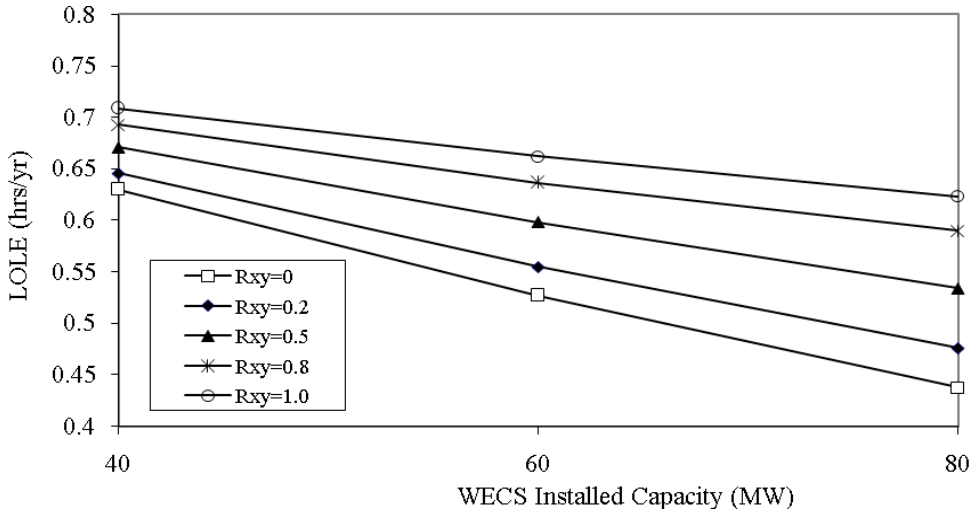


Figure 4.12: The RBTS LOLE for a peak load of 185 MW with varying WECS installed capacity and wind speed correlation level

Figure 4.12 shows that the system LOLE decreases as the WECS installed capacity increases. The benefits associated with different WECS installed capacities increase as the degree of wind speed correlation between the two wind sites decrease. The effect of the wind speed correlation level on the system reliability become more obvious as the wind penetration level increases.

Section 4.5 examines the adequacy impacts associated with adding two dependent wind energy conversion systems (WECS) to an existing generating system. The state sampling Monte Carlo

simulation method and an analytical method are applied to calculate the LOLE and LOEE reliability indices. The studies show that generating correlated random numbers with uniform distributions and a specified correlation coefficient in the state sampling method can be used to conduct adequacy assessment in power systems containing correlated WECS. This is a potentially extremely important development as it permits correlated WECS to be incorporated in large practical system studies without requiring excessive increases in computer solution time. An important benefit is that this method can also be used in bulk system reliability studies.

## 4.6. Bulk System Adequacy Assessment Incorporating Two Correlated WECS

This section presents the effects of incorporating large scale dependent wind energy facilities in bulk system adequacy evaluation using the state sampling Monte Carlo simulation technique. The wind penetration levels for the study systems are approximately 15% in these studies. The multi-state WECS models shown in Table 4.3 are used in MECORE to represent WECS. Wind speed correlation coefficients (R) of 0, 0.5 and 1.0 between the Regina and Swift Current wind sites are used to represent independent, moderately dependent and completely dependent cases respectively. Each WECS is considered to be connected to the test system through a transmission line. The assumed carrying capacity of the circuit is the installed capacity of the WECS. The impacts of wind speed correlation levels, wind farm locations and system load are examined.

### 4.6.1. Study Systems

The RBTS is shown in Figure 2.4. It is a relatively small system with some designed in weaknesses, one of which is the radial supply to Bus 6 [20, 56]. The IEEE-RTS shown in Figure 2.5 is a system with a strong transmission network and a weak generation system [21, 56]. The weaknesses of RBTS and IEEE-RTS are also illustrated by using factor analysis in this study. The analysis results of examining the reliability of the RBTS and IEEE-RTS when the generation system or the transmission system is assumed to be 100% reliable are shown in Table 4.9 and 4.10 respectively. The values designated as Generation Failures (GF) are the EENS based on outages caused only by the generation system with the transmission system 100% reliable. The values designated as Transmission Failures (TF) are based on outages caused only by the transmission system with the generation system 100% reliable.

Table 4.9: Factor analysis EENS for the RBTS

| Peak Load (MW) | System EENS (MWh/yr) | | |
|---|---|---|---|
| | GF & TF | GF | TF |
| 165 | 124.73 | 1.64 | 123.07 |
| 175 | 136.50 | 5.00 | 131.43 |
| 185 | 150.82 | 12.24 | 138.43 |
| 195 | 174.68 | 28.68 | 145.56 |
| 205 | 228.00 | 71.44 | 155.28 |

Table 4.9 shows that the reliability indices for the RBTS increase with peak load for both generation and transmission system failures. The contribution due to transmission failures, however, is much larger than that due to generation failures. The transmission failures at Bus 6 dominate the system reliability.

Table 4.10: Factor analysis EENS for the IEEE-RTS

| Peak Load (MW) | System EENS (MWh/yr) | | |
|---|---|---|---|
| | GF & TF | GF | TF |
| 2450 | 81.22 | 80.75 | 0.67 |
| 2550 | 167.82 | 167.44 | 0.70 |
| 2650 | 408.79 | 408.23 | 0.73 |
| 2750 | 767.80 | 766.99 | 0.75 |
| 2850 | 1674.80 | 1673.46 | 0.78 |
| 2950 | 2904.98 | 2903.17 | 0.81 |
| 3050 | 5808.39 | 5805.10 | 0.84 |

The weakness of the IEEE-RTS can be observed from Table 4.10 as the system reliability indices are dominated by generation system failures.

The two composite test systems, the RBTS and the IEEE-RTS, were modified to create four test systems to represent general conditions that exist in actual power systems. Factor analysis of a composite system base case is used to illustrate the modified system weaknesses.

***The Modified RBTS (MRBTS)***

The single line diagram of the MRBTS is shown in Figure 4.13. As noted previously, one RBTS weakness is the radial supply to Bus 6. The RBTS is, therefore, modified by adding a transmission line designated as Line 10 between Bus 5 and Bus 6. Line 10 has the same

parameters as Line 9. The modified system is designated as the MRBTS [66]. The MRBTS has 240 MW of installed capacity in 11 generating units, and the peak load is 185 MW.

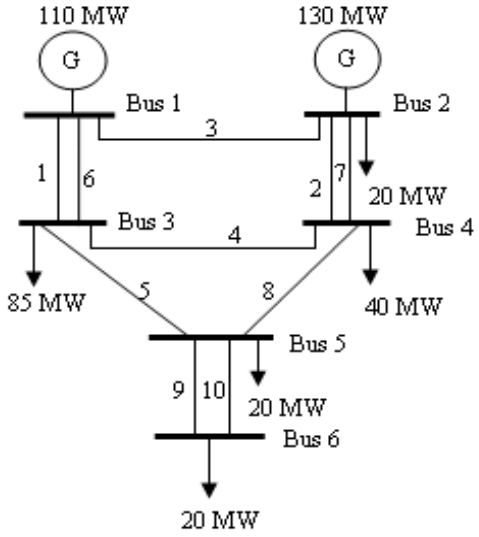


Figure 4.13: Single line diagram of the MRBTS

Figure 4.14 shows how the system EENS changes as a function of the peak load using factor analysis.

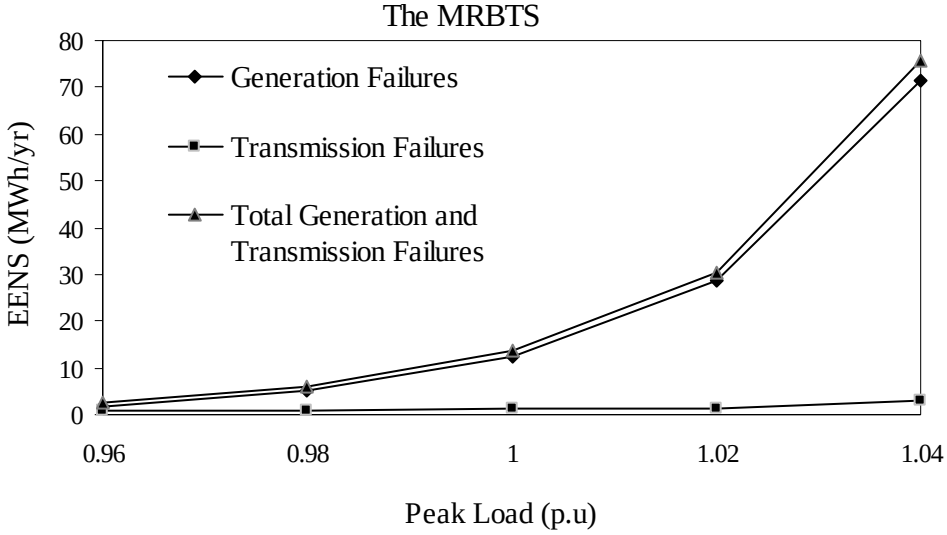


Figure 4.14: Factor analysis of the MRBTS

Figure 4.14 illustrates that the MRBTS is a relatively balanced system which has an adequate generation system and a weak transmission system. The base case MRBTS annual system and load point EENS values are shown in Table 4.11. The system EENS is dominated by the

performance at Bus 3. Load curtailment in this system is based on an outage cost priority order. Bus 3 has the lowest Interrupted Energy Assessment Rate (IEAR) and is therefore interrupted first.

Table 4.11: The system and load point EENS (MWh/yr) indices for the MRBTS

| Bus Name | Bus 3 | Bus 4 | Bus 5 | Bus 6 |
|---|---|---|---|---|
| Bus EENS | 12.566 | 0.029 | 0.293 | 0.674 |
| System EENS | 13.562 | | | |

***The Reinforced MRBTS (MRRBTS)***

The MRBTS noted above is modified as follows: The load level of all delivery points are increased to 1.3 p.u. of the original values. Two 20 MW and one 20 MW generating units are added at Bus 2 and Bus 1 respectively. The total installed generating capacity is 300 MW. The system peak load is 240 MW. The MRBTS with the above modifications is designated as the MRRBTS [66]. The single line diagram of the MRRBTS is the same as that of the MRBTS shown in Figure 4.13.

The load center of the MRRBTS is located in the southern area and the generation center is in the northern area. Figure 4.15 shows the factor analysis results for the MRRBTS.

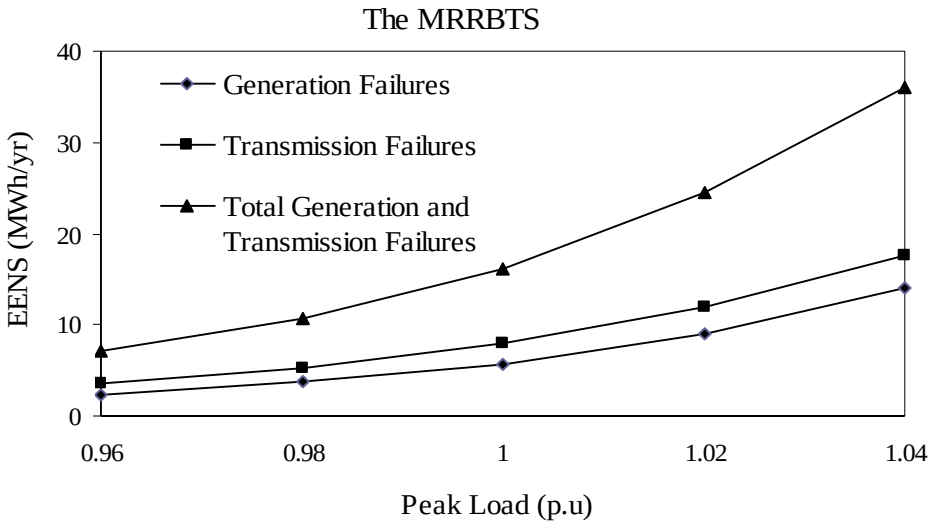


Figure 4.15: Factor analysis of the MRRBTS

It can be seen from Figure 4.15 that the MRRBTS has a strong generation system, but the system tends to be transmission weak. The annual system and load point EENS results obtained are shown in Table 4.12.

Table 4.12: The system and load point EENS (MWh/yr) indices for the MRRBTS

| Bus Name | Bus 3 | Bus 4 | Bus 5 | Bus 6 |
|---|---|---|---|---|
| Bus EENS | 15.088 | 0.020 | 0.376 | 0.713 |
| System EENS | 16.198 | | | |

***The Modified RTS (MRTS)***

The original IEEE-RTS shown in Figure 2.5 has a very strong transmission network and a weak generation system. In the studies described in this thesis, the original IEEE-RTS is modified to create a more practical system with a relatively strong transmission network and a weak generation system. The modified RTS is designated as the MRTS [66]. The total installed capacity in the RTS is 3405 MW in 32 generating units and the peak load is 2850 MW.

Two steps are used to modify the IEEE-RTS to create the MRTS:

Step 1: Generating unit modifications: The FOR of the four 20 MW units are changed from 0.1 to 0.015 and the mean time to repair (MTTR) modified from 50 to 55 hrs. The FOR of the two 400 MW units are changed from 0.12 to 0.08 and the MTTR modified from 150 to 100 hrs.

Step 2: Transmission line modifications: The lengths of all the 138 KV lines were doubled except for Line 10 which is a 25.6 km cable. The 230 KV lines were extended as follows: the lengths of lines L21, L22, L31, L38 were increased by a factor of three; the lengths of lines L18 to L20, L23, L25 to L27 were increased by a factor of four; the lengths of lines L24, L28 to L30, and L32 to L37 were increased by a factor of six. The transmission line unavailabilities are modified based on Canadian Electricity Association data [67]. The overall transmission line unavailabilities in the studies include terminal related forced outages using the data in the Appendix D.

The single diagram of the MRTS is the same as that of the IEEE-RTS shown in Figure 2.5. The total installed capacity of the MRTS is 3405 MW and the system peak load is 2850 MW. The

factor analysis of the MRTS is shown in Figure 4.16. This indicates that the MRTS is a generation deficient system. The system and load point EENS for the MRTS are shown in Table 4.13. Bus 19, Bus 9 and Bus 15 are the least reliable load points in the MRTS using the economic load curtailment policy.

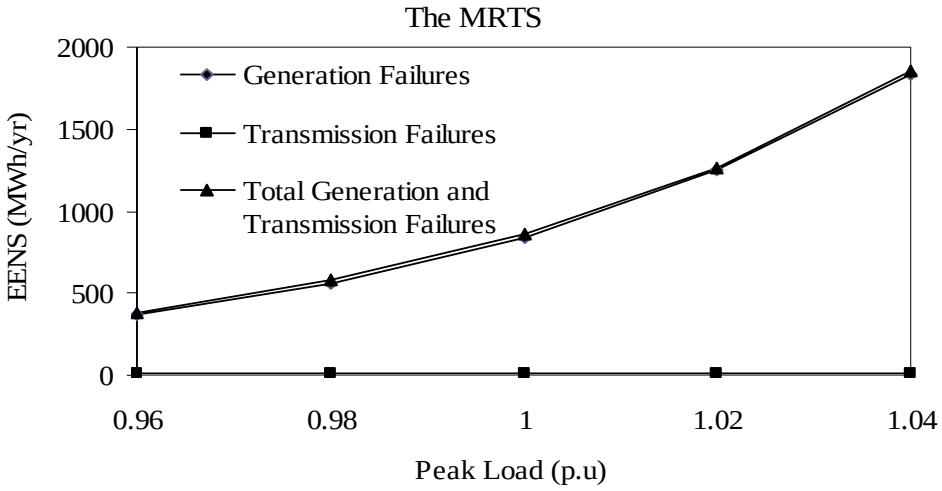


Figure 4.16: Factor analysis of the MRTS

Table 4.13: The system and load point EENS (MWh/yr) indices for the MRTS

| No. Bus | EENS |
|---|---|
| 2 | 0.067 |
| 3 | 0.034 |
| 4 | 1.703 |
| 6 | 6.257 |
| 7 | 0.092 |
| 8 | 0.448 |
| 9 | 214.888 |
| 10 | 0.513 |
| 13 | 0.003 |
| 14 | 40.246 |
| 15 | 158.024 |
| 16 | 8.912 |
| 18 | 5.672 |
| 19 | 412.935 |
| 20 | 6.716 |
| Overall System EENS = 856.509 | |

***The Modified MRTS (M1MRTS)***

The MRTS is modified to create a system designated as the M1MRTS in which there is increased utilization of the transmission network. The load levels at all the delivery points are increased to 1.5 p.u. of the original load values. The generating units are doubled at Buses 16, 18, 21, 22, 23. The rating of Line 10 is increased to 1.1 p.u. of the original rating. The total number of generating units in the M1MRTS is now 44 units. The total system capacity is 5320 MW and the peak load is 4275 MW. The single line diagram of the M1MRTS is the same as that of the IEEE-RTS and the MRTS shown in Figure 2.5.

There is significant transmission utilization in the M1MRTS as a considerable amount of power is transferred from the northern to the southern portion of the system. The factor analysis shown in Figure 4.17 illustrates that the M1MRTS is a system with a relatively strong generation system and a weak transmission network.

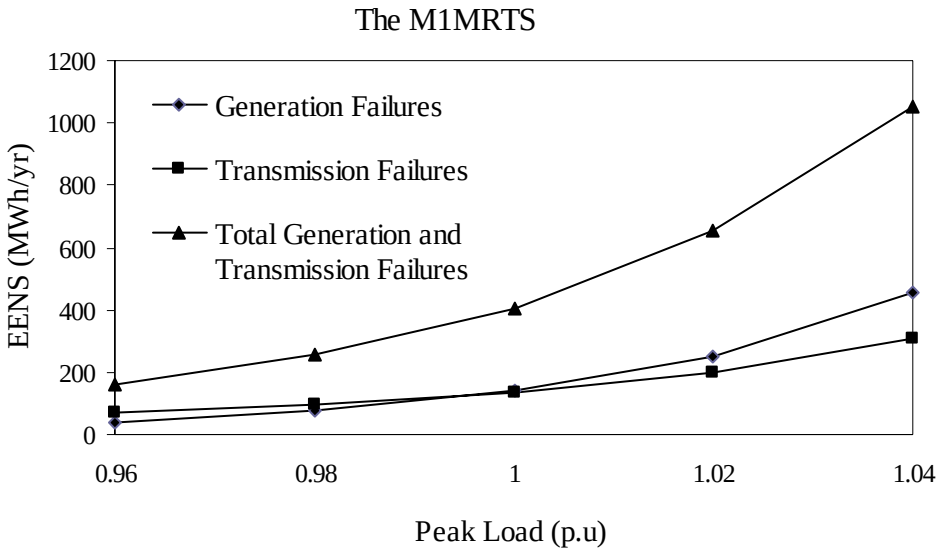


Figure 4.17: Factor analysis of the M1MRTS

The annual system and load point EENS for the M1MRTS are shown in Table 4.14. The EENS at Bus 6 increases compared to the case of the MRTS, as transmission system failures make additional contributions to the EENS at Bus 6 in the M1MRTS.

Table 4.14: The system and load point EENS (MWh/yr) indices for the M1MRTS

| No. Bus | EENS |
|---|---|
| 1 | 0.142 |
| 2 | 5.986 |
| 3 | 52.187 |
| 4 | 1.742 |
| 5 | 1.392 |
| 6 | 60.435 |
| 7 | 1.522 |
| 8 | 12.223 |
| 9 | 73.407 |
| 10 | 52.625 |
| 13 | 2.445 |
| 14 | 60.012 |
| 15 | 15.572 |
| 16 | 1.164 |
| 18 | 0.278 |
| 19 | 62.245 |
| 20 | 0.536 |
| Overall System EENS = 403.915 | |

The original RBTS and IEEE-RTS have been modified to represent conditions that exist in a wide range of practical systems. The four systems are used as basic study configurations to examine the effects of adding WECS with different degrees of correlation at different points in transmission networks. The modified RBTS designated as the MRBTS is considered to be a balanced system with acceptable generation and transmission. The modified IEEE-RTS designated as the MRTS has a strong transmission network and weak generation. The modified reinforced RBTS designated as the MRRBTS and the modified MRTS designated as the M1MRTS are composite systems with adequate generation and transmission deficiencies.

### 4.6.2. Studies on a Balanced System (the MRBTS)

The wind penetration level is 14.3% when the two 20 MW WECS are added to the MRBTS. A single transmission line with an unavailability of 0.00114 and an average repair time of 10 hrs is used to connect a WECS to a MRBTS bus. Three cases described as follows are used to illustrate the effect on the adequacy of the MRBTS of adding two WECS with different wind speed correlation levels. In the two WECS studies described in the studies described in this thesis, the

first WECS utilizes the Regina wind data and the second WECS utilizes the Swift Current wind data.

Case 1: 20 MW WECS are added at Buses 1 and 2.

Case 2: 20 MW WECS are added at Buses 3 and 5.

Case 3: 20 MW WECS are added at Buses 3 and 6.

The system EENS values are shown in Table 4.15. Table 4.16 shows the EENS at Bus 3 for the three cases with variation in the wind speed correlation between the two wind sites.

Table 4.15: The MRBTS EENS (MWh/yr) indices obtained by adding the two WECS at different locations

| Original MRBTS | | R=0 | R=0.5 | R=1.0 | The change (%) between R=0 and R=0.5 | The change (%) between R=0.5 and R=1.0 |
|---|---|---|---|---|---|---|
| 13.562 | Case 1 | 6.995 | 7.643 | 8.215 | 9.26 | 7.48 |
| | Case 2 | 6.875 | 7.444 | 7.943 | 8.28 | 6.70 |
| | Case 3 | 6.875 | 7.444 | 7.943 | 8.28 | 6.70 |

Table 4.15 shows that the system reliability is affected when the two wind farms are added at various locations in the MRBTS, but the effect is not very significant. There are 8.28% to 9.26% changes in the system EENS due to considering independence and partially dependent wind speed correlation. These changes in the system EENS are 6.70% - 7.48% when the wind speed correlation coefficient changes from 0.5 to 1.0 in the three cases.

Table 4.16: The EENS (MWh/yr) at Bus 3 indices obtained by adding the two WECS at different locations

| Original MRBTS | | R=0 | R=0.5 | R=1.0 | The change (%) between R=0 and R=0.5 | The change (%) between R=0.5 and R=1.0 |
|---|---|---|---|---|---|---|
| 12.566 | Case 1 | 6.181 | 6.806 | 7.366 | 10.11 | 8.23 |
| | Case 2 | 6.127 | 6.761 | 7.336 | 10.35 | 8.50 |
| | Case 3 | 6.127 | 6.761 | 7.336 | 10.35 | 8.50 |

Table 4.16 shows that the addition of WECS at the different locations also has a relatively small

effect on the EENS at Bus 3. The percentage changes in the EENS at Bus 3 are higher than the the percentage changes in the system EENS, that is, the reliability benefits at Bus 3 are more than the benefit to the overall system as the wind speed correlation decreases.

### 4.6.3. Studies on a Generation Deficient System (the MRTS)

Two 300 MW WECS are added through transmission lines at different buses in the southern portion (138 KV) of the MRTS. The wind penetration level is 15%. The unavailability and average repair time of the facility connection line is 0.00058 and 10 hrs respectively.

The three cases listed below and shown in Figure 4.18 are used to investigate the effects on the adequacy of the system and the load points when two wind farms with various wind speed correlations are added at different locations.

Case 1: WECS are added at Bus 1 and Bus 3.

Case 2: WECS are added at Bus 1 and Bus 4.

Case 3: WECS are added at Bus 1 and Bus 6.

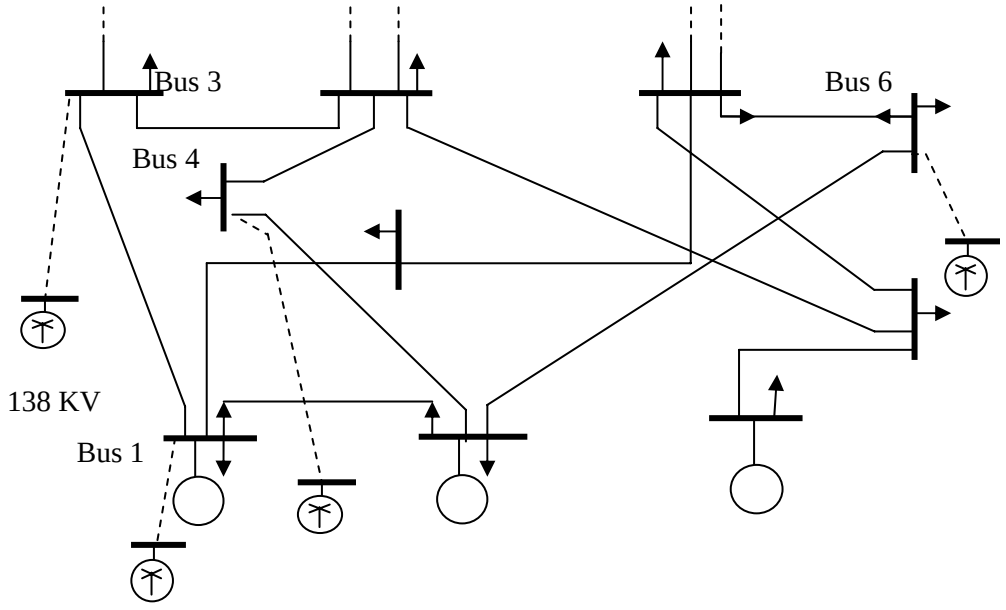


Figure 4.18: Adding the two 300 MW WECS at different locations in the MRTS

The system reliability indices for the MRTS with the two 300 MW WECS at different locations are shown in Table 4.17. Table 4.18 shows the selected load point EENS values for the three cases.

Table 4.17: The MRTS EENS (MWh/yr) indices obtained by adding the two WECS at different locations

| Original MRTS | | R=0 | R=0.5 | R=1.0 | The change (%) between R=0 and R=0.5 | The change (%) between R=0.5 and R=1.0 |
|---|---|---|---|---|---|---|
| 856.510 | Case 1 | 422.814 | 466.452 | 514.723 | 10.32 | 10.35 |
| | Case 2 | 422.227 | 465.036 | 513.344 | 10.14 | 10.39 |
| | Case 3 | 418.416 | 462.049 | 509.015 | 10.43 | 10.16 |

Table 4.18: The MRTS selected Bus EENS (MWh/yr) indices obtained by adding the two WECS at different locations

| No. Bus (Base case EENS) | | R=0 | R=0.5 | R=1.0 | The change (%) between R=0 and R=0.5 | The change (%) between R=0.5 and R=1.0 |
|---|---|---|---|---|---|---|
| Bus 19 (412.935) | Case 1 | 201.154 | 222.558 | 244.511 | 10.64 | 9.86 |
| | Case 2 | 200.506 | 222.179 | 244.330 | 10.81 | 9.97 |
| | Case 3 | 200.545 | 222.262 | 244.488 | 10.83 | 10.00 |
| Bus 9 (214.888) | Case 1 | 102.211 | 113.843 | 126.459 | 11.38 | 11.08 |
| | Case 2 | 102.831 | 114.317 | 126.823 | 11.17 | 10.94 |
| | Case 3 | 102.767 | 114.471 | 127.227 | 11.39 | 11.14 |
| Bus 15 (158.024) | Case 1 | 73.932 | 81.535 | 91.252 | 10.28 | 11.92 |
| | Case 2 | 73.852 | 81.530 | 91.266 | 10.40 | 11.94 |
| | Case 3 | 73.782 | 81.446 | 91.266 | 10.39 | 12.06 |

Tables 4.17 and 4.18 show that the system and load point EENS values are almost unchanged when the two wind farms are added at various locations in the MRTS. This is due to the fact that the MRTS has a very strong transmission network and a weak generation system. When the degree of wind speed correlation changes from low to moderate and from moderate to high, the

percentage changes in the system EENS are about 10%. The percentage changes in the EENS at Bus 19, Bus 9 and Bus 15 are similar to the the percentage changes in the system EENS.

### 4.6.4. Studies on Transmission Deficient Systems (the MRRBTS and the M1MRTS)

***The MRRBTS Analysis***

As noted earlier, the total installed generating capacity of the MRRBTS is 300 MW. In order to retain the 14.3% wind penetration level used in the MRBTS, the MRRBTS is extended by adding two 25 MW WECS. The unavailability and average repair time of the wind facility connection line is 0.00114 and 10 hrs respectively. The three cases of adding the two 25 MW WECS at various buses in the MRRBTS are the same as those used earlier in the MRBTS analysis. The system and Bus 3 EENS values when the two wind farms are added at difference locations in the MRRBTS are shown in Tables 4.19 and 4.20 respectively.

Table 4.19: The MRRBTS EENS (MWh/yr) indices obtained by adding the two WECS at different locations

| Original MRRBTS | | R=0 | R=0.5 | R=1.0 | The change (%) between R=0 and R=0.5 | The change (%) between R=0.5 and R=1.0 |
|---|---|---|---|---|---|---|
| 16.198 | Case 1 | 11.141 | 11.452 | 11.928 | 2.79 | 4.16 |
| | Case 2 | 7.183 | 8.085 | 9.224 | 12.56 | 14.09 |
| | Case 3 | 7.183 | 8.085 | 9.224 | 12.56 | 14.09 |

Table 4.20: The EENS (MWh/yr) at Bus 3 indices obtained by adding the two WECS at different locations in the MRRBTS

| No. Bus | | R=0 | R=0.5 | R=1.0 | The change (%) between R=0 and R=0.5 | The change (%) between R=0.5 and R=1.0 |
|---|---|---|---|---|---|---|
| Bus 3 | Case 1 | 10.212 | 10.523 | 10.998 | 3.05 | 4.51 |
| | Case 2 | 6.602 | 7.582 | 8.720 | 14.84 | 15.01 |
| | Case 3 | 6.602 | 7.582 | 8.720 | 14.84 | 15.01 |

Tables 4.19 and 4.20 show that connecting the two wind farms in the southern part of the MRRBTS (Cases 2 and 3) results in higher reliability improvement for the overall system and for

Bus 3 than that for the wind farms added in the northern part (Case 1). The loads are mainly concentrated in the southern part of the MRRBTS. In addition, the increased utilization of the transmission network in Case 1 causes more obvious transmission concerns than in the other cases. The percentage changes in the system and Bus 3 EENS values when the wind speed correlation coefficient varies from 0 to 0.5, or from 0.5 to 1.0 are much higher in Cases 2 and 3 than when the two wind farms are located at the north (Case 1). The reliability benefits to the system and Bus 3 are relatively insignificant in Case 1 as the degree of wind speed correlation decreases. The system and load point reliability indices, and the reliability benefits due to having a low degree of wind speed correlation are highly influenced by connecting the WECS at different locations in the MRRBTS.

***The M1MRTS analysis***

The M1MRTS installed generating capacity is 5320 MW. The system wind penetration level is 15% with the addition of 940 MW WECS. The unavailability and average repair time of the wind facility connection line is 0.00058 and 10 hrs respectively. The locations of the two 470 MW WECS at various buses in the M1MRTS are the same as in the three cases described earlier and shown in Figure 4.18. The system and selected load point reliability indices for the M1MRTS with the two WECS at different locations are shown in Tables 4.21 and 4.22 respectively.

Table 4.21: The M1MRTS EENS (MWh/yr) indices obtained by adding the two WECS at different locations

| Original M1MRTS | | R=0 | R=0.5 | R=1.0 | The change (%) between R=0 and R=0.5 | The change (%) between R=0.5 and R=1.0 |
|---|---|---|---|---|---|---|
| 403.915 | Case 1 | 220.705 | 243.605 | 266.144 | 10.38 | 9.25 |
| | Case 2 | 213.107 | 238.304 | 262.246 | 11.82 | 10.05 |
| | Case 3 | 195.156 | 222.062 | 240.835 | 13.79 | 8.45 |

Table 4.21 shows that the different WECS locations have different impacts on system reliability improvement in the M1MRTS.

Table 4.22: The M1MRTS selected load bus EENS (MWh/yr) indices obtained by adding the two WECS at different locations

| No. Bus (Base case EENS) | | R=0 | R=0.5 | R=1.0 | The change (%) between R=0 and R=0.5 | The change (%) between R=0.5 and R=1.0 |
|---|---|---|---|---|---|---|
| Bus 19 (62.245) | Case 1 | 27.176 | 31.021 | 35.197 | 14.15 | 13.46 |
| | Case 2 | 27.277 | 31.116 | 35.239 | 14.07 | 13.25 |
| | Case 3 | 27.626 | 31.280 | 35.225 | 13.23 | 12.61 |
| Bus 9 (73.407) | Case 1 | 30.360 | 34.819 | 39.725 | 14.69 | 14.09 |
| | Case 2 | 28.097 | 33.563 | 39.171 | 19.45 | 16.71 |
| | Case 3 | 29.085 | 34.636 | 40.967 | 19.09 | 18.28 |
| Bus 6 (60.435) | Case 1 | 57.055 | 57.537 | 58.084 | 0.84 | 0.95 |
| | Case 2 | 56.334 | 56.818 | 57.287 | 0.86 | 0.83 |
| | Case 3 | 28.491 | 29.599 | 29.648 | 3.89 | 0.16 |

It can be seen from Table 4.22 that the reliability indices at Bus 19 are slightly impacted by the WECS location as the indices at this bus are dominated by generation failures. The effect of wind speed correlation at Buses 19 and 9 indices are higher than those in the overall system. The effect of wind speed correlation on the EENS at Bus 6, however, is insignificant as the reliability indices at Bus 6 are dominated by connected transmission lines failures. There are higher reliability benefits at Bus 6 when a WECS is connected to Bus 6 in Case 3 than in the other cases. The impacts of wind speed correlation on the system reliability indices and on the load point indices in the M1MRTS are obviously different. These impacts are very dependent on the transmission network topology.

Studies conducted on the two transmission deficient systems show that the effects of wind speed correlation on the system and load point reliability indices are significantly influenced by connecting the WECS at different locations in a system. The MRRBTS system reliability indices are dominated by the Bus 3 indices due to the economic load curtailment policy and therefore the reliability impact of adding the two WECS on the overall system are similar to those at Bus 3. The M1MRTS system reliability indices are not dominated by the values at a single bus, and therefore the reliability impacts of wind speed correlation on the system reliability indices are not similar to those on a single load point. The reliability benefits at a load point considering a low wind speed correlation are very dependent on the factors that cause load point failure. Bus 19 has

the lowest curtailment priority in the M1MRTS and the reliability indices at Bus 19 are dominated by generation failures. Although Bus 6 has a higher priority, failures at Bus 6 are dominated by connected transmission line failures. The reliability improvements at Bus 19, therefore, are higher than those at Bus 6 with decrease in wind speed correlation.

## 4.7. Conclusions

A genetic algorithm method is used to adjust the ARMA models to simulate hourly wind speeds based on the degree of wind speed correlation between the wind sites. The studies show that generating correlated random numbers with uniform distributions and a specified correlation coefficient in the state sampling method can be used to conduct adequacy assessment in power systems containing correlated WECS. The multi-state WECS models created for independent wind sites can be used in the state sampling simulation method to represent WECS considering wind speed correlation between the wind farms.

A series of analyses using the state sampling Monte Carlo simulation method was conducted on the RBTS generating system incorporating WECS with different wind speed correlations. The studies show the system reliability benefits increase as the degree of wind speed correlation between the two wind sites decrease. The effect of the wind speed correlation level on the system reliability for the RBTS generating system become more obvious as the wind penetration level increases.

This chapter presents quantitative reliability results for bulk systems incorporating large-scale wind energy facilities considering wind speed correlation. There are obvious reliability improvements when the four developed systems are augmented with WECS at a 14-15% wind penetration level. The degree of wind speed correlation affects the system and load point reliability indices. This effect, however, is very dependent on the system conditions. In a generation deficient system, portrayed by the MRTS, the percentage changes in the system EENS and the less reliable load points when the correlation coefficient changes from 0 to 0.5, or from 0.5 to 1.0, are about 10% no matter where the two WECS are located in the system. In a balanced system, portrayed by the MRBTS, the system and load point reliability indices are

affected when the two wind farms are added at various locations in the system, but the effect is not very significant. There are 6-10% changes in the system EENS due to considering independent, partially dependent and totally dependent wind speeds.

Transmission deficient environments were created in both the MRRBTS and the M1MRTS by increasing the system load in each system and the generating capacity. The studies conducted on the MRRBTS and the M1MRTS show that the system and load point reliability improvements are significantly influenced by connecting the WECS at different locations in a transmission deficient system. When the wind speed correlation level varies from independent to moderately dependent, there is less than a 3% change in the system EENS when the WECS are located in transmission weak areas in the MRRBTS. In other cases, the percentage changes in the system EENS are higher than 12%. The studies on the M1MRTS show that the impacts of wind speed correlation on the system reliability indices and on the load point indices are different. In the M1MRTS, the EENS has about a 10% change when the correlation coefficient varies from 0 to 0.5. Under these conditions, the percentage change in the EENS at Bus 19 is up to 14% and at Bus 6 is less than 1%. The effects of wind speed correlation on system and load point reliability are dependent on the transmission network topology.

The actual numerical values in these studies of the representative test systems are obviously system dependent. The studies illustrate, however, that it is possible to quantitatively assess the reliability implications associated with adding WECS to a bulk system including the effects of multiple correlated wind sites. The methods and study results presented in this chapter should assist system planners and operators to evaluate the reliability benefits of adding wind power to their systems.

# 5. Wind Integrated Bulk System Adequacy Assessment Considering Wind Energy Seasonal Characteristics

## 5.1. Introduction

Seasonal variations in the speed and direction of the wind result from seasonal changes in the relative inclination of the earth towards the sun. In general, monthly and seasonal variations have a significant effect on wind power plant performance. The detailed performances of the seasonal wind characteristics at specific regions have been investigated and the wind energy resource assessed for these areas in [68-70]. The effects of period wind power output and load demand on the adequacy assessment of the RBTS and the IEEE-RTS are investigated in this chapter. The ability to utilize period wind capacity and load models in bulk system adequacy assessment is examined. The effects of seasonal wind speed cross-correlation are also considered. Regina and Swift Current wind speed data are used in the studies presented in this chapter.

## 5.2. Actual Wind Speeds for the Two Sites

Hourly wind speed time data from 1996-2003 (8 year series) for Regina and Swift Current wind sites can be found in the National Climate Data and Information Archive on the Environment Canada web site [71]. Monthly mean wind speed variations for the overall period and for two individual years are shown in Figure 5.1.

Figure 5.1 shows that the monthly wind speed variations for the individual years are different. In general, higher monthly wind speeds occur in winter and lower monthly wind speeds occur in summer. In this chapter, it is assumed that a year consists of two seasons: summer and winter. Summer runs from April to September and contains 4392 hours, and winter consists of two parts: January to March, and October to December. The total number of hours in winter is 4368 hours.The actual wind speed correlation between the Regina and Swift Current sites was calculated using the basic cross-correlation coefficient and 8 years of hourly wind speed data.

The annual wind speed correlation coefficient (R) between the two sites is 0.48. R values of 0.5 and 0.47 respectively obtained using the summer and winter hourly wind speed data indicate that seasonal wind speeds between the two sites are moderately correlated. A wind speed correlation coefficient of 0.5 is, therefore, used in the studies described in this chapter.

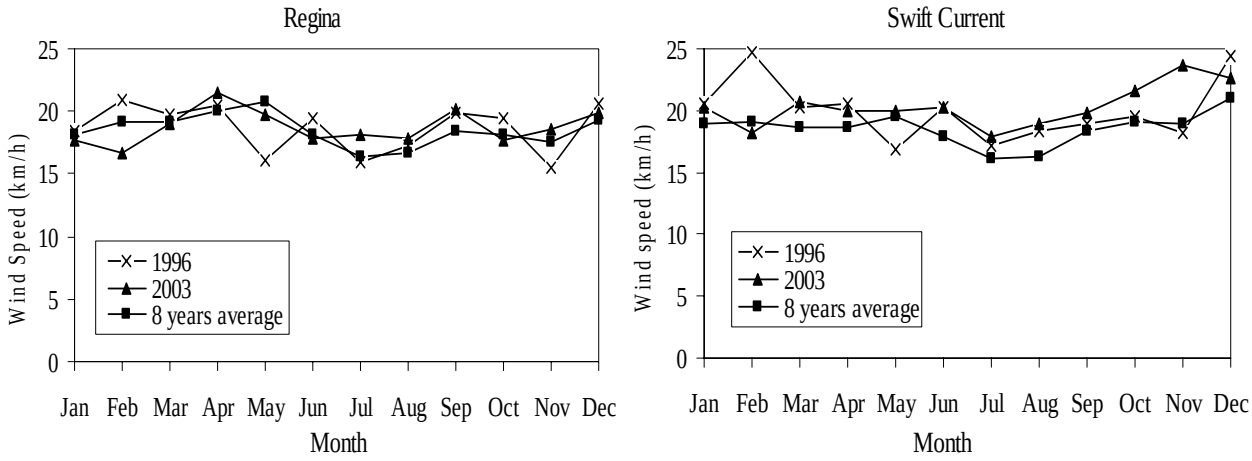


Figure 5.1: Monthly mean wind speeds for two specific years and for an eight year period for the two wind sites

## 5.3. Period WECS Models for the Two Sites

### 5.3.1. Period Wind Speed Models

The hourly wind speed time data from 1996-2003 (8 year series) obtained from Environment Canada were used to develop period ARMA models. Hourly wind speed data from 1984-2003 (20 years) at the Regina and Swift Current wind sites were used to calculated the period hourly mean speed and standard deviation. Reference 52 developed the Swift Current ARMA model using the ARMASA Toolbox [72-74] associated with the System Identification Toolbox [75] in the MATLAB program. The ARMASA Toolbox is also used in this study to develop the period ARMA(n, n-1) models for the two wind sites. In the ARMASA Toolbox, the function of SIG2ARMA is used to estimate autoregressive moving average models from the input data (wind speed data) and select a model with optimal predictive qualities. The Ljung-Box Q-statistic test and P-value are calculated to test if a time-series is independently distributed [73]. The time series are considered in this study to be independent if the P-value is greater than 0.01.

**Annual Wind Speed Models**

The annual ARMA models for the Regina and Swift Current sites are given in (5. 1) and (5. 2).

Regina: ARMA (4, 3)

$$y_t = 1.0144\, y_{t-1} + 0.3494\, y_{t-2} - 0.4485\, y_{t-3} + 0.0351\, y_{t-4} + \alpha_t - 0.3299\, \alpha_{t-1} - 0.4198\, \alpha_{t-2} + 0.1622\, \alpha_{t-3} \quad (5.1)$$

$$\alpha_t \in NID(0, 0.492112^2)$$

Swift Current: ARMA (4, 3)

$$y_t = 1.1772\, y_{t-1} + 0.1001\, y_{t-2} - 0.3572\, y_{t-3} + 0.0379\, y_{t-4} + \alpha_t - 0.5030\, \alpha_{t-1} - 0.2924\, \alpha_{t-2} + 0.1317\, \alpha_{t-3} \quad (5.2)$$

$$\alpha_t \in NID(0, 0.524760^2)$$

It should be noted that the wind speed model for the Regina wind site shown in Equation 5.1 is different from that developed in [46] due to using hourly wind speed data for different years. The ARMA model for the Swift Current site shown in Equation 5.2 is the same as that developed in [52].

**Seasonal Wind Speed Models**

The seasonal ARMA models for the two sites are as follows. Summer runs from April to September and winter is from October to March.

Regina: Summer ARMA (4, 3)

$$y_t = 0.5322\, y_{t-1} + 0.4600\, y_{t-2} - 0.1264\, y_{t-3} + 0.0116\, y_{t-4} + \alpha_t + 0.1089\, \alpha_{t-1} - 0.2290\, \alpha_{t-2} + 0.0534\, \alpha_{t-3} \quad (5.3)$$

$$\alpha_t \in NID(0, 0.534785^2)$$

Regina: Winter ARMA (4, 3)

$$y_t = 1.1946\, y_{t-1} + 0.0605\, y_{t-2} - 0.3644\, y_{t-3} + 0.0625\, y_{t-4} + \alpha_t - 0.4526\, \alpha_{t-1} - 0.2551\, \alpha_{t-2} + 0.1501\, \alpha_{t-3} \quad (5.4)$$

$$\alpha_t \in NID(0, 0.445096^2)$$

Swift Current: Summer ARMA (4, 3):

$$y_t = 1.4469\, y_{t-1} - 0.9768\, y_{t-2} + 0.4537\, y_{t-3} - 0.0199\, y_{t-4} + \alpha_t - 0.7964\, \alpha_{t-1} + 0.5947\, \alpha_{t-2} - 0.1313\, \alpha_{t-3} \quad (5.5)$$

$$\alpha_t \in NID(0, 0.565728^2)$$

Swift Current: Winter ARMA (4, 3):

$$y_t = 0.9534\, y_{t-1} + 0.2793\, y_{t-2} - 0.3237\, y_{t-3} + 0.0307\, y_{t-4} + \alpha_t - 0.2519\, \alpha_{t-1} - 0.2969\, \alpha_{t-2} + 0.1195\, \alpha_{t-3} \quad (5.6)$$

$$\alpha_t \in NID\,(0, 0.479435^2)$$

**Monthly Wind Speed Models**

The hourly wind speed data from 1996 to 2003 were used to build monthly wind speed models. The monthly ARMA (4, 3) models using Swift Current data are shown in (5.7) to (5.18). These wind speed models are used to simulated period hourly wind speeds and create WECS models for monthly period reliability analysis at HL-I.

January:

$$y_t = 0.6446\, y_{t-1} + 0.4154\, y_{t-2} - 0.2287\, y_{t-3} + 0.0742\, y_{t-4} + \alpha_t + 0.0477\, \alpha_{t-1} - 0.2364\, \alpha_{t-2} + 0.1439\, \alpha_{t-3} \quad (5.7)$$

$$\alpha_t \in NID\,(0, 0.481769^2)$$

February:

$$y_t = 1.0482\, y_{t-1} + 0.0174\, y_{t-2} - 0.2688\, y_{t-3} + 0.1305\, y_{t-4} + \alpha_t - 0.3396\, \alpha_{t-1} - 0.1303\, \alpha_{t-2} + 0.1909\, \alpha_{t-3} \quad (5.8)$$

$$\alpha_t \in NID\,(0, 0.468049^2)$$

March:

$$y_t = 0.9278\, y_{t-1} + 0.1896\, y_{t-2} - 0.1486\, y_{t-3} - 0.0389\, y_{t-4} + \alpha_t - 0.1795\, \alpha_{t-1} - 0.1725\, \alpha_{t-2} + 0.0214\, \alpha_{t-3} \quad (5.9)$$

$$\alpha_t \in NID\,(0, 0.478180^2)$$

April:

$$y_t = 0.8428\, y_{t-1} - 0.0145\, y_{t-2} + 0.1777\, y_{t-3} - 0.0933\, y_{t-4} + \alpha_t - 0.1322\, \alpha_{t-1} + 0.0567\, \alpha_{t-2} - 0.1367\, \alpha_{t-3} \quad (5.10)$$

$$\alpha_t \in NID\,(0, 0.499477^2)$$

May:

$$y_t = 0.3662\, y_{t-1} + 0.1057\, y_{t-2} + 0.3433\, y_{t-3} - 0.0052\, y_{t-4} + \alpha_t + 0.3021\, \alpha_{t-1} + 0.2376\, \alpha_{t-2} - 0.1047\, \alpha_{t-3} \quad (5.11)$$

$$\alpha_t \in NID\,(0, 0.541976^2)$$

June:

$$y_t = 0.9984\, y_{t-1} + 0.0102\, y_{t-2} - 0.1892\, y_{t-3} + 0.0831\, y_{t-4} + \alpha_t - 0.3878\, \alpha_{t-1} - 0.1056\, \alpha_{t-2} + 0.1351\, \alpha_{t-3} \quad (5.12)$$

$$\alpha_t \in NID\,(0, 0.574636^2)$$

July:
$$y_t = 0.5714\ y_{t-1} + 0.2381\ y_{t-2} - 0.040\ y_{t-3} + 0.0632\ y_{t-4} + \alpha_t + 0.070\ \alpha_{t-1} - 0.0879\ \alpha_{t-2} + 0.0395\ \alpha_{t-3} \quad (5.13)$$
$$\alpha_t \in NID\ (0, 0.609286^{\ 2})$$

August:
$$y_t = 0.4104\ y_{t-1} + 0.4112\ y_{t-2} - 0.0098\ y_{t-3} - 0.0042\ y_{t-4} + \alpha_t + 0.2101\ \alpha_{t-1} - 0.1521\ \alpha_{t-2} - 0.0075\ \alpha_{t-3} \quad (5.14)$$
$$\alpha_t \in NID\ (0, 0.611003^{\ 2})$$

September:
$$y_t = -0.0228\ y_{t-1} + 0.4100\ y_{t-2} + 0.3956\ y_{t-3} - 0.0355\ y_{t-4} + \alpha_t + 0.6882\ \alpha_{t-1} + 0.2293\ \alpha_{t-2} - 0.1062\ \alpha_{t-3} \quad (5.15)$$
$$\alpha_t \in NID\ (0, 0.550853^{\ 2})$$

October:
$$y_t = 0.7581\ y_{t-1} - 0.0266\ y_{t-2} + 0.2245\ y_{t-3} - 0.0760\ y_{t-4} + \alpha_t - 0.0661\ \alpha_{t-1} + 0.1327\ \alpha_{t-2} - 0.0830\ \alpha_{t-3} \quad (5.16)$$
$$\alpha_t \in NID\ (0, 0.504692^{\ 2})$$

November:
$$y_t = 0.4284\ y_{t-1} + 0.7649\ y_{t-2} - 0.2540\ y_{t-3} - 0.0323\ y_{t-4} + \alpha_t + 0.2521\ \alpha_{t-1} - 0.4164\ \alpha_{t-2} + 0.0542\ \alpha_{t-3} \quad (5.17)$$
$$\alpha_t \in NID\ (0, 0.474193^{\ 2})$$

December:
$$y_t = 1.2048\ y_{t-1} - 0.6442\ y_{t-2} + 0.2345\ y_{t-3} + 0.0996\ y_{t-4} + \alpha_t - 0.5021\ \alpha_{t-1} + 0.4733\ \alpha_{t-2} + 0.0154\ \alpha_{t-3} \quad (5.18)$$
$$\alpha_t \in NID\ (0, 0.477504^{\ 2})$$

The average wind speeds in July and December for the Regina wind sites as shown in Figure 5.1 are the lowest and highest respectively. The wind speed data in July and December were, therefore, used to create monthly ARMA models. The July and December ARMA models are shown in Equations 5.19 and 5.20 respectively.

July:
$$y_t = 0.6083\ y_{t-1} + 0.1261\ y_{t-2} + 0.0470\ y_{t-3} + 0.0470\ y_{t-4} + \alpha_t + 0.0215\ \alpha_{t-1} + 0.0172\ \alpha_{t-2} + 0.0213\ \alpha_{t-3} \quad (5.19)$$
$$\alpha_t \in NID\ (0, 0.578970^{\ 2})$$

December:
$$y_t = 0.5599\ y_{t-1} + 0.3660\ y_{t-2} - 0.1328\ y_{t-3} + 0.0793\ y_{t-4} + \alpha_t + 0.1856\ \alpha_{t-1} - 0.0600\ \alpha_{t-2} + 0.1487\ \alpha_{t-3} \quad (5.20)$$
$$\alpha_t \in NID\ (0, 0.440162^{\ 2})$$

### 5.3.2. Period WECS Models

The developed ARMA models and the functional relationship between the power output of the WTG and the wind speed are used to create the wind power output models. The WTG units used in the studies are assumed to have a rated capacity of 2 MW, and cut-in, rated, and cut-out speeds of 14.4, 36 and 80 km/h, respectively. The WECS consists of identical WTG units with zero forced outage rate. Five-state WECS models for the Regina and Swift Current sites were created using the approach described in [47] and 8,000 simulated years of Regina and Swift Current hourly data. The annual and seasonal five-state models for the two sites are shown in Tables 5.1 and 5.2 respectively.

Table 5.1: The annual and seasonal WECS five-state models - Regina site

| | Annual | Summer | Winter |
|---|---|---|---|
| Average wind speed (km/h) | 19.66 | 19.18 | 20.13 |
| Capacity Outage (%) | Probability | Probability | Probability |
| 0 | 0.09521 | 0.08682 | 0.10305 |
| 25 | 0.06570 | 0.06062 | 0.07075 |
| 50 | 0.11635 | 0.11030 | 0.12260 |
| 75 | 0.21913 | 0.21728 | 0.22114 |
| 100 | 0.50361 | 0.52498 | 0.48246 |

Table 5.2: The annual and seasonal WECS five-state models - Swift Current site

| | Annual | Summer | Winter |
|---|---|---|---|
| Average wind speed (km/h) | 19.52 | 18.35 | 20.70 |
| Capacity Outage (%) | Probability | Probability | Probability |
| 0 | 0.07021 | 0.05446 | 0.08558 |
| 25 | 0.05944 | 0.04771 | 0.07093 |
| 50 | 0.11688 | 0.09960 | 0.13380 |
| 75 | 0.24450 | 0.23418 | 0.25463 |
| 100 | 0.50897 | 0.56405 | 0.45506 |

It can be seen from Tables 5.1 and 5.2 that although the average winter wind speed is higher than that in summer at the Regina and Swift Current sites, the WECS models at these locations have similar general characteristics for the winter and summer periods. The probabilities of having higher capacity levels in the WECS seasonal multi-state capacity models increase as the average wind speeds increase in the winter period. The probabilities of having no WECS capacity increase with the lower average wind speeds in the summer period.

The monthly WECS models for July and December with Regina data are shown in Table 5.3. The monthly WECS model with Swift Current data are shown in Table 5.4.

Table 5.3: The monthly WECS five-state models - Regina Site

| | July | December |
|---|---|---|
| Average wind speed (km/h) | 16.96 | 20.12 |
| Capacity Outage (%) | Probability | Probability |
| 0 | 0.04326 | 0.108469 |
| 25 | 0.04191 | 0.071965 |
| 50 | 0.08958 | 0.121907 |
| 75 | 0.21303 | 0.215334 |
| 100 | 0.61222 | 0.482325 |

Table 5.4: The monthly WECS five-state models – Swift Current site

| | January | February | March | April |
|---|---|---|---|---|
| Average wind speed (km/h) | 21.85 | 20.86 | 19.51 | 19.67 |
| Capacity Outage (%) | Prob. | Prob. | Prob. | Prob. |
| 0 | 0.11512 | 0.08560 | 0.07512 | 0.07718 |
| 25 | 0.08373 | 0.07425 | 0.06149 | 0.06104 |
| 50 | 0.14487 | 0.13976 | 0.11873 | 0.11756 |
| 75 | 0.24588 | 0.25751 | 0.23916 | 0.24043 |
| 100 | 0.41040 | 0.44288 | 0.50550 | 0.50379 |
| | May | June | July | August |
| Average wind speed (km/h) | 20.27 | 18.96 | 16.39 | 16.73 |
| Capacity Outage (%) | Prob. | Prob. | Prob. | Prob. |
| 0 | 0.08898 | 0.05887 | 0.03003 | 0.02658 |
| 25 | 0.06557 | 0.05354 | 0.03165 | 0.03002 |
| 50 | 0.12231 | 0.11024 | 0.07530 | 0.07515 |
| 75 | 0.24196 | 0.24508 | 0.21263 | 0.22570 |
| 100 | 0.48118 | 0.53227 | 0.65039 | 0.64255 |
| | September | October | November | December |
| Average wind speed (km/h) | 18.22 | 20.08 | 19.94 | 22.05 |
| Capacity Outage (%) | Prob. | Prob. | Prob. | Prob. |
| 0 | 0.04753 | 0.07505 | 0.05971 | 0.10318 |
| 25 | 0.04557 | 0.06045 | 0.06155 | 0.08465 |
| 50 | 0.09896 | 0.12003 | 0.12894 | 0.15300 |
| 75 | 0.24058 | 0.25553 | 0.26843 | 0.26443 |
| 100 | 0.56736 | 0.48894 | 0.48137 | 0.39474 |

Tables 5.3 and 5.4 reflect the monthly variability in the Regina and Swift Current wind speed profiles.

### 5.3.3. RBTS Generating Capacity System Analysis Using the Period WECS Models

The effects of period WECS and load models on the system reliability indices for the RBTS at HL-I are illustrated in this section using the analytical method. The chronological hourly load values for the IEEE-RTS [9, 10] are used in this study. A 40 MW WECS with the three Swift Current models shown in Table 5.2 is used to investigate the difference in the system LOLE and LOEE between using seasonal WECS and load models and annual models in an RBTS analysis. These system risk indices are shown in Table 5.5.

Table 5.5: HL-I indices for the RBTS with a 40 MW WECS using Swift Current data and the analytical method

| WECS Model | LOLE (hrs/yr) | LOEE (MWh/yr) |
|---|---|---|
| Annual | 0.7798 | 6.9562 |
| Winter (4368 hrs) | 0.5732 | 5.1364 |
| Summer (4392 hrs) | 0.1900 | 1.6511 |
| Summation of winter and summer | 0.7632 | 6.7875 |

Table 5.5 shows that the risk indices decrease slightly when using two seasonal periods rather than a single annual period.

The monthly system reliability indices obtained using the models shown in Table 5.4 and the analytical method are shown in Table 5.6. This table shows that the maximum system risk occurs in December during the winter period. The highest mean hourly wind speeds for the Swift Current site also occur in the winter period with the highest values in the month of December. A comparison of Table 5.5 with Table 5.6 shows that the annual wind and load models provide the highest estimate of the annual reliability indices followed by the seasonal model analysis value. When monthly periods are used, the system risk indices decrease further due to the increased recognition of the correlation between the chronological load profile and the wind speed.

Table 5.6: HL-I adequacy indices for the each month using the analytical method

| | LOLE (hrs/yr) | LOEE (MWh/yr) |
|---|---|---|
| January | 0.0550 | 0.5105 |
| February | 0.0183 | 0.1591 |
| March | 0.0029 | 0.0208 |
| April | 0.0087 | 0.0781 |
| May | 0.0470 | 0.4242 |
| June | 0.0850 | 0.7319 |
| July | 0.0320 | 0.2745 |
| August | 0.0076 | 0.0617 |
| September | 0.0040 | 0.0302 |
| October | 0.0180 | 0.1603 |
| November | 0.1226 | 1.0101 |
| December | 0.3337 | 3.0375 |
| Summation of monthly result | 0.7348 | 6.4989 |

The correlation between the chronological load profile and the wind speed at the WECS location is not retained in most analytical techniques or in a state sampling Monte Carlo approach and therefore load and wind correlation is not inherently incorporated in analyses conducted using these methods. The research described in this section shows that studies can be done using period analysis, i.e. seasonal periods or monthly periods, and the annual risk obtained by summing the period risks. This is the basic approach used in conventional generating capacity evaluation to include scheduled maintenance considerations and can also be used in bulk system analysis.

## 5.4. Bulk System Analysis Using Period WECS and Load Models

The effects of using seasonal and monthly WECS and load models on the system reliability indices for the RBTS and IEEE-RTS are illustrated in this section. The load duration curve (LDC) on an annual basis (8760 hours) is created by arranging the hourly load values for the IEEE-RTS in descending order. A similar procedure was used to create LDC for summer (4392) and winter (4368) period. These seasonal LDC are designated as SLDC, and WLDC. The MECORE software uses a stepped LDC representation in the analysis. The annual and period LDC are divided into the twenty non-uniform load steps shown in Table 5.7. Table 5.7 shows that the highest load level in summer is 92% of the system peak load.

Table 5.7: The IEEE-RTS annual and seasonal LDC

| Level (%) | Probability | | |
|---|---|---|---|
| | Annual | Summer | Winter |
| 1.00 | 0.00023 | 0 | 0.00046 |
| 0.99 | 0.00011 | 0 | 0.00023 |
| 0.98 | 0.00057 | 0 | 0.00114 |
| 0.97 | 0.00171 | 0 | 0.00343 |
| 0.95 | 0.00171 | 0 | 0.00343 |
| 0.93 | 0.00331 | 0 | 0.00664 |
| 0.92 | 0.00616 | 0.00068 | 0.01168 |
| 0.90 | 0.00970 | 0.00296 | 0.01648 |
| 0.88 | 0.01153 | 0.00615 | 0.01694 |
| 0.86 | 0.0161 | 0.01207 | 0.02015 |
| 0.85 | 0.02363 | 0.01776 | 0.02953 |
| 0.83 | 0.02546 | 0.02231 | 0.02862 |
| 0.81 | 0.02386 | 0.02163 | 0.02610 |
| 0.80 | 0.03311 | 0.02846 | 0.03777 |
| 0.78 | 0.03459 | 0.03666 | 0.03251 |
| 0.76 | 0.01632 | 0.01753 | 0.01511 |
| 0.75 | 0.08219 | 0.09358 | 0.07074 |
| 0.70 | 0.23162 | 0.23452 | 0.22871 |
| 0.60 | 0.21553 | 0.19854 | 0.23260 |
| 0.50 | 0.26256 | 0.30715 | 0.21772 |

The period WECS multi-state models shown in Tables 5.1 to 5.4 are used in the RBTS and IEEE-RTS analyses. In the first case a single WECS is installed in each system. Two WECS with identical installed capacity are installed in the systems in the second case and wind speed cross-correlation between the two wind sites is considered. As noted earlier, a wind speed correlation coefficient of 0.5 between the two wind sites is used as both the annual and period wind speeds between the two sites are moderately correlated.

### 5.4.1. RBTS System Analysis

**RBTS with a Single WECS**

A single 40 MW WECS with data from the Swift Current site was added at Bus 3 since Bus 3 has the lowest IEAR value and the largest load. The differences in the system EENS obtained using annual, seasonal and monthly WECS and load models are investigated. The monthly

system EENS for the RBTS associated with a single 40 MW WECS obtained using monthly WECS models with monthly LDC are shown in Figure 5.2.

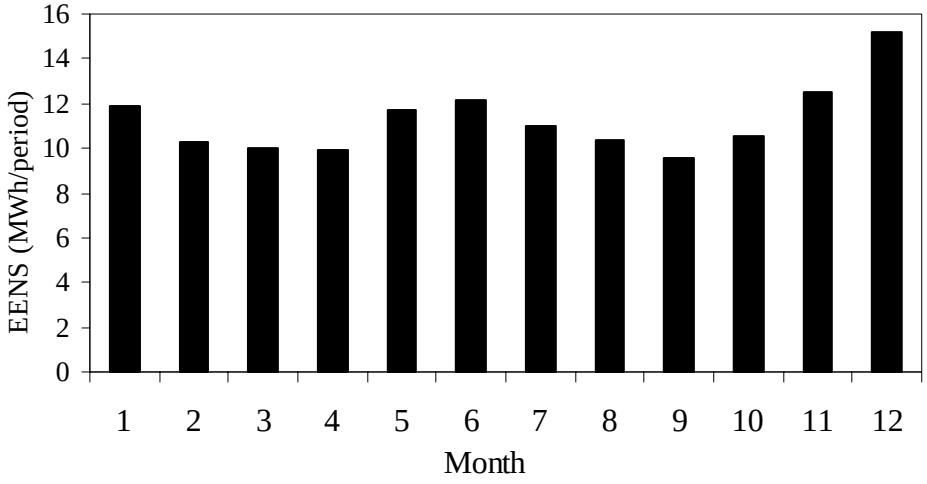


Figure 5.2: Monthly system EENS for a peak load of 185 MW

Figure 5.2 shows that the highest monthly risk occurs in December as the system load demand in December is higher than that in other months. The highest mean hourly wind speeds for the Swift Current site also occur in the month of December as shown in Table 5.4.

The seasonal system EENS as a function of system peak load obtained using corresponding models are shown in Figure 5.3.

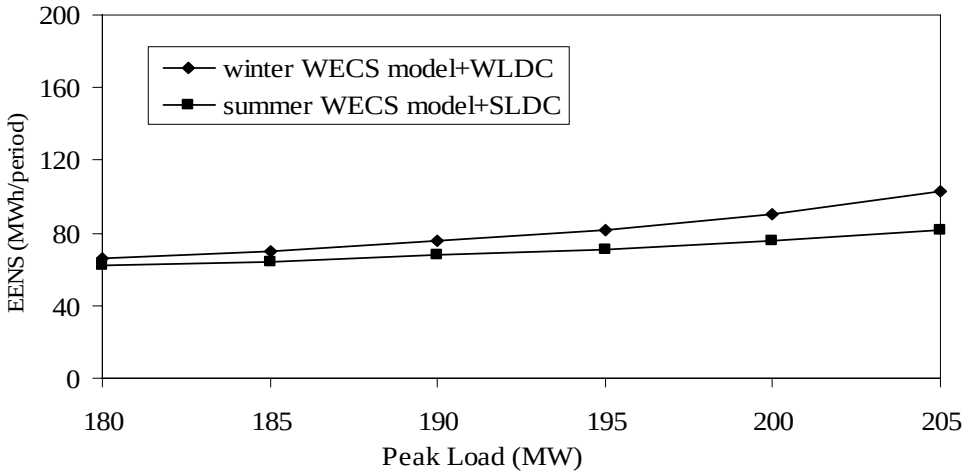


Figure 5.3: Seasonal system EENS for the RBTS with a single 40 MW WECS

It can be seen from Figure 5.3 that the RBTS system EENS in the winter season is higher than that in the summer as the load demand in winter is much higher than in the summer as shown in Table 5.7. The RBTS is considered to be transmission deficient, as bus 6 is supplied by a single line as shown in Figure 2.4. A large segment of system EENS is contributed by failure of line 9 resulting in an outage of bus 6. This event is not related to the season and is the reason why there are not much difference in the system EENS in the winter and summer periods.

A comparison of the summation of the system EENS obtained utilizing monthly and seasonal period WECS and load models and the EENS obtained using annual models is shown in Figure 5.4. This figure shows that the summation of the system EENS obtained utilizing the monthly and seasonal WECS and load models is very similar to that obtained using annual models.

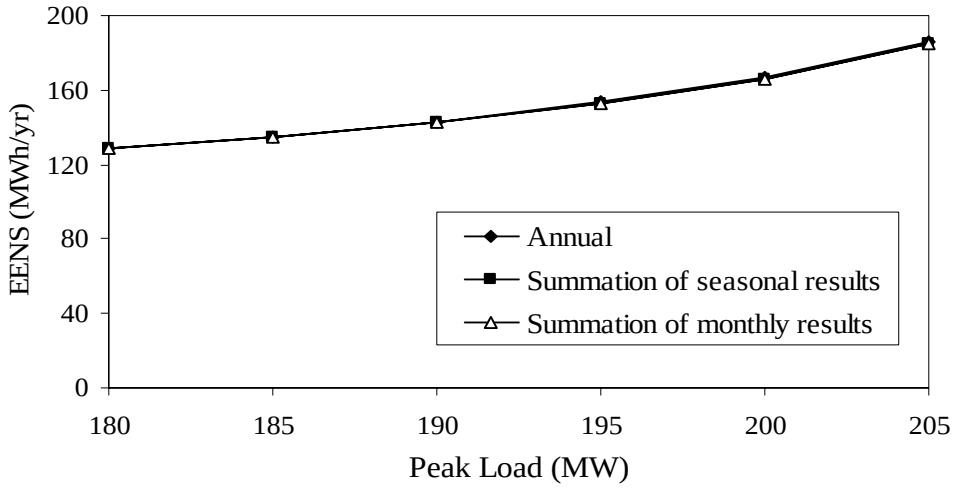


Figure 5.4: A comparison of the system EENS obtained using annual, seasonal and monthly models for the RBTS with the single WECS

**RBTS with Two WECS Analysis**

Two 20 MW WECS with data from the Regina and Swift Current sites are added at Buses 3 and 5 respectively. The wind speed data in July and December for the two wind sites are used to conduct the study to examine the effect of monthly wind parameters in bulk system adequacy assessment. The monthly system EENS using monthly WECS and load models are shown in Figure 5.5.

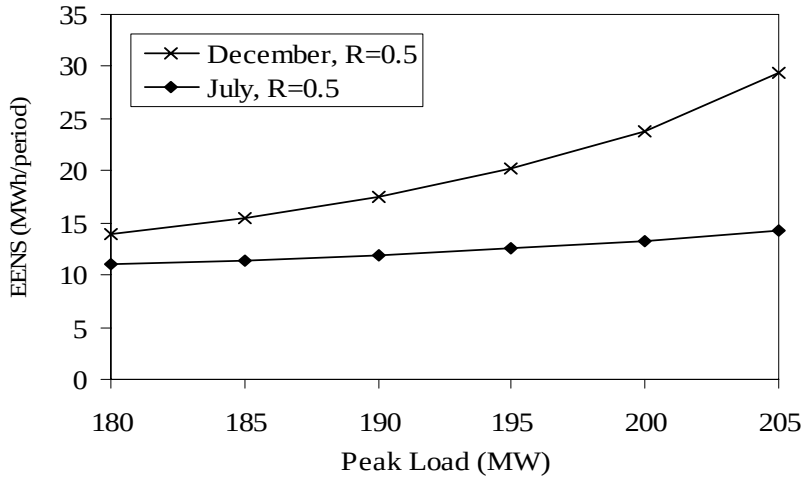


Figure 5.5: Monthly system EENS for the RBTS using monthly LDC and WECS models

Figure 5.5 shows that the system risks in July are smaller than in December as the maximum load demand in July is 0.88 of the annual system peak load. The increases in the system EENS in July as the system peak load increases are relatively small. Although wind speeds in December are higher than those in July, and the WECS provide more power output to the system in December, the load demands in December make a higher contribution to the system risks. The total risk is highly influenced by the radial line 9 in the RBTS.

The system EENS for the RBTS with the two WECS obtained using seasonal WECS models with seasonal LDC and annual WECS models with annual LDC are shown in Figure 5.6.

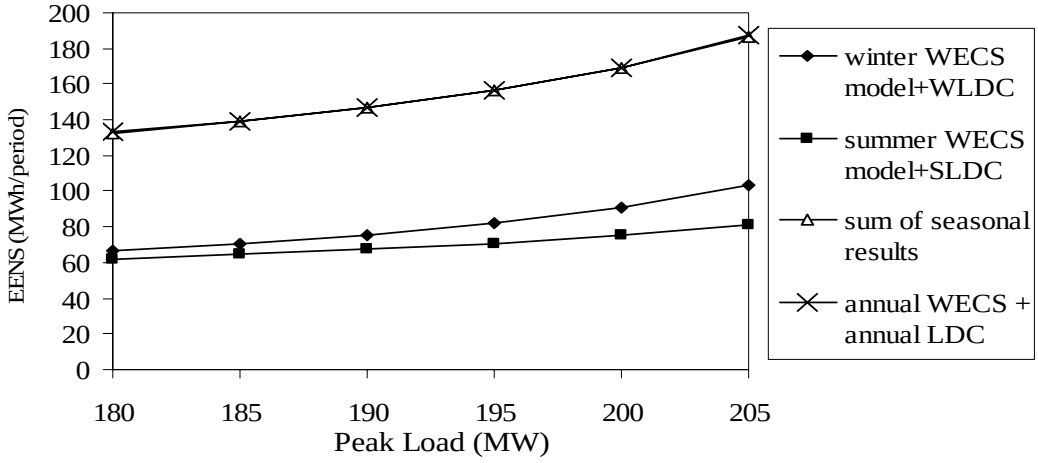


Figure 5.6: The system EENS for the RBTS with the two wind farms using annual and seasonal WECS and load models

Figure 5.6 illustrates that the summation of the system EENS obtained utilizing seasonal WECS and load models are very close to those obtained using the annual models.

The study was extended to examine seasonal wind speeds with different degree of correlation. In this chapter, it is assumed that the low wind speeds (in summer) have a low wind speed correlation level and the higher wind speeds (in winter) have a strong correlation level. Wind speed correlation coefficients (R) of 0.2 and 0.8 are used to represent weakly and strongly dependent cases respectively. Figure 5.7 shows the effect of seasonal wind speed correlations on the seasonal EENS values for the RBTS. A comparison of the annual EENS results obtained using the annual models and the summation of the seasonal EENS results considering variations in the seasonal wind speed correlations are also shown in this figure.

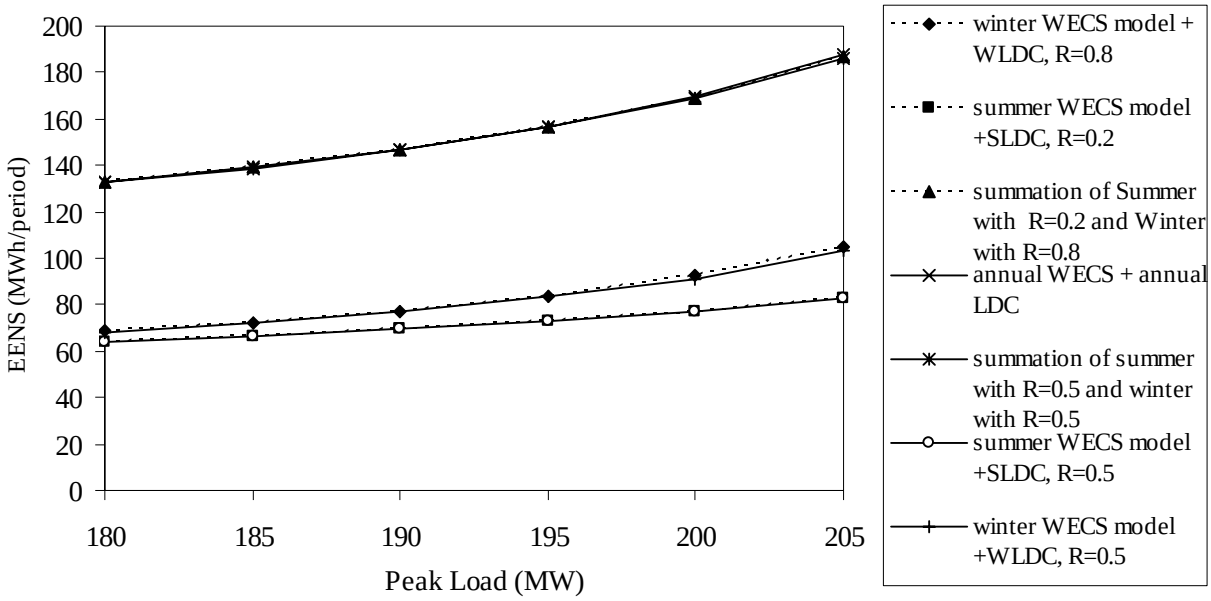


Figure 5.7: The system EENS using annual and seasonal WECS models considering seasonal wind speed correlations

Figure 5.7 shows that the annual EENS indices for the RBTS obtained by summing the winter EENS with strong wind speed correlation and the summer EENS with weak wind speed correlation are similar to those obtained by summing the two season EENS with moderately dependent wind speeds. This may not be the case in other systems and is considered in the following by application to the IEEE-RTS.

### 5.4.2. IEEE-RTS Analysis

A similar analysis was conducted on the IEEE-RTS with 600 MW WECS. The load center is located in the southern portion (138 KV) of the IEEE-RTS. Each WECS, therefore, is added through a transmission line at selected buses in the southern portion of the system.

**IEEE-RTS with a Single WECS**

A single 600 MW WECS using data from the Swift Current site is added at Bus 1. The system EENS obtained by considering monthly and seasonal WECS and LDC models are shown in Figure 5.8 and Figure 5.9 respectively. The system peak load is 2850 MW in the study described by Figure 5.8.

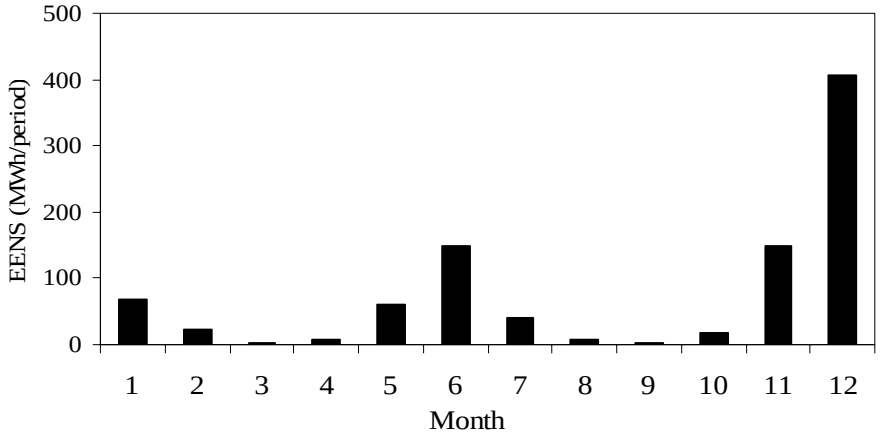


Figure 5.8: Monthly system EENS for the IEEE-RTS with a single 600 MW WECS using monthly LDC and WECS models

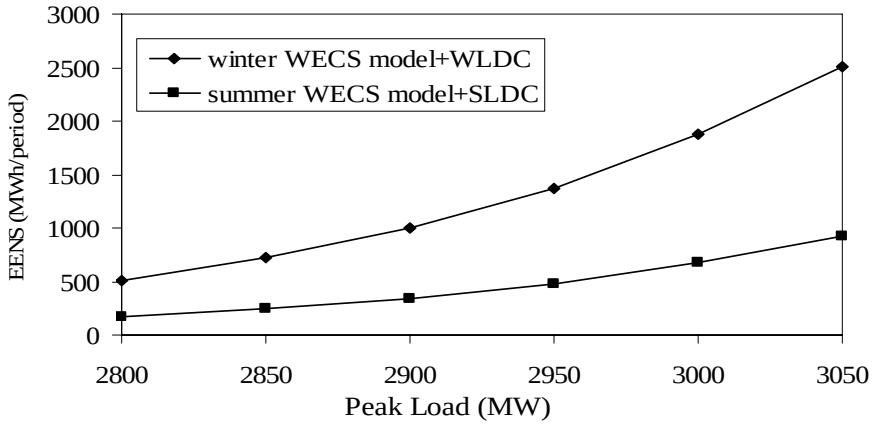


Figure 5.9: Seasonal system EENS for the IEEE-RTS with a single 600 MW WECS using seasonal LDC and WECS models

The IEEE-RTS is a relatively large system compared to the RBTS and the IEEE-RTS system indices are not dominated by a single component. Figure 5.8 and 5.9 show that there are considerable differences in the monthly and seasonal risk values in these cases.

A comparison of the IEEE-RTS EENS using annual, seasonal and monthly WECS and load models is shown in Figure 5.10.

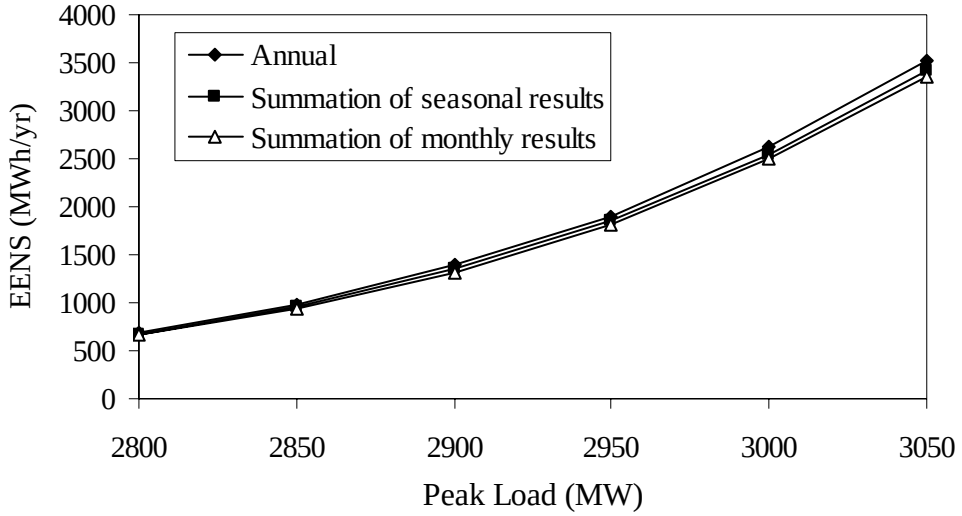


Figure 5.10: A comparison of the IEEE-RTS EENS using different period WECS and load models

Figure 5.10 shows that the system EENS obtained utilizing monthly and seasonal WECS and load models are close to those obtained using the annual models when the system has a single WECS.

**IEEE-RTS with the Two WECS**

The two moderately correlated 300 MW WECS were added to Bus 1 and Bus 3 in the IEEE-RTS. The two monthly system EENS for the IEEE-RTS with these two WECS using monthly WECS and load models are shown in Figure 5.11.

Figure 5.11 shows that the increase in system risks in July as the system peak load increases is smaller than that in December, as the load demand in December makes much more contribution to the system risk than that in the month of July.

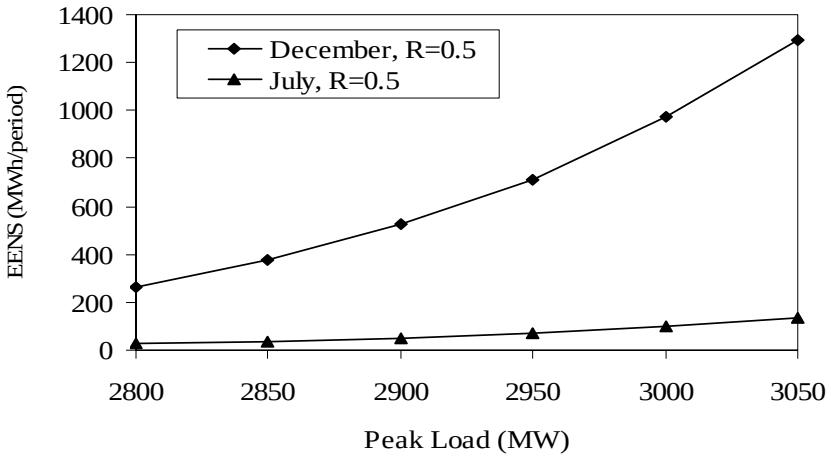


Figure 5.11: Monthly system EENS for the IEEE-RTS with the two 300 MW WECS using monthly LDC and WECS models

The system EENS for the IEEE-RTS with the two WECS obtained using seasonal WECS models with seasonal LDC and annual WECS models with annual LDC are shown in Figure 5.12.

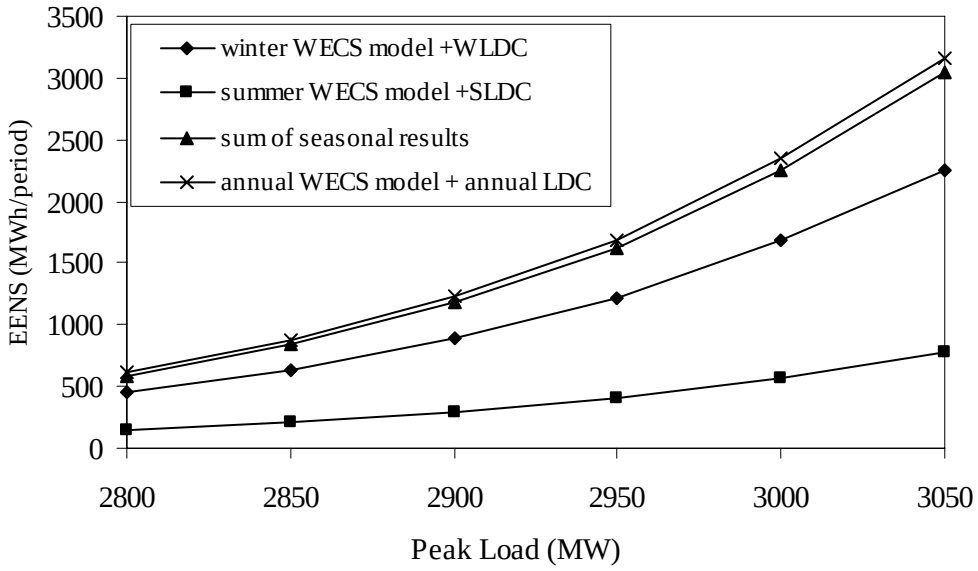


Figure 5.12: A comparison of the system EENS for the IEEE-RTS with the two 300 MW WECS using annual and seasonal WECS and load models

It can seen from Figure 5.12 that the system EENS obtained utilizing seasonal WECS and seasonal load models are close to those obtained using the annual models when the system has two correlated WECS. This is a similar conclusion to that drawn for the RBTS analysis. This

indicates that it is possible to create period time series wind speed models and load models and use them to create accurate annual analyses.

The case of the IEEE-RTS with the two WECS was extended to examine seasonal wind speeds with different correlation degrees. It is assumed in this study that the low wind speeds in summer have a low wind speed correlation level (R=0.2) and the higher wind speeds in winter have a strong correlation level (R=0.8). The effect of seasonal wind speed correlations on the seasonal EENS values for the IEEE-RTS is shown in Figure 5.13. A comparison of annual EENS results obtained using the annual models and the summation of the seasonal EENS results considering variations in the seasonal wind speed correlations are also shown in Figure 5.13.

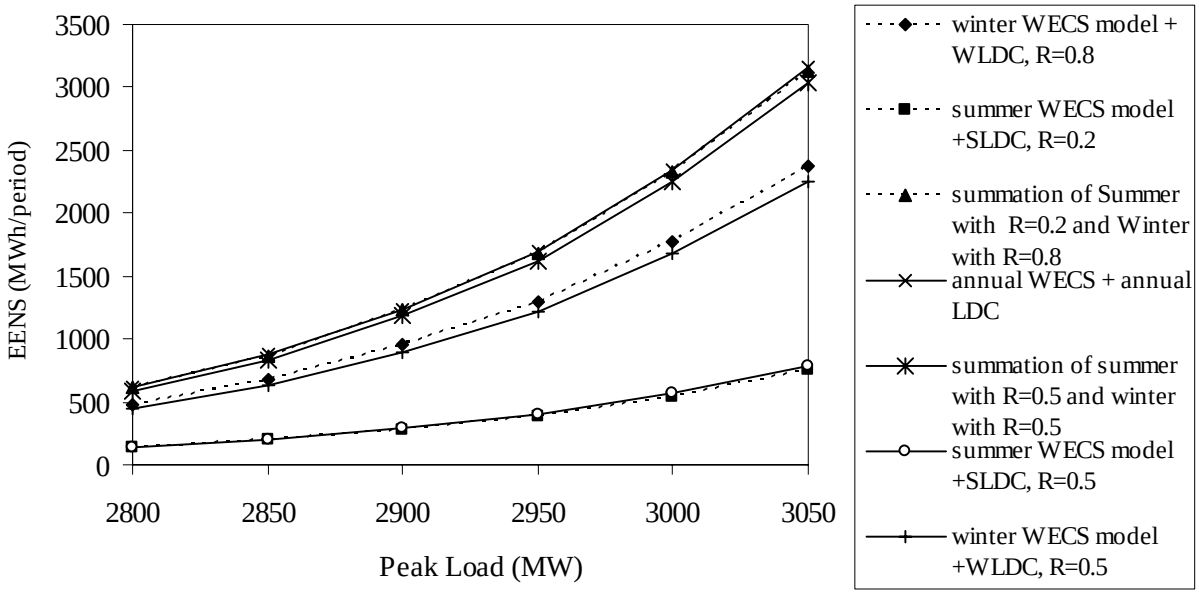


Figure 5.13: The system EENS for the IEEE-RTS with the two 300 MW WECS using annual and seasonal WECS models considering seasonal wind speed correlations

Figure 5.13 shows that the annual EENS indices for the IEEE-RTS obtained by summing the winter EENS with strong wind speed correlation and the summer EENS with weak wind speed correlation are similar to those obtained by summing the two season EENS with moderately dependent wind speeds. There are very small differences between the annual EENS obtained using annual profiles and those obtained by summing the seasonal EENS considering different wind speed correlations.

The conclusion can be drawn based on the analyses of the RBTS and IEEE-RTS, that the annual wind profile is an acceptable representation and that annual studies can be done directly using this profile. The annual system reliability indices are not significantly impacted by variation in the seasonal wind speed correlation between the two wind sites.

The procedures described for creating monthly and seasonal WECS models should prove useful in time period analyses in which specified generating units are removed from service to conduct maintenance or planned refurbishment. When units are removed from service for periodic inspection and maintenance in accordance with a planned program, the annual reliability indices can be obtained by dividing the year into periods and calculating period indices using the appropriate WECS capacity and load models [9]. The WECS multi-state models provide convenient and reasonable tools to construct modified capacity models for systems incorporating large-scale wind farms.

## 5.5. Conclusions

Models for period wind speed, WECS capacity, and load are illustrated in this chapter and were used to investigate the effects of period wind power output and load demands on bulk system reliability assessment. The seasonal and monthly WECS capacity models show that the probability of having the full WECS capacity is higher in a period with higher average wind speed than it is in a time period with a lower average wind speed and the probability of having zero capacity is significantly lower. The degree of correlation between the chronological wind speed and the hourly load profiles were examined in a RBTS generating capacity evaluation. The results show that the correlation between the chronological load profile and the wind speed at the WECS location can be recognized in the analytical and state sampling methods by using period analysis.

The developed seasonal and monthly load profiles and the corresponding WECS models were utilized in the RBTS and IEEE-RTS HL-II studies using the state sampling Monte Carlo simulation approach. The analysis results show that the system risk indices obtained utilizing seasonal and monthly WECS and load models are close to those obtained using the annual

models when the system has a single or two correlated WECS. The degree of correlation between the chronological wind speed and the hourly load profiles does not significantly impact the system risk in the composite generation and transmission systems studied. The annual wind profile is, therefore, an acceptable representation and annual studies can be done directly using this profile. The variations in the system reliability indices for different time periods are obviously dependent on system conditions. The procedures described for creating monthly and seasonal WECS models should prove useful in situations where time period models are required to incorporate scheduled maintenance of generation and transmission facilities.

# 6. Wind Integrated Bulk System Planning Using a Joint Deterministic-Probabilistic Criterion

## 6.1. Introduction

Reliability evaluation of bulk power systems has been a major system planning concern for many years. As previously noted in Chapter 1, bulk electric system (BES) reliability assessment can be divided into two basic aspects designated as system adequacy and system security. Bulk electric system adequacy assessment is focused on the existence of sufficient facilities within the system to satisfy the consumer load demand within the basic system operational constraints. A bulk electric system includes the facilities necessary to generate sufficient energy and the associated transmission required to transport the energy to the actual bulk supply points. Security considerations in BES are generally considered by focusing on the operation of the system in different operating conditions designated as normal, alert, emergency and extreme emergency states [14, 77-80]. A BES security assessment normally utilizes the traditional deterministic criterion known as the N-1 security criterion [13] in which the loss of any BES component (a contingency) will not result in system failure. The deterministic N-1 planning criterion has been used by many electric power utilities for many years due to attractive characteristics such as, simple implementation, straightforward understanding, assessment and judgment. The N-1 criterion has generally resulted in acceptable security levels, but in its basic simplest form does not provide an assessment of the actual system reliability as it does not incorporate the probabilistic nature of system behaviour and component failures.

Probabilistic approaches to BES reliability evaluation can respond to the significant factors that affect the reliability of a system. There is, however, considerable reluctance to use probabilistic techniques in many areas due to the difficulty in interpreting the resulting numerical indices. A survey conducted as part of an EPRI project indicated that many utilities had difficulty in interpreting the expected load curtailment indices as the existing models were based on adequacy

analysis and in many cases did not consider realistic operating conditions. These concerns were expressed in response to the survey and are summarized in the project report [80].

There is considerable interest in combining deterministic considerations with probabilistic indices to monitor the wellbeing of an electric power system, and evaluate the quantitative The system well-being approach proposed in [77, 78] is based on security constrained adequacy evaluation and provides the ability to incorporate the deterministic criteria used in static security assessment into the probabilistic framework utilized in conventional adequacy evaluation. The well-being concept was extended and applied to composite generation and transmission systems in [81-86] using analytical and Monte Carlo simulation methods. Although the system well-being concept provides system engineers and risk managers with comprehensive information on the degree of system vulnerability, a complete system well-being analysis can require considerable computing time particularly on large practical electrical power systems. A developed alternate approach to the well-being technique, which would also incorporate deterministic and probabilistic considerations in a single risk assessment framework, is designated as the joint deterministic-probabilistic (D-P) approach and is based on the non sequential Monte Carlo simulation method [15]. Reference 15 presents the utilization of D-P method in a bulk system with conventional generation units. Unlike conventional generation sources, wind power is variable due to its intermittent and diffuse nature and traditional planning methods will have to adapt to ensure bulk power system reliability levels are maintained as wind power penetration levels increase. This chapter extends this approach to wind integrated bulk power system planning.

The MRBTS shown in Figure 4.13 is used in this chapter as a base study system. This chapter examines the capacity value of wind generation using various approaches and how this capacity value can be utilized under a deterministic N-1 criterion. The application of capacity credit in the conventional N-1 approach is the first step in the application of the D-P method. Factors such as wind farm location, wind farm correlation levels, and installed wind capacity are considered in the studies. This chapter also illustrates the traditional deterministic N-1 criterion (D), the basic probabilistic (P) criterion and the D-P criterion by application to a bulk power system incorporating wind energy.

## 6.2. Study Methods

The joint deterministic-probabilistic (D-P) approach includes both deterministic and probabilistic criteria and is defined as follows: The system is required to satisfy a deterministic criterion (N-1) and also meet an acceptable risk criterion under the designated (N-1) outage condition [15, 87]. The procedure for D-P analysis of a bulk electric system using MECORE is briefly illustrated in the following steps:

Step 1: Apply the deterministic N-1 criterion to the given bulk electric system.

Step 2: Probabilistic analysis is then conducted using the MECORE program. The analysis is conducted on the bulk electric system with the element designated as the most severe contingency removed from the system.

Step 3: The system reliability index value under the most severe contingency is then compared with the defined index criterion.

The D-P technique provides a bridge between the accepted deterministic and probabilistic methods. The basic deterministic N-1 technique results in a variable risk level under each assigned outage condition. This is particularly true when the critical outage switches from a transmission element to a generating unit or vice versa. The D-P approach introduces an element of consistency in the assessment by introducing the concept of an acceptable risk level under the critical element outage condition.

## 6.3. Wind Capacity Credit Analysis under the Deterministic Criterion

The application of the D method in a composite system associated with wind power involves the determination of the most severe single contingency for the system. When wind power is incorporated to a power system, the requirement for conventional capacity is reduced. The saving in conventional capacity is called the “capacity credit” of the wind power. Both utilities and developers need to accurately assess the capacity value of wind. The Effective Load Carrying Capacity (ELCC) method [88], Capacity Factor method [89] and the Derated Adjusted Forced Outage Rate [9] of a wind farm (DAFORW) method [47] are used in this chapter to calculate the wind capacity credit under the D criterion.

In this study, the analyses are conducted on the MRBTS. The single line diagram of the MRBTS is shown in Figure 4.13. The five-state WECS model with Regina and Swift Current wind speed data shown in Table 4.3 are used in the MECORE program applications described in this chapter. The probability of a wind unit residing in the full down state is designated as DAFORW. The DAFORW values for the two wind sites and the corresponding five-state models are shown in Table 6.1.

Table 6.1: The independent WECS five-state models and DAFORW

| | Regina Site | Swift Current Site |
|---|---|---|
| Capacity Outage (%) | Probability | Probability |
| 0 | 0.07585 | 0.07021 |
| 25 | 0.06287 | 0.05944 |
| 50 | 0.11967 | 0.11688 |
| 75 | 0.23822 | 0.24450 |
| 100 | 0.50340 | 0.50897 |
| DAFORW | 0.75761 | 0.76564 |

### 6.3.1. ELCC Method

The Effective Load Carrying Capacity (ELCC) reliability measure was developed in order to measure the adequacy impacts of generating unit additions [88]. The ELCC method is also a popular reliability-based approach to assess wind capacity credit [52, 90-93]. The basic concept in this approach is to gradually increase the system peak load until the level of system reliability in the wind assisted system is the same as that of the original system without WECS and therefore determine the increase in load carrying capability. The most commonly used reliability index in the ELCC approach is the Loss of Load Expectation (LOLE).

The wind capacity credit of the 20 MW WECS with the Regina site data shown in Table 6.1 was calculated using this method. The original system LOLE for the MRBTS is 1.095 hrs/yr utilizing the chronological load profile and the analytical method. Figure 6.1 shows that after a 20 MW WECS with Regina site data is added to the MRBTS, the combined system can carry a peak load of 189.2 MW at a LOLE of 1.095 hrs/yr. The incremental peak load carrying capability (ELCC) in this case is 4.2 MW. The WECS, therefore, has a 4.2 MW capacity credit using the ELCC

method. A 4.0 MW wind capacity credit for a 20 MW WECS with Swift Current site data was obtained using the same approach.

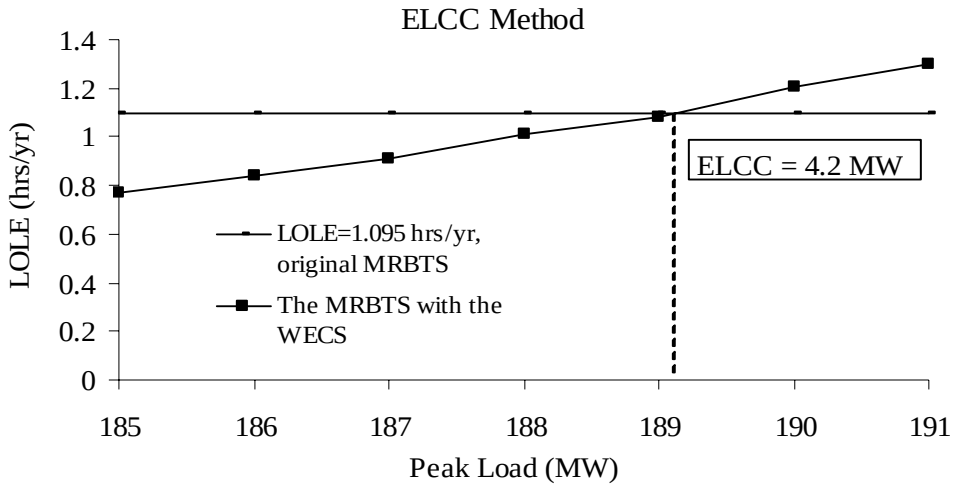


Figure 6.1: The wind capacity credit of a 20 MW WECS with Regina site data

### 6.3.2. Capacity Factor Method

The Capacity Factor (CF) can be used to measure the productivity of a wind turbine or any power production facility. The CF compares the plant's actual production over a given period of time with the power the plant would have produced if it had run at full capacity for the same amount of time [89]. References 94 to 96 use an approximate method to obtain a wind capacity factor that can be used to assess wind capacity credit. Although modern utility-scale wind turbines typically operate 65% to 90% of the time, they often run at less than full capacity. Therefore, a capacity factor of 25% to 40% is common, although they may achieve higher capacity factors during windy weeks or months [89]. Reference 94 indicates that the overall yearly wind capacity value is approximately 20% for all scenarios in the Independent Electricity System Operator (IESO), Ontario, Canada.

The PJM Interconnection which is a regional transmission organization in North American and the New York Independent System Operator (NYISO) define capacity value as the capacity factor during those hours of the day when the peak load is likely to occur in the peak months of June, July, and August [95, 96]. Reference 96 defines Peak Hours as those ending at 3, 4, 5, and 6 p.m. local prevailing time.

The PJM Peak Hours and Peak Months were applied to calculate WECS capacity factors for the Regina and Swift Current wind sites. The basic procedure is described in the following:

Step 1: Peak hour wind speed and wind power output in June, July and August are obtained using the annual ARMA model shown in Equations 4.3 and 4.4. Selected peak hour wind speeds for one year are shown in Table 6.2.

Table 6.2: The first year peak hour wind speeds (km/h) at the two wind site

| | Regina | | | | Swift Current | | | |
|---|---|---|---|---|---|---|---|---|
| Date | 3:00 p.m | 4:00 p.m | 5:00 p.m | 6:00 p.m | 3:00 p.m | 4:00 p.m | 5:00 p.m | 6:00 p.m |
| June, 1 | 43.26 | 42.09 | 37.60 | 36.49 | 15.58 | 17.72 | 19.38 | 19.08 |
| June, 2 | 29.57 | 32.97 | 32.17 | 21.75 | 26.20 | 18.70 | 24.73 | 21.04 |
| …<br>…<br>… | …<br>…<br>… | …<br>…<br>… | …<br>…<br>… | …<br>…<br>… | …<br>…<br>… | …<br>…<br>… | …<br>…<br>… | …<br>…<br>… |
| August, 31 | 20.60 | 15.70 | 8.72 | 7.37 | 16.23 | 13.00 | 7.79 | 17.57 |

Step 2: The peak hour wind power outputs are obtained using the functional relationship between the power output of the WTG and the wind speed. The selected peak hour wind power outputs are shown in Table 6.3.

Table 6.3: The first year peak hour wind power outputs (MW) at the two wind site

| | Regina | | | | Swift Current | | | |
|---|---|---|---|---|---|---|---|---|
| Date | 3:00 p.m | 4:00 p.m | 5:00 p.m | 6:00 p.m | 3:00 p.m | 4:00 p.m | 5:00 p.m | 6:00 p.m |
| June, 1 | 2 | 2 | 2 | 2 | 0.05 | 0.14 | 0.24 | 0.22 |
| June, 2 | 1.14 | 1.57 | 1.46 | 0.39 | 0.78 | 0.20 | 0.64 | 0.35 |
| …<br>…<br>… | …<br>…<br>… | …<br>…<br>… | …<br>…<br>… | …<br>…<br>… | …<br>…<br>… | …<br>…<br>… | …<br>…<br>… | …<br>…<br>… |
| August, 31 | 0.32 | 0.05 | 0 | 0 | 0.07 | 0 | 0 | 0 |

Step 3: The summed peak hour wind power output during the peak months is determined after simulating 3,000 years.

Step 4: The summed wind power in Step 3 is divided by the wind power that would have been produced if the WECS operated at maximum output 100% of the time to obtain the wind capacity factor.

The wind capacity factor at peak hours is approximately 29.5% for the WECS with Regina wind site data and is 25.8% for the WECS with Swift Current wind site data.

It should be noted that the wind capacity credit of a WECS will vary in this method with the definition of Peak Hours or Peak Months. For example, the PJM wind capacity factor method was used to calculate the wind capacity credit for a winter period (Peak Months). The wind capacity factor for a 20 MW WECS with Regina site data in a winter period is 29.3%, and the factor is 30.5% for a 20 MW WECS with Swift Current site data assuming that the winter period consists of January, February, November and December with the four peak hours from 3:00 p.m. to 6:00 p.m.

### 6.3.3. DAFORW Method

The two-state generating unit has been used in many conventional generating capacity adequacy studies. The probability of a unit residing in the full down state is known as the DAFOR [9]. The effects of wind variability can be aggregated to produce a DAFOR statistic similar in form that used for conventional generating units. This statistic is designated as DAFORW and it is used to present the probability of a WTG residing in the full down state. The DAFORW for the two 20 MW WECS is 0.7576 and 0.7656 as shown in Table 6.1. Based on the concept of DAFORW, the wind capacity credit for the WECS located with Regina site data is $20\times(1-0.75761) = 4.9$ MW. The wind capacity credit for the WECS with Swift Current site data is $20\times(1-0.7654) = 4.1$ MW.

### 6.3.4. Comparison of Wind Capacity Credit Obtained Using the Three Methods

The wind capacity credits for the 20 MW WECS obtained using the three methods are shown in Table 6.4. The capacity percentage values are between 20% and 30% for the two WECS. It can be seen from Table 6.4 that the individual site wind capacity credit values obtained using the three methods are relatively similar.

Table 6.4: Wind capacity credit (MW) for the 20 MW WECS

| Method | Wind Capacity Credit (MW) (Percentage value %) | |
|---|---|---|
| | Regina Site | Swift Current Site |
| ELCC method | 4.2 (21%) | 4.0 (20%) |
| Capacity Factor method | 5.9 (29.5%) | 5.1 (25.5%) |
| DAFORW method | 4.9 (24.5%) | 4.1 (20.5%) |

The ELCC method calculations in this thesis are conducted using reliability assessments that consider generating unit outage statistics and the hourly annual load demand. The simplified Capacity Factor approach provides an approximate wind capacity value that only considers the historical contribution made to serving the system load during the designated peak period. The Peak Hours and Peak Months in the Capacity Factor method will differ for different systems, and will depend on the specific characteristics of the region and the demand shape. The DAFORW method uses the probability distribution of the annual wind power instead of the specified time period profile used in the Capacity Factor approach. The DAFORW and the Capacity Factor techniques are decoupled from the conventional generating capacity and therefore do not incorporate system reliability parameters or evaluation. The ELCC approach uses all these factors in the assessment and is the most comprehensive approach. The wind capacity credits obtained using the ELCC method are used in the following studies using the deterministic (D) criterion.

### 6.3.5. Sensitivity Study of Wind Capacity Credit Under the Deterministic Criterion

The effects of wind capacity credit on the system peak load carrying capacity (PLCC) using the deterministic N-1 method is illustrated in this section by assuming the wind capacity credit increases from 0% to 100% in 20% increments. The study system is the MRBTS with a 20 MW WECS with Regina site data. Line 1 (L1) is the weakest element in the MRBTS as the utilization of Line 1 is approximately 85% of the line rating for the system peak load condition. An L1 outage is, therefore, selected as the most severe single contingency in this study. The system PLCC values with variation in wind capacity credit are given in Table 6.5 with the WECS connected to different buses. These PLCC values are graphically shown in Figure 6.2.

Table 6.5: The PLCC (MW) of the MRBTS with a 20 MW WECS with different wind capacity credits under L1 outage condition

| Wind capacity credit value (%) | WECS at Bus 1 | WECS at Bus 2 | WECS at Bus 3 |
|---|---|---|---|
| 0% (No wind capacity ) | 189 | 189 | 189 |
| 20% | 189 | 192 | 194 |
| 40% | 189 | 195 | 199 |
| 60% | 189 | 197 | 203 |
| 80% | 189 | 200 | 207 |
| 100% (Full wind capacity) | 189 | 202 | 211 |

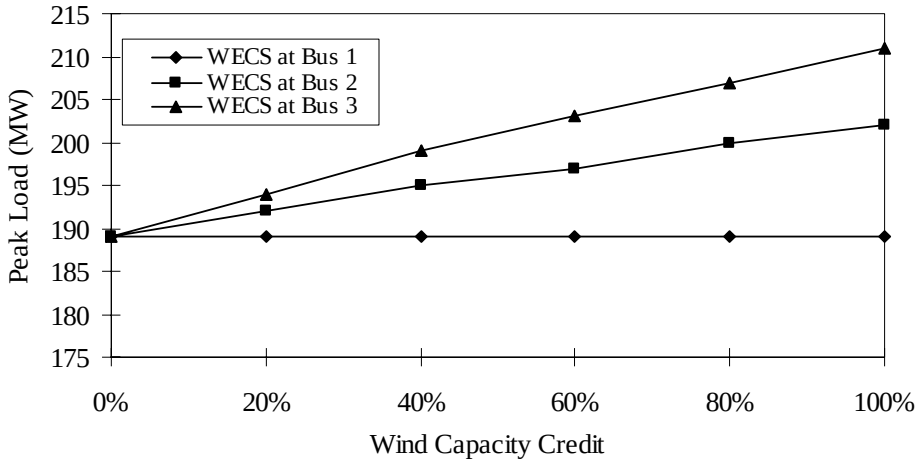


Figure 6.2: The PLCC of the MRBTS with a 20 MW WECS with varying wind capacity credits

It can be seen from Table 6.5 and Figure 6.2 that when the WECS is located at Bus 1, there is no system PLCC benefit as the wind capacity credit increases because adding a WECS at Bus 1 does not reduce the stress on Line 1. The PLCC increases as the wind capacity credit increases when the WECS is connected to Bus 2 or Bus 3 and the benefits of adding the WECS at Bus 3 are higher than those obtained by adding the WECS at Bus 2.

The system PLCC benefits with increase in the wind capacity credit are obviously impacted by the WECS location and the system condition. Considering the WECS as firm generation capacity under the deterministic approach is relatively straightforward. The actual magnitude of firm capacity to assign to a WECS, however, is not obvious. Capacity credit assignments of 0% to

100% obviously understate and overstate respectively the actual benefits. The ELCC of the WECS can, however, be used to provide a consistent approach that recognizes the factors that impact the overall system reliability.

## 6.4. The Effect of a Single WECS on the System PLCC Values Using the D, P and D-P Techniques

This section illustrates the application of the D, P and D-P methods in assessing the adequacy of the MRBTS including wind energy. The improvement in system PLCC due to adding wind power to the MRBTS is examined using the three approaches. The wind penetration level is 7.7% when a 20 MW WECS is added to the MRBTS. A 20 MW WECS with Regina site data is assumed to be connected to Bus 3 in the MRBTS. The diagram of the MRBTS with the single WECS is shown in Figure 6.3.

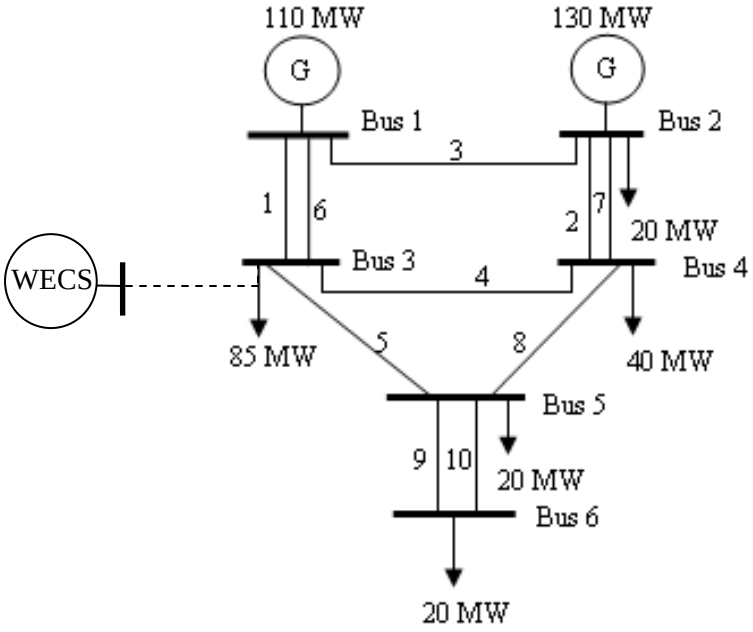


Figure 6.3: The diagram of the MRBTS with a single WECS

The Severity Index (SI) [9] expressed in System Minutes/year (SM/yr) is used as the representative reliability index in this chapter. The SI is a normalized form of EENS obtained by dividing the EENS by the system peak load. The SI is a relative index that can be used in planning and system development studies [9]. This index is also designated as the Delivery Point

Unreliability Index (DPUI) and used by all the major Canadian electric power utilities to measure the reliability performance of their bulk electric power systems [97]. The SI (or DPUI) is a useful and appropriate index for comparing systems of different sizes and with different peak loads.

### 6.4.1. Application of the D Approach

The application of the D method involves the determination of the most severe single contingency for the studied system. The previous wind capacity credit studies show that the wind capacity credit of a 20 MW WECS with Regina site data is 21% using the ELCC method. The WECS is, therefore, considered as 4.2 MW of firm generation capacity to determine the PLCC for the MRBTS under the D criterion. The largest generating unit in the MRBTS has a capacity of 40 MW and therefore a WECS outage does not constitute the most severe contingency under the D criterion. In Table 6.6, the designation G1-40/ G2-40 indicates the removal of a 40 MW unit at Bus 1 or Bus 2 and L1 means Line 1 is removed from service. The PLCC for the original MRBTS and the MRBTS with the 20 MW WECS are shown in Table 6.6.

Table 6.6: The system PLCC (MW) values under the D criterion

| Outage | Original MRBTS | The MRBTS with the WECS |
|---|---|---|
| L1/L6 | 189 | 194 |
| G2-40/G1-40 | 200 | 204 |
| L5/L8 | 239 | 244 |

Table 6.6 shows that the PLCC for the original MRBTS and the MRBTS with a WECS exceeds 185 MW under all outage conditions and meets the N-1 criterion at that load level. L6 is in parallel with L1, and therefore all comments for L1 also apply to L6. The L5 and L8 outage conditions are less severe than G1-40, G2-40 and L1 outages, and therefore, are not included in the following studies.

Table 6.6 also shows that an L1 outage is the most severe single contingency for the original MRBTS and the MRBTS with wind energy. As noted earlier, when the WECS is added at Bus 3,

which is located at the load center of the MRBTS, it reduces the transmission deficiency problem and the system PLCC increases from 189 MW to 194 MW.

### 6.4.2. Application of the P Approach

The WECS with the five-state models shown in Table 6.1 are used to evaluate the SI index for the MRBTS with wind energy. The SI as a function of the peak load for the original MRBTS and the MRBTS incorporating a WECS are shown in Table 6.7 and Figure 6.4. Table 6.7 shows that the original MRBTS risk at the 185 MW reference peak load expressed by the SI is 4.4 SM/yr. A probabilistic criterion Rc of 4.4 SM/yr is therefore used in the following probabilistic analyses.

Table 6.7: The system SI (SM/yr) obtained using the P approach.

| Peak Load (MW) | 185 | 190 | 195 | 200 | 205 | 210 |
|---|---|---|---|---|---|---|
| Original MRBTS | 4.40 | 7.05 | 9.91 | 15.39 | 24.54 | 29.33 |
| The MRBTS with the WECS | 3.03 | 4.65 | 7.02 | 10.32 | 15.37 | 22.71 |

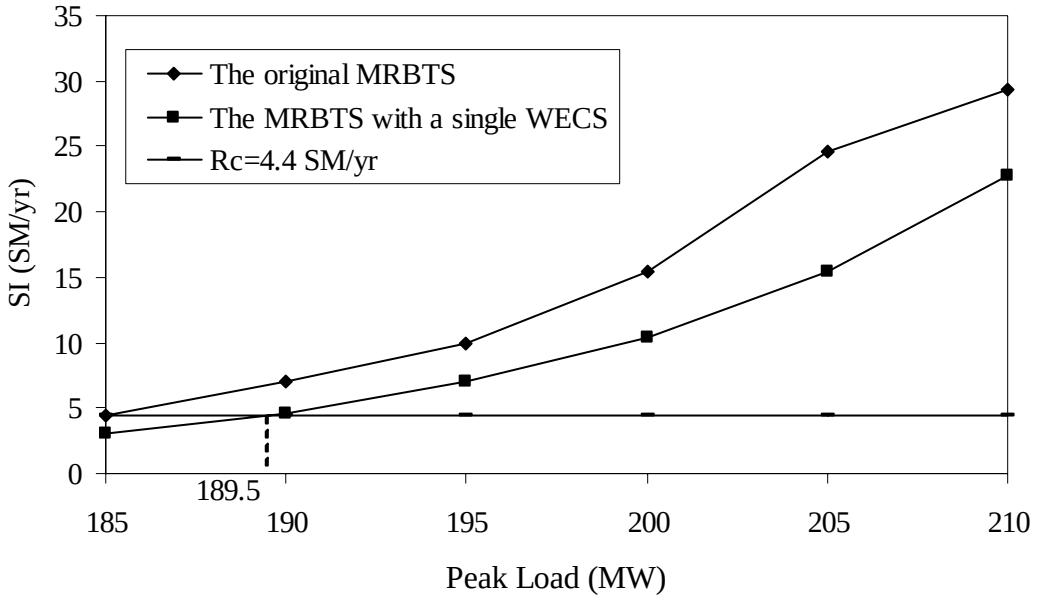


Figure 6.4: Annual SI indices for the original MRBTS and the MRBTS with the WECS using the P approach

Figure 6.4 indicates that the system PLCC for the MRBTS with the WECS is 189.5 MW using the probabilistic method.

### 6.4.3. Application of the D-P Approach

**The Original MRBTS**

The D-P criterion is a combination of the deterministic N-1 criterion and a quantitative SI criterion designated as Pc. Table 6.8 shows the system SI for the original MRBTS as a function of the system peak load under different contingencies.

Table 6.8: Annual SI (SM/yr) for the original MRBTS utilizing the D-P method

| Peak Load (MW) | 185 | 189 | 190 | 195 | 200 | 205 |
|---|---|---|---|---|---|---|
| L1 | 22.08 | 33.57 | n/a | n/a | n/a | n/a |
| G2-40 | 121.64 | 163.24 | 169.89 | 249.73 | 362.71 | n/a |
| G1-40 | 96.05 | 130.23 | 131.76 | 201.93 | 296.57 | n/a |

As noted earlier, the reference peak load for the original MRBTS is 185 MW. Table 6.8 shows that the SI at this load level is 121.64 SM/yr under a G2-40 contingency. This is the largest contingency risk in Table 6.8 at the reference peak of 185 MW. A Pc value of 121 SM/yr was selected as the SI criterion in the following MRBTS D-P studies. The G2-40 outage is a more severe contingency than an L1 outage when the system peak load is less than 189 MW. At this peak load level, the SI is 33.57 SM/yr under an L1 contingency, which is less than the Pc value of 121 SM/yr. The magnitude of the Pc affects the system PLCC and is a management decision. Table 6.8 indicates that the L1 outage condition violates the deterministic N-1 criterion when the peak load exceeds 189 MW. The system PLCC is, therefore, 189 MW using the D-P method.

**The MRBTS with a Single WECS**

Using the joint D-P approach, the following two steps are applied to combine the deterministic N-1 framework with probabilistic analysis for a WECS [98].

Step 1: Determine whether the firm capacity associated with the WECS is or is not the most severe outage condition.

Step 2: If the WECS is not the critical contingency in the study system, determine the PLCC under the critical contingency and conduct a probabilistic evaluation with the WECS represented by a multi-state model in the form shown in Table 6.1.

Previous study under the deterministic N-1 criterion indicates that the 20 MW WECS with Regina site data is not the most severe single contingency for the MRBTS. The annual SI for the MRBTS with the 20 MW WECS is calculated using the WECS model shown in Table 6.1. Table 6.6 shows that L1 is the maximum impact element in the MRBTS with wind energy. The annual system SI for the MRBTS with the single WECS under the L1 outage condition are shown in Figure 6.5 utilizing the D-P method.

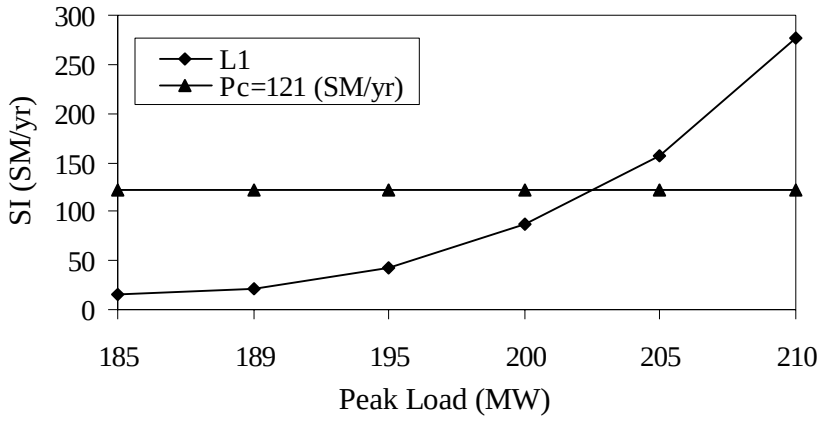


Figure 6.5: The annual SI for the MRBTS with the 20 MW WECS using the D-P method

Figure 6.5 shows that the PLCC value is 202 MW at the Pc criterion. As noted above, a particular Pc value is a management decision to accept a specified system risk level. The D-P approach is a deterministic framework with an embedded probabilistic criterion. The system is, therefore, first required to satisfy the N-1 criterion. Table 6.6 shows that the system PLCC is 194 MW using the D approach. The system PLCC is, therefore, 194 MW using the D-P method.

### 6.4.4. Comparison of the System PLCC Values Using the Three Techniques

The PLCC values for the original MRBTS and the MRBTS with the single WECS determined using the three methods are shown in Table 6.9.

Table 6.9: Comparison of the PLCC values (MW) using the three techniques

| | D | P | D-P |
|---|---|---|---|
| Original MRBTS | 189 | 185 | 189 |
| The MRBTS with the 20 MW WECS | 194 | 189.5 | 194 |

It can be seen from Table 6.9 that when a single 20 MW WECS is incorporated in the MRBTS, the improvements in the system PLCC obtained using the three techniques are similar.

## 6.5. The MRBTS Associated with WECS Planning Using the D, P and D-P Techniques

### 6.5.1. Wind Farm Planning

Wind capacity was added in 20 MW increments to the MRBTS. The impact of these additions is examined in this section using the D, P and D-P methods. The wind capacity credit of the WECS with varying installed capacity obtained utilizing the ELCC method is shown in Table 6.10.

Table 6.10: The wind capacity credits for the WECS using Regina and Swift Current site data

| WECS Installed Capacity (MW) | | 20 | 40 | 60 | 80 |
|---|---|---|---|---|---|
| Regina | ELCC (MW) | 4.2 | 5.9 | 6.5 | 7.1 |
| | Wind capacity credit (%) | 21% | 14.75% | 10.83% | 10.13% |
| Swift Current | ELCC (MW) | 4.0 | 5.7 | 6.4 | 6.9 |
| | Wind capacity credit (%) | 20% | 14.25% | 10.67% | 8.63% |

The WECS capacity credit percentage value decreases as the WECS installed capacity increases, although the ELCC increases as the WECS installed capacity increases. The WECS capacity credits are less than 40 MW which is the capacity of the largest unit in the MRBTS. The loss of WECS capacity is, therefore, not the largest single contingency under the deterministic N-1 criterion. The results shown in Table 6.10 are used in the D and D-P methods to analysis the MRBTS with the WECS.

Two possible wind farm planning schemes are considered. The total wind capacity is equally divided between the two locations in Scheme 2.

Scheme 1: A single WECS with Regina site data is added at Bus 3.

Scheme 2: Two identical installed capacity WECS with data from the Regina and Swift Current sites are added at Buses 3 and 6 respectively. The wind speeds between the two wind farms are considered to be moderately correlated.

The wind capacity credits shown in Table 6.10 are directly applied to conduct the analysis of Scheme 1 using the D approach. As two moderately correlated wind farms are considered in Scheme 2, it is necessary to determine the wind capacity credits of the two dependent WECS using the ELCC method. The procedure described in Section 4.4.3 of Chapter 4 is used to determine the total wind capacity credit considering wind speed correlation between the two wind farms. The total wind capacity credits for the two WECS considering different correlation levels are shown in Table 6.11 using the ELCC method.

Table 6.11: Wind capacity credits (MW) for the two correlated wind farms using the ELCC method

| *Site 1: 20 MW WECS , Site 2: 20 MW WECS* | | |
|---|---|---|
| Correlation coefficient | Site 1: Regina<br>Site 2: Swift Current | Site 1: Swift Current<br>Site 2: Regina |
| 0.2 | 7.4 | 7.3 |
| 0.5 | 6.7 | 6.7 |
| 0.8 | 6.3 | 6.3 |
| *Site 1: 40 MW WECS, Site 2: 20 MW WECS* | | |
| Correlation coefficient | Site 1: Regina<br>Site 2: Swift Current | Site 1: Swift Current<br>Site 2: Regina |
| 0.2 | 8.8 | 8.8 |
| 0.5 | 8.4 | 8.3 |
| 0.8 | 7.4 | 7.4 |

Table 6.11 shows that the overall wind capacity credit decreases with increase in the degree of wind speed correlation. The results shown in Table 6.10 and Table 6.11 indicate that it is reasonable to divide the total wind capacity credit between the two wind farms based on the ratio of the installed capacity of each wind farm to the total installed wind capacity. For example, when the correlation coefficient is 0.2, the effective wind capacity of Site 1 with Regina site data and 40 MW of installed capacity is 5.86 MW ($\left(\frac{40}{40+20}\right)\times 8.8$ MW ). This value is very close to that of an independent 40 MW WECS with Regina site data as shown in Table 6.10. When the two WECS have identical installed capacities, the total wind capacity credit is evenly divided between the two farms. This is used in the following studies described in this thesis.

The system PLCC results for the two schemes obtained using the D method and the P method are shown in Figure 6.6 and Figure 6.7 respectively.

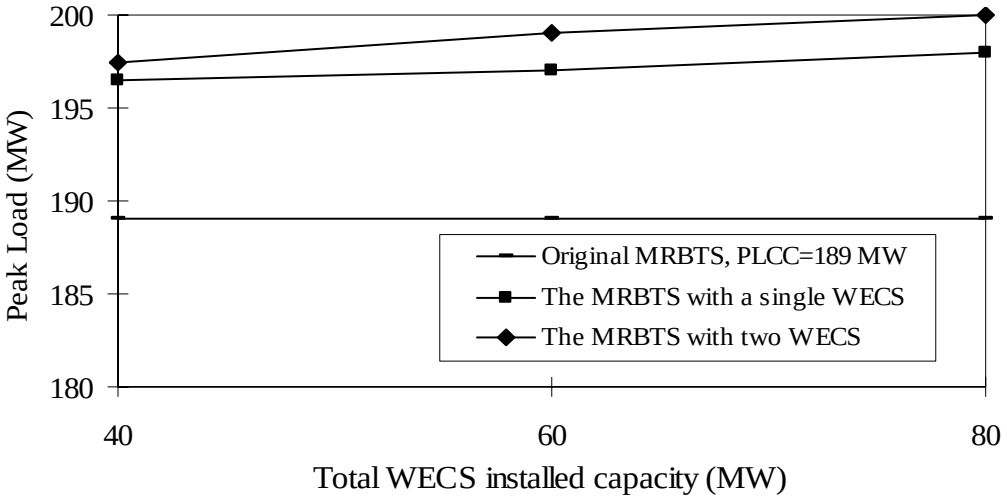


Figure 6.6: Comparison of the PLCC values for the two schemes using the D method

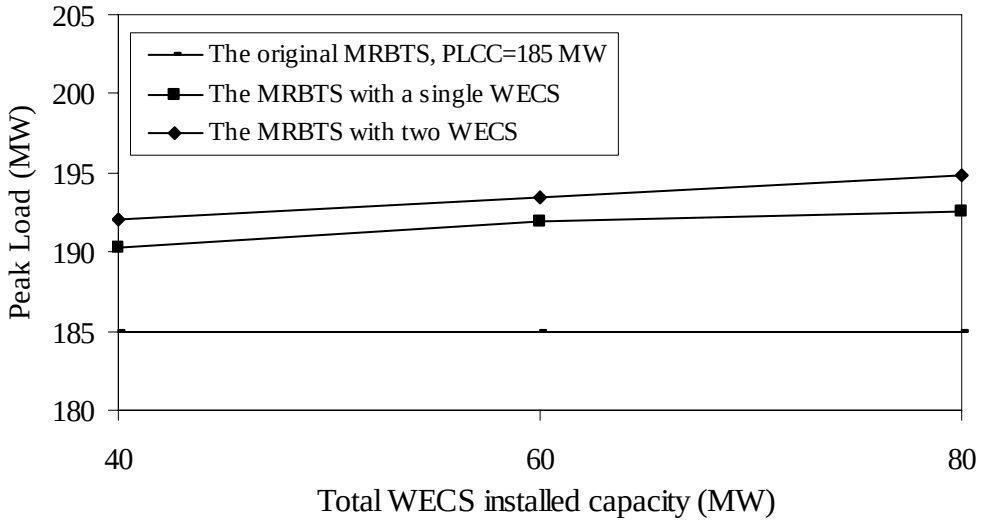


Figure 6.7: A comparison of the PLCC values for the two schemes using the P method

As noted earlier, the most severe single contingency for the MRBTS with wind energy is an L1 outage. The annual SI values for the system under the D-P criterion with L1 on outage are shown in Figure 6.8.

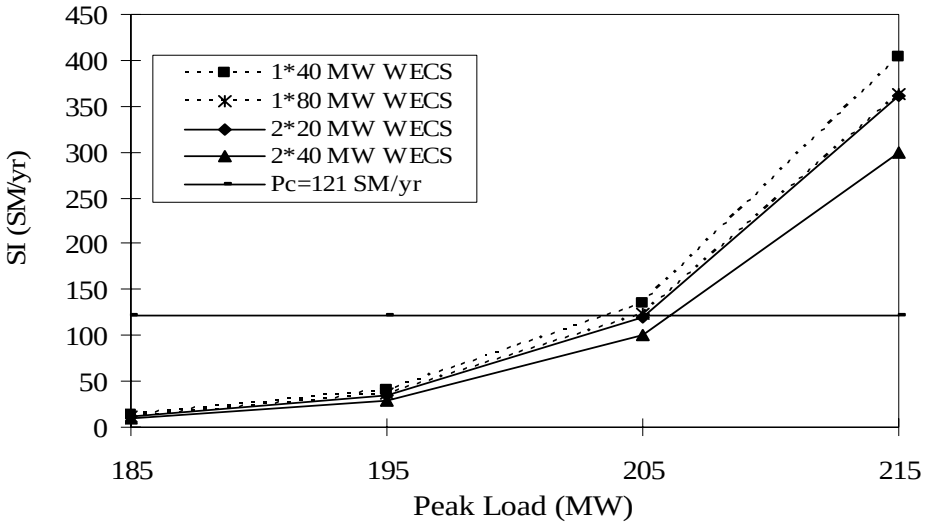


Figure 6.8: A comparison of the annual SI values for the two schemes using the D-P method under the L1 outage condition

Figure 6.8 illustrates that the system PLCC values exceed 200 MW at the specified Pc value. As noted earlier, the D-P method is predicated on the deterministic N-1 criterion with an added probabilistic perspective and the deterministic N-1 criterion is the pre-condition before applying the probabilistic criterion. The system PLCC values obtained using the D-P method are, therefore, the same in this case as those obtained using the D method shown in Figure 6.6.

The results show that the system PLCC benefits for the MRBTS associated with the two correlated wind farms are higher than those for the system with a single wind farm using the three techniques. Two WECS with identical installed capacities are used in the following studies. The first WECS utilizes the Regina data and the second WECS utilizes the Swift Current data.

### 6.5.2. Effect of the Two WECS Locations in the MRBTS

When the two WECS are added at various locations in the MRBTS, the effect of the system risk is analyzed using the D, P and D-P method. Three cases described as follows are used to illustrate the effect on the adequacy of the MRBTS of adding two WECS to different locations.

Case 1: 20 MW WECS are added at Buses 1 and 2.

Case 2: 20 MW WECS are added at Buses 3 and 2.

Case 3: 20 MW WECS are added at Buses 3 and 6.

The system PLCC rounded values for the three cases obtained using the D method are shown in Table 6.12. The table shows that the system PLCC obtained using the D approach is obviously impacted by the WECS locations in the MRBTS.

Table 6.12: The system PLCC (MW) for the three cases using the D method

| The most severe outage | Case 1 | Case 2 | Case 3 |
|---|---|---|---|
| L1 | 192 | 196 | 197 |

The system SI and PLCC results for the three cases applying the P method are shown in Figure 6.9. This figure illustrates that the impacts on the system PLCC are not very significant when the WECS are added at different locations utilizing the P method. The PLCC value is 192 MW using the probabilistic criterion when the two 20 MW WECS are added in the MRBTS.

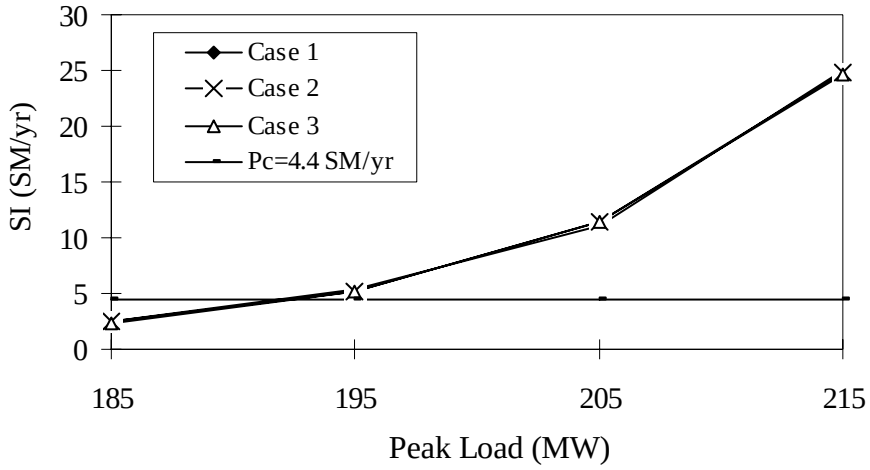


Figure 6.9: The system SI for the three cases using the P method

The system SI and the PLCC values for the three cases obtained using the D-P method are illustrated in Figure 6.10. It can be seen that the effects of the WECS locations on the system SI are obvious under the L1 outage condition. The system PLCC values are, however, 192 MW, 196 MW and 197 MW respectively using the D-P method as the system must first satisfy the D criterion for applying the D-P approach.

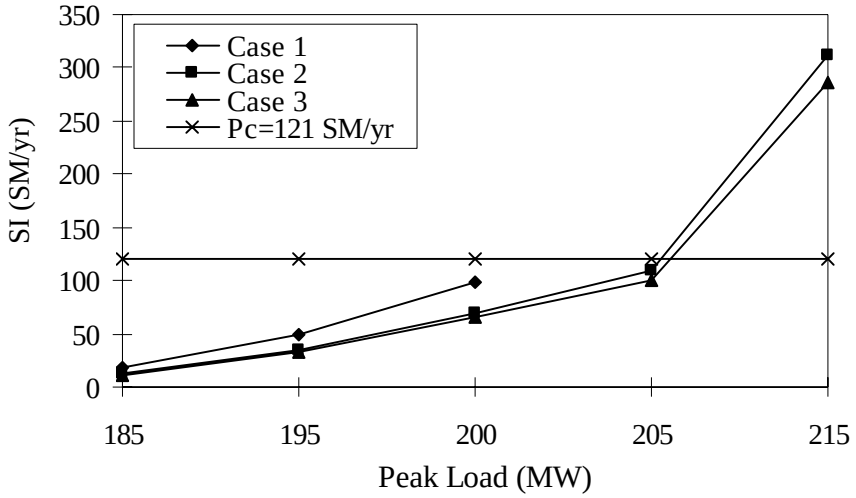


Figure 6.10: The system SI for the three cases using the D-P method under the L1 outage condition

The results shown in Table 6.12 and Figures 6.9 and 6.10 indicate that the WECS locations have an impact on the system risk using the D and D-P method with a transmission line outage. The effect of WECS location on the system PLCC is very small when using the P method as the system is no longer transmission limited. The impacts on the system risk of WECS location using the D, P and D-P techniques are different and depend on the system condition.

### 6.5.3. MRBTS Planning Incorporating Two WECS Using the D, P and D-P Techniques

The basic objective of this section is to examine the system PLCC for the MRBTS with wind energy in a system planning context under the D, P and D-P criteria. The two correlated wind farms are located in the load center (Bus 3 and Bus 6) of the MRBTS in the following studies. All studies conducted on the original MRBTS are considered as Base Case studies in this analysis and are described as follows [98]:

***Base Case**:*

Base Case 1 (B-C1): The MRBTS system

Base Case 2 (B-C2): The MRBTS system with 20 MW WECS at both Bus 3 and Bus 6

Base Case 3 (B-C3): The MRBTS system with 40 MW WECS at both Bus 3 and Bus 6

Two possible planning alternatives are considered, and the three cases were studied under each alternative. The six scenarios are as follows.

***Alternative 1:***

Alternative 1- Case 1 (A1-C1): Three 20 MW generating units are added at Bus 2.

Alternative 1- Case 2 (A1-C2): Three 20 MW generating units are added at Bus 2, and 20MW WECS are added at both Bus 3 and Bus 6.

Alternative 1- Case 3 (A1-C3): Three 20 MW generating units are added at Bus 2, and 40 MW WECS are added at both Bus 3 and Bus 6.

***Alternative 2:***

Alternative 2- Case 1(A2-C1): Alternative 1- Case 1 and an additional transmission line between Bus 1 and Bus 3.

Alternative 2- Case 2 (A2-C2): Alternative 1- Case 2 and an additional transmission line between Bus 1 and Bus 3.

Alternative 2- Case 3 (A2-C3): Alternative 1- Case 3 and an additional transmission line between Bus 1 and Bus 3.

**Planning Alternatives Using the D method**

The wind capacity credits for the 20 MW and 40 MW WECS are approximately 3.4 MW and 4.8 MW respectively using the ELCC method assuming moderate wind speed correlation between the two wind sites. The rounded system PLCC values using the D method are shown in Table 6.13.

Table 6.13: The system PLCC (MW) for the base case and the two alternatives using the D method

| | Case | PLCC (MW) | The most severe contingency |
|---|---|---|---|
| Base Case | B-C1 | 189 | L1 |
| | B-C2 | 197 | L1 |
| | B-C3 | 200 | L1 |
| Alternative 1 | A1-C1 | 226 | L1 |
| | A1-C2 | 234 | L1 |
| | A1-C3 | 237 | L1 |
| Alternative 2 | A2-C1 | 260 | G2-40 |
| | A2-C2 | 268 | G2-40 |
| | A2-C3 | 271 | G2-40 |

It can be seen from Table 6.13 that the planning alternatives result in significant improvements in the system PLCC under the deterministic N-1 criterion. The PLCC for Alternative 1 are limited

by a L1 contingency. The transmission stress on L1 is, however, reduced by adding a line between Bus 1 and Bus 3 in Alternative 2. The system PLCC values are improved by adding the WECS to the system.

**Planning Alternatives Using the P method**

The system PLCC values obtained using the probabilistic approach and the Rc criterion of 4.4 SM/yr are shown in Table 6.14.

Table 6.14: System PLCC obtained using the P method

| | Case | PLCC (MW) |
|---|---|---|
| Base Case | B-C1 | 185 |
| | B-C2 | 192 |
| | B-C3 | 195 |
| Alternative 1 | A1-C1 | 246 |
| | A1-C2 | 254 |
| | A1-C3 | 257 |
| Alternative 2 | A2-C1 | 253 |
| | A2-C2 | 259 |
| | A2-C3 | 262 |

Table 6.14 shows that under the probabilistic criterion, the PLCC value for each case of Alternative 1 are significantly higher than the corresponding base case value due to the fact that the additional three units are added at Bus 2. The addition of a line between Bus 1 and Bus 3 in Alternative 2 provides a small additional benefit to the system PLCC in Alternative 1. Adding the two WECS in the southern part of the system has an obvious impact on the system PLCC using a probabilistic criterion.

**Planning Alternatives Using the D-P method**

The system SI values for the three base cases determined using the D-P method are shown in Figure 6.11. As noted earlier, the deterministic N-1 criterion is the pre-condition in the D-P method. The system PLCC for B-C1, B-C2 and B-C3 are, therefore, 189 MW, 197 MW and 200 MW respectively.

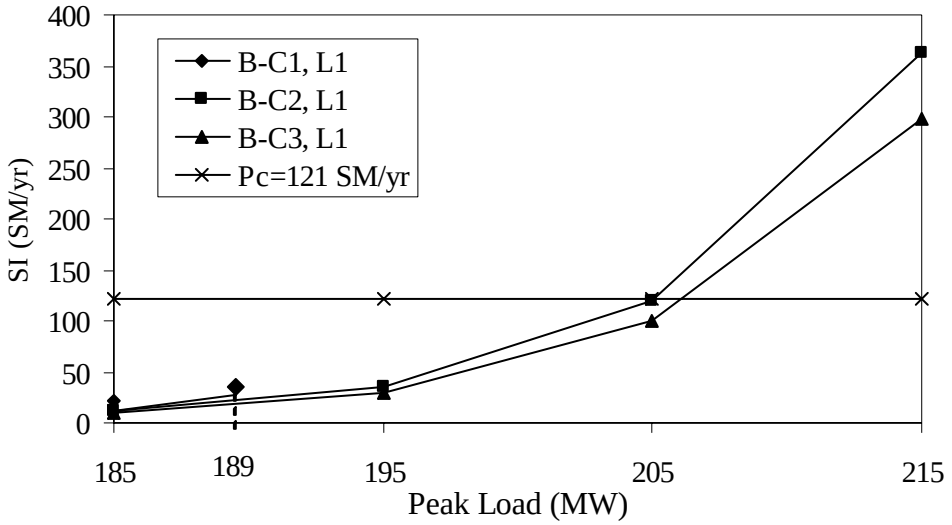


Figure 6.11: The system SI values for the Base cases using the D-P method

The SI values for each case of Alternative 1 are shown in Figure 6.12.

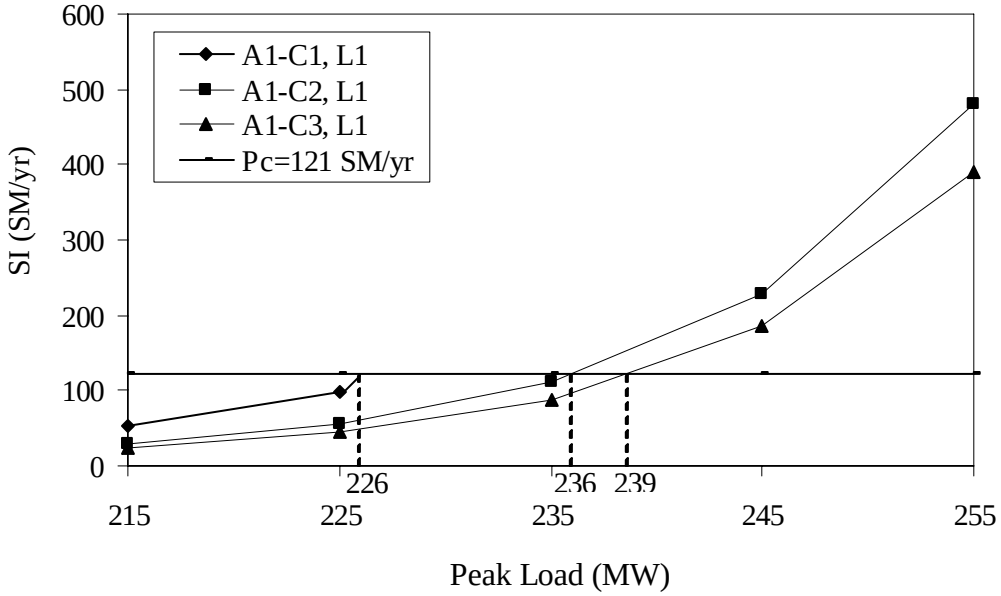


Figure 6.12: The PLCC values for the Alternative 1 cases using the D-P method

It can be seen from Table 6.12 that the system PLCC under A1-C1 is 226 MW which is the same as that obtained utilizing the D method. The reason is that conventional generation units are added to the system under A1-C1. The peak loads for A1-C2 and A1-C3 236 MW and 239 MW

respectively to satisfy the Pc value. The PLCC for A1-C2 and A1-C3 become 234 MW and 237 MW respectively based on the PLCC results obtained using the D method.

The system SI values as a function of peak load for each case of Alternative 2 are shown in Figure 6.13. This figure shows that the system PLCC value for A2-C1, A2-C2 and A2-C3 are 254 MW, 262 MW and 265 MW respectively.

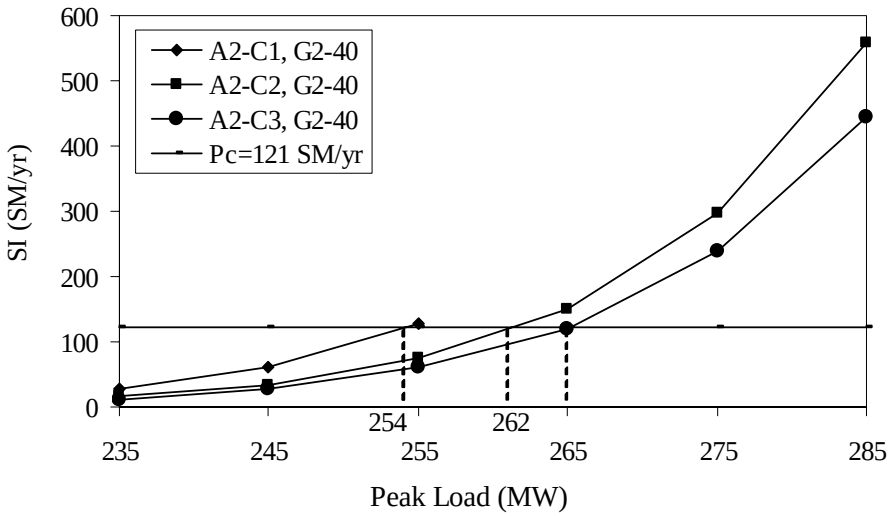


Figure 6.13: The PLCC values for the Alternative 2 cases using the D- P method

The system PLCC values for the study cases obtained using the D-P method under a probabilistic risk criterion Pc of 121 SM/yr are shown in Table 6.15.

Table 6.15: System PLCC for all cases obtained using the D-P criterion

| | Case | PLCC (MW) | The most severe contingency |
|---|---|---|---|
| Base Case | B-C1 | 189 | L1 |
| | B-C2 | 197 | L2 |
| | B-C3 | 200 | L1 |
| Alternative 1 | A1-C1 | 226 | L1 |
| | A1-C2 | 234 | L1 |
| | A1-C3 | 237 | L1 |
| Alternative 2 | A2-C1 | 254 | G2-40 |
| | A2-C2 | 262 | G2-40 |
| | A2-C3 | 265 | G2-40 |

It can be seem from Table 6.15 that there are significant increases in the system PLCC values with the two alternatives obtained using the D-P method.

**Technique Comparison**

The system PLCC results shown in Tables 6.13, 6.14 and 6.15 obtained using the D, P and D-P methods respectively are repeated in Table 6.16 for comparison purposes.

Table 6.16: Comparison of the system PLCC (MW) values obtained using the three techniques

| | | D | P | D-P |
|---|---|---|---|---|
| Case 1 | B-C1 | 189 | 185 | 189 |
| | A1-C1 | 226 | 246 | 226 |
| | A2-C1 | 260 | 253 | 254 |
| Case 2 | B-C2 | 197 | 192 | 197 |
| | A1-C2 | 234 | 254 | 234 |
| | A2-C2 | 268 | 259 | 262 |
| Case 3 | B-C3 | 200 | 195 | 200 |
| | A1-C3 | 237 | 257 | 237 |
| | A2-C3 | 271 | 262 | 265 |

*Case 1 (no wind):*

In this case, B-C1 and A1-C1 are situations in which the system is transmission limited. The system PLCC values under B-C1 and A1-C1 obtained using the D method are the same as those obtained using the D-P method due to the deterministic N-1 criterion pre-condition before applying the probabilistic criterion in the D-P method. The PLCC for the A1-C1 determination using the P approach is higher due to the relatively low transmission line failure rates. A2-C1 is a case in which the system is generation limited and the P and D-P PLCC values are very similar. The D PLCC is the largest of the three values.

*Case2 (with 40 MW WECS):*

In B-C2 and A1-C2, the PLCC values under the D-P criterion are the same as those under the D criterion. The PLCC value for the P criterion is the highest of the three alternatives for this condition. In A2-C2, the D PLCC value is the largest of the three methods. The D-P PLCC value is close to the PLCC for the P approach. Although the criteria for the three techniques are different, the degrees of improvement in the PLCC due to adding the two 20 MW WECS are very similar for the three techniques.

*Case 3 (with 80 MW WECS):*

The general conclusions in Case 2 also apply in Case 3. It is interesting to note that the additional 40 MW wind capacity in Case 3 results an increase in the PLCC of only 3 MW over the PLCC in Case 2 using the three techniques.

### 6.5.4. The Effect of the Probability Criterion on the System PLCC

Table 6.16 shows the system PLCC values for all study cases obtained using the three techniques. It is impossible to compare the risk associated with different contingencies under the D criterion as this approach does not provide any quantitative information. The P and D-P methods involve an evaluation of the quantitative system risk. The PLCC under various selected risk criterion values obtained using the two methods are analyzed to investigate the impact of the risk criterion on the system risk level.

The effect of the probabilistic criterion (Rc) in the P method are investigated using the study cases. It is assumed that the Rc values are 4.4, 10, 15 and 20 SM/yr respectively. The system PLCC results with varying selected Rc values are shown in Table 6.17.

Table 6.17: The system PLCC (MW) for each case with the variation of Rc values

| | | P method | | | |
|---|---|---|---|---|---|
| | | Rc=4.4 SM/yr | Rc=10 SM/yr | Rc=15 SM/yr | Rc=20 SM/yr |
| Base Case | B-C1 | 185 | 195 | 200 | 204 |
| | B-C2 | 192 | 203 | 207 | 211 |
| | B-C3 | 195 | 205 | 210 | 214 |
| Alternative 1 | A1-C1 | 246 | 257 | 262 | 266 |
| | A1-C2 | 254 | 265 | 270 | 274 |
| | A1-C3 | 257 | 268 | 273 | 277 |
| Alternative 2 | A2-C1 | 253 | 263 | 268 | 272 |
| | A2-C2 | 259 | 270 | 275 | 279 |
| | A2-C3 | 262 | 273 | 278 | 282 |

Table 6.17 shows that the selection of an Rc value impacts the system acceptable risk level using the P approach. Although the system peak load carrying capacity is improved with the increase in the criterion value Rc, this is accomplished at a higher risk level.

The effects of the Pc value on the system PLCC in the D-P approach are conducted using the nine study cases by assuming that the Pc values are 35, 50, 85, 120 and 200 SM/yr respectively. The system PLCC values with the variation in Pc are shown in Table 6.18. The system PLCC values for A2-C2 with varying Pc values are graphically shown in Figure 6.14 to illustrate the impact.

Table 6.18: The system PLCC (MW) for each case with the variation of Pc values for the D-P method

| Case | | D-P Method | | | | | D Method |
|---|---|---|---|---|---|---|---|
| | | Pc=35 SM/yr | Pc=50 SM/yr | Pc=85 SM/yr | Pc=120 SM/yr | Pc=200 SM/yr | |
| Base Case | B- C1 | 189 | 189 | 189 | 189 | 189 | 189 |
| | B- C2 | 195 | 197 | 197 | 197 | 197 | 197 |
| | B- C3 | 196 | 199 | 200 | 200 | 200 | 200 |
| Alternative 1 | A1-C1 | 209 | 214 | 222 | 226 | 226 | 226 |
| | A1-C2 | 218 | 223 | 231 | 234 | 234 | 234 |
| | A1-C3 | 221 | 226 | 234 | 237 | 237 | 237 |
| Alternative 2 | A2-C1 | 238 | 242 | 249 | 254 | 260 | 260 |
| | A2-C2 | 245 | 250 | 257 | 262 | 268 | 268 |
| | A2-C3 | 248 | 253 | 260 | 265 | 271 | 271 |

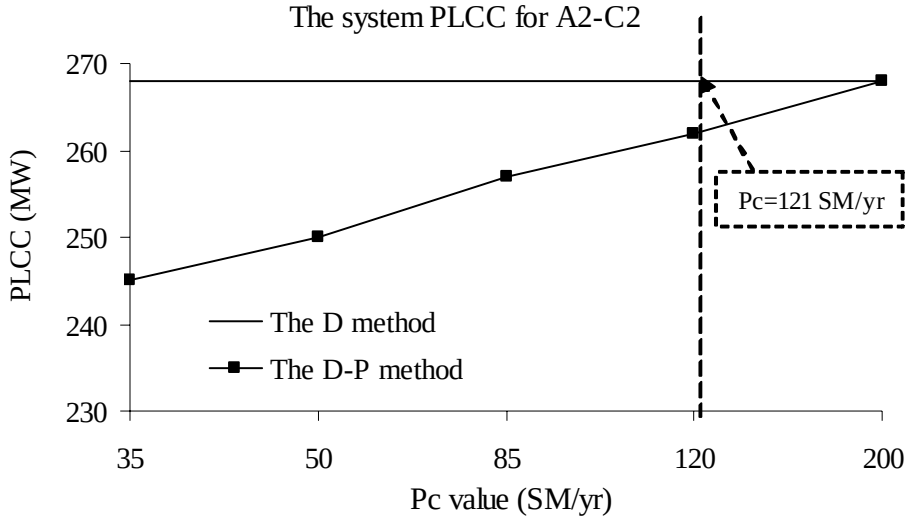


Figure 6.14: Comparison of the system PLCC obtained using the D and D-P with varying Pc values

It can be seen from Table 6.18 and Figure 6.14 that the system PLCC increases with increase in the selected Pc value. The system PLCC values for the Base case obtained using the D-P approach are the same as those obtained using the D method when the Pc values is greater than 85 SM/yr. The PLCC values for Alternatives 1 and 2 also illustrate that the D and D-P approaches provide the same results when the Pc is more than or equal to 120 SM/yr and 200 SM/yr respectively. The application of the D-P method in these conditions can not provide more stringent results for a system than the D method. Under the 35 SM/yr Pc condition, the results obtained using the D-P method are lower than those in the D method. The advantage of the D-P method is that it provides more stringent results. The particular Pc value used in the D-P method is very dependent on the utility management philosophy and what constitute an acceptable risk level.

## 6.6. Conclusions

The joint deterministic-probabilistic technique can be applied as a planning tool in bulk power systems containing wind energy. The first step in both the D and D-P approaches is the determination of the wind capacity credit. The capacity contribution of a wind generation conversion system is not obvious due to its variable and intermittent characteristics. This chapter examines wind capacity credit using the ELCC, Capacity Factor and DAFORW approaches.

Although the wind capacity credit values obtained using the ELCC, Capacity Factor and DAFORW approaches are not significantly different, the ELCC method is the most comprehensive approach as generating unit outage parameters, hourly load demands and system reliability parameters are considered in the analysis. The ELCC method is used in WECS studies described in this thesis. Sensitivity studies of wind capacity credit indicate that the benefits in system PLCC with increase in the wind capacity credit are impacted by the WECS location and system condition.

When a WECS is not the maximum impact element in a D-P analysis based on its capacity credit value, a WECS in the form of a multi-state model is applied in the resulting probabilistic reliability assessment using the state-sampling Monte Carlo simulation method.

The analyses conducted on the MRBTS associated with a single WECS show that adding the WECS results in different PLCC improvement values for the D, P and the D-P methods. In expanding the total installed wind capacity, the system PLCC benefits due to adding two wind farms in the MRBTS are higher than those for a single wind farm.

The D, P, and D-P techniques are used in a WECS planning context in this chapter. The study results indicate that none of the three approaches produce the highest or lowest PLCC in all cases. The D method produces a hard limit in which WECS is considered as a firm generating unit. The P approach provides a much softer limit since it recognizes the variable nature of a WECS. In the D-P approach the system must first satisfy the D criterion. The system risk given that the critical element has failed must then be equal to or less than a specified probabilistic risk criterion. If this risk is less than or equal to the criterion value, the D and D-P approaches provide the same result. If the risk exceeds this value then the load must be reduced to meet the acceptable risk level. The application of the D-P method provides more stringent results for a system with wind energy than the D method because the D-P technique is driven by the deterministic N-1 criterion with an added probabilistic perspective which recognizes the power output characteristics of a WECS.

# 7. Large-Wind Integrated Bulk System Reinforcement Planning

## 7.1. Introduction

The primary function of a power system is to provide electrical energy to its customers economically and with an acceptable degree of continuity and quality [9]. System planners and owners are therefore expected to evaluate the reliability and economic parameters with considerable detail in grid planning where the problem involves many uncertainties including those of investment budgets, reliability criteria, load forecasts and system characteristics, etc. [99]. The deterministic N-1 (D) planning criterion for transmission systems has been used for many years and will continue to be a benchmark criterion [25]. The likelihood of the designated single element failing is not included in an analysis using the D approach. In the probabilistic (P) approach this likelihood is included together with similar probabilities for all the elements in the system to calculate the system risk. The P method is used in transmission planning [25, 100-102] as it provides quantitative indices which can be used to decide if the system performance is acceptable or if changes need to be made, and can be used for performing economic analyses. There is a growing interest in combing deterministic considerations with probabilistic assessment in order to evaluate the quantitative system risk and conduct bulk power system planning [103, 104]. As noted in Chapter 6, the D-P technique is one of the approaches that incorporate deterministic considerations with probabilistic assessment. The D-P approach provides an element of consistency in the assessment by introducing the concept of an acceptable risk level under the critical element outage condition.

This chapter presents technical and economic assessments using the D-P method in large wind integrated bulk system planning. A comparison of the P and the D-P methods for long-term bulk system planning was also conducted using a representative study. Careful study of the uncertainty in the growing demand is required due to the fact that load uncertainty is inherent in any electric power system. The impacts on the system risk indices and investments in the planning period by considering load forecast uncertainty are examined in this chapter.

## 7.2. Study System

The MRTS is shown in Section 4.6.1 of Chapter 4. A new modified system was created based on the MRTS and designated as the M2MRTS in order to conduct studies using the D, D-P and P techniques. The numbers of generating units were doubled at Buses 16, 18 and 21, and 2×50 MW and 1×155 MW generating units were added at Bus 22 and Bus 23 respectively. The rating of Line 10 was increased to 1.1 p.u. of the original rating. The total number of generating units in the M2MRTS is now 38 units. The total system capacity is 4615 MW. The load value at each load points was increased by a factor of 1.28. The reference peak load of the M2MRTS is 3650 MW. The single line diagram of the M2MRTS is shown in Figure 7.1.

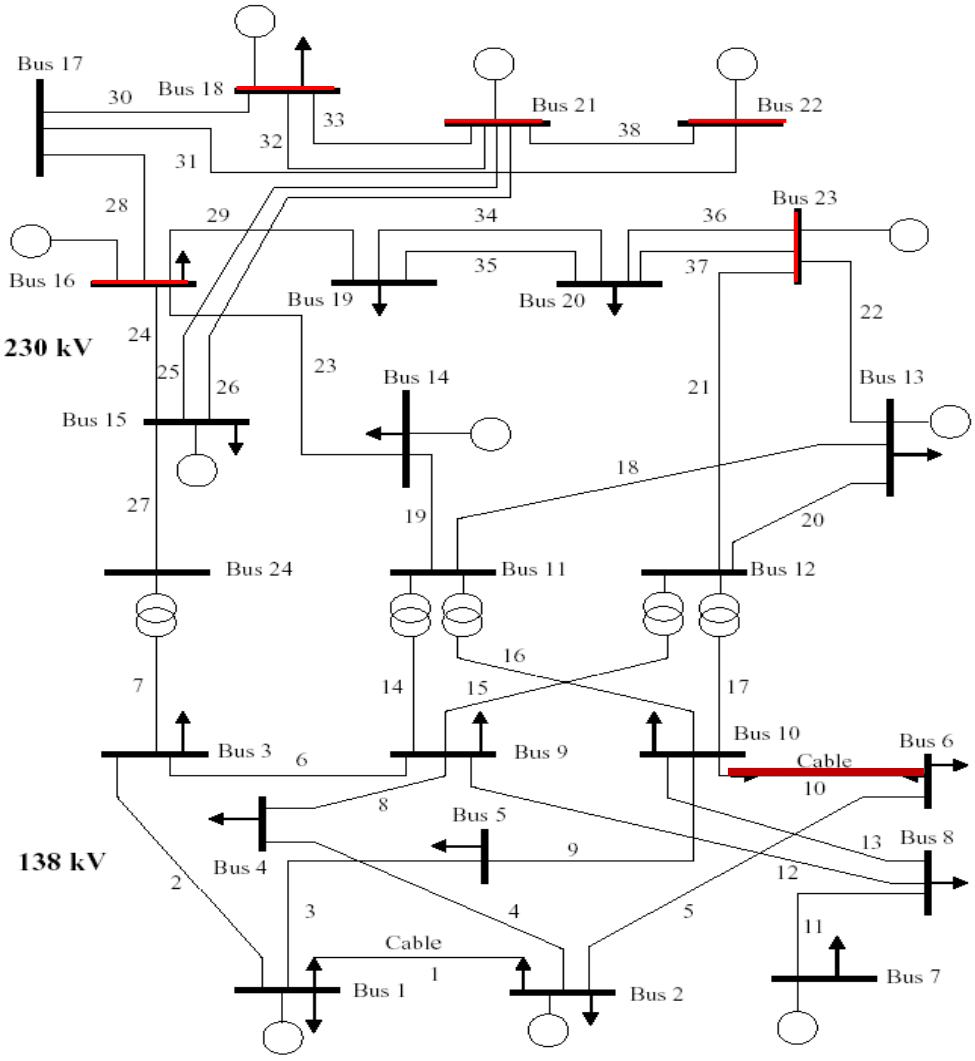


Figure 7.1: Single line diagram of the M2MRTS

A contingency list for the M2MRTS was obtained by applying the D criterion, involving single generating unit or single transmission elements. The purpose of a contingency selection process is to reduce and limit the set of outage components to be considered. In the case of generation facilities, the largest generating units at different locations in the system are considered. In the case of transmission facilities, the transmission line selections can be done through power flow analyses. The most severe single contingency can be determined from the contingency analysis list. The rank contingency order and the corresponding system PLCC for the M2MRTS are shown in Table 7.1.

Table 7.1: Contingency list for the M2MRTS under the deterministic N-1 criterion

| Rank Order | Outage | PLCC (MW) |
|---|---|---|
| 1 | L10 | 3670 |
| 2 | L23 | 3732 |
| 3 | L7/ L27 | 3783 |
| 4 | L5 | 4031 |
| 5 | L19 | 4086 |
| 6 | L21 | 4104 |
| 7 | G23_350 | 4210 |
| 8 | G18_400 | 4213 |
| 9 | G21_400 | 4213 |
| 10 | L8 | 4239 |

Table 7.1 shows that the line outages tend to have a higher rank than generating unit outages and an L10 outage is the most severe contingency in this system. The M2MRTS has obvious transmission deficiencies, especially in the southeast part of the system. Table 7.1 shows that the system PLCC value using the D approach is 3670 MW.

A probabilistic analysis was conducted using the MECORE program with Line 10 removed from the system. The system SI (SM/yr) as a function of the system peak load obtained utilizing the D-P method are shown in Table 7.2.

Table 7.2: The system SI (SM/yr) for the M2MRTS obtained using the D-P method

| Peak Load (MW) | 3650 | 3670 |
|---|---|---|
| SI | 33.75 | 34.19 |

When using the P approach, the M2MRTS system EENS and SI indices at the reference peak load of 3650 MW are 175 MWh/yr and 2.9 SM/yr respectively.

## 7.3. M2MRTS Analysis with WECS

Two moderately correlated 470 MW WECS with Regina and Swift Current site data are added in the M2MRTS through transmission lines. The five-state models for the two WECS shown in Table 6.1 are used in the studies described in this chapter. The length of each transmission line is 88 km. The admittance, unavailability and repair time of the facility connection line is 4.73485 (p.u.), 0.00058, 10 hrs respectively. The assumed carrying capacity of the circuit is the installed capacity of the WECS.

### 7.3.1. WECS Wind Capacity Credit

The ELCC method described in Chapter 6 is used to evaluate the 470 MW WECS wind capacity credit. The system LOLE for the M2MRTS is 0.75 hrs/yr utilizing a chronological load profile. The combined system can carry a peak load of 3770 MW at a LOLE of 0.75 hrs/yr after the two 470 MW WECS are added. The increase in peak load carrying capability is 120 MW. Previous studies described in Chapter 6 show that it is reasonable to evenly divide the total wind capacity credit between the two farms when the two WECS have identical installed capacities. The wind capacity credit for each 470 MW WECS is therefore 60 MW and is used in the following studies described in this chapter. The largest generating unit in the M2MRTS has a capacity of 400 MW, and a WECS outage does not therefore constitute the most severe contingency under the D criterion.

### 7.3.2. Effect of the WECS Location

The WECS locations in the M2MRTS are considered in two cases:

Case 1: the WECS are added at Buses 1 and 3.

Case 2: the WECS are added at Buses 1 and 6.

The study results for the M2MRTS with and without WECS using the D, D-P and P techniques are shown in Tables 7.3 to 7.5.

Table 7.3: The rank orders for the M2MRTS and the two cases using the D method

| | M2MRTS | | Case 1 | | Case 2 | |
|---|---|---|---|---|---|---|
| Rank Order | Outage | PLCC (MW) | Outage | PLCC (MW) | Outage | PLCC (MW) |
| 1 | L10 | 3670 | L10 | 3670 | L23 | 3910 |
| 2 | L23 | 3732 | L23 | 3940 | L7/L27 | 3958 |
| 3 | L7/L27 | 3783 | L7/L27 | 3958 | L19 | 4275 |
| 4 | L5 | 4031 | L5 | 4046 | L21 | 4286 |
| 5 | L19 | 4086 | L21 | 4286 | G18_400/G21_400 | 4334 |
| 6 | L21 | 4104 | L19 | 4305 | G23_350 | 4378 |
| 7 | G23_350 | 4210 | G18_400/G21_400 | 4334 | L10 | 4487 |

Table 7.4: The system SI obtained using the D-P method

| | | | |
|---|---|---|---|
| M2MRTS (L10) | Peak load (MW) | 3650 | 3670 |
| | SI (SM/yr) | 33.75 | 34.19 |
| Case 1 (L10) | Peak load (MW) | 3650 | 3670 |
| | SI (SM/yr) | 33.68 | 33.89 |
| Case 2 (L23) | Peak load (MW) | 3650 | 3910 |
| | SI (SM/yr) | 86.48 | 157.78 |

Table 7.5: The system SI (SM/yr) obtained using the P method

| Peak load (MW) | M2MRTS | Case 1 | Case 2 |
|---|---|---|---|
| 3650 | 2.9 | 1.74 | 1.506 |
| 3750 | 4.98 | 2.765 | 2.617 |
| 3850 | 8.84 | 4.715 | 4.52 |
| 3950 | 16.01 | 8.472 | 8.153 |
| 4050 | 27.92 | 14.678 | 14.364 |
| 4150 | 49.04 | 25.774 | 25.29 |
| 4250 | 83.04 | 43.613 | 42.793 |
| 4350 | 137.27 | 72.314 | 71.074 |
| 4450 | n/a | 119.155 | 117.135 |
| 4550 | n/a | 187.834 | 184.529 |

It can be seen from Tables 7.3 and 7.4 that the system PLCC improves to 3910 MW in Case 2 due to the fact that the transmission stress on Line 10 is reduced by adding a WECS at Bus 6. Under the D criterion, the system PLCC value for Case 1 is 3670 MW which is the same as that of the M2MRTS. Table 7.5 shows that the system SI benefits due to adding WECS at different locations are similar using the P method. There are very small SI benefits obtained using the D-P

method in Case 1. The conclusion can be drawn that the WECS location results in different system SI benefits when using the P and D-P methods. The M2MRTS with WECS located at Bus 1 and Bus 6 (Case 2) is considered as the base system in the following planning studies described in this chapter.

## 7.4. Reinforcement Planning Technical Analysis

### 7.4.1. Base System Analysis

As noted earlier, the M2MRT with the two 470 MW WECS located in Bus 1 and Bus 6 is designated as the base system in these studies. The total installed generation capacity includes 4615 MW of conventional capacity and 940 MW of wind power. The system peak load is 3650 MW.

The analysis results for the base system obtained using the three methods are given in Tables 7.6 to 7.8. Table 7.6 shows that the most critical element contingency for the base system is a L23 outage. The variation in the system SI as a function of the peak load is shown in Table 7.7 obtained using the P method. Table 7.8 indicates that under the most critical contingency, the base system PLCC is 3910 MW using the D-P method and a Pc of 157.78 SM/yr.

Table 7.6: The system PLCC (MW) for the base system using the D method

| Rank Order | Outage | PLCC |
|---|---|---|
| 1 | L23 | 3910 |
| 2 | L7/L27 | 3958 |
| 3 | L19 | 4275 |
| 4 | L21 | 4286 |
| 5 | G18_400/ G21_400 | 4334 |
| 6 | G23_350 | 4378 |
| 7 | L10 | 4487 |
| 8 | L6 | 4487 |
| 9 | L1/L2/L8/L9 | 4531 |
| 10 | L5/L4/L12/L13 | 4534 |

Table 7.7: The system SI (SM/yr) for the base system using the P method

| Peak Load (MW) | 3650 | 3750 | 3850 | 3950 | 4050 | 4150 | 4250 | 4350 | 4450 | 4550 |
|---|---|---|---|---|---|---|---|---|---|---|
| SI | 1.506 | 2.617 | 4.520 | 8.153 | 14.364 | 25.290 | 42.793 | 71.074 | 117.135 | 184.529 |

Table 7.8: The system SI (SM/yr) for the base system using the D-P method

| Peak Load (MW) | 3650 | 3910 |
|---|---|---|
| SI | 86.48 | 157.78 |

Table 7.9 shows the yearly peak loads in a next ten year planning time frame assuming that the peak load in Year 0 is 3900 MW and each year has a 2% peak load growth.

Table 7.9: Annual peak load (MW)

| Year | 0 | 1 | 2 | 3 | 4 | 5 | 6 | 7 | 8 | 9 | 10 |
|---|---|---|---|---|---|---|---|---|---|---|---|
| Peak Load (MW) | 3900 | 3980 | 4060 | 4140 | 4220 | 4300 | 4390 | 4480 | 4570 | 4660 | 4760 |

Table 7.9 shows that the base system PLCC of 3910 MW obtained using the D-P method cannot meet the system peak load growth over the next ten years. The system risk index SI is approximately 158 SM/yr at the system PLCC of 3910 MW using the D-P method. The analysis conducted on the MRBTS in Chapter 6 shows that the selection of the Pc and Rc values impact the system acceptable risk level using the D-P and P approaches. A high Pc value indicates the acceptance of a high risk and could result in there being no difference between the system PLCC values obtained using the D and the D-P approaches. A Pc of 50 SM/yr and a Rc of 10 SM/yr are applied as the base system risk criteria respectively in the following studies.

The planning time frame is an eleven year period and is considered to include two stages:
Stage 1 is from the $0^{th}$ to $4^{th}$ year to meet the system peak load of 4220 MW.
Stage 2 is from the $5^{th}$ to $10^{th}$ year to meet the system peak load of 4760 MW.

### 7.4.2. The System Planning Using the D-P Approach

The intent of this study is not to cover all the aspects of the planning process. The focus is on

transmission reinforcement planning. It is assumed that generation expansion has determined that 6×50 MW conventional generating units will be installed at Bus 22, 1×350 MW and 3×155 MW units will be added at Bus 23. The total installed conventional generating capacity therefore increases to 5730 MW in the eleven year planning time frame.

The deterministic N-1 criterion is the precondition in using the D-P method. The selection of planning alternatives to meet the N-1 criterion over a planning time frame is the first step in using the D-P method. Six expansion planning alternatives are proposed based on practical planning considerations. In the case of a large-scale transmission system, it is reasonable to limit the study to an area or subsystem. Doing so can provide more realistic results than evaluating the whole system [25]. These alternatives are listed as follows:

**Alternative 1**

The procedure applied in Alternative 1 is as follows. The most severe contingency in each step of Alternative 1 and the corresponding system PLCC values are shown in Table 7.10.

***Alternative 1_Stage 1***

*Step 1: Double Line 23 and Line 19.*

Bus 14 has a high load curtailment priority and a weak transmission connection (only Lines 19 and 23), which means that Bus 14 will suffer not only from generation deficiencies but also from the removal of Line 19 or Line 23. The base system PLCC ranking shown in Table 7.5 indicates that Line 23 is the most critical element outage for the base system. The first step in reinforcing the transmission network is, therefore, to double Lines 23 and 19. The system PLCC under this condition is 4080 MW as shown in Table 7.10.

*Step 2: Double Line 6.*

The rank order for Step 1 shown in Table 7.10 indicates that an L7 outage is the most critical contingency after reinforcing Lines 19 and 23. Lines 6, 13 and 28 experience overload conditions which cause load curtailment at Bus 3 in the normal system state. The transmission stress is diminished by doubling Line 6. The system PLCC in Step 2 is 4250 MW as shown in Table 7.10. It can be seen from Table 7.10 that the system PLCC value under the D criterion meet the 4$^{th}$

year load demand in Step 2. The system is in a generation deficient condition after reinforcing the transmission network as the system peak load increases.

***Alternative 1_Stage 2***

*Step 3: Add 6×50 MW units at Bus 22, a 350 MW and 3×155 MW units at Bus 23.*

The generation deficiency problem is solved by adding generating units to the system. Bus 8 is connected to the system by Lines 12, 13 and 11. The removal of Line 11 is not considered as in this case Bus 7 will be isolated. Bus 8 risk indices are, therefore, sensitive to a contingency on Lines 12 and 13. Table 7.10 shows that the system most critical contingency in Step 3 is the removal of Line 12 or Line 13. The system PLCC under this condition is 4575 MW as shown in Table 7.10.

*Step 4: Double Line 12 or 13.*

The transmission stress in Lines 12, 13 and 17 is reduced by doubling Line 12 or Line 13. Table 7.10 indicates that the system PLCC now becomes 4835 MW which satisfies the $10^{th}$ year system peak load under the most critical contingency of a Line 21 outage.

Table 7.10: The system PLCC under the most critical contingency for Alt. 1 using the D method

| Alternative 1 | | Most severe outage condition | PLCC (MW) |
|---|---|---|---|
| Stage 1 (0-$4^{th}$ yr) | Step 1: Double Line 23 and Line 19 | L7 | 4080 |
| | Step 2: Double Line 6 | G23_350 | 4250 |
| Stage 2 ($5^{th}$- $10^{th}$ yr) | Step 3: Add 6×50 MW units at Bus 22, a 350 MW and 3×155 MW units at Bus 23 | L12 or L13 | 4575 |
| | Step 4: Double Line 12 | L21 | 4835 |

**Alternative 2**

The procedure applied in Alternative 2 is as follows. The most severe contingency in each step of Alternative 2 and the corresponding system PLCC values are shown in Table 7.11.

***Alternative 2_Stage 1***

*Step1: Add a line between Bus 11 and Bus 15.*

A new line was added between Buses 11 and 15 and designated as Line 39. The parameters of Line 39 are the same as those of Line 27. Bus14 has a weak transmission connection problem which is solved by adding this line. The most severe element outage event is now a Line 7 outage. The system PLCC under this condition is 4060 MW as shown in Table 7.11.

*Step 2: Double Line 6.*

The situation is similar to that described previously for Alternative 1 for which the solution was to double Line 6. Generation deficiency is again the main problem for the system after adding the additional line and doubling Line 6. The outage of a 400 MW unit at Bus 18 is the most critical contingency in Step 2. The system PLCC in Step 2 is 4330 MW and exceeds the system load in the $4^{th}$ year.

***Alternative 2_Stage 2***

*Step 3: Add 6×50 MW units at Bus 22, a 350 MW and 3×155 MW units at Bus 23.*

The system generation deficiency problem is solved by adding the designated generating units. The most severe element outage for Step 3 is now Line 12 or 13 shown in Table 7.11. The system PLCC is now 4575 MW.

*Step 4: Double Line 12 or 13.*

The transmission stress in Lines 12, 13 and 17 is reduced by doubling Line 12 or 13. The system PLCC is now 4800 MW under a Line 21outage condition as shown in Table 7.11.

Table 7.11: The system PLCC under the most critical contingency for Alt. 2 using the D method

| Alternative 2 | | Most severe outage condition | PLCC (MW) |
|---|---|---|---|
| Stage 1 (0-$4^{th}$ yr) | Step 1: Add a line between Bus 11 and Bus 15 | L7 | 4060 |
| | Step 2: Double Line 6 | G18_400 | 4330 |
| Stage 2 ($5^{th}$- $10^{th}$ yr) | Step 3: Add 6×50 MW units at Bus 22, a 350 MW and 3×155 MW units at Bus 23 | L12/L13 | 4575 |
| | Step 4: Double Line 12 | L21 | 4800 |

It can be seen from Table 7.11 that the system peak loads at each stage are satisfied for Alternative 2.

**Alternative 3**

The procedure applied in Alternative 3 is as follows. The most severe contingency in each step of Alternative 3 and the corresponding system PLCC values are shown in Table 7.12.

***Alternative 3_Stage 1***

*Step1: Double Line 23.*

Doubling Line 23 results in the system PLCC increasing from 3910 MW to 4080 MW. The most critical contingency is now a Line 7 outage.

*Step 2: Double Line 7 and Line 27.*

The transmission system risk is further reduced by doubling Lines 7 and 27. The most critical system condition is now an outage of a 350 MW unit at Bus 23. The system PLCC under the G23-350 condition is 4250 MW which exceeds the required 4220 MW at the end of Stage 1.

***Alternative 3_Stage 2***

*Step 3: Add 6×50 MW units at Bus 22, a 350 MW and 3×155 MW units at Bus 23.*

The system generation deficiency problem is alleviated with the addition of these generating units. The most severe element outage for Step 3 is now Line 12 or 13 as shown in Table 7.12. The system PLCC is 4575 MW under this condition.

*Step 4: Add a line between Bus 6 and Bus 8.*

Studies indicate that the PLCC can be enhanced with the addition of a line between Buses 6 and 8. The new transmission line is designated as Line 40 and has the same parameters as Line 12. The system PLCC now increases to 4880 MW. System transmission stress in the eastern part of the 138 KV system still exists and the removal of Line 12 or 13 remains the most severe element outage event in the reinforced system.

Table 7.12: The system PLCC under the most critical contingency for Alt. 3 using the D method

| Alternative 3 | | Most severe outage condition | PLCC (MW) |
|---|---|---|---|
| Stage 1 (0-4$^{th}$ yr) | Step 1: Double Line 23 | L7 | 4080 |
| | Step 2: Double Line 7 and Line 27 | G23_350 | 4250 |
| Stage 2 (5$^{th}$- 10$^{th}$ yr) | Step 3: Add 6×50 MW units at Bus 22, a 350 MW and 3×155 MW units at Bus 23 | L12/L13 | 4575 |
| | Step 4: Add a line between Bus 6 and Bus 8 | L12 | 4880 |

Table 7.12 shows that the system peak load at each stage can be satisfied using Alternative 3.

**Alternative 4**

The transmission system reinforcement analysis in Alternative 4 is similar to that in Alternative 1. The generation expansion is now conducted in two stages. The system PLCC values for each step of Alternative 4 are shown in Table 7.13.

Table 7.13: The system PLCC under the most critical contingency for Alt. 4 using the D method

| Alternative 4 | | Most severe outage condition | PLCC (MW) |
|---|---|---|---|
| Stage 1 (0-4$^{th}$ yr) | Step 1: Double Line 23 and Line 19; Add 6×50 MW units at Bus 22 and a 350 MW at Bus 23 | L7 | 4080 |
| | Step 2: Double Line 6 | L12/L13 | 4575 |
| Stage 2 (5$^{th}$- 10$^{th}$ yr) | Step 3: Double Line 12/13 | G23_350 | 4680 |
| | Step 4: Add 3×155 MW units at Bus 23 | L21 | 4835 |

**Alternative 5**

The transmission system reinforcement analysis in Alternative 5 is similar to that in Alternative 2. The generation expansion is now conducted in two stages. The system PLCC in each step of Alternative 5 are shown in Table 7.14.

Table 7.14: The system PLCC under the most critical contingency for Alt. 5 using the D method

| Alternative 5 | | Most severe outage condition | PLCC (MW) |
|---|---|---|---|
| Stage 1 (0-4$^{th}$ yr) | Step 1: Add a line between Buses 11 and 15; Add 6×50 MW units at Bus 22 and a 350 MW at Bus 23 | L7 | 4080 |
| | Step 2: Double Line 6 | L12/L13 | 4575 |
| Stage 2 (5$^{th}$- 10$^{th}$ yr) | Step 3: Double Line 12 | L7 | 4760 |
| | Step 4: Add 3×155 MW units at Bus 23 | L21 | 4800 |

**Alternative 6**

The transmission system reinforcement analysis in Alternative 6 is similar to that in Alternative 3. The generation expansion is now conducted in two stages. The most critical contingency in each step and the corresponding system PLCC values are shown in Table 7.15.

Table 7.15: The system PLCC under the most critical contingency for Alt. 6 using the D method

| Alternative 6 | | Most severe outage condition | PLCC (MW) |
|---|---|---|---|
| Stage 1 (0-4th yr) | Step 1: Double Line 23; Add 6×50 MW units at Bus 22 and a 350 MW at Bus 23 | L7 | 4080 |
| | Step 2: Double Line 7 and Line 27 | L12/L13 | 4575 |
| Stage 2 (5th- 10th yr) | Step 3: Add a line between Buses 6 and 8 | G23_350 | 4720 |
| | Step 4: Add 3×155 MW units at Bus 23 | L21 | 4880 |

It can be seen from Tables 7.13 to 7.15 that the system PLCC values for Alternatives 4, 5, and 6 meet the load growth at the end of each stage.

The study results for the six alternatives shown in Tables 7.10 to 7.15 are presented in Table 7.16 for comparison purposes. It can be seen from Table 7.16 that under the D criterion, the system PLCC values for the six alternatives at the end of Stage 1 meet the load requirements in the $4^{th}$ year, and the system PLCC values at Stage 2 for each alternative exceed the system load requirement in the $10^{th}$ year (4760 MW). The conclusion can be drawn that the six alternatives determined using the D method meet the future forecast load requirements.

Table 7.16: The system PLCC value for the six alternatives using the D method

| Alternative 1 | | Most severe outage condition | PLCC (MW) |
|---|---|---|---|
| Stage 1 (0-4th year) | Step 1: Double Lines 23 and 19 | L7 | 4080 |
| | Step 2: Double Line 6 | G23_350 | 4250 |
| Stage 2 (5th- 10th year) | Step 3: Add 6×50 MW units at Bus 22, a 350 MW and 3×155 MW units at Bus 23 | L12/L13 | 4575 |
| | Step 4: Double Line 12 | L21 | 4835 |
| Alternative 2 | | Most severe outage condition | PLCC (MW) |
| Stage 1 (0-4h year) | Step 1: Add a line between Buses 11 and 15 | L7 | 4060 |
| | Step 2: Double Line 6 | G18_400 | 4330 |
| Stage 2 (5th- 10th year) | Step 3: Add 6×50 MW units at Bus 22, a 350 MW and 3×155 MW units at Bus 23 | L12/L13 | 4575 |
| | Step 4: Double Line 12 | L21 | 4800 |
| Alternative 3 | | Most severe outage condition | PLCC (MW) |
| Stage 1 (0-4th year) | Step 1: Double Line 23 | L7 | 4080 |
| | Step 2: Double Lines 7 and 27 | G23_350 | 4250 |
| Stage 2 (5th- 10th year) | Step 3: Add 6×50 MW units at Bus 22, a 350 MW and 3×155 MW units at Bus 23 | L12/L13 | 4575 |
| | Step 4: Double Line 12 | L12 | 4880 |
| Alternative 4 | | Most severe outage condition | PLCC (MW) |
| Stage 1 (0-4th year) | Step 1: Double Lines 23 and 19, add 6×50 MW units at Bus 22 and a 350 MW at Bus 23 | L7 | 4080 |
| | Step 2: Double Line 6 | L12/L13 | 4575 |
| Stage 2 (5th- 10th year) | Step 3: Double Line 12 | G23_350 | 4680 |
| | Step 4: Add 3×155 MW units at Bus 23 | L21 | 4835 |
| Alternative 5 | | Most severe outage condition | PLCC (MW) |
| Stage 1 (0-4th year) | Step 1: Add a line between Buses 11 and 15, add 6×50 MW units at Bus 22 and a 350 MW at Bus 23 | L7 | 4080 |
| | Step 2: Double Line 6 | L12/L13 | 4575 |
| Stage 2 (5th- 10th year) | Step 3: Double Line 12 | L7 | 4760 |
| | Step 4: Add 3×155 MW units at Bus 23 | L21 | 4800 |
| Alternative 6 | | Most severe outage condition | PLCC (MW) |
| Stage 1 (0-4th year) | Step 1: Double Line 23, add 6×50 MW units at Bus 22 and a 350 MW at Bus 23 | L7 | 4080 |
| | Step 2: Double Lines 7 and 27 | L12/L13 | 4575 |
| Stage 2 (5th- 10th year) | Step 3: Add a line between Buses 6 and 8 | G23_350 | 4720 |
| | Step 4: Add 3×155 MW units at Bus 23 | L21 | 4880 |

In applying the D-P method, the D analysis described above is followed by probabilistic analysis to determine the system risk under each critical outage condition. A probabilistic evaluation for each alternative is conducted with the most severe contingency to determine the system risk for the alternative in the planning time period. The system load requirement at the end of Stage 1 and Stage 2 are 4220 MW and 4760 MW respectively. The system SI values for the peak load of 4220 MW and 4760 MW under the D criterion are shown in Table 7.17.

Table 7.17: The system SI values (SM/yr) for the alternatives at the end of two stages obtained using the D- P method

| | Alt. 1 | Alt. 2 | Alt. 3 | Alt. 4 | Alt. 5 | Alt. 6 |
|---|---|---|---|---|---|---|
| Stage 1 (peak load in the $4^{th}$ year : 4220 MW ) | 175 | 184 | 168 | 38.4 | 39 | 37.5 |
| Stage 2 (peak load in the $10^{th}$ year : 4760 MW ) | 36 | 41 | 40 | 36 | 41 | 40 |

As noted earlier, a Pc of 50 SM/yr and a Rc of 10 SM/yr were selected as system criteria in this study. Table 7.17 shows that the system SI for Alternatives 1, 2 and 3 exceed 50 SM/yr in Stage 1. Alternatives 1, 2 and 3 were, therefore, eliminated from the candidate planning list due to their inability to meet the designated Pc value in the first planning time period and Alternatives 4, 5 and 6 are therefore acceptable planning alternatives using the D-P method.

### 7.4.3. System Planning Using the P Approach

The probabilistic evaluation for the six alternatives over the planning time frame was conducted using MECORE. The system SI values for the peak loads of 4220 MW and 4760 MW are shown in Table 7.18.

Table 7.18: The system SI values (SM/yr) for the alternatives obtained using the P method

| | Alt. 1 | Alt. 2 | Alt. 3 | Alt. 4 | Alt. 5 | Alt. 6 |
|---|---|---|---|---|---|---|
| Stage 1 (peak load in the 4th yr : 4220 MW ) | 39.8 | 2.72 | 31.5 | 2.95 | 2.04 | 1.64 |
| Stage 2 (peak load in the 10th yr : 4760 MW ) | 8 | 9.8 | 5.5 | 7.2 | 9.8 | 5.4 |

It can be seen from Table 7.18 that although the six alternatives meet the system load requirement in the second planning time period based on the Rc of 10 SM/yr, the system SI values for Alternatives 1 and 3 exceed the designated Rc in Stage 1. Alternatives 1 and 3 are unacceptable schemes using the P method.

The selected planning schemes for the three techniques are shown in Table 7.19. It can be seen from this table that the planning alternatives selected are different for the different criteria. All six alternatives are satisfied under the D criterion. Alternatives 4, 5 and 6 are acceptable using the D-P method. Alternatives 2, 4, 5 and 6 are candidate planning schemes using the P method.

Table 7.19: The selected planning schemes for the three techniques

| Method | D | P | D-P |
|---|---|---|---|
| Selected Alternatives | 1, 2, 3, 4, 5, 6 | 2, 4, 5, 6 | 4, 5, 6 |

## 7.5. Economic Analysis in Reinforcement Planning

Power system planning includes examining the predicted level of reliability and the investment and operating costs associated with the various alternatives. Economic analyses are conducted on the selected alternatives in order to determine the optimum planning option. The total cost includes the required investment and system operational costs and the customer interruption costs due to electric supply outage [25, 100, 101]. In this study, the best alternative is considered to be the one that achieves the minimum total cost while satisfying the applied reliability criterion.

### 7.5.1. Basic Concepts and Methods

The total cost includes the three costs [25] shown in Equation 7.1.

$$\text{Min } T = I + O + R \qquad (7.1)$$

where, I, O and R are the investment, operating and risk costs respectively.

The operating cost is not included in the evaluation in the study described in this chapter. The added generating capacity is basically the same for each alternative and the system operating

costs will be very similar for each alternative. Only the investment cost is considered in the D-P method and the investment and risk costs are included in the P method.

The risk cost is the customer interruption damage cost due to random system component outages. The Expected Damage Cost (EDC) is an important index that can be used to include economic analysis in composite system adequacy assessment. As noted in Chapter 2, MECORE calculates this index by multiplying the EENS of the overall system by the system IEAR. The system IEAR of the IEEE-RTS can be calculated using the data in Table 2.2, and is 4.22 $/kWh [34]. An IEAR of 4.22 $/kWh is a relatively low value based on a unit interrupted cost of 9.08 $/kWh indicated in [106]. The IEAR values shown in Table 2.2 were therefore increased by a factor of two and applied in the M2MRTS. The values for each load point of the M2MRTS and the corresponding priority order are shown in Table 7.20. The system IEAR of the M2MRTS is 8.44 $/kWh.

Table 7.20: Bus IEAR values and priority order in the M2MRTS

| Bus No. | IEAR ($/kWh) | Priority Order |
|---|---|---|
| 1 | 12.40 | 1 |
| 2 | 9.78 | 9 |
| 3 | 10.60 | 8 |
| 4 | 11.24 | 3 |
| 5 | 12.22 | 2 |
| 6 | 11.0 | 4 |
| 7 | 10.82 | 5 |
| 8 | 10.80 | 6 |
| 9 | 4.60 | 16 |
| 10 | 8.28 | 10 |
| 13 | 10.78 | 7 |
| 14 | 6.82 | 14 |
| 15 | 6.02 | 15 |
| 16 | 7.08 | 13 |
| 18 | 7.50 | 11 |
| 19 | 4.58 | 17 |
| 20 | 7.28 | 12 |

The annual cash flow of the annual investment cost is estimated using the capital return factor (CRF) [25, 26] shown as follows:

$$A = V \times CRF \tag{7.2}$$

$$CRF = \frac{i(1+i)^n}{(1+i)^n - 1} \tag{7.3}$$

where $A$ is the annual equivalent capital, $V$ is the actual investment in a given year, $i$ is the discount or present worth rate, $n$ is the economic life (year) of the investment $V$.

The present value method which captures the time values of the costs is used to calculate the total cost over a cash flow.

$$PV = \sum_{j=1}^{m} \frac{A_j}{(1+i)^{j-1}} \tag{7.4}$$

where, $PV$ is the present value, $A_j$ the annual cost in year j, $i$ the discount rate, and $m$ the number of years considered in the system plan. The present value of the total investment cost ($TI$) for a period of $m$ years assuming that there is the same annual equivalent investment in the period of $m$ years can be calculated by:

$$TI = V \frac{i(1+i)^n}{(1+i)^n - 1} \sum_{j=1}^{m} \frac{1}{(1+i)^{j-1}} \tag{7.5}$$

Reference 25 illustrates the procedure for calculating the present value of a multi-stage investment. As noted earlier, the planning period in this study is divided into two segments. The required investment for each stage is determined and the total cash flow evaluated. The cash flow for each individual investment can be obtained using Equations 7.2 and 7.3. Each cash flow has a time length equal to the economic life of the investment, with each year having equal annual equivalent capital. The cash flows corresponding to the different investment stages show a time shift between them and can be superimposed to obtain the total cash flow for the two stage investment. The concept is illustrated in Figure 7.2. Investments 1 and 2 are assumed be in place in years $T_1$ and $T_2$, with annual equivalent capitals $A_1$ and $A_2$ respectively. The planning span is from $T_1$ to $T_3$ (the dashed line). The total cash flow for the two-stage investments within the planning span should be calculated in such a way that the annual capital between $T_1$ and $T_2$ is $A_1$, the one between $T_2$ and $T_3$ is $A_1+A_2$. Equation 7.4 is used to calculate the present value after the total cash flow is obtained.

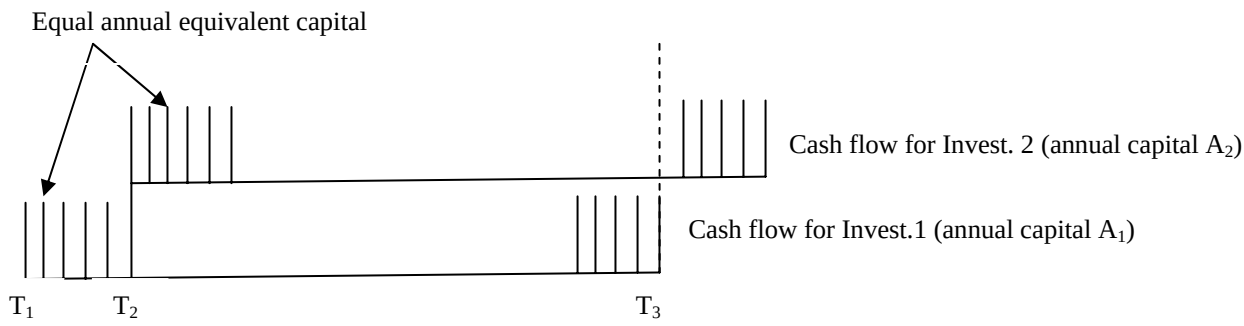


Figure 7.2: Cash flows for two-stage investments

### 7.5.2. Investment Costs Analysis

The investment cost of the four transmission reinforcement alternatives shown in Table 7.19 were calculated using the following assumptions:

Capitalized unit cost [26]: 50 MW hydro unit: 1200 $/KW,
155 MW fossil steam unit: 1400$/KW,
350 MW fossil steam unit: 1400$/KW

Investment cost of a 230/138 KV transformer (400 MVA) addition: 13M$

Investment cost of a transmission line: a 238 KV overhead line =0.8 M$/mile
a 138 KV overhead line =0.5 M$/mile

Transmission line length: 138 KV: L40 =86 mile, L6=62 mile, L12=86 mile.
230 KV: L19=116 mile, L23=108 mile
L27=144 mile, L39=144 mile

The investment cost of a second line is assumed to be 50% of the cost of the first line when a double circuit structure is used.

Useful lifetime considered=50 years

Discount rate (present worth rate) =8% per year

$$\mathrm{CRF} = \frac{0.08 \times (1+0.08)^{50}}{(1+0.08)^{50} - 1} = 0.08174$$

As noted above, Alternatives 4, 5 and 6 are the selected alternatives in the planning time period based the technical analysis conducted using the D-P and P methods. In addition, Alternative 2 is selected in the P method. In order to illustrate the procedure, the investment cost for Alternative

4 is presented in the following. The capital investment cost in Stage 1 is considered to be in place in the starting year (0 year) and is in place in the 5th year in Stage 2. Transmission cost is designated as “T”, and generating unit cost is represented by “G”.

*Alternative 4_ Stage 1: Double Lines 19, 23 and 6; Add 6×50 MW and 1×350 MW units at Buses 22 and 23 respectively.*

The project actual investment cost in the starting year of Stage 1:

$$\begin{aligned} V_{41} &= V_{41T} + V_{41G} \\ &= (0.5 \times (0.8 \times 108 + 0.8 \times 116 + 0.5 \times 62)) + (6 \times 50 \times 1.2 + 1 \times 350 \times 1.4) \\ &= 105.1 + 850 \\ &= 955.1 \ \text{(M\$)} \end{aligned}$$

The annual capital payment in Stage 1:

$$\begin{aligned} A_{41} &= A_{41T} + A_{41G} \\ &= (V_{41T} + V_{41G}) \times CRF \\ &= (105.1 + 850) \times 0.08174 \\ &= 8.59 + 69.48 \\ &= 78.07 \ \text{(M\$)} \end{aligned}$$

The present value of the total investment in Stage 1:

$$\begin{aligned} TI_{41} &= TI_{41T} + TI_{41G} \\ &= (8.59 + 69.48) \times \left( \frac{1}{(1+0.08)^{1-1}} + \frac{1}{(1+0.08)^{2-1}} + \frac{1}{(1+0.08)^{3-1}} + \frac{1}{(1+0.08)^{4-1}} + \frac{1}{(1+0.08)^{5-1}} \right) \\ &= 37.05 + 299.60 \\ &= 336.65 \ \text{(M\$)} \end{aligned}$$

*Alternative 4_Stage 2: Add 3×150 MW units at Bus 23 and double Line 12.*

The project actual investment cost in the starting year of Stage 2:

$$\begin{aligned} V_{42} &= V_{42T} + V_{42G} \\ &= 0.5 \times (0.5 \times 86) + (3 \times 155 \times 1.4) \\ &= 21.5 + 651 \\ &= 672.5 \ \text{(M\$)} \end{aligned}$$

The annual capital payment in Stage 2:

$$
\begin{aligned}
A_{42} &= A_{42T} + A_{42G} \\
&= (V_{42T} + V_{42G}) \times CRF \\
&= 1.76 + 53.21 \\
&= 54.97 (M\$)
\end{aligned}
$$

The present value of the total investment in Stage 2:

$$
\begin{aligned}
TI_{42} &= (A_{41} + A_{42}) \times \left( \frac{1}{(1+0.08)^{6-1}} + \frac{1}{(1+0.08)^{7-1}} + \frac{1}{(1+0.08)^{8-1}} + \frac{1}{(1+0.08)^{9-1}} + \frac{1}{(1+0.08)^{10-1}} + \frac{1}{(1+0.08)^{11-1}} \right) \\
&= (A_{41T} + A_{42T}) \times 3.40 + (A_{41G} + A_{42G}) \times 3.40 \\
&= 10.35 \times 3.40 + 122.69 \times 3.40 \\
&= 35.16 + 416.90 \\
&= 452.06 (M\$)
\end{aligned}
$$

Finally, the present value of the total investment for Alternative 4:

$$
\begin{aligned}
TI_4 &= TI_{4T} + TI_{4G} \\
&= (37.05 + 35.16) + (299.60 + 416.90) \\
&= 72.21 + 716.50 \\
&= 788.71 \ (M\$)
\end{aligned}
$$

The calculation of the investment costs for Alternatives 2, 5, and 6 is similar to that shown for Alternative 4 and is provided in Appendix E. The investment costs of the four alternatives are summarized in Table 7.21.

Alternatives 4, 5 and 6 are the selected alternatives in the planning time period based on the D-P method. A comparison of the investment cost for Alternatives 4, 5 and 6 shown in Table 7.21 indicates that the generation expansion cost for the three alternatives are the same and that the transmission reinforcement planning investment cost for Alternative 4 is less than that for Alternatives 5 and 6. Alternative 4 is, therefore, the best planning option in the D-P approach.

Table 7.21: The investment costs (PV in $0^{th}$ year M$) of the alternatives in an eleven-year planning period

| **Alternative 2** | | T | G | T+G |
|---|---|---|---|---|
| Stage 1 | $V_1$ | 130.7 | 0 | 130.7 |
| | $A_1$ | 10.68 | 0 | 10.68 |
| | $TI_1$ | 46.07 | 0 | 46.07 |
| Stage 2 | $V_2$ | 21.5 | 1501 | 1522.5 |
| | $A_2$ | 1.76 | 122.69 | 124.45 |
| | $TI_2$ | 42.27 | 416.90 | 459.17 |
| The present value of the total investment ($TI_1$+ $TI_2$) | | ***88.34*** | ***416.90*** | ***505.24*** |
| **Alternative 4** | | T | G | T+G |
| Stage 1 | $V_1$ | 105.1 | 850 | 955.1 |
| | $A_1$ | 8.59 | 69.48 | 78.07 |
| | $TI_1$ | 37.05 | 299.60 | 336.65 |
| Stage 2 | $V_2$ | 21.5 | 651 | 672.5 |
| | $A_2$ | 1.76 | 53.21 | 54.97 |
| | $TI_2$ | 35.16 | 416.90 | 452.06 |
| The present value of the total investment ($TI_1$+ $TI_2$) | | ***72.21*** | ***716.50*** | ***788.71*** |
| **Alternative 5** | | T | G | T+G |
| Stage 1 | $V_1$ | 130.7 | 850 | 980.7 |
| | $A_1$ | 10.68 | 69.48 | 80.16 |
| | $TI_1$ | 46.07 | 299.60 | 345.67 |
| Stage 2 | $V_2$ | 21.5 | 651 | 672.5 |
| | $A_2$ | 1.76 | 53.21 | 54.97 |
| | $TI_2$ | 42.27 | 416.90 | 459.17 |
| The present value of the total investment ($TI_1$+ $TI_2$) | | ***88.34*** | ***716.50*** | ***804.84*** |
| **Alternative 6** | | T | G | T+G |
| Stage 1 | $V_1$ | 113.8 | 850 | 963.80 |
| | $A_1$ | 9.30 | 69.48 | 78.78 |
| | $TI_1$ | 40.11 | 299.60 | 339.71 |
| Stage 2 | $V_2$ | 43 | 651 | 694 |
| | $A_2$ | 3.51 | 53.21 | 56.73 |
| | $TI_2$ | 43.55 | 416.90 | 460.45 |
| The present value of the total investment ($TI_1$+ $TI_2$) | | ***83.66*** | ***716.50*** | ***800.16*** |

### 7.5.3. Risk Cost Analysis

The IEAR of 8.44 $/kWh previous noted was used in MECORE to calculate the annual system risk cost (EDC) in K$/yr. The annual EDC values for the selected alternatives are shown in Table 7.22.

Table 7.22: The system annual EDC (K$/yr) for the alternatives obtained using the P method

| | Year | Peak Load (MW) | Alternative 2 | Alternative 4 | Alternative 5 | Alternative 6 |
|---|---|---|---|---|---|---|
| Stage 1 | 0 | 3900 | 312.18 | 780.72 | 331.34 | 268.74 |
| | 1 | 3980 | 447.68 | 894.71 | 427.94 | 344.34 |
| | 2 | 4060 | 663.11 | 1052.82 | 574.99 | 458.83 |
| | 3 | 4140 | 1039.59 | 1323.81 | 826.79 | 663.23 |
| | 4 | 4220 | 1615.21 | 1748.48 | 1209.41 | 972.27 |
| Stage 2 | 5 | 4300 | 764.21 | 498.34 | 746.30 | 148.81 |
| | 6 | 4390 | 1048.18 | 748.21 | 1044.28 | 280.84 |
| | 7 | 4480 | 1550.57 | 1122.47 | 1533.16 | 532.03 |
| | 8 | 4570 | 2437.85 | 1748.62 | 2471.56 | 1007.38 |
| | 9 | 4660 | 3901.30 | 2763.06 | 3914.64 | 1872.55 |
| | 10 | 4760 | 6524.15 | 4788.68 | 6541.38 | 3585.91 |

The present value of the total cost due to the system unreliability (TR) in the planning period is given by [25]:

$$TR = \sum_{j=1}^{m} \frac{EDC_j}{(1+i)^{j-1}} \qquad (7.6)$$

The present values of TR for the four alternatives are as follows:

*Alternative 2:*

$$TR_2 = \frac{312.18}{(1+0.08)^{1-1}} + \frac{447.68}{(1+0.08)^{2-1}} + \frac{663.11}{(1+0.08)^{3-1}} + \ldots + \frac{6524.15}{(1+0.08)^{11-1}}$$
$$= 11683.73\,(K\$)$$
$$= 11.68(M\$)$$

*Alternative 4:*

$$TR_4 = \frac{780.72}{(1+0.08)^{1-1}} + \frac{894.71}{(1+0.08)^{2-1}} + \frac{1052.82}{(1+0.08)^{3-1}} + \ldots + \frac{4788.68}{(1+0.08)^{11-1}}$$
$$= 10858.49\,(K\$)$$
$$= 10.86\,(M\$)$$

*Alternative 5:*

$$TR_5 = \frac{331.34}{(1+0.08)^{1-1}} + \frac{427.94}{(1+0.08)^{2-1}} + \frac{574.99}{(1+0.08)^{3-1}} + \ldots + \frac{6541.38}{(1+0.08)^{11-1}}$$
$$= 11149.93\,(\text{K\$})$$
$$= 11.50\,(\text{M\$})$$

*Alternative 6:*

$$TR_6 = \frac{268.74}{(1+0.08)^{1-1}} + \frac{344.34}{(1+0.08)^{2-1}} + \frac{458.83}{(1+0.08)^{3-1}} + \ldots + \frac{3585.91}{(1+0.08)^{11-1}}$$
$$= 5952.74\ (\text{K\$})$$
$$= 5.95\ (\text{M\$})$$

The total cost for Alternatives 2, 4, 5, and 6 are listed in Table 7.23. This table shows that the risk cost of Alternative 2 is higher than in other schemes which means Alternative 2 is the least reliable alternative. The investment cost of Alternative 2 in the planning time frame is, however, the lowest cost due to the fact that generation expansion is only considered in Stage 2. Alternative 5 has the highest investment cost followed by Alternatives 6, 4, and 2. Although the investment cost of Alternative 6 is higher than Alternatives 2 and 4, the risk cost of Alternative 6 is the lowest of the four alternatives.

Table 7.23: The investment, risk, and total cost in M$ of the four alternatives for the planning period

| | Alternative 2 | Alternative 4 | Alternative 5 | Alternative 6 |
|---|---|---|---|---|
| Investment | 505.24 | 788.71 | 804.85 | 800.16 |
| Risk | 11.68 | 10.86 | 11.15 | 5.95 |
| Total | 516.92 | 799.57 | 816.00 | 806.11 |

Table 7.24 shows the rank order of the total cost in the planning period for the D-P and P techniques.

Table 7.24: Rank order of the total cost in the planning period

| Rank Order | D-P method | P method |
|---|---|---|
| 1 | Alt. 4 | Alt. 2 |
| 2 | Alt. 6 | Alt. 4 |
| 3 | Alt. 5 | Alt. 6 |
| 4 | n/a | Alt. 5 |

It can be seen from Table 7.24 that the rank orders for the two approaches are different. Although Alternative 2 has the lowest total cost using the P approach, it cannot meet the single contingency requirement under the D-P criterion.

## 7.6. The Effect of Load Forecast Uncertainty on the Selected Planning Schemes

It is extremely unlikely that the forecast load will be the same as the actual load and therefore there is a degree of uncertainty in the forecast value. Long-term load forecasting is directed at periods longer than a year and is used to perform long-term planning in the decision-making process of facility additions and power plan investments. The impacts on system risk indices and investments in the planning period due to considering long-term load forecast uncertainty (LFU) for the candidate alternatives are examined in this section. The variability in the forecast load is considered by assuming that the standard deviation describing the uncertainty is 2% of the forecast peak load. *Method 1* described in Chapter 3 was applied to incorporate the LFU in MECORE.

### 7.6.1. Analysis Using the D-P Method

In the D-P method, LFU is considered in the probabilistic procedure applied under the most severe single contingency condition. The system SI results for Alternatives 4, 6 and 5 with and without incorporating LFU are presented in Tables 7.25, 7.26 and 7.27 respectively.

Table 7.25: Alt. 4 system SI (SM/yr) with and without considering LFU using the D-P method

| | year | SI (without LFU) | SI (with 2% LFU) | Difference (%) |
|---|---|---|---|---|
| Stage 1 | 0 | 16.62 | 17.07 | 2.7 |
| | 1 | 20.47 | 21.07 | 2.9 |
| | 2 | 25.06 | 25.87 | 3.2 |
| | 3 | 31.03 | 32.19 | 3.7 |
| | 4 | 38.44 | 39.88 | 3.7 |
| Stage 2 | 5 | 3.47 | 3.76 | 8.5 |
| | 6 | 5.34 | 6.01 | 12.5 |
| | 7 | 8.74 | 9.72 | 11.2 |
| | 8 | 13.73 | 15.60 | 13.6 |
| | 9 | 21.54 | 24.73 | 14.8 |
| | 10 | 35.72 | 40.51 | 13.4 |

Table 7.26: Alt. 6 system SI (SM/yr) with and without considering LFU using the D-P method

| | year | SI (without LFU) | SI (with 2% LFU) | Difference (%) |
|---|---|---|---|---|
| Stage 1 | 0 | 16.44 | 16.84 | 2.4 |
| | 1 | 20.17 | 20.74 | 2.8 |
| | 2 | 24.56 | 25.34 | 3.2 |
| | 3 | 30.35 | 31.45 | 3.6 |
| | 4 | 37.49 | 38.86 | 3.6 |
| Stage 2 | 5 | 4.15 | 4.70 | 13.4 |
| | 6 | 6.69 | 7.57 | 13.2 |
| | 7 | 10.76 | 12.02 | 11.6 |
| | 8 | 16.88 | 18.69 | 10.7 |
| | 9 | 25.81 | 28.44 | 10.2 |
| | 10 | 40.09 | 43.74 | 9.1 |

Table 7.27: Alt. 5 system SI (SM/yr) with and without considering LFU using the D-P method

| | year | SI (without LFU) | SI (with 2% LFU) | Difference (%) |
|---|---|---|---|---|
| Stage 1 | 0 | 16.98 | 17.44 | 2.7 |
| | 1 | 20.95 | 21.52 | 2.7 |
| | 2 | 25.52 | 26.33 | 3.2 |
| | 3 | 31.56 | 32.72 | 3.7 |
| | 4 | 39.05 | 40.45 | 3.6 |
| Stage 2 | 5 | 4.23 | 4.72 | 11.5 |
| | 6 | 6.60 | 7.41 | 12.2 |
| | 7 | 10.31 | 11.64 | 12.8 |
| | 8 | 16.20 | 18.27 | 12.8 |
| | 9 | 25.36 | 28.53 | 12.5 |
| | 10 | 40.91 | 45.71 | 11.8 |

Tables 7.25 to 7.27 show that the quantitative effects of load forecast uncertainty on the system SI indices for the three alternatives. The effect of LFU on the system SI of each alternative is lower in Stage 1 than that in Stage 2. The system annual SI values for the three alternatives still meet the specified Pc value of 50 SM/yr in the D-P method considering the LFU.

### 7.6.2. Analysis Using the P Method

Using the P approach, the annual system SI(SM/yr) values for Alternatives 2, 4 and 6 with and without considering 2% LFU in the planning period are shown in Tables 7.28, 7.29 and 7.30 respectively.

Table 7.28: Alt. 2 system SI (SM/yr) with and without considering LFU using the P method

| | year | SI (without LFU) | SI (with 2% LFU) | Difference (%) |
|---|---|---|---|---|
| Stage 1 | 0 | 0.57 | 0.62 | 9.4 |
| | 1 | 0.80 | 0.89 | 11.2 |
| | 2 | 1.16 | 1.31 | 12.7 |
| | 3 | 1.78 | 2.02 | 13.3 |
| | 4 | 2.72 | 3.10 | 14.0 |
| Stage 2 | 5 | 1.26 | 1.33 | 5.5 |
| | 6 | 1.70 | 1.87 | 10.4 |
| | 7 | 2.46 | 2.85 | 16.1 |
| | 8 | 3.79 | 4.33 | 14.2 |
| | 9 | 5.95 | 6.75 | 13.4 |
| | 10 | 9.75 | 10.95 | 12.4 |

Table 7.29: Alt. 4 system SI (SM/yr) with and without considering LFU using the P method

| | year | SI (without LFU) | SI (with 2% LFU) | Difference (%) |
|---|---|---|---|---|
| Stage 1 | 0 | 1.42 | 1.46 | 2.6 |
| | 1 | 1.60 | 1.65 | 3.4 |
| | 2 | 1.84 | 1.97 | 6.8 |
| | 3 | 2.27 | 2.44 | 7.6 |
| | 4 | 2.95 | 3.22 | 9.3 |
| Stage 2 | 5 | 0.82 | 0.90 | 9.5 |
| | 6 | 1.21 | 1.34 | 10.8 |
| | 7 | 1.78 | 2.00 | 12.5 |
| | 8 | 2.72 | 3.12 | 14.7 |
| | 9 | 4.21 | 4.91 | 16.6 |
| | 10 | 7.15 | 8.14 | 13.8 |

Table 7.30: Alt. 6 system SI (SM/yr) with and without considering LFU using the P method

| | year | SI (without LFU) | SI (with 2% LFU) | Difference (%) |
|---|---|---|---|---|
| Stage 1 | 0 | 0.49 | 0.52 | 5.8 |
| | 1 | 0.61 | 0.66 | 7.4 |
| | 2 | 0.80 | 0.89 | 10.8 |
| | 3 | 1.14 | 1.27 | 11.2 |
| | 4 | 1.64 | 1.85 | 12.7 |
| Stage 2 | 5 | 0.25 | 0.30 | 22.4 |
| | 6 | 0.45 | 0.56 | 23.6 |
| | 7 | 0.84 | 1.05 | 24.0 |
| | 8 | 1.57 | 1.93 | 23.1 |
| | 9 | 2.86 | 3.48 | 21.9 |
| | 10 | 5.36 | 6.42 | 19.8 |

Table 7.28 shows that the annual system SI for Alternative 2 at the $10^{th}$ year when the load forecast uncertainty is considered is 10.95 which exceeds the specified Rc value (10 SM/yr). Alternative 5 and Alternative 2 have the same transmission reinforcement structure. The generation expansion for Alternative 2 is conducted in Stage 2. The generation expansion in Alternative 5 is spread over both stages and the system configuration of Alternative 5 at the end of the planning period is the same as that of Alternative 2. Alternatives 2 and 5 are, therefore, not qualified as candidate schemes when LFU is considered. Tables 7.29 and 7.30 indicate that the system SI values for Alternatives 4 and 6 meet the Rc requirement with LFU.

The annual risk cost EDC (K$/yr) of Alternatives 4 and 6 with and without LFU are shown in Tables 7.31 and 7.32 respectively.

Table 7.31: The annual risk cost EDC (K$/yr) of Alt. 4 with and without considering LFU using the P method

| | year | EDC (without LFU) | EDC (with 2% LFU) |
|---|---|---|---|
| Stage 1 | 0 | 780.72 | 800.77 |
| | 1 | 894.71 | 925.41 |
| | 2 | 1052.82 | 1217.77 |
| | 3 | 1323.81 | 1424.31 |
| | 4 | 1748.48 | 1822.38 |
| Stage 2 | 5 | 498.34 | 545.93 |
| | 6 | 748.21 | 828.96 |
| | 7 | 1122.47 | 1262.98 |
| | 8 | 1748.62 | 2004.99 |
| | 9 | 2763.06 | 3221.45 |
| | 10 | 4788.68 | 5450.08 |
| The total risk cost (PV in the starting year M$) | | 10.86 | 12.02 |

Table 7.32: The annual risk cost EDC (K$/yr) of Alternative 6 with and without considering LFU using the P method

| | year | EDC (without LFU) | EDC(with 2% LFU) |
|---|---|---|---|
| Stage 1 | 0 | 268.74 | 284.22 |
| | 1 | 344.34 | 369.87 |
| | 2 | 458.83 | 508.33 |
| | 3 | 663.23 | 737.26 |
| | 4 | 972.27 | 1095.64 |
| Stage 2 | 5 | 148.81 | 182.18 |
| | 6 | 280.84 | 346.99 |
| | 7 | 532.03 | 659.63 |
| | 8 | 1007.38 | 1239.64 |
| | 9 | 1872.55 | 2282.91 |
| | 10 | 3585.91 | 4297.38 |
| The total risk cost (PV in the starting year M$) | | 5.95 | 6.98 |

Tables 7.31 indicates that the total risk cost of Alternative 4 increases from 10.86 M$ to 12.02 M$ by including a LFU of 2%. Table 7.32 shows that the risk cost of Alternative 6 increases from 5.95 to 6.98 M$.

### 7.6.3. Comparison of the Two Methods

The ranked total cost of the selected alternatives in the planning period using the D-P and P method when load forecast uncertainty is considered are shown in Table 7.33.

Table 7.33: Rank order of the total cost (PV in the starting year M$) in the planning period considering 2% LFU

| **D-P method** | | | | |
|---|---|---|---|---|
| Rank Order | | Total cost | Investment cost | |
| 1 | Alt. 4 | 788.71 | 788.71 | |
| 2 | Alt. 6 | 800.16 | 800.16 | |
| 3 | Alt. 5 | 804.85 | 804.85 | |
| **P method** | | | | |
| Rank Order | | Total cost | Investment cost | Risk cost |
| 1 | Alt. 4 | 800.73 | 788.71 | 12.02 |
| 2 | Alt. 6 | 807.14 | 800.16 | 6.98 |

A comparison of Table 7.24 and Table 7.33 indicates that the selected candidate alternatives cost ranking and the corresponding total costs are not significantly impacted by the LFU, using the D-P method. Alternatives 2 and 5 are eliminated from candidate planning schemes in the P method due to their inability to meet the risk criterion of 10 SM/yr at the end of planning time period. In the P method, the LFU affects the total cost ranking and the selected planning scheme risk indices and the corresponding costs increase by considering the LFU. Based on the data used in the analyses, Alternative 4 is recommended as the optimum option from the viewpoint of economic and technical analyses using the D-P and P techniques and considering load forecast uncertainty.

## 7.7. Conclusions

This chapter focuses on the application of a joint deterministic and probabilistic criterion in wind integrated bulk system reinforcement planning. The M2MRTS was created in order to conduct planning analysis using the D, P and D-P techniques. WECS location analysis shows that the system SI benefits of incorporating WECS differ when using the P and D-P methods. The M2MRTS with WECS located at Bus 1 and Bus 6 was used as the base system in the planning studies described in this chapter.

Six planning alternatives, each of which satisfies the deterministic N-1 planning criterion, are proposed as candidate development options in this chapter. The deterministic N-1 criterion is a precondition in the D-P approach. Probabilistic analyses were conducted under the most critical contingency to determine the system SI value for the six alternatives over the planning time period. The planning period is divided into two stages. Analysis shows that the SI values for Alternatives 1, 2, 3 do not meet the specified Pc requirement at the end of Stage 1. Alternatives 1, 2, and 3 are therefore removed as candidate planning alternatives. Alternatives 4, 5, and 6 are then selected as the candidate planning alternatives based on the D-P method and used in an economic assessment to determine the best choice.

The six designated alternatives in the planning time period are also examined using the P method. Alternatives 1 and 3 are eliminated from the candidate list due to their inability to meet

the specified Rc value. Economic analysis is then conducted on selected Alternatives 2, 4, 5 and 6 to determine the optimum planning option. The reliability analyses show that the application of the D-P and P techniques can result in the selection of different planning alternatives.

In this chapter, the best alternative should achieve the minimum total cost which includes the investment, operating and risk costs. The investment cost is considered in the D-P method, and both the investment and risk costs are included in the P method. The present value method which captures the time values of the annual costs is used to calculate the total cost. The present value of a two-stage investment process is utilized in this study. The study results indicate that the rank order of the total cost for the selected alternatives in the D-P and P approaches are different.

The study results obtained using the D-P method show that although the annual system risk index values for the selected three alternatives increase by considering load forecast uncertainty, the total cost rank order for the three alternatives do not change and the system risk index values still meet the specified probabilistic risk criterion. The analysis results obtained using the P approach indicate that load forecast uncertainty can significantly affect the risk indices and the corresponding risk costs for the selected planning schemes. Two alternatives were eliminated from the four candidate planning list due to their inability to meet the probabilistic criterion at the end of the planning time period when the load forecast uncertainty was considered in the P method.

The research work described in this chapter illustrates that the joint deterministic-probabilistic approach can be effectively used to integrate wind power in bulk electric system planning.

# 8. Summary and Conclusion

Wind power is receiving considerable attention in the continued growth and development of electric power systems due to its tremendous environmental, social and economic benefits, together with public support and government incentives. Since wind power production is dependent on the wind, the output of a turbine and a wind farm varies over time, under the influence of meteorological fluctuations. The fundamentally different operating characteristics of wind energy affect power system reliability in a different manner than conventional technology systems. The reliability impact of such a highly variable power source is an important aspect that must be assessed when the wind power penetration is significant. The research described in this thesis is focused on the utilization of state sampling Monte Carlo simulation in wind integrated bulk electric system reliability analysis and the application of these concepts in system planning and decision making. The MECORE program initially developed at the University of Saskatchewan is based on the state sampling approach and this program has been utilized in the research described in this thesis to conduct bulk system adequacy studies. The capabilities of this software and basic adequacy indices provided by the MECORE program are illustrated in Chapter 2.

Load forecast uncertainty is an extremely important parameter and in the light of the financial, societal and environmental uncertainties which electric power utilities face may be the most important single parameter in generating capacity reliability assessment. Two basic methods for considering load forecast uncertainty in generating capacity or bulk system reliability assessment are described in Chapter 3. The conducted studies show that the two methods provide virtually identical system reliability indices in a generating capacity study. The basic method designated in this thesis as Method 2 involves the use of a modified load duration curve with a large number of load steps. The capability limit of the MECORE software, as currently formatted in order to reduce the computation time, restricts the application of this method in the reliability evaluation of bulk systems. It becomes necessary to reduce the number of steps in the load profile in order to use the modified load duration model as input data to MECORE. Two approximate

approaches were developed to reduce the number of steps in the modified load duration curve. Analysis shows that the two approximate approaches provide reasonably accurate reliability index results in a generating capacity study. The number of load steps in the load duration models obtained using the two approximate approaches is dependent on the standard deviation of the load forecast uncertainty. The analyses conducted on the RBTS and the IEEE-RTS indicate that the utilization of the approximate approach provides similar system reliability indices as those obtained using the basic method. The studies conducted on the two study systems show that the system reliability indices increase with increased load forecast uncertainty. The effects of load forecast uncertainty on individual load point EENS are quite different and are very dependent on the topology of the system, and the system load curtailment philosophy.

In an actual power system incorporating WECS, wind farms are neither completely dependent nor independent but are correlated to some degree if the distances between sites are not large. The techniques and models developed to permit dependent wind energy facilities to be incorporated in generating and bulk system adequacy evaluation using the state sampling Monte Carlo simulation technique are presented in Chapter 4. The effect of wind speed correlation between two wind sites is examined using the ARMA time series models developed for Swift Current and Regina. In this thesis, a genetic algorithm method is used to adjust the ARMA models to simulate hourly wind speeds based on the degree of wind speed correlation between the wind sites.

A state sampling Monte Carlo simulation method and an analytical method were applied to calculate reliability indices in a generating system incorporating two dependent wind farms. Both techniques can be extended to consider more than two dependent wind sites. The method of generating correlated random numbers with uniform distributions and a specified correlation coefficient in the state sampling method was proposed and used to conduct adequacy assessment in generating systems and in bulk electric systems containing correlated WECS. This is an important development as it permits correlated WECS to be incorporated in large practical system studies at both HL-I and HL-II without requiring excessive increases in computer solution time. The MECORE software was modified based on this conclusion to generate correlated and uncorrelated random numbers in the simulation process in order to incorporate

two dependent wind farms and used to conduct the studies described in this thesis. The multi-state WECS models created for independent wind sites can be used in the state sampling simulation method to represent WECS considering wind speed correlation between the wind farms.

The analyses using the state sampling Monte Carlo simulation method were conducted on generating and bulk systems incorporating WECS with different wind speed correlations. The studies show the system reliability benefits increase as the degree of wind speed correlation between the two wind sites decrease. The effects of the wind speed correlation level on the system reliability of generating and bulk systems become more obvious as the wind penetration level increases.

The original RBTS and IEEE-RTS were modified to create four systems in order to represent the conditions existing in a wide range of practical systems. There are obvious reliability improvements when the four developed systems are augmented with WECS at a large wind penetration level. The degree of wind speed correlation affects the system and load point reliability indices. The actual numerical index values from these studies on the representative test systems are obviously system dependent. The studies described in Chapter 4, however, clearly illustrate that it is possible to quantitatively assess the reliability implications associated with adding WECS to a bulk system including the effects of multiple correlated wind sites.

The output of a wind turbine generator and a wind farm varies over time, under the influence of meteorological fluctuations. These variations occur on all time scales: by seconds, minutes, hours, days, months, seasons and years. The procedures described for creating monthly and seasonal WECS models are presented in Chapter 5. The developed seasonal and monthly load profiles and the corresponding WECS models were utilized in composite RBTS and IEEE-RTS studies using the state sampling Monte Carlo simulation approach. The analysis results show that the system risk indices obtained utilizing seasonal and monthly WECS and load models are close to those obtained using the annual models when the system has a single or two correlated WECS. The degree of correlation between the chronological wind speed and the hourly load profiles does not significantly impact the system risk in the composite generation and transmission

systems studied. The annual wind profile is, therefore, an acceptable representation and annual studies can be done directly using this profile. The variations in the system reliability indices for different time periods are obviously dependent on system characteristics. The procedures described in this thesis for creating monthly and seasonal WECS models should prove useful in situations where time period models are required to incorporate scheduled maintenance of generation and transmission facilities.

Most electric power utilities use deterministic techniques such as the traditional N-1 security criterion to assess system reliability in transmission system planning. These deterministic approaches are not consistent and do not provide an accurate basis for comparing alternate equipment configurations and performing economic analyses as they do not incorporate the probabilistic or stochastic nature of system behavior and component failures. There is therefore growing interest in combining deterministic considerations with probabilistic assessment in order to evaluate the quantitative system risk and conduct bulk power system planning. A relatively new approach that incorporates deterministic and probabilistic considerations in a single risk assessment framework has been designated as the joint deterministic-probabilistic approach. The increasing use of wind power as an important electrical energy source clearly indicates the importance of considering the impacts of wind power in power system planning and design, and developing appropriate evaluation techniques. Chapter 6 illustrates the application of the joint deterministic-probabilistic (D-P) technique as a planning tool in bulk power systems containing wind energy. The D-P method incorporates deterministic (D) and probabilistic (P) considerations in a single risk assessment framework.

The wind capacity credit of a WECS is examined using the Effective Load Carrying Capacity (ELCC) method, Capacity Factor method and the Derated Adjusted Forced Outage Rate of a wind farm (DAFORW) method. Analysis shows that the wind capacity credit values obtained using these approaches are not significantly different. The ELCC method is the most comprehensive approach as generating unit outage parameters, hourly load demands and system reliability parameters are considered in the analysis. Sensitivity studies indicate that the benefits in system peak load carrying capacity (PLCC) with increase in the assigned wind capacity credit are impacted by the WECS location and system condition.

The D, P, and D-P techniques are used in a WECS planning context in Chapter 6. The study results indicate that none of the three approaches produce the highest or lowest PLCC in all cases. The D method produces a hard limit in which WECS is considered as a firm generating unit. The P approach provides a much softer limit since it recognizes the variable nature of a WECS. In the D-P approach the system must first satisfy the D criterion. The system risk given that the critical element has failed must then be equal to or less than a specified probabilistic risk criterion. If this risk is less than or equal to the criterion value, the D and D-P approaches provide the same result. If the risk exceeds this value then the load must be reduced to meet the acceptable risk level. The studies described in this thesis show that the application of the D-P method provides more stringent results for a system with wind energy than the deterministic N-1 method because the joint deterministic-probabilistic technique is driven by the deterministic N-1 criterion with an added probabilistic perspective which recognizes the power output characteristics of a WECS.

The objective of power system planning is to select the most economical and reliable plan in order to meet the expected future load growth at minimum cost and optimum reliability subject to economic and technical constraints. Chapter 7 illustrates the application of the D-P and P methods in reinforcement planning for a wind integrated bulk transmission system. This analysis considers both technical and economic considerations. The studies conducted indicate that the results when applying the P method are more sensitive to load forecast uncertainty than those when applying the D-P method. The reliability analyses show that the application of the D-P and P techniques can result in the selection of different planning alternatives. The economic study results indicate that the rank order of the total cost for the selected alternatives in the D-P and P approaches are different. The research work illustrates that the joint deterministic-probabilistic approach can be effectively used to integrate wind power in bulk electric system planning.

It is believed that the models, methodologies, results and discussion presented in this thesis should assist system planners and operators to evaluate the reliability benefits of adding wind power to their systems.

# REFERENCES


1. R. Billinton, "Bibliography on the Application of Probability Methods in Power System Reliability Evaluation," *IEEE Transactions on Power Apparatus and Systems*, Vol. 91, 1972, pp. 649-660.
2. R. N. Allan, R. Billinton, and S. H. Lee, "Bibliography on the Application of Probability Methods in Power System Reliability Evaluation: 1977-1982," *IEEE Transactions on Power Apparatus and Systems*, Vol. 103, 1984, pp. 275-282.
3. R. N. Allan, R. Billinton, S. M. Shahidehpour and C. Singh, "Bibliography on the Application of Probability Methods in Power System Reliability Evaluation: 1982-1987," *IEEE Transactions on Power Apparatus and Systems*, Vol. 3, No.4, November 1988, pp. 1555-1564.
4. M. Th. Schilling, R. Billinton, A. M. Leite da Silva, M.A. El-kady, "Bibliography on composite system reliability 1964-1988," *IEEE Transactions on Power Systems*, Vol. 4, No. 3, August 1989, pp. 1122-1132.
5. R. N. Allan, R. Billinton, A. M. Breipohl, and C. H. Grigg, "Bibliography on the application of probability methods in power system reliability evaluation: 1987-1991," *IEEE Transactions on Power Systems*, Vol. 9, No. 4, February 1994, pp. 275-282.
6. R. N. Allan, R. Billinton, A.M. Breipohl, and C. H. Grigg, "Bibliography on the application of probability methods in power system reliability evaluation: 1992-1996", *IEEE Transactions on Power Systems*, Vol. 14, No. 1, February 1999, pp. 51-57.
7. R. C. Bansal, T. S. Bhatti, and D. P. Kothari, "Discussion of "Bibliography on the Application of Probability Methods in Power System Reliability Evaluation,"" *IEEE Transactions on Power Systems*, Vol. 17, No. 3, August 2002, pp. 924.
8. Roy Billinton, Mahmud Fotuhi-Firuzabad, and Lina Bertling, "Bibliography on the application of probability methods in power system reliability evaluation: 1996-1999," *IEEE Transactions on Power Systems*, Vol. 16, No. 4, November 2001, pp. 595-602.
9. R. Billinton and R. Allan, *Reliability evaluation of power systems*, 2nd Edition, Plenum Press, New York, 1996.

10. R. Billinton and W. Li, *Reliability Assessment of Electrical Power System Using Monte* Carlo Methods, Plenum Press, New York, 1994.
11. "Glossary of Terms," North American Electric Reliability Council, Glossary of Terms Task Force, February 2008.
12. R. Billinton, R. Allan and L. Salvaderi, *Applied Reliability Assessment in Electric Power Systems*, IEEE Press, New York, 1991.
13. North American Electric Reliability Council Planning Standards.
    Available at: http://www.nerc.com (August, 2007)
14. R. Billinton, G. Lian. "Composite Power System Health Analysis Using a Security Constrained Adequacy Evaluation Procedure", *IEEE Transactions on Power Systems*, Vol. 9, No. 2, May 1994, pp. 936-941.
15. R. Billinton, H. Bao and R. Karki, "A Joint Deterministic- Probabilistic Approach To Bulk System Reliability Assessment," *Proceedings of the Probability Methods Applied to Power System Symposium*, Puerto Rico, USA, June, 2008.
16. R. Billinton, "Composite System Adequacy Assessment – the Contingency Enumeration Approach", IEEE Tutorial Course 90EHO311-1-PWR, 1990.
17. Globe Wind Energy Council, Globe Wind Report 2008.
    Available at: http://www.gwec.net (February, 2009)
18. Utility Wind Integration Group (UWIG), Utility Wind Integration State of the Art, Available at: http://www.uwig.org (September, 2007)
19. W. Li, *Installation Guide and User's Manual for the MECORE Program*, July 1998.
20. R. Billinton and et al, "A Reliability Test System for Educational Purposes Basic Data," *IEEE Transactions on Power Systems*, Vol. PWRS-3, No. 4, August 1989, pp. 1238-1244.
21. IEEE Task Force, "IEEE Reliability Test System," *IEEE Transactions on Power Apparatus and Systems*, Vol. PAS-98, Nov/Dec. 1979, pp. 2047-2054.
22. M. Mitchell, *An Introduction to Genetic Algorithms*, The MIT Press, 1996.
23. L. Chambers, *Practical Handbook of Genetic Algorithms*, BocaRaton: CRC Press, 1995.
24. GENETIC ALGORITHMS, http://cs.felk.cvut.cz/~xobitko/ga/ (December, 2007).

25. W. Li, *Risk Assessment of Power Systems: Models, Methods, and Applications*, John Wiley &Sons, Hoboken, NJ, 2005.
26. H. G. Stoll, *Least-Cost Electric Utility Planning*, New York, Wiley, 1989.
27. E. J. Henley and H. Kumamoto, *Probability Risk Assessment: Reliability Engineering, Design and Analysis*, IEEE Press, New York, 1992.
28. R. Billinton and W. Li, "Hybrid Approach for Reliability Evaluation of Composite Generation and Transmission Systems Using Monte Carlo Simulation and Enumeration Technique," *IEE Proceedings-C*, Vol. 138, No. 3, 1991, pp. 233-241.
29. M. V. F. Pereira, M. E. P. Maceira, G. C. Oliveira and L. M. V. G. Pinto, "Combining Analytical Models and Monte Carlo Techniques in Probabilistic Power System Analysis", *IEEE Transactions on Power Systems*, Vol. 7, No. 1, February 1992, pp. 265-272.
30. R. Billinton and W. Li, "A System State Transition Sampling Method for Composite System Reliability Evaluation", *IEEE Transactions on Power Systems,* Vol. 8, No. 3, August 1993, pp.761-771.
31. R. Billinton and A. Sankarakrishnan, "A System State Transition Sampling Technique for Reliability Evaluation", *Reliability Engineering and System Safety*, Vol. 44, 1994, pp. 131-134.
32. R. Ubeda and R. N. Allan, "Sequential Simulation Applied to Composite System Reliability Evaluation", IEE Proceeding-C, Vol. 139, No. 2, March 1992.
33. R. Billinton and W. Wangdee, "Impact of Utilizing Sequential and Non-Sequential Simulation Techniques in Bulk Electric System Reliability Assessment", *IEE Proc. of Generation, Transmission and Distribution,* Vol. 152, No. 5, September 2005, pp. 623-628.
34. X. Tang, "*Considerations in Bulk System Reliability Assessment"*, M.Sc. thesis, University of Saskatchewan, 2000.
35. K. L. Lo and Y. K. Wu, "Risk Assessment Due to Local Demand Forecast Uncertainty in the Competitive Supply Industry", *IEE Proceedings of Generation, Transmission and Distribution,* Vol. 150, Issue 5, September 2003, pp. 573- 581.

36. A. P. Douglas, A. M. Breipohl, F.N. Lee, and R. Adapa, "Risk due to Load Forecast Uncertainty in Short Term Power System Planning", *IEEE Transactions on Power Syst*ems, Vol. 13, No. 4, 1998, pp. 1493–1499.
37. J. Hoffer and M. Prill, "On the Models of Peak Load Forecast Uncertainty in Probabilistic Production Costing Algorithms", *International Journal of Electrical Power & Energy Systems*, Vol. 18, Issue 3, March 1996, pp. 153-160.
38. D. Zhai, A. M. Breipohl, F. N. Lee, and R. Adapa, "The Effect of Load Uncertainty on Unit Commitment Risk," *IEEE Transactions on Power Syst*ems, Vol. 9, No. 1, February 1994, pp. 510–517.
39. F. Ali El-Sheikhi and R. Billinton, "Load Forecast Uncertainty Considerations in Generating Unit Preventive Maintenance Scheduling for Single Systems," *Proceedings of the 3rd International Conference of Probabilistic Methods Applied to Electric Power Systems*, July 1991, pp. 241–245.
40. R. Billinton and D. Huang, "Effects of Load Forecast Uncertainty on Bulk Electric System Reliability Evaluation", *IEEE Transactions on Power Systems*, Vol. 23, Issue 2, May 2008, pp. 418 – 425.
41. W. Li and R. Billinton, "Effect of bus load uncertainty and correlation in composite system adequacy evaluation," *IEEE Transactions on Power Systems*, Vol. 6, No. 4, November 1991, pp. 1522–1529.
42. "*Utility Wind Integration State of the Art*", prepared by Utility Wind Integration Group incorporated with American Public Power Association (APPA), Edison Electric Institute (EEI) and National Rural Electric Cooperative Association (NRECA), May 2006, available on: http://www.uwig.org
43. J. C. Smith, M. R. Milligan, E. A. DeMeo and B. Parsons, "Utility Wind Integration and Operating Impact State of the Art", *IEEE Transactions on Power Systems*, Vol. 22, No. 3, August 2007, pp. 900-908.
44. M. R. Haghifam and M. Omidvar, "Wind Farm Modeling in Reliability Assessment of Power System", *the 9th International Conference on PMAPS*, Stockholm, Sweden, June 2006.

45. A. A. Chowdhury, “Reliability Models for Large Wind Farms in Generation System Planning”, *IEEE Power Engineering Society General Meeting, 2005* , Vol. 2, pp. 1926-1933.
46. R. Billinton, H. Chen and R. Ghajar, “Time-series Models for Reliability Evaluation of Power Systems Including Wind Energy”, *Microelectronics Reliability*, Vol. 36, No. 9, 1996, pp. 1253-1261.
47. R. Billinton and Y. Gao, “Multistate Wind Energy Conversion System Models for Adequacy Assessment of Generating Systems Incorporating Wind Energy”, *IEEE Transactions on Energy Conversion*, Vol. 23, No. 1, March 2008, pp. 163 - 170.
48. S. H. Karaki, B. A. Salim and R. B. Chedid, “ Probabilistic Model of a Two-Site Wind Energy Conversion System”, *IEEE Transactions on Energy Conversion*, Vol. 17, No. 4, December 2002, pp. 530-536.
49. F.C. Sayas and R. N. Allan, “Generation Availability Assessment of Wind Farms”, *IEE proceedings, Generation, Transmission & Distribution*, Vol. 143, Issue 5, September 1996, pp. 507-518.
50. H. Holttinen, “Hourly Wind Power Variations in the Nordic Countries”, *Wind Energy*, Vol. 8, No. 2, April-June 2005, pp. 173-195.
51. J.R. Ubeda and M.A.R. Rodriguez Garcia, “ Reliability and Production Assessment of Wind Energy Production Connected to the Electric Network Supply”, *IEE proceedings, Generation, Transmission & Distribution*, Vol. 146, No. 2, March 1999, pp. 169-175.
52. W. Wangdee and R. Billinton, “Considering Load-carrying Capability and Wind Speed Correlation of WECS in Generation Adequacy Assessment”, *IEEE Transactions on Energy Conversion*, Vol. 21, No. 3, September 2006, pp. 734-741.
53. M. S. Miranda and R.W. Dunn, “Spatially Correlated Wind Speed Modelling for Generation Adequacy Studies in the UK”, 2007 *IEEE PES General Meeting* Tampa, Florida USA.
54. F. Vallee, J. Lobry and O. Deblecker, “Impact of the Wind Geographical Correlation Level for Reliability Studies”, *IEEE Transactions on Power Systems*, Vol. 22, No. 4, November 2007. pp. 2232-2239.

55. N.B. Negra, O.Holmstrom, B.Bak-Jesen and P. Sorensen, “Aspects of Relevance in Offshore Wind Farm Reliability Assessment”. *IEEE Transactions on Energy Conversion*, Vol. 22, No. 1, March 2007. pp. 159-166.
56. R. Billinton and Y. Gao, “Adequacy Assessment of Composite Power Generation and Transmission Systems with Wind Energy”, *International Journal of Reliability and Safety*, Vol. 2, No. 1/2, 2008, pp. 79-98.
57. R. Billinton and G. Bai, “Generating Capacity Adequacy Associated with Wind Energy”, *IEEE Transactions on Energy Conversion*, Vol. 19, No. 3, September 2004, pp. 641-646.
58. W. Wangdee and R. Billinton, “Reliability Assessment of Bulk Electric Systems Containing Large Wind Farms”, *Electrical Power and Energy Systems*, 29 (2007), pp. 759-766.
59. R. Billinton and W. Wangdee, “Reliability-Based Transmission Reinforcement Planning Associated With Large-Scale Wind Farms”, *IEEE Transactions on Power Systems*, Vol. 22, No. 1, February 2007, pp. 34-41.
60. R. Billinton and A. Sankarakrishnan, “A comparison of Monte Carlo simulation techniques for composite power system reliability assessment”, *Proceedings of the IEEE WESCANEX 95. Communications, Power, and Computing. Conference.* Vol. 1, May 1995, pp. 145 – 150.
61. R. Billinton, Bagen and Y. Cui, “Reliability evaluation of small stand-alone wind energy conversion systems using a time series simulation model”, *IEE Proceedings, Generation, Transmission and Distribution*, Vol. 150, Issue 1, January 2003, pp. 96-100.
62. Y. Gao and R. Billinton, "Adequacy Assessment of Generating Systems Containing Wind Power Considering Wind Speed Correlation", *IET Renewable Power Generation*, Vol. 3, Issue 2, June 2009, pp. 217-226.
63. P. Giorsetto and K. F. Utsurogi, “Development of A New Procedure for Reliability Modeling of Wind Turbine Generators”, *IEEE Transactions on Power Apparatus and Systems*, Vol. PAS-102, No. 1, 1983, pp. 134-143.

64. R. Billinton and Y. Li, “Incorporating Multi-state Models in Composite System Adequacy Evaluation”, *Proceedings of the 8th International Conference on Probabilistic Method Applied to Power Systems*, Ames, Iowa, September 2004.
65. Papoulis, S. Unnikrishna Pillai, *Probability, Random Variables, and Stochastic Processes*, 4th Edition, McGraw-Hill, Boston, 2002.
66. R. Billinton, Y. Gao and R. Karki, "Composite System Adequacy Assessment Incorporating Large-Scale Wind Energy Conversion Systems Considering Wind Speed Correlation", *IEEE Transactions on Power Systems*, Vol. 24, Issue 3 , August 2009 pp. 1375 – 1382.
67. 2004 Forced Outage Performance of Transmission Equipment, Canadian Electricity Association.
68. M. Li and X. Li, “Investigation of Wind Characteristics and Assessment of Wind Energy Potential for Waterloo Region, Canada”, *Energy Conversion and Management*, Vol. 46, No. 18-19 , November 2005, pp. 3014-3033.
69. D. Weisser, “A Wind Energy analysis of Grenada: an estimation using the ‘Weibull’ density function”, *Renew Energy* 28 (2003), pp. 1803–1812.
70. A. R. Daniel and A. A. Chen, “Stochastic Simulation and Forecasting of Hourly Average Wind Speed Sequences in Jamaica”, *Solar Energy*, Vol. 46, No. 1, 1999, pp. 1-11.
71. Canada’s National Climate Archive,
Available at: http://www.climate.weatheroffice.ec.gc.ca (July, 2008)
72. P. M. T. Broersen, ARMASA Matlab Toolbox [online].
Available at: http://www.tn.tudelft.nl/mmr/downloads. (June, 2008)
73. P. M. T. Broersen and S. de Waele, “Finite Sample Properties of ARMA Order Selection”, *IEEE Transactions on Instrumentation and Measurement*, Vol. 53, No. 3, June 2004, pp. 645-651.
74. P. M. T. Broersen “ Autogressive Model Orders for Durbin’s MA and ARMA estimaters”, *IEEE Transactions on Signal Processing*, Vol. 48, No. 8, August 2000, pp. 2454-2457.
75. L. Ljung, *System Identification Toolbox for Use with MATLAB, User’s Guide Version 7.2*, The MathWorks Inc., 2008.

76. Y. Gao, R. Billinton and R. Karki, "Composite Generation and Transmission System Adequacy Assessment Considering Wind Energy Seasonal Characteristics", *Proceeding of the IEEE General Meeting 2009*, July 2009, Calgary, Alberta, Canada.
77. E. Khan and R. Billinton, "A Hybrid Model for Quantifying Different Operating States of Composite Systems", *IEEE Transactions on Power Systems*, Vol. 7, No. 1, February 1992, pp. 187-193.
78. R. Billinton, E. Khan, "A security based approach to composite power system reliability evaluation", *IEEE Transactions on Power Systems*, Vol. 7, Issue 1, February 1992, pp. 65 – 72.
79. L. H. Fink and K. Carlsen, "Operating Under Stress and Strain", *IEEE Spectrum*, Vol. 15, No. 3, March 1978, pp. 48-53.
80. EPRI Final Report, *Composite-System reliability Evaluation: Phase 1 – Scoping Study*, Tech. report EPRI EL-5290, Dec. 1987.
81. R. Billinton and G. Lian, "Consideration of Dependent Outages in Security Constrained Adequacy Evaluation of Composite Systems", *IEE Proceedings-C*, Vol. 141, No. 1, January 1994, pp. 47-52.
82. L. Goel and C. Feng, "Well-being framework for composite generation and transmission system reliability evaluation," in *Proc. Inst. Elect. Eng. Gener. Trans. Distrib.*, Vol. 146, September 1999, pp. 528–534.
83. A. M. L. da Silva, L. C. de Resende, L. A. da F. Manso, and R. Billinton, " Well-Being Analysis for Composite Generation and Transmission Systems", *IEEE Transactions on Power Systems*, Vol. 19, No. 4, November 2004, pp. 1763-1770.
84. R. Billinton, R. Karki, "Application of Monte Carlo Simulation to Generating System Well-Being Analysis", *IEEE Transactions on Power Systems*, Vol. 14, No. 3, August, 1999, pp. 1172-1177.
85. R. N. Allan and R. Billinton, "Probabilistic Assessment of Power Systems", *Proceedings of the IEEE*, Vol. 88, No. 2, February 2000, pp. 140-162.
86. W. Wangdee and R. Billinton, "Bulk Electric System Well-Being Analysis Using Sequential Monte Carlo Simulation", *IEEE Transactions on Power Systems*, Vol. 21, No. 1, February 2006, pp. 188-193.

87. H. Bao, *Application of Deterministic-Probabilistic (D-P) Criterion to Bulk Electric System Planning*, M.Sc thesis, University of Saskatchewan, 2007.
88. L. Garver, Effective Load-Carrying Capability of Generating Units, *IEEE Trans. Power Apparatus & Sys*. V. PAS-85, No. 8 (1966), pp. 910–919.
89. American Wind Energy Association,
Available at: http://www.awea.org/faq/wwt_basics.html. (December, 2008)
90. R. Billinton, H. Chen, "Assessment of Risk-Based Capacity Benefit Factors Associated With Wind Energy Conversion Systems", *IEEE Transactions on Power Systems*, Vol. 13, No. 3, August 1998, pp. 1191-1198.
91. M. Milligan, "*Measuring Wind Plant Capacity Value*", National Renewable Energy Laboratory, USA, 2005.
92. M. Milligan, "*Capacity Credit for Wind*", Consultant National Renewable Energy Laboratory, April 26, 2007.
93. E. P. kahn, "Effective Load Carrying Capability of Wind Generation: Initial Results with Public Data", *The Electricity Journal*, Vol. 17, Issue 10, December 2004, pp. 85-95.
94. Independent Electricity System Operator (IESO) Canadian Wind Energy Association (CanWEA) for Ontario Wind Integration Study.
Available at: http://www.ieso.ca/imoweb/pubs/marketreports/OPA-Report-200610-1.pdf (December, 2008)
95. The Effects of Integrating Wind Power on Transmission System Planning, Reliability, and Operations, Report on Phase 2: System Performance Evaluation, The New York State Energy Research and Development Authority and GE Energy, Energy Consulting, March 4, 2005.
96. PJM-Manual 21: Rules and Procedures for Determination of Generating Capability Appendix B: Calculating Capacity Values for Intermittent Capacity Resources, 2008. http://www.pjm.com/committees/working-groups/irwg/downloads/20081014-item-03-manual-21.pdf (December, 2008).
97. Canadian Electricity Association, "Report on Bulk Electricity System Delivery Point Interruptions & Significant Power Interruptions", 2007.

98. R. Billinton, Y. Gao and R. Karki, “Application of a Joint Deterministic-Probabilistic Criterion to Wind Integrated Bulk Power System Planning”, accepted in IEEE Transactions on Power Systems, November 2009.
99. Fang R. and Hill D. J., “A New Strategy for Transmission Expansion in Competitive Electricity Markets”, *IEEE Trans. on Power Systems*, Vol. 18, No. 1, February 2003, pp. 374-380.
100. W. Li, P. Choudhury, “Probabilistic Transmission Planning”, *IEEE Power and Energy Magazine*, September-October, 2007, Vol. 5, Issue 5, pp. 46-53.
101. J.G.Dalton, D.L. Garrison and C.M. Fallon, “Value-Based Reliability Transmission Planning”, *IEEE Trans. on Power Systems*, Vol. 11, No. 3, August 1996, pp. 1400-1408.
102. A.A.Chowdhury and D. O. Koval, “Application of Customer Interruption Costs in Transmission Network Reliability Planning”, *IEEE Trans. on Industry Applications*, Vol. 37, No. 6, Nov./Dec. 2001, pp. 1590-1596.
103. W. Wangdee, W. Li, W. Shum and P. Choudhury, Member, IEEE “Assessing Transfer Capability Requirement for Wind Power Generation Using a Combined Deterministic and Probabilistic Approach”, *IEEE PES GM*, Calgary, July, 2009.
104. R. Billiton and R. Mo, “Deterministic/probabilistic Contingency Evaluation in Composite Generation and Transmission Systems” *IEEE PES GM*, Denver, June, 2004.
105. Goel, L. and R. Billinton. "Utilization of Interrupted Energy Assessment Rates to Evaluate Reliability Worth in Electric Power Systems”. *IEEE Transactions on Power Systems*, Vol. 8, No. 3, 1993, pp. 929-936.
106. British Columbia Transmission Corporation, “Benefit/Cost Analysis Based on Reliability and Transmission Loss Considerations for Central Vancouver Island Transmission Project”, Report No. 2007-REL-03.2, September, 2007.

# APPENDIX A. BASIC DATA FOR THE RBTS AND THE IEEE RTS

Tables A.1-A.3 and A.4-A.6 present the bus, transmission line and generator data for the RBTS and the IEEE-RTS respectively.

Table A.1: Bus data for the RBTS

| Bus No. | Load (p.u.) | | $P_g$ | $Q_{max}$ | $Q_{min}$ | $V_0$ | $V_{max}$ | $V_{min}$ |
|---|---|---|---|---|---|---|---|---|
| | Active | Reactive | | | | | | |
| 1 | 0.00 | 0.0 | 1.0 | 0.50 | -0.40 | 1.05 | 1.05 | 0.97 |
| 2 | 0.20 | 0.0 | 1.2 | 0.75 | -0.40 | 1.05 | 1.05 | 0.97 |
| 3 | 0.85 | 0.0 | 0.0 | 0.00 | 0.00 | 1.00 | 1.05 | 0.97 |
| 4 | 0.40 | 0.0 | 0.0 | 0.00 | 0.00 | 1.00 | 1.05 | 0.97 |
| 5 | 0.20 | 0.0 | 0.0 | 0.00 | 0.00 | 1.00 | 1.05 | 0.97 |
| 6 | 0.20 | 0.0 | 0.0 | 0.00 | 0.00 | 1.00 | 1.05 | 0.97 |

Table A.2: Line data for the RBTS

| Line | Bus | | R | X | B/2 | Tap | Current Rating (p.u.) | Failure Rate (occ/yr) | Repair Time (hrs) | Failure Prob. |
|---|---|---|---|---|---|---|---|---|---|---|
| | I | J | | | | | | | | |
| 1,6 | 1 | 3 | 0.0342 | 0.18 | 0.0106 | 1.0 | 0.85 | 1.50 | 10.0 | 0.00171 |
| 2,7 | 2 | 4 | 0.1140 | 0.60 | 0.0352 | 1.0 | 0.71 | 5.00 | 10.0 | 0.00568 |
| 3 | 1 | 2 | 0.0912 | 0.48 | 0.0282 | 1.0 | 0.71 | 4.00 | 10.0 | 0.00455 |
| 4 | 3 | 4 | 0.0228 | 0.12 | 0.0071 | 1.0 | 0.71 | 1.00 | 10.0 | 0.00114 |
| 5 | 3 | 5 | 0.0228 | 0.12 | 0.0071 | 1.0 | 0.71 | 1.00 | 10.0 | 0.00114 |
| 8 | 4 | 5 | 0.0228 | 0.12 | 0.0071 | 1.0 | 0.71 | 1.00 | 10.0 | 0.00114 |
| 9 | 5 | 6 | 0.0228 | 0.12 | 0.0071 | 1.0 | 0.71 | 1.00 | 10.0 | 0.00114 |

Table A.3: Generator data for the RBTS

| Unit No. | Bus No. | Rating (MW) | Failure Rate (occ/yr) | Repair Time (hrs) | Failure Prob. |
|---|---|---|---|---|---|
| 1 | 1 | 40.0 | 6.0 | 45.0 | 0.03 |
| 2 | 1 | 40.0 | 6.0 | 45.0 | 0.03 |
| 3 | 1 | 10.0 | 4.0 | 45.0 | 0.02 |
| 4 | 1 | 20.0 | 5.0 | 45.0 | 0.025 |
| 5 | 2 | 5.0 | 2.0 | 45.0 | 0.01 |
| 6 | 2 | 5.0 | 2.0 | 45.0 | 0.01 |
| 7 | 2 | 40.0 | 3.0 | 60.0 | 0.02 |
| 8 | 2 | 20.0 | 2.4 | 55.0 | 0.015 |
| 9 | 2 | 20.0 | 2.4 | 55.0 | 0.015 |
| 10 | 2 | 20.0 | 2.4 | 55.0 | 0.015 |
| 11 | 2 | 20.0 | 2.4 | 55.0 | 0.015 |

Table A.4: Bus data for the IEEE-RTS

| Bus No. | Load (p.u.) | | $P_g$ | $Q_{max}$ | $Q_{min}$ | $V_0$ | $V_{max}$ | $V_{min}$ |
|---|---|---|---|---|---|---|---|---|
| | Active | Reactive | | | | | | |
| 1 | 1.08 | 0.22 | 1.92 | 1.20 | -0.75 | 1.00 | 1.05 | 0.95 |
| 2 | 0.97 | 0.20 | 1.92 | 1.20 | -0.75 | 1.00 | 1.05 | 0.95 |
| 3 | 1.80 | 0.37 | 0.00 | 0.00 | 0.00 | 1.00 | 1.05 | 0.95 |
| 4 | 0.74 | 0.15 | 0.00 | 0.00 | 0.00 | 1.00 | 1.05 | 0.95 |
| 5 | 0.71 | 0.14 | 0.00 | 0.00 | 0.00 | 1.00 | 1.05 | 0.95 |
| 6 | 1.36 | 0.28 | 0.00 | 0.00 | 0.00 | 1.00 | 1.05 | 0.95 |
| 7 | 1.25 | 0.25 | 3.00 | 2.70 | 0.00 | 1.00 | 1.05 | 0.95 |
| 8 | 1.71 | 0.35 | 0.00 | 0.00 | 0.00 | 1.00 | 1.05 | 0.95 |
| 9 | 1.75 | 0.36 | 0.00 | 0.00 | 0.00 | 1.00 | 1.05 | 0.95 |
| 10 | 1.95 | 0.40 | 0.00 | 0.00 | 0.00 | 1.00 | 1.05 | 0.95 |
| 11 | 0.00 | 0.00 | 0.00 | 0.00 | 0.00 | 1.00 | 1.05 | 0.95 |
| 12 | 0.00 | 0.00 | 0.00 | 0.00 | 0.00 | 1.00 | 1.05 | 0.95 |
| 13 | 2.65 | 0.54 | 5.91 | 3.60 | 0.00 | 1.00 | 1.05 | 0.95 |
| 14 | 1.94 | 0.39 | 0.00 | 3.00 | -0.75 | 1.00 | 1.05 | 0.95 |
| 15 | 3.17 | 0.64 | 2.15 | 1.65 | -0.75 | 1.00 | 1.05 | 0.95 |
| 16 | 1.00 | 0.20 | 1.55 | 1.20 | -0.75 | 1.00 | 1.05 | 0.95 |
| 17 | 0.00 | 0.00 | 0.00 | 0.00 | 0.00 | 1.00 | 1.05 | 0.95 |
| 18 | 3.33 | 0.68 | 4.00 | 3.00 | -0.75 | 1.00 | 1.05 | 0.95 |
| 19 | 1.81 | 0.37 | 0.00 | 0.00 | 0.00 | 1.00 | 1.05 | 0.95 |
| 20 | 1.28 | 0.26 | 0.00 | 0.00 | 0.00 | 1.00 | 1.05 | 0.95 |
| 21 | 0.00 | 0.00 | 4.00 | 3.00 | -0.75 | 1.00 | 1.05 | 0.95 |
| 22 | 0.00 | 0.00 | 3.00 | 1.45 | -0.90 | 1.00 | 1.05 | 0.95 |
| 23 | 0.00 | 0.00 | 6.60 | 4.50 | -0.75 | 1.00 | 1.05 | 0.95 |
| 24 | 0.00 | 0.00 | 0.00 | 0.00 | 0.00 | 1.00 | 1.05 | 0.95 |

Table A.5: Line data for the IEEE-RTS

| Line No. | Bus | | R | X | B/2 | Tap | Current Rating (p.u.) | Failure Rate (occ/yr) | Repair Time (hrs) |
|---|---|---|---|---|---|---|---|---|---|
| | I | J | | | | | | | |
| 1 | 1 | 2 | 0.0260 | 0.0139 | 0.2306 | 1.00 | 1.75 | 0.240 | 16.0 |
| 2 | 1 | 3 | 0.0546 | 0.2112 | 0.0286 | 1.00 | 1.75 | 0.510 | 10.0 |
| 3 | 1 | 5 | 0.0218 | 0.0845 | 0.0115 | 1.00 | 1.75 | 0.330 | 10.0 |
| 4 | 2 | 4 | 0.0328 | 0.1267 | 0.0172 | 1.00 | 1.75 | 0.390 | 10.0 |
| 5 | 2 | 6 | 0.0497 | 0.1920 | 0.0260 | 1.00 | 1.75 | 0.480 | 10.0 |
| 6 | 3 | 9 | 0.0308 | 0.1190 | 0.0161 | 1.00 | 1.75 | 0.380 | 10.0 |
| 7 | 3 | 24 | 0.0023 | 0.0839 | 0.0000 | 1.00 | 4.00 | 0.020 | 768.0 |
| 8 | 4 | 9 | 0.0268 | 0.1037 | 0.0141 | 1.00 | 1.75 | 0.360 | 10.0 |
| 9 | 5 | 10 | 0.0228 | 0.0883 | 0.0120 | 1.00 | 1.75 | 0.340 | 10.0 |
| 10 | 6 | 10 | 0.0139 | 0.0605 | 1.2295 | 1.00 | 1.75 | 0.330 | 35.0 |
| 11 | 7 | 8 | 0.0159 | 0.0614 | 0.0166 | 1.00 | 1.75 | 0.300 | 10.0 |
| 12 | 8 | 9 | 0.0427 | 0.1651 | 0.0224 | 1.00 | 1.75 | 0.440 | 10.0 |
| 13 | 8 | 10 | 0.0427 | 0.1651 | 0.0224 | 1.00 | 1.75 | 0.440 | 10.0 |
| 14 | 9 | 11 | 0.0023 | 0.0839 | 0.0000 | 1.00 | 4.00 | 0.020 | 768.0 |
| 15 | 9 | 12 | 0.0023 | 0.0839 | 0.0000 | 1.00 | 4.00 | 0.020 | 768.0 |
| 16 | 10 | 11 | 0.0023 | 0.0839 | 0.0000 | 1.00 | 4.00 | 0.020 | 768.0 |
| 17 | 10 | 12 | 0.0023 | 0.0839 | 0.0000 | 1.00 | 4.00 | 0.020 | 768.0 |
| 18 | 11 | 13 | 0.0061 | 0.0476 | 0.0500 | 1.00 | 5.00 | 0.400 | 11.0 |
| 19 | 11 | 14 | 0.0054 | 0.0418 | 0.0440 | 1.00 | 5.00 | 0.390 | 11.0 |
| 20 | 12 | 13 | 0.0061 | 0.0476 | 0.0500 | 1.00 | 5.00 | 0.400 | 11.0 |
| 21 | 12 | 23 | 0.0124 | 0.0966 | 0.1015 | 1.00 | 5.00 | 0.520 | 11.0 |
| 22 | 13 | 23 | 0.0111 | 0.0865 | 0.0909 | 1.00 | 5.00 | 0.490 | 11.0 |
| 23 | 14 | 16 | 0.0050 | 0.0389 | 0.0409 | 1.00 | 5.00 | 0.380 | 11.0 |
| 24 | 15 | 16 | 0.0022 | 0.0173 | 0.0364 | 1.00 | 5.00 | 0.330 | 11.0 |
| 25 | 15 | 21 | 0.0063 | 0.0490 | 0.0515 | 1.00 | 5.00 | 0.410 | 11.0 |
| 26 | 15 | 21 | 0.0063 | 0.0490 | 0.0515 | 1.00 | 5.00 | 0.410 | 11.0 |
| 27 | 15 | 24 | 0.0067 | 0.0519 | 0.0546 | 1.00 | 5.00 | 0.410 | 11.0 |
| 28 | 16 | 17 | 0.0033 | 0.0259 | 0.0273 | 1.00 | 5.00 | 0.350 | 11.0 |
| 29 | 16 | 19 | 0.0030 | 0.0231 | 0.0243 | 1.00 | 5.00 | 0.340 | 11.0 |
| 30 | 17 | 18 | 0.0018 | 0.0144 | 0.0152 | 1.00 | 5.00 | 0.320 | 11.0 |
| 31 | 17 | 22 | 0.0135 | 0.1053 | 0.1106 | 1.00 | 5.00 | 0.540 | 11.0 |
| 32 | 18 | 21 | 0.0033 | 0.0259 | 0.0273 | 1.00 | 5.00 | 0.350 | 11.0 |
| 33 | 18 | 21 | 0.0033 | 0.0259 | 0.0273 | 1.00 | 5.00 | 0.350 | 11.0 |
| 34 | 19 | 20 | 0.0051 | 0.0396 | 0.0417 | 1.00 | 5.00 | 0.380 | 11.0 |
| 35 | 19 | 20 | 0.0051 | 0.0396 | 0.0417 | 1.00 | 5.00 | 0.380 | 11.0 |
| 36 | 20 | 23 | 0.0028 | 0.0216 | 0.0228 | 1.00 | 5.00 | 0.340 | 11.0 |
| 37 | 20 | 23 | 0.0028 | 0.0216 | 0.0228 | 1.00 | 5.00 | 0.340 | 11.0 |
| 38 | 21 | 22 | 0.0087 | 0.0678 | 0.0712 | 1.00 | 5.00 | 0.450 | 11.0 |

Table A.6: Generator data for the IEEE-RTS

| Unit No. | Bus No. | Rating (MW) | Failure Rate (occ/yr) | Repair Time (hrs) | Failure Prob. |
|---|---|---|---|---|---|
| 1 | 22 | 50 | 4.42 | 20 | 0.01 |
| 2 | 22 | 50 | 4.42 | 20 | 0.01 |
| 3 | 22 | 50 | 4.42 | 20 | 0.01 |
| 4 | 22 | 50 | 4.42 | 20 | 0.01 |
| 5 | 22 | 50 | 4.42 | 20 | 0.01 |
| 6 | 22 | 50 | 4.42 | 20 | 0.01 |
| 7 | 15 | 12 | 2.98 | 60 | 0.02 |
| 8 | 15 | 12 | 2.98 | 60 | 0.02 |
| 9 | 15 | 12 | 2.98 | 60 | 0.02 |
| 10 | 15 | 12 | 2.98 | 60 | 0.02 |
| 11 | 15 | 12 | 2.98 | 60 | 0.02 |
| 12 | 15 | 155 | 9.13 | 40 | 0.04 |
| 13 | 7 | 100 | 7.30 | 50 | 0.04 |
| 14 | 7 | 100 | 7.30 | 50 | 0.04 |
| 15 | 7 | 100 | 7.30 | 50 | 0.04 |
| 16 | 13 | 197 | 9.22 | 50 | 0.05 |
| 17 | 13 | 197 | 9.22 | 50 | 0.05 |
| 18 | 13 | 197 | 9.22 | 50 | 0.05 |
| 19 | 1 | 20 | 19.47 | 50 | 0.10 |
| 20 | 1 | 20 | 19.47 | 50 | 0.10 |
| 21 | 1 | 76 | 4.47 | 40 | 0.02 |
| 22 | 1 | 76 | 4.47 | 40 | 0.02 |
| 23 | 2 | 20 | 9.13 | 50 | 0.10 |
| 24 | 2 | 20 | 9.13 | 50 | 0.10 |
| 25 | 2 | 76 | 4.47 | 40 | 0.02 |
| 26 | 2 | 76 | 4.47 | 40 | 0.02 |
| 27 | 23 | 155 | 9.13 | 40 | 0.04 |
| 28 | 23 | 155 | 9.13 | 40 | 0.04 |
| 29 | 23 | 350 | 7.62 | 100 | 0.08 |
| 30 | 18 | 400 | 7.96 | 150 | 0.12 |
| 31 | 21 | 400 | 7.96 | 150 | 0.12 |
| 32 | 16 | 155 | 9.13 | 40 | 0.04 |

Tables A.7-A.9 give the per-unit load model for the RBTS and IEEE-RTS.

Table A.7: The weekly peak load as a percent of annual peak

| Week | Peak load | Week | Peak load | Week | Peak load | Week | Peak load |
|---|---|---|---|---|---|---|---|
| 1 | 86.2 | 14 | 75.0 | 27 | 75.5 | 40 | 72.4 |
| 2 | 90.0 | 15 | 72.1 | 28 | 81.6 | 41 | 74.3 |
| 3 | 87.8 | 16 | 80.0 | 29 | 80.1 | 42 | 74.4 |
| 4 | 83.4 | 17 | 75.4 | 30 | 88.0 | 43 | 80.0 |
| 5 | 88.0 | 18 | 83.7 | 31 | 72.2 | 44 | 88.1 |
| 6 | 84.1 | 19 | 87.0 | 32 | 77.6 | 45 | 88.5 |
| 7 | 83.2 | 20 | 88.0 | 33 | 80.0 | 46 | 90.9 |
| 8 | 80.6 | 21 | 85.6 | 34 | 72.9 | 47 | 94.0 |
| 9 | 74.0 | 22 | 81.1 | 35 | 72.6 | 48 | 89.0 |
| 10 | 73.7 | 23 | 90.0 | 36 | 70.5 | 49 | 94.2 |
| 11 | 71.5 | 24 | 88.7 | 37 | 78.0 | 50 | 97.0 |
| 12 | 72.7 | 25 | 89.6 | 38 | 69.5 | 51 | 100.0 |
| 13 | 70.4 | 26 | 86.1 | 39 | 72.4 | 52 | 95.2 |

Table A.8: Daily peak load as a percentage of weekly load

| Day | Peak Load |
|---|---|
| Monday | 93 |
| Tuesday | 100 |
| Wednesday | 98 |
| Thursday | 96 |
| Friday | 94 |
| Saturday | 77 |
| Sunday | 75 |

Table A.9: Hourly peak load as a percentage of daily peak

| Hour | Winter Weeks 1-8&44-52 | | Summer Weeks 18-30 | | Spring/Fall Weeks 9-17&31-43 | |
|---|---|---|---|---|---|---|
| | Wkdy | Wknd | Wkdy | Wknd | Wkdy | Wknd |
| 12-1am | 67 | 78 | 64 | 74 | 63 | 75 |
| 1-2 | 63 | 72 | 60 | 70 | 62 | 73 |
| 2-3 | 60 | 68 | 58 | 66 | 60 | 69 |
| 3-4 | 59 | 66 | 56 | 65 | 58 | 66 |
| 4-5 | 59 | 64 | 56 | 64 | 59 | 65 |
| 5-6 | 60 | 65 | 58 | 62 | 65 | 65 |
| 6-7 | 74 | 66 | 64 | 62 | 72 | 68 |
| 7-8 | 86 | 70 | 76 | 66 | 85 | 74 |
| 8-9 | 95 | 80 | 87 | 81 | 95 | 83 |
| 9-10 | 96 | 88 | 95 | 86 | 99 | 89 |
| 10-11 | 96 | 90 | 99 | 91 | 100 | 92 |
| 11-noon | 95 | 91 | 100 | 93 | 99 | 94 |
| Noon-1pm | 95 | 90 | 99 | 93 | 93 | 91 |
| 1-2 | 95 | 88 | 100 | 92 | 92 | 90 |
| 2-3 | 93 | 87 | 100 | 91 | 90 | 90 |
| 3-4 | 94 | 87 | 97 | 91 | 88 | 86 |
| 4-5 | 99 | 91 | 96 | 92 | 90 | 85 |
| 5-6 | 100 | 100 | 96 | 94 | 92 | 88 |
| 6-7 | 100 | 99 | 93 | 95 | 96 | 92 |
| 7-8 | 96 | 97 | 92 | 95 | 98 | 100 |
| 8-9 | 91 | 94 | 92 | 100 | 96 | 97 |
| 9-10 | 83 | 92 | 93 | 93 | 90 | 95 |
| 10-11 | 73 | 87 | 87 | 88 | 80 | 90 |
| 11-12 | 63 | 81 | 72 | 80 | 70 | 85 |

Note: Wkdy-Weekday, Wknd-Weekend.

# APPENDIX B. THE RTS LOAD DURATION CURVE DATA

Table B.1: The RTS 20-step load duration curve data

| Load level | Probability |
|---|---|
| 1.000 | 0.00023 |
| 0.990 | 0.00011 |
| 0.983 | 0.00057 |
| 0.966 | 0.00171 |
| 0.949 | 0.00171 |
| 0.932 | 0.00331 |
| 0.915 | 0.00616 |
| 0.898 | 0.00970 |
| 0.881 | 0.01153 |
| 0.864 | 0.01610 |
| 0.847 | 0.02363 |
| 0.830 | 0.02546 |
| 0.813 | 0.02386 |
| 0.800 | 0.03311 |
| 0.780 | 0.03459 |
| 0.760 | 0.01632 |
| 0.750 | 0.08219 |
| 0.700 | 0.23162 |
| 0.600 | 0.21553 |
| 0.500 | 0.26256 |

# APPENDIX C. GENETIC ALGORITHM TERMS

Genetic algorithms (GAS) are numerical optimisation algorithms inspired by both natural selection and natural genetics. Much of the terminology used by the GA community is based on that used by biologists [22].

**Chromosome**: A candidate solution to a problem, often encoded as a bit string. Each chromosome consists of "genes" (e.g., bits).

**String size**: A bit string size.

**Offspring**: New solutions (Children).

**Selection**: This operator selects chromosomes in the population for reproduction. The fitter the chromosomes, the more times it is likely to be selected to reproduce.

**Crossover**: This operator randomly chooses a locus and exchanges the subsequence before and after that locus between two chromosomes to create two offspring. For example, the strings 10000100 and 11111111 could be crossed over after the third locus in each to produce the two offspring 10011111 and 11100100. The crossover operator roughly mimics biological recombination between two single-chromosome organisms.

**Mutation**: This operator randomly flips some of the bits in a chromosome. For example, the string 00000100 might be mutated in its second position to yield 01000100. Mutation can occur at each bit position in a string with some probability, usually very small.

**Outline of the Basic Genetic Algorithm**

1. [Start] Generate random population of *n* chromosomes (suitable solutions for the problem)
2. [Fitness] Evaluate the fitness *f(x)* of each chromosome *x* in the population
3. [New population] Create a new population by repeating following steps until the new population is complete
    3.1 [Selection] Select a pair of parent chromosomes from the current population, the probability of selection being an increasing function of fitness.
    3.2 [Crossover] With a crossover probability cross over the parents to form a new offspring (children). If no crossover was performed, offspring is an exact copy of parents.
    3.3 [Mutation] With a mutation probability mutate new offspring at each locus (position in chromosome).
    3.4 [Accepting] Place new offspring in a new population
4. [Replace] Replace the current population with the new population.
5. [Loop] Go to step 2.

# APPENDIX D. STATISTIC OF TRANSMISSION EQUIPMENT FORCED OUTAGES

Statistic of transmission equipment forced outages is obtained from 2004 Forced Outage Performance of Transmission Equipment, Canadian Electricity Association.

Table D.1: Statistic of Transmission Equipment Forced Outages

| | Frequency | Mean duration (h) |
|---|---|---|
| 230 KV transmission lines statistics for a line-related sustained forced outage | 0.3205 /per 100 km | 34.5 |
| 230 KV transmission lines statistics for a terminal-related forced outage | 0.1653 | 16.1 |
| 138 KV transmission lines statistics for a line-related sustained forced outage | 0.9317 /per 100 km | 8.5 |
| 138 KV transmission lines statistics for a terminal-related forced outage | 0.1454 | 12.9 |
| 138 KV cable statistics for a cable-related sustained forced outage | 1.6675 /per 100 km. | 147.4 |
| 138 KV cable statistics for a terminal-related forced outage | 0.0376 | 284.8 |
| 230 KV transformer bank statistics for forced outages involving integral subcomponents | 0.0568 | 226.3 |
| 230 KV transformer bank statistics for terminal equipment | 0.0781 | 76 |

# APPENDIX E. THE INVESTMENT COSTS FOR PLANNING ALTERNATIVES

The procedure for calculating the investment costs for Alternatives 2, 5, and 6 introduced on pages 148, 151 and 152 respectively are shown as follows:

**Alternative 2**

*Stage 1: Add a line between Lines 23 and 9, and double Line 6.*

The project actual investment cost in the starting year of Stage 1:

$$V_{21} = V_{21T} = 0.8 \times 144 + 0.5 \times (0.5 \times 62) = 130.7 \text{ (M\$)}$$

The annual capital payment for Stage 1:

$$A_{21} = A_{21T} = V_{21T} \times \text{CRF} = 130.7 \times 0.08174 = 10.68 \text{ (M\$)}$$

The present value of the total investment for Stage 1:

$$\begin{aligned} TI_{21} = TI_{21T} &= 10.68 \times \left( \frac{1}{(1+0.08)^{1-1}} + \frac{1}{(1+0.08)^{2-1}} + \frac{1}{(1+0.08)^{3-1}} + \frac{1}{(1+0.08)^{4-1}} + \frac{1}{(1+0.08)^{5-1}} \right) \\ &= 10.68 \times 4.312 \\ &= 46.07 \text{ (M\$)} \end{aligned}$$

*Stage 2: Add 6×50 MW at Bus 22, 1×350 MW and 3×155 MW units at Bus 23;*

*Double Line 12.*

The project actual investment cost in the 5th year:

$$\begin{aligned} V_{22} &= V_{22T} + V_{22G} \\ &= (0.5 \times (0.5 \times 86)) + (6 \times 50 \times 1.2 + (3 \times 155 + 350) \times 1.4) \\ &= 21.5 + 1501 \\ &= 1522.5 \text{ (M\$)} \end{aligned}$$

The annual capital payment for Stage 2:

$$
\begin{aligned}
A_{22} &= A_{22T} + A_{22G} \\
&= (V_{22T} + V_{22G}) \times \text{CRF} \\
&= (21.5 + 1501) \times 0.08174 \\
&= 1.76 + 122.69 \\
&= 124.45 \text{ (M\$)}
\end{aligned}
$$

The present value of the total investment for Stage 2:

$$
\begin{aligned}
TI_{22T} &= (A_{21T} + A_{22T}) \times \left( \frac{1}{(1+0.08)^{6-1}} + \frac{1}{(1+0.08)^{7-1}} + ..... + \frac{1}{(1+0.08)^{11-1}} \right) \\
&= (10.68 + 1.76) \times 3.40 \\
&= 42.27 \text{ (M\$)}
\end{aligned}
$$

$$
\begin{aligned}
TI_{22G} &= (A_{21G} + A_{22G}) \times \left( \frac{1}{(1+0.08)^{6-1}} + \frac{1}{(1+0.08)^{7-1}} + ..... + \frac{1}{(1+0.08)^{11-1}} \right) \\
&= (0 + 122.69) \times 3.40 \\
&= 416.90 \text{ (M\$)}
\end{aligned}
$$

The present value of the total investment for Alternative 2:

$$
\begin{aligned}
TI_2 &= TI_{2T} + TI_{2G} \\
&= (46.07 + 42.27) + 416.90 \\
&= 88.34 + 416.90 \\
&= 505.24 \text{ (M\$)}
\end{aligned}
$$

**Alternative 5**

*Stage 1: Add a line between Bus 11 and Bus 15 and double Line 6;*

*Add 6×50 MW and 1×350 MW units at Buses 22 and 23 respectively.*

The project actual investment cost in the starting year of Stage 1:

$$
\begin{aligned}
V_{51} &= V_{51T} + V_{51G} \\
&= (0.8 \times 144 + 0.5 \times (0.5 \times 62)) + (6 \times 50 \times 1.2 + 1 \times 350 \times 1.4) \\
&= 130.7 + 850 \\
&= 980.7 \text{ (M\$)}
\end{aligned}
$$

The annual capital payment of Stage 1:

$$\begin{aligned} A_{51} &= A_{51T} + A_{51G} \\ &= (V_{51T} + V_{51G}) \times \mathrm{C}RF \\ &= 10.68 + 69.48 \\ &= 80.16 \text{ (M\$)} \end{aligned}$$

The present value of the total investment for Stage 1:

$$\begin{aligned} TI_{51} &= TI_{51T} + TI_{51G} \\ &= (10.68 + 69.48) \times \left( \frac{1}{(1+0.08)^{1-1}} + \frac{1}{(1+0.08)^{2-1}} + \frac{1}{(1+0.08)^{3-1}} + \frac{1}{(1+0.08)^{4-1}} + \frac{1}{(1+0.08)^{5-1}} \right) \\ &= 46.07 + 299.60 \\ &= 345.67 \text{ (M\$)} \end{aligned}$$

*Stage 2: Add 3×155 MW units at Bus 23 and double Line 12.*

The project actual investment cost in the 5th year:

$$\begin{aligned} V_{52} &= V_{52T} + V_{52G} \\ &= 0.5 \times (0.5 \times 86) + (3 \times 155 \times 1.4) \\ &= 21.5 + 651 \\ &= 672.5 \text{ (M\$)} \end{aligned}$$

The annual capital payment of Stage 2:

$$\begin{aligned} A_{52} &= A_{52T} + A_{52G} \\ &= (V_{52T} + V_{52G}) \times CRF \\ &= 1.76 + 53.21 \\ &= 54.97 \text{ (M\$)} \end{aligned}$$

The present value of the total investment for Stage 2:

$$\begin{aligned} TI_{52} &= (A_{51} + A_{52}) \times \left( \frac{1}{(1+0.08)^{6-1}} + \frac{1}{(1+0.08)^{7-1}} + \ldots\ldots + \frac{1}{(1+0.08)^{11-1}} \right) \\ &= (A_{51T} + A_{52T}) \times 3.40 + (A_{51G} + A_{52G}) \times 3.40 \\ &= 12.44 \times 3.40 + 122.69 \times 3.40 \\ &= 42.27 + 416.90 \\ &= 459.17 \text{(M\$)} \end{aligned}$$

The present value of the total investment for Alternative 5:

$$\begin{aligned} TI_5 &= TI_{51} + TI_{52} \\ &= 345.67 + 459.17 \\ &= 804.84 \text{ (M\$)} \end{aligned}$$

**Alternative 6**

*Stage 1: Double Lines 23, 27 and 7;*

*Add 6×50 MW and 1×350 MW units at Buses 22 and 23 respectively.*

The project actual investment cost in the starting year of Stage 1:

$$\begin{aligned} V_{61} &= V_{61T} + V_{61G} \\ &= (0.5\times(0.8\times108 + 0.8\times144) + 13) + (6\times50\times1.2 + 1\times350\times1.4) \\ &= 113.8 + 850 \\ &= 963.8\,(\text{M\$}) \end{aligned}$$

The annual capital payment for Stage 1:

$$\begin{aligned} A_{61} &= A_{61T} + A_{61G} \\ &= (V_{61T} + V_{61G}) \times \text{C}RF \\ &= 9.30 + 69.48 \\ &= 78.78 \text{ (M\$)} \end{aligned}$$

The present value of the total investment for Stage 1:

$$\begin{aligned} TI_{61} &= TI_{61T} + TI_{61G} \\ &= (9.30 + 69.48) \times \left( \frac{1}{(1+0.08)^{1-1}} + \frac{1}{(1+0.08)^{2-1}} + \frac{1}{(1+0.08)^{3-1}} + \frac{1}{(1+0.08)^{4-1}} + \frac{1}{(1+0.08)^{5-1}} \right) \\ &= 40.11 + 299.60 \\ &= 339.71\,(\text{M\$}) \end{aligned}$$

*Stage 2: Add a line between Buses 6 and 8, add 3×155 MW units at Bus 23.*

The project actual investment cost in the 5th year:

$$\begin{aligned} V_{62} &= V_{62T} + V_{62G} \\ &= (0.5\times 86) + (3\times 155\times 1.4) \\ &= 43 + 651 \\ &= 694\,(\text{M\$}) \end{aligned}$$

The annual capital payment for Stage 2:

$$\begin{aligned} A_{62} &= A_{62T} + A_{62G} \\ &= (V_{62T} + V_{62G}) \times CRF \\ &= 3.51 + 53.21 \\ &= 56.73\ (\text{M\$}) \end{aligned}$$

The present value of the total investment for Stage 2:

$$\begin{aligned} TI_{62} &= (A_{61} + A_{62}) \times \left( \frac{1}{(1+0.08)^{6-1}} + \frac{1}{(1+0.08)^{7-1}} + ..... + \frac{1}{(1+0.08)^{11-1}} \right) \\ &= (A_{61T} + A_{62T}) \times 3.40 + (A_{61G} + A_{62G}) \times 3.40 \\ &= 12.82 \times 3.40 + 122.69 \times 3.40 \\ &= 43.55 + 416.90 \\ &= 460.45\,(\text{M\$}) \end{aligned}$$

The present value of the total investment for Alternative 6:

$$\begin{aligned} TI_6 &= TI_{61} + TI_{62} \\ &= 339.71 + 460.45 \\ &= 800.16\ (\text{M\$}) \end{aligned}$$